Elucidation of anti-viral strategies in *Streptomyces*

Bente Ursula Rackow

Mitglied der Helmholtz-Gemeinschaft

JÜLICH
Forschungszentrum

Elucidation of anti-viral strategies in *Streptomyces*

Bente Ursula Rackow

The thesis has been conducted at the Institute of Bio- and Geosciences, IBG-1: Biotechnology Forschungszentrum Jülich, from October 2021 until March 2025 under the supervision of Prof. Dr. Julia Frunzke.

Published by permission of the

Faculty of Mathematics and Natural Sciences at

Heinrich-Heine-University Düsseldorf

Supervisor:　　　　Prof. Dr. Julia Frunzke

Institute of Bio- and Geosciences, IBG-1: Biotechnology

Forschungszentrum Jülich

Jülich

Co-supervisor:　　　Prof. Dr. Nick Wierckx

Institute of Bio- and Geosciences, IBG-1: Biotechnology

Forschungszentrum Jülich

Jülich

"Now, here, you see, it takes all the running you can do, to keep in the same place. If you want to get somewhere else, you must run at least twice as fast as that!" Red Queen

– Lewis Carroll (Through the Looking-Glass, and what Alice found there)

Publications

The research presented in this dissertation has been published in the following manuscript:

B. Rackow, C. Rolland, I. Mohnen, J. Wittmann, M. Müsken, J. Overmann & J. Frunzke (2024). „Isolation and characterization of the new *Streptomyces* phages Kamino, Geonosis, Abafar and Scarif infecting a broad range of host species", Microbiology Spectrum, Vol 14, No. 11: https://doi.org/10.1128/spectrum.00663-24

Table of contents

Abbreviations

a.U.	Arbitrary Units
Abi	Abortive infection
AME	Aminoglycoside modifying enzyme
BGC	Biosynthetic gene cluster
bp	Base pairs
Cas	CRISPR-associated
CBASS	Cyclic oligonucleotide-based antiphage signalling system
CRISPR	Clustered regularly interspaced short palindromic repeats
DNA	Deoxyribonucleic acid
dsDNA	double stranded DNA
dsRNA	double stranded RNA
e.g.	*exempli gratia*
et al.	*et alii*
i.e.	*id est*
HGT	Horizontal gene transfer
MM	Minimal medium
OD	Optical density
PADLOC	Prokaryotic Antiviral Defense LOCator
PCR	Polymerase chain reaction
PFU	Plaque forming units
R-M	Restriction-modification
RNA	Ribonucleic acid
SM	Spent medium
ssDNA	single stranded DNA
ssRNA	single stranded RNA
TEM	Transmission electron microscope
TPM	Transcripts per million

Further abbreviations not included in this section are used according to international standards, which are listed in the author guidelines of the Journal of Cell Biology (https://rupress.org/jcb/pages/standard-abbreviations).

Abbreviations

Summary

Streptomyces species have been highly studied for decades for their multicellular development and their distinguished ability to produce a myriad of different bioactive small molecules. In recent years the interaction between these multicellular bacteria and their predatory viruses, the bacteriophages (or phages for short) came into the focus of research. It was recently discovered that specialized metabolites produced by *Streptomyces* not only protect from competing bacteria but also from phage infections. Both aminoglycosides and anthracyclines, small molecules produced by *Streptomyces* have been shown to efficiently inhibit phage infection, but the exact mechanism of action remained elusive. This multi functionality of small molecules piqued the interest. This work sets out to elucidate such anti-viral strategies of *Streptomyces* and to integrate the chemical defense mediated by small molecules into the context of the bacterial immune system.

Initially, spent medium of natural aminoglycoside producing *Streptomyces spp.* was tested for its anti-phage potential, showing different degrees of defense potential, specific to the molecule produced as well as the phage tested. Extracellular effects of spent medium could only be determined for phages infecting less related species, such as *Corynebacterium glutamicum*. Furthermore, isolation and characterization of novel *Streptomyces* phages broadened the repertoire of phages that can be used to understand the interaction between host and phage and how chemical defense affects this interaction. Three of the four newly isolated phages infect several different species. These broad host range phages pose to be good tools to understand also the influence of the host background on the efficiency of chemical defense.

Large screenings of small molecules mediating chemical defense with two different collections of phages revealed several sensitivity determinants of phages to chemical defense and showed that the efficiency of chemical defense is a delicate process influenced by a manifold of factors. *Streptomyces* phages showed sensitivity towards most of the compounds tested, whereas coliphages only showed sensitivity towards DNA intercalating molecules. Redirecting the focus of this work towards the mechanism of action of the anthracycline daunorubicin, many insights in the inhibitory effect of this small molecule were obtained. Daunorubicin acts intracellularly, after the genome injection of phages but before DNA replication. The host background influences the potency of daunorubicin-mediated defense and synergy between chemical defense and intracellular defense systems could be determined.

Even though the direct mechanism of action of chemical defense remains yet elusive, several important insights were gained and provide basis for further research in this area of anti-phage defense.

Summary

1. Introduction

1.1 Bacteriophages

Bacteriophages (or phages for short) are the predatory viruses of bacteria and the most abundant biological entity on earth, outnumbering bacteria by a factor of 10, reaching estimated numbers of 10^{31} total particles (Hendrix, 2002; Hendrix, Smith, Burns, Ford, & Hatfull, 1999). The term bacteriophage is Greek for "bacteria eater" and describes the first observations that were connected to the discovery of the small viruses by Frederick Twort (1915) and Felix d'Herelle (1917) independently, where empty spots or "plaques" on bacterial lawns were identified (d'Herelle, 1917; Twort, 1915). These "ultramicroscopic viruses" or "invisible microbes" could only be visualized with electron microscopy, where the morphological description of the phages started (Luria, Delbrück, & Anderson, 1943; Ruska, 1940). With about 10^{24} infections per second (Naureen et al., 2020) phages harbour great potential to shape the bacterial world. Furthermore, their ability to kill bacteria in a very specific manner made phages interesting tools for therapeutic treatment of bacterial infections (Clokie, 2011; Rehman, Ali, Khan, Bostan, & Naseem, 2019; Rose et al., 2014; Uyttebroek et al., 2022). However, since phages and bacteria are in a continuous arms race and bacteria are able to evolve defense mechanism against phages, the reliability of phage therapy suffered and antibiotic treatment was the more consistent choice. Therefore, phage research shifted from therapy to molecular tool development (Salmond & Fineran, 2015). Moreover, the limited diversity of phages available for therapeutic approaches further diminished the strength of phage therapy in former times (Ly-Chatain 2014; Salmond & Fineran, 2015). Considering the sheer quantity of phages, research on their molecular composition, lifestyle, morphology, and genomes ensured the discovery of a previously unknown diversity of said traits (Ofir & Sorek, 2018). With the onset of the "Phage Treaty" by Max Delbrück and colleagues in the 1940s, research in bacteriophages focused on the T-phages infecting *Escherichia coli.* This research uncovered multiple important insights into the fundamental principles of biology, such as the structure of genes, the triplet nature of the genetic code or the phenomenon of "enzyme induction" (Salmond & Fineran, 2015). This time span of phage research was the "birth" of molecular biology, leading to the discovery of various molecular tools. For example restriction-modification systems (RM), the T4 DNA ligase or the T7 polymerase. However, the broad diversity of phages completely was completely disregarded, which is in the focus of the phage research nowadays in the renaissance of phage biology (Salmond & Fineran, 2015).

1.1.1 Phage lifestyle, morphology and diversity

Like every virus, phages are dependent on their host for replication of viral DNA, production of proteins and the final assembly of the phage particle (Clokie, 2011; Ofir & Sorek, 2018). Regarding the

infection and replication of phages, different life styles of phages are known, spanning from lytic infection over lysogenisation of the host to chronic infections. During lytic infections the phage infects its host, hijacks the host replication machinery and uses it for its own replication. Once the phage particles are assembled the host cell is lysed and the offspring of phages is set free (Salmond & Fineran, 2015). Virulent phages, which have a strictly lytic lifestyle, have a huge impact on bacterial populations and shape their ecological niches, however the phage abundance is tightly coupled to the host abundance leading to a balance of the players in the co-evolutionary game (Clokie, 2011) (Figure 1). Temperate phages are able to enter both the lytic or the lysogenic lifecycle, where the phage genome is integrated into the host genome or carried as an extrachromosomal plasmid and is stably inherited (Salmond & Fineran, 2015) (Figure 1). In the lysogenic state the dormant phage is called prophage and it is tightly associated with the host both in terms of replication and fitness, forming a symbiotic relationship (Bondy-Denomy et al., 2016). Upon extrinsic stress signals, which can range from UV-radiation, DNA targeting antibiotics or infection of another phage, the prophage can be induced and enters the lytic cycle (Salmond & Fineran, 2015). Induction of the prophage can also happen in the absence of extrinsic signals, so called spontaneous induction. The model phage which was highly studied to understand the switch between lytic and lysogenic lifecycle is the temperate coliphage λ. Here, the decision between lytic or lysogenic lifecycle is mainly dependent on the concentrations of phage repressor proteins (Oppenheim, Kobiler, Stavans, Court, & Adhya, 2005). Furthermore, a
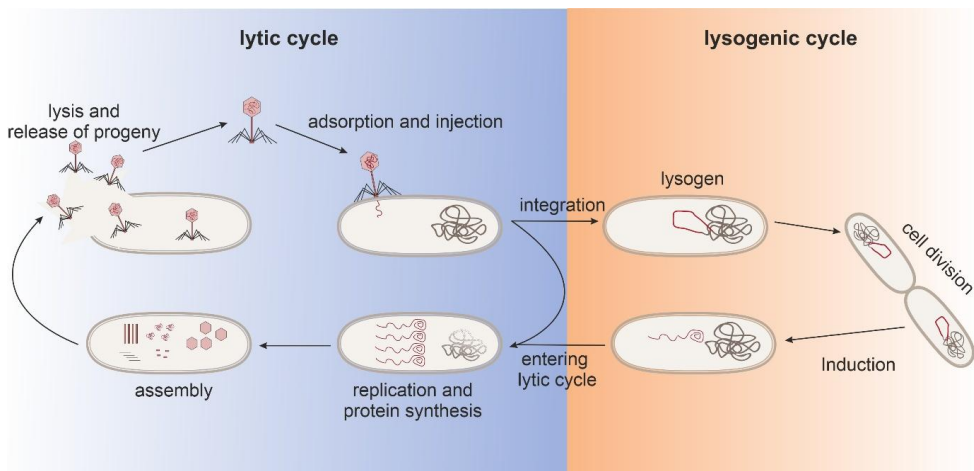
Figure 1: Lytic and lysogenic lifecycle of phages. Each phage infection starts with the recognition of the host cell, followed by adsorption and injection of the phage genome. Once inside the cell two routes can be followed, temperate phages can instead of only following the lytic cycle decide to integrate their genome into the host genome or form an extrachromosomal plasmid (not shown), forming a stable association with the host which is called the lysogenic cycle. Virulent phages in contrast can only follow the route of the lytic cycle, hijacking the host machinery for its own replication and protein synthesis, followed by phage particle assembly and finally lysis of the host cell and release of the phage progeny. Upon encountering stress factors, such as UV-radiation, SOS-response inducing factors or even phage infection, the so-called prophage within the lysogenic cycle can be induced, excise itself from the host genome and enter the lytic cycle. The Figure is inspired by Salmond & Fineran 2015.

lifestyle known as chronic infection exists where after infection of the host, the phage replicates within the host and phage particles are shed from the cell over a long period of time without killing the host. This kind of lifestyle is known for archaeal viruses or filamentous viruses, like M13, and will not be further discussed in this work (Clokie, 2011).

Given the immense estimated number of phage particles on the planet, it is not surprising that their traits, including genetic material and morphological forms, exhibit a high degree of diversity (Dion, Oechslin, & Moineau, 2020; Krupovic, Prangishvili, Hendrix, & Bamford, 2011). Genetic information is conserved in the form of both DNA and RNA in the single-stranded or double-stranded form (Figure 2) (Ackermann, 2006). Regarding phage morphology and genetic material, which can be determined using electron microscopy, the majority of isolated phages have the morphotype of tailed phages with double stranded DNA, the *Caudoviricetes*, belonging to the realm of Duplodnaviria (Ackermann, 2007; Krupovic et al., 2021) (Figure 2). Other dsDNA morphotypes such as lipid-containing polyhedral, classified as Varidnaviria, or lipid pleomorphic phages which are unclassified have been described as well (Krupovic et al., 2021) (Figure 2). Furthermore, ssDNA phages with a polyhedral or filamentous shape, classified as Monodnaviria, as well as dsRNA and ssRNA phages with a polyhedral morphology, classified as Riboviria are described in literature. However, those phages make up only 4 % of all phages that were isolated and characterized (Ackermann, 2007; Ofir & Sorek, 2018) (Figure 2). Isolated phages that are fully characterized and described are often highly biased due to the methods used for their isolation, the availability of suitable host organisms for cultivation, and the enrichment techniques chosen by researchers. In contrast, viral "dark matter" identified in metagenomics data suggests a different distribution of phage families, highlighting the challenges in isolating certain phage types currently underrepresented in phage isolates. According to metagenomics data RNA viruses are more abundant than currently depicted in phage libraries (Creasy, Rosario, Leigh, Dishaw, & Breitbart, 2018; Neri et al., 2022). Taxonomic classification of phages was classically based only on the morphological shape of the phage capsid, which is outdated, as morphological similarities completely disregard the genomic relatedness of phages (Turner, Kropinski, & Adriaenssens, 2021). Nowadays, taxonomic classification is based on genetic information instead of only morphological traits and is regulated by the International Committee on Taxonomy of Viruses (ICTV) (Krupovic et al., 2021).

Phage geobiological distribution is tightly coupled to the distribution of its host, a phenomenon that is best studied in marine cyanobacteriophages (Clokie, 2011). This, however, holds true in more structured environments, such as soil or the mammalian gut, where phages and hosts share ecological niches and influence the abundance of the respective counterpart (Clokie, 2011). This direct and constant physical interaction leads to the ever ongoing evolutionary adaption and counter adaption of
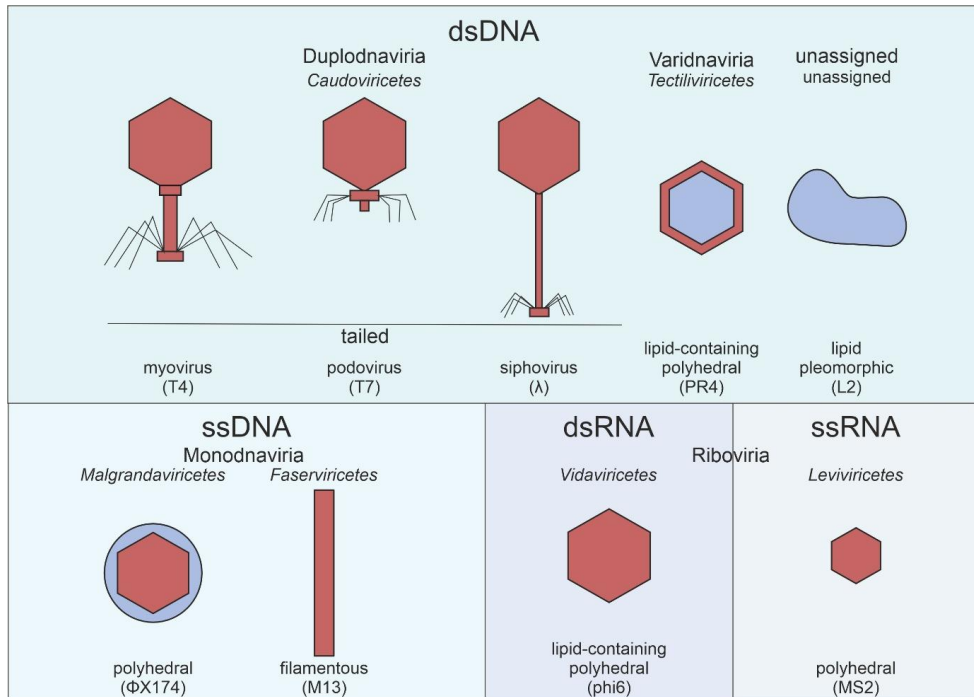
Figure 2: Phage morphology, genetic material and classification. Phage genomes can contain dsDNA, ssDNA, dsRNA or ssRNA. Double-stranded DNA phages are classified as Duplodnaviria, Varidnaviria or unassigned. Duplodnaviria are tailed phages belonging to the class *Caudoviricetes* that can be distinguished in the morphotypes of myovirus with a medium sized, contractile tail, podovirus with a short stubby tail and siphovirus with a long non-contractile tail. Model phages of those morphologies are T4, T7 and λ respectively. Varidnaviria and unassigned phages of the dsDNA phages are of lipid-containing polyhedral or lipid pleomorphic morphology respectively, model phages for those classes are PR4 (*Tectilviricetes*) and L2 (unassigned) respectively. ssDNA phages are classified as Monodnaviria and have either polyhedral or filamentous morphologies with ΦX174 (*Malgrandaviricetes*) and M13 (*Faserviricetes)* as example phages. Finally RNA phages belong to the realm of Riboviria and are categorized into dsRNA phages and ssRNA phages, classified as *Vidaviricetes* (e.g. phi6) and *Leviviricetes* (e.g. MS2) respectively. Both types have a polyhedral morphology. Design of the Figure was inspired by Ofir & Sorek 2018 and based on the newest taxonomic information of the International Committee on Taxonomy of Viruses (ICTV, 2022).

phages and bacteria ensuring to the evolutional arms race that is described in the "red queen hypothesis" (Stern & Sorek, 2011; Van Valen, 1973).

1.1.2 Phage-host interactions

Rather than simply being a two-player game, interactions between phages and their bacterial hosts form a complex network (Rostøl & Marraffini, 2019; Salmond & Fineran, 2015). Phages can either be specialists, infecting only one strain of bacteria with high efficiency, or generalists, capable of infecting multiple strains or even different bacterial species within a given environment (Rackow et al., 2024; Stern & Sorek, 2011). Temperate phages that integrate into the host genome and persist as prophages can provide adaptive benefits to the host. These horizontally transferred elements might include genes for anti-phage defense or antibiotic resistance cassettes, as well as mechanisms for superinfection exclusion and other advantageous traits (Bondy-Denomy et al., 2016; Stern & Sorek,

1. Introduction

2011; X. Wang et al., 2010). Superinfection refers to instances where multiple phage particles infect the same bacterial cell simultaneously, resulting in competition or cooperation between phages within the same host (Stern & Sorek, 2011). A notable example of this phenomenon is the BASEL (BActeriophage SElection for your Laboratory) phage collection, which comprises 69 newly isolated coliphages that infect the same host strain (Maffei et al., 2021) (Figure 3). This collection serves as a valuable tool for studying phage-host interactions, particularly the evolutionary "arms race" between phages and bacteria. Its taxonomic diversity reflects the natural variety of phages, enabling comparative studies (Maffei et al., 2021) (Figure 3). By manipulating the host's immune system, researchers can observe how different phages respond to bacterial defenses and evolve over time. Fortunately, the collection is completely characterized, providing information about the phages genome size and composition, first and secondary receptors, as well as sensitivity and resistance to anti-phage defense systems (Maffei et al., 2021). With these information at hand the BASEL collection is a solid basis for in depth studies, allowing to correlate results to the available information about the individual phages (Maffei et al., 2021).
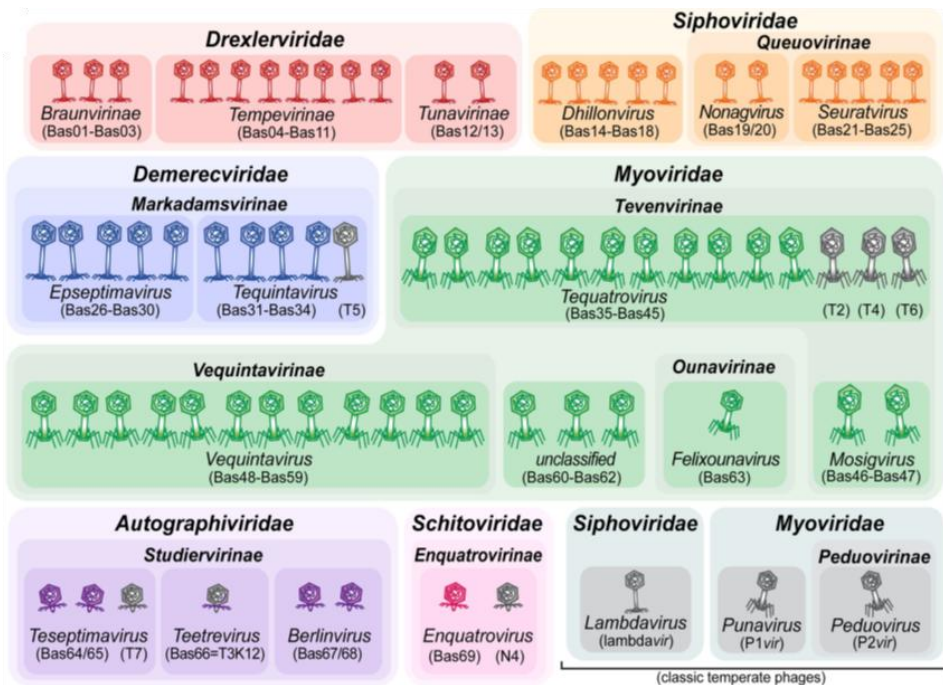
Figure 3: Overview of the BASEL phage collection. Taxonomic overview and visual representation of the 69 BASEL phages including the Phage family, subfamily and genus including the model phages T2-T7 as well as λ, N4, P1*vir* and P2*vir* for classification reference in grey. All phages in this collection infect the same *E. coli* strain, K12 MG1655 ΔRM and are virulent phages except for the three grey in the bottom row which are exclusively classic temperate model phages. Figure adapted from Maffei et al., 2021.

1.2 Anti-viral defense strategies of bacteria

Due to their constant co-evolution with phages, bacteria have developed a diverse array of anti-phage defense systems, collectively known as the bacterial immune system, which has been extensively studied in recent years (Millman et al., 2022; Stern & Sorek, 2011; Nitzan Tal & Sorek, 2022). Many of these studies have been conducted using *E. coli* as a model organism, given its well-documented biology and extensively characterized genomic composition (Doron et al., 2018; Hochhauser, Millman, & Sorek, 2023; Maffei et al., 2021; Millman et al., 2022). In the following chapter an overview of the bacterial immune system will be provided.

1.2.1 Bacterial anti-phage defense systems

Since the concept of defense islands was discovered, the identification of new anti-phage defense systems increased in speed in recent years. Defense islands are genomic regions within the bacterial genome that contain multiple anti-phage defense systems, e.g. CRISPR-Cas, a toxin-antitoxin system and a retron system, which are often horizontally transferred together (Doron et al., 2018; Makarova, Wolf, Snir, & Koonin, 2011). This led to the discovery of multiple new defense systems that show high degrees of conservation between prokaryotic and eukaryotic anti-viral defense systems (Georjon & Bernheim, 2023). Similarly to the eukaryotic immune systems, the bacterial immune systems can be categorized into the innate and the adaptive immune system (Doron et al., 2018). The innate immune system consist of the classic anti-phage defense systems such as restriction-modification or abortive infection systems (abi systems) (Figure 4). These systems are today tools in molecular biology due to research in the early days of phage biology by Delbrück, Luria and colleagues (Loenen, Dryden, Raleigh, & Wilson, 2013; Luria & Human, 1952; Pleška et al., 2016). Restriction-modification (RM) systems are able to discriminate self- from non-self DNA by modification of the host DNA, such as the methylation of cytosines in a sequence dependent manner (Bair & Black, 2007; Loenen et al., 2013; Pingoud, Wilson, & Wende, 2014; Rao, Dryden, & Bheemanaik, 2013). RM systems are nuclease based defense systems which typically have paired methyltransferase and endonuclease activities exerted by two to three enzymes which act in concert to detect and cleave foreign DNA and protect their host DNA (Bair & Black, 2007) (Figure 4). These nuclease-based defense systems are categorized into four types, according to their modification pattern, recognition site and cleavage pattern and they are present in over 90 % of the sequenced bacterial genomes (Stern & Sorek, 2011). Type I RM systems consist of three subunits, a restriction, a modification and a specificity enzyme. These enzymes recognize a specific DNA sequence but cleave the DNA at random sites distant from the recognition site (Loenen et al., 2013). Type II RM systems have independently acting restriction endonucleases and methylases which recognise specific palindromic DNA sequences and cleave within or close to the recognition site (Pingoud et al., 2014). The third type of RM systems, type III is constructed of two subunits, one for

modification and one for restriction. These enzymes recognise specific, non-palindromic DNA sequences and cleave at sites in a short distance from the recognition site (Rao et al., 2013). In contrast to the other RM systems, type IV RM systems recognize and cleave modified DNA sequences, however they lack methyltransferase subunits (Bair & Black, 2007). RM systems are able to stop ongoing phage infections and ensure the viability of the single cell (Nitzan Tal & Sorek, 2022). In contrast to this, abortive infection is the general term for a pre-mature cell death as reaction upon phage entry and is a means to protect the bacterial population from spread of the phage infection by sacrificing single cells (Aframian & Eldar, 2023; Lopatina, Tal, & Sorek, 2020). Even though abortive infection systems have been known and described for decades, the molecular mechanism of many of these systems remains elusive (Maffei et al., 2021). Adaptive immunity is characterized by the possibility to acquire resistance towards new phages by editing the system. One example is the CRISPR/Cas system, where the integration of new spacer sequences broadens the resistance too phage infections (Makarova et al., 2020). The adaptive immune system comprises various systems such as CRISPR-Cas, sensing-signalling systems, nucleotide depletion systems, retron systems, toxin-antitoxin systems and many more (Georjon & Bernheim, 2023). Systems such as CRISPR-Cas have been highly studied and are nowadays used in biotechnology as tools to specifically modify DNA making use of the spacer sequences, which are originally used to detect and identify invading phage DNA (Makarova et al., 2020) (Figure 4). Similar to RM systems, CRISPR systems are distinguished into different classes regarding their effector modules and interference pattern (Makarova et al., 2020). Another important defense system for this work are retron systems, which are genetic elements composed of a specialized reverse transcriptase (RT) and a non-coding RNA which work in concert with an effector protein (Millman et al., 2020). Retrons are described to act as a second line of defense. Once the cell recognizes the failure of first line defenses, the retron system gets activated and leads subsequently to an abortive infection, thereby protecting neighbouring cells from the spread of phage infection (Millman et al., 2020). Triggers of the different anti-phage defense systems are highly diverse and range from invading DNA to the corruption of host protein complexes and span the whole phage lifecycle, leading to phage specific defense mechanism (Georjon & Bernheim, 2023). Defense systems are clustered in the genomes of bacteria and form so-called defense islands, which are prone to horizontal gene transfer (HGT) and thus are less conserved within the genome (Doron et al., 2018; Makarova et al., 2011). Within bacterial genomes often more than one defense system can be identified, with a mean of 5.3 systems per genome (Georjon & Bernheim, 2023). These systems can act as layers of defense, for either different phages that are able to infect the host or different stages of infection (Doron et al., 2018; Gao et al., 2020). Another kind of anti-phage defense which was first described in the 1950s but was only recently rediscovered is the small molecule mediated anti-phage

defense, termed chemical defense (Hardy, Kever, & Frunzke, 2023). Secreted small molecules, e.g. aminoglycosides and anthracylines, provide protection against a broad range of phages (Kever et al., 2022; Kronheim et al., 2018; Zuo, Yu, Alvarez, & Dozois, 2021) (Figure 4).
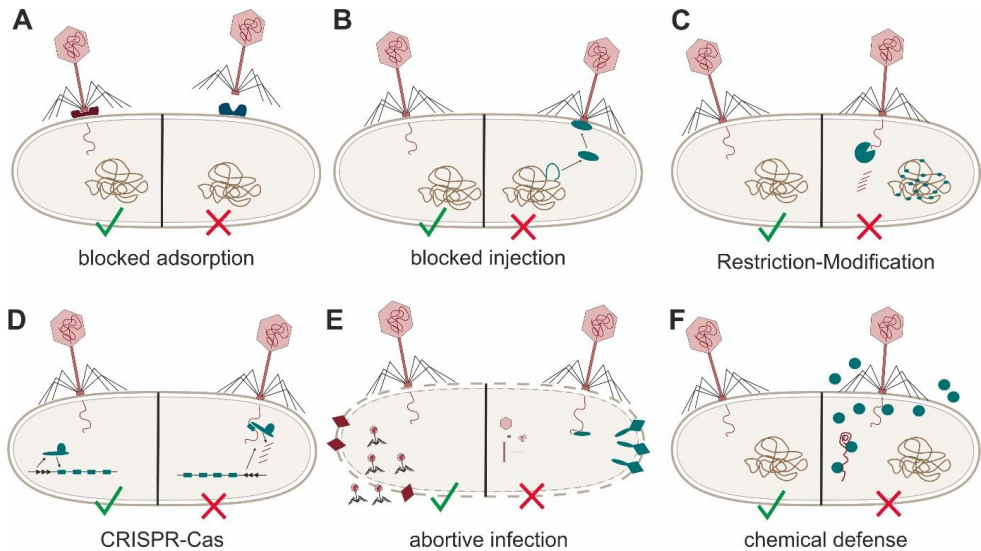
Figure 4: Selection of anti-phage defense systems. A general overview of several anti-phage defense systems and which step of phage infection is inhibited. A) Blocking of adsorption, by masking the phage receptor or decorating it with sugar or protein residues. The phage is blocked from the irreversible binding to the host cell. B) Blocking of injection is often mediated by prophage encoded genes that inhibit superinfection and recognise phage infection in the very early stages. C) Restriction modification systems are cellular encoded systems which distinguish foreign from own DNA by a methylation pattern which was added to the host DNA by the methylase of the RM system. The restriction enzyme recognises unmodified DNA sequences and subsequently cleaves invading DNA. D) CRISPR-Cas belongs to the adaptive immune system of bacteria and can identify phage DNA very specifically through spacer sequences in the host-genome. Upon encounter of the spacer sequence the Cas enzyme will cleave the invading DNA. E) Abortive infection mechanism recognise ongoing phage infection by e.g. the RecBCD complex and will lead to premature cell-lysis, prior to the completion of the phage lifecycle, inhibiting the release of phage progeny and thereby protecting the population from a spread of the phage infection. F) Chemical defense mediated by small molecules leads to an inhibition of phage infection in the early steps of the infection, likely by intercalating into the DNA and blocking the replication/transcription. Many more defense systems are known and described, however this selection of defense systems gives a concise overview of the distribution of protein/RNA mediated and other defense systems. The green tick indicates successful phage infection and the red cross indicates the inhibited phage infection by the respective defense system. Phage related DNA, proteins or effectors are shown in shades of red, host DNA is shown in brown and host proteins and effectors are shown in dark turquoise. The design of this Figure was inspired by Georjon & Bernheim 2023 and the dissertation of Dr. Tom Luthe.

1.2.2 Synergy between different defense systems

Regarding the metabolic burden associated with the simultaneous expression of multiple anti-phage defense systems, there must be an adaptive benefit to certain combinations of these systems (Tesson & Bernheim, 2023). This idea is supported by the findings of Wu and colleagues, who demonstrated the synergistic effects of different anti-phage defense systems (Wu et al., 2024). Synergism is defined as the interaction between two systems that produce a combined effect greater than the sum of their individual effects (Wu et al., 2024). In the context of anti-phage defense, co-occurring systems within defense islands can confer synergistic defense properties (Tesson & Bernheim, 2023; Wu et al., 2024).

1. Introduction

These combinations may also be jointly transferred via HGT, providing fitness advantages to recipient bacteria—particularly in phage-dense environments (Wu et al., 2024). In this work, the focus on synergistic effects lies in the interplay between intracellular defense systems (e.g., restriction-modification systems or retrons) and extracellular defense mechanisms, such as chemical defenses mediated by secreted small molecules.

1.2.3 From single cell defense to pan-immunity

Bacteria, outside the controlled conditions of a laboratory, exist in diverse microbial communities rather than monoclonal cultures. These communities are composed of multiple bacterial strains and species, each contributing unique anti-phage defense systems (Bernheim & Sorek, 2020). Together, these systems provide resistance to a wide variety of phages, functioning as a shared resource within the population (Bernheim & Sorek, 2020). Defined as the pan-immune system by Aude Bernheim and colleagues, this shared resource underscores the idea that not a single bacterium carries all the necessary defense mechanisms. Instead, the collective immune potential of the community ensures population-wide survival in the face of phage threats (Bernheim & Sorek, 2020; Doron et al., 2018; Hochhauser et al., 2023). In this context, chemical defense mechanisms mediated by small molecules hold significant potential as a community-wide strategy for protection against phage infections (Hardy et al., 2023; Kever et al., 2022; Kever et al., 2024; Kronheim et al., 2018). Unlike defense systems acting on individual bacteria, small molecules can diffuse through the microbial environment, potentially offering protection to neighbouring cells within the community. This shared chemical defense might not only enhance the resilience of the microbial population but also highlights the importance of understanding the breadth and specificity of protection these molecules provide. The defense spectrum conferred by small molecules is therefore highly relevant, as it determines the range of phages that can be neutralized or inhibited by such mechanisms and will be a significant part of this work (Hardy et al., 2023; Luthe, Kever, Thormann, & Frunzke, 2023b).

1.3 Chemical anti-phage defense

The inhibitory effect of antibiotics on phage infection was first described in the 1950s, however this was never connected to the bacterial immune system and therefore not followed up on (Hardy et al., 2023). Within the last decade, several research groups rediscovered this phenomenon independently and set out to understand the mechanism of action of small molecule mediated anti-phage defense (Jiang, Wei, Liang, Peng, & Li, 2020; Kever et al., 2022; Kronheim et al., 2018). Naturally produced small molecules that have been shown to mediate anti-phage defense are mainly produced by Actinomycetes belonging to the genera *Streptomyces* and *Micromonospora* and span from aminoglycosides and anthracyclines to peptide antibiotics such as actinomycin D, glycopeptide antibiotics such as bleomycin or the piperidine alkaloid abikoviromycin (Gurevich, Kolosov, Korobko,

& Onoprienko, 1968; Hardy et al., 2023; Scholz, Meissner, & Rosenthal, 1979). The following chapter will elaborate on chemical defense mediated by aminoglycosides and anthracyclines as recent studies focused on these two classes of molecules and will summarize what is known about the anti-phage defense properties of these small molecules (Kever et al., 2022; Kronheim et al., 2018).

1.3.1 Aminoglycoside mediated anti-phage defense

One of the two main classes of small molecules described to exert anti-phage activity is the class of aminoglycoside antibiotics which are produced by bacteria of the genera *Streptomyces* and *Micromonospora* (Forge & Schacht, 2000). Aminoglycosides are translation inhibiting antibiotics targeting the 16S rRNA of the small ribosomal subunit, leading to a blockage of translation or mistranslation and subsequently to cell death (Bruni & Kralj, 2020; Forge & Schacht, 2000). Aminoglycosides have a structure consisting of three to four cyclitol rings and five- or six-membered sugars which are linked via glycosidic bonds. The hallmark of aminoglycosides are the attached amino groups to the various rings of the structure (see Figure 19B), as well as hydroxyl groups which allow for high water solubility (Forge & Schacht, 2000). Aminoglycosides have been reported by multiple researchers to possess anti-phage properties (Jiang et al., 2020; Kever et al., 2022; Zuo et al., 2021). For example, apramycin has been shown to efficiently block the infection of dsDNA phages during the early stages of the infection process (Kever et al., 2022) (Figure 5). This effect has been observed not only in ecologically closely related phage-host pairs but also across different genera of phage-host systems, highlighting its broad-spectrum potential in interfering with phage infection dynamics (Kever et al., 2022). The mechanism of action for this anti-phage defense has been narrowed down to a specific stage of infection occurring after the phage genome is injected into the host cell but likely before genome replication begins (Kever et al., 2022)(see Figure 5). Evidence for this was provided by Kever and colleagues, who demonstrated a significant reduction in phage titer in the presence of apramycin. This reduction coincided with potassium efflux, suggesting active genome injection by the phage, yet no subsequent DNA replication was detectable (Kever et al., 2022). Interestingly, this effect was not limited to experiments using the purified apramycin compound. Similar results were observed when spent medium from the apramycin-producing organism, *Streptoalloteichus tenebrarius*, was used (Kever et al., 2022). These findings highlight the physiological relevance and potential multi-functionality of apramycin, reinforcing its potential as a natural anti-phage defense mechanism that operates at the community level (Kever et al., 2022). However, the exact molecular mechanism of action remains to be determined.

1.3.2 Anthracycline mediated anti-phage defense

Anthracyclines, the second class of molecules that have been described to have anti-phage defense potential, are natural products of different *Streptomyces* species and are especially known for their anti-cancer potential (Barka et al., 2016; Hardy et al., 2023; Stutzman-Engwall & Hutchinson, 1989; Tse & Boger, 2004). Anthracyclines are type II aromatic polyketides which have an aglycone scaffold with additional sugar residues and are known to intercalate into DNA and inhibit the topoisomerase II, thereby leading to physical distortion of DNA (Tse & Boger, 2004). Kronheim and colleagues could show that daunorubicin and doxorubicin, two anthracyclines produced by *Streptomyces peucetius,* show a broad anti-phage effect on several dsDNA phages spanning a host range from *E. coli, Pseudomonas aeruginosa* to *Streptomyces coelicolor* (Kronheim et al., 2018). Similar to the work of Kever and colleagues, Kronheim et al. could show that daunorubicin acts on a step of phage infection after the genome injection but prior to DNA replication, leading to the general hypothesis of an early blockage of the lytic phage lifecycle (Kever et al., 2022; Kronheim et al., 2018) (see Figure 5). It was also shown for daunorubicin that neither the morphotype of the phage, nor the phage lifestyle were conditional for the efficiency of daunorubicin, as both virulent and temperate phages are inhibited by
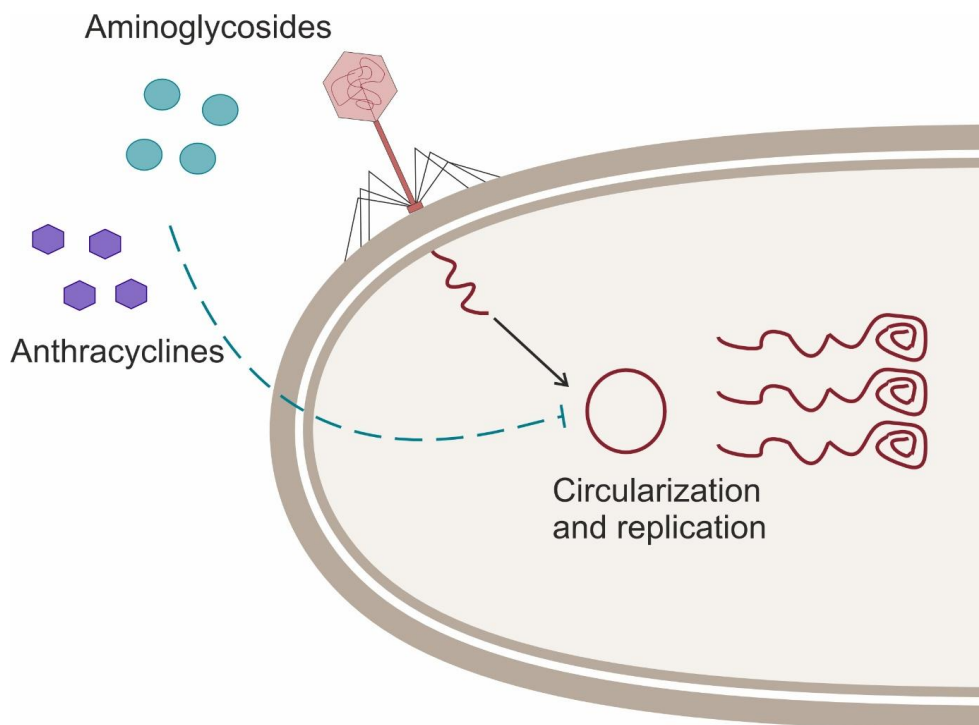
Figure 5: General hypothesis of anti-phage defense conducted by small molecules. Inhibition of phage infection by anthracyclines (purple) and aminoglycosides (turquoise) likely occurs after injection of the phage genome but previous to DNA replication. One possible step of interference could be the phage genome circularization, which is the eminent step after genome injection. Design of the Figure was inspired by Hardy, Kever & Frunzke 2023

the small molecule as well as all morphotypes of the *Caudoviricetes* (Kronheim et al., 2018)*.* Nevertheless, similar to the work of Kever and colleagues, the specific molecular mechanism of phage inhibition by daunorubicin or anthracyclines in general remains elusive (Kronheim et al., 2018).

1.4 *Streptomyces* species and their specialized metabolism

Streptomyces is a genus of Gram-positive bacteria within the phylum Actinomycetota, renowned for their complex multicellular development and prolific specialized metabolism (Zambri, Williams, & Elliot, 2022). These bacteria exhibit a multicellular lifestyle, forming intricate networks of branching hyphae that resemble fungal mycelia (Figure 6). This distinctive morphological development enables them to thrive in diverse soil environments, where they play a vital role in organic matter decomposition and nutrient cycling (Zambri et al., 2022). One striking feature of *Streptomyces* is their expansive genomes, which are among the largest in the bacterial domain, often exceeding 8–10 Mb (Gomez-Escribano et al., 2021). These genomes are highly GC-rich (~70 %) and packed with biosynthetic gene clusters (BGCs) encoding a wide variety of specialized metabolites. These compounds include antibiotics, antifungals, antitumor agents, and other bioactive small molecules (Barka et al., 2016). The production capacity of *Streptomyces* species make them an important work horses in biotechnology. Approximately 70 % of all naturally produced antibiotics stem from *Streptomyces*, emphasising the clinical and biotechnological relevance (Bibb, 2013). *Streptomyces* genomes typically harbour at least 20–40 BGCs, showcasing their unparalleled biosynthetic potential (Baltz, 1998). Advances in genome sequencing and transcriptomic analysis have revealed that many of these clusters remain "cryptic" and are not expressed under standard laboratory conditions, representing a vast reservoir of unexplored chemical diversity (Barka et al., 2016). The small molecules produced by *Streptomyces* serve as a sophisticated arsenal of defense mechanisms, allowing them to outcompete microbial rivals and resist environmental pressures (Zambri et al., 2022). These compounds also protect against bacteriophages, which are a major threat to bacterial populations (Hardy et al., 2023). Two important model organism for the multicellular development and specialised metabolism of *Streptomyces* are *Streptomyces coelicolor* and *Streptomyces venezuelae* (Gomez-Escribano & Bibb, 2011; Gomez-Escribano et al., 2021; Kieser, Bibb, Buttner, Charter, & Hopwood, 2000), which are used throughout this work to investigate phage infection dynamics in *Streptomyces.* The following chapter will delve deeper into the significance of *Streptomyces* as producers of bioactive small molecules, particularly in the context of phage infection.

1.4.1 Complex specialized metabolism as key to chemical defense

As sessile, soil-dwelling organisms, *Streptomyces* rely on alternative strategies to protect themselves from competing microorganisms, as locomotion-based avoidance is not feasible (Zambri et al., 2022). The soil represents one of the most diverse and densely populated environments, characterized by its

highly structured spatial organization (Fierer, 2017). In this environment, spatial movement is heavily restricted, and competition for nutrients, space, and protection is exceptionally intense (Fierer, 2017). *Streptomyces* species are equipped with several BGC's for the expression of various bioactive specialized metabolites, enabling them to thrive in this highly competitive environment (Zambri et al., 2022). The regulation of small molecule production is tightly coupled to the developmental stages of *Streptomyces.* The production of specialized metabolites coincides with the onset of aerial hyphae formation and is followed by programmed cell death of parts of the mycelium to provide nutrients for the offspring cells (Bibb, 2013; Luthe et al., 2023a) (Figure 6). Typically, producer strains are resistant to the compounds they produce to avoid self-toxicity, which is fundamental for the small molecules to confer protection not only against competing bacteria but also against phages. This leads to the decoupling of the anti-bacterial and anti-phage properties of a compound through presence of a resistance cassette, which is key to the anti-phage defense mediated by aminoglycosides in particular (Hardy et al., 2023; Kever et al., 2022; Kever et al., 2024).
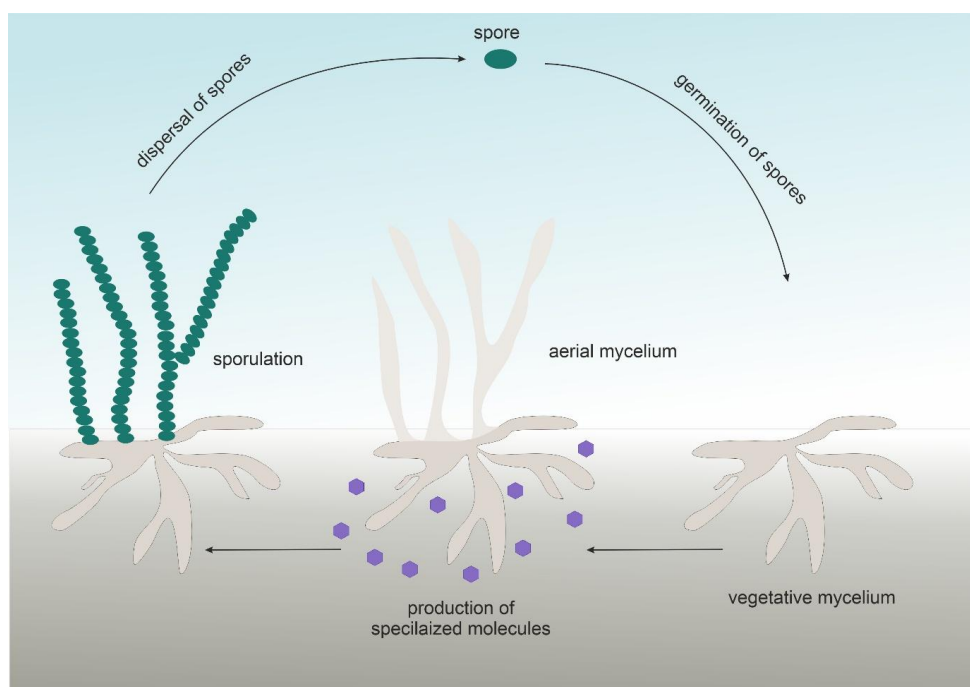
Figure 6: Schematic representation of *Streptomyces* developmental stages in the multicellular lifestyle of the actinomycetes. Upon the encounter of favourable conditions, the *Streptomyces* lifecycle starts with the germination of a single spore. The germinated spore grows into a highly branched vegetative mycelium which expands by tip extension and has connected compartments often harbouring more than one genome. Programmed cell death of the old vegetative mycelium precedes the erection of unbranched aerial hyphae upon nutrient depletion or stress condition, which coincides with the onset of specialized molecule production. Aerial hyphae are highly hydrophobic and grow out of the soil into the air. From aerial hyphae unigenomic spore chains are formed by the formation of cell walls and mature spores are further dispersed through air. Design of the Figure was inspired by Zacharia et al. 2021

1.4.2 *Streptomyces* interaction with bacteriophages

In the last couple of years extensive efforts were made in isolating and describing new phages infecting Actinobacteria, e.g. with School or Bachelor courses such as the Science Education Alliance- Phage Hunters Advancing Genomics and Evolutionary Sciences (SEA-PHAGES) (Hatfull, 2015) or the school outreach program of the SPP2330 (Going Viral) (Erdrich et al., 2024). These efforts led to about 5380 available sequenced phage genomes available on an Actinobacteriophage database (phagesdb.org, January 2025) infecting 14 different Actinobacteria genera. These phages are great tools to investigate how phage infection can act as potential trigger for the specialized metabolism in *Streptomyces,* how developmental programmes in the multicellular organisms are altered upon infection and how multicellular organism defend themselves against phage infection in a greater sense (Luthe et al., 2023b). Multiple phages infecting various *Streptomyces* species have been isolated, characterized and described in detail. Different phenotypic changes in the infected host upon infection could be observed, which are due to the multicellularity of Streptomyces as well as their prolific specialized metabolism. This cannot be observed in unicellular organisms such as *E. coli, Bacillus subtilis* or other well-studied model organism (Hardy, Sharma, Kever, & Frunzke, 2020; Kever et al., 2022; Kronheim et al., 2023; Luthe et al., 2023a; Ongenae et al., 2022a; Ongenae et al., 2023; Ongenae et al., 2022b; Rackow et al., 2024). One such phenotypic alteration upon phage infection is the increased secretion of specialized metabolites in the lysis zone of the phage, particularly described for *S. coelicolor*. This strain was shown to produce the colourful metabolites actinorhodin and undecylprodigiosine after being infected by different phages (Figure 7) (Hardy et al., 2020; Kronheim et al., 2023; Rackow et al., 2024). Specialised metabolites as anti-phage defense has already been described in this work and must be present previous to the infection of the respective phage to confer protection. However, the increased secretion of metabolites after the phage infection might protect yet uninfected neighbouring cells (Kronheim et al., 2023). Another striking reaction to phage infection was observed in *S. venezuelae*, *Streptomyces griseus* and *S. coelicolor,* which showed increased sporulation around the plaque interface of phage infection as containment strategy of the phage infection (Figure 7) (Luthe et al., 2023a). Changes in the development of *Streptomyces* upon phage infection are to be expected, as several known *Streptomyces* phages encode developmental genes within their genomes, such as *whiB* or *whiB*-like genes (Sharma, Hardy, Luthe, & Frunzke, 2021). The presence of these genes strongly suggests that phages have the potential to disrupt or manipulate *Streptomyces* development during the course of infection (Luthe et al., 2023a). Furthermore, the developmental stage of the *Streptomyces* host during the encounter of the phage infection seems to play a crucial role for the infection efficiency, as older mycelium is much more resistant to phage infection compared to germinating spores or young mycelium which seems to be very sensitive to phage infection (Luthe et

al., 2023a; Luthe et al., 2023b). Lastly, as Gram-positive bacteria, *Streptomyces* possess a thick cell wall, which plays a crucial role in both the adsorption of phages and their egress mechanisms (Ongenae et al., 2022b). Interestingly, one described defense strategy involves the conversion of *Streptomyces* into a cell-wall-deficient state, which was shown to still be viable in osmoprotective environments (Ongenae et al., 2022b). This reversible cell wall shedding significantly reduces phage progeny, thereby providing protection to the host population (Ongenae et al., 2022b). Important to notice is that the immune system of actinobacteria, *Streptomyces spp*. in particular, has a unique make up. Usually frequent systems being rare or absent and normally rare systems being enriched in the genome of the hosts, especially in comparison to proteobacteria (Georjon, Tesson, Shomar, & Bernheim, 2023). The genetic structure of *Streptomyces* enhances this unique feature, since core defense systems such as RM systems are encoded near the genomic core region whereas other systems (e.g. Wadjet) tend to be encoded in the extremities of the *Streptomyces* genome which are prone to HGT (Georjon et al., 2023).
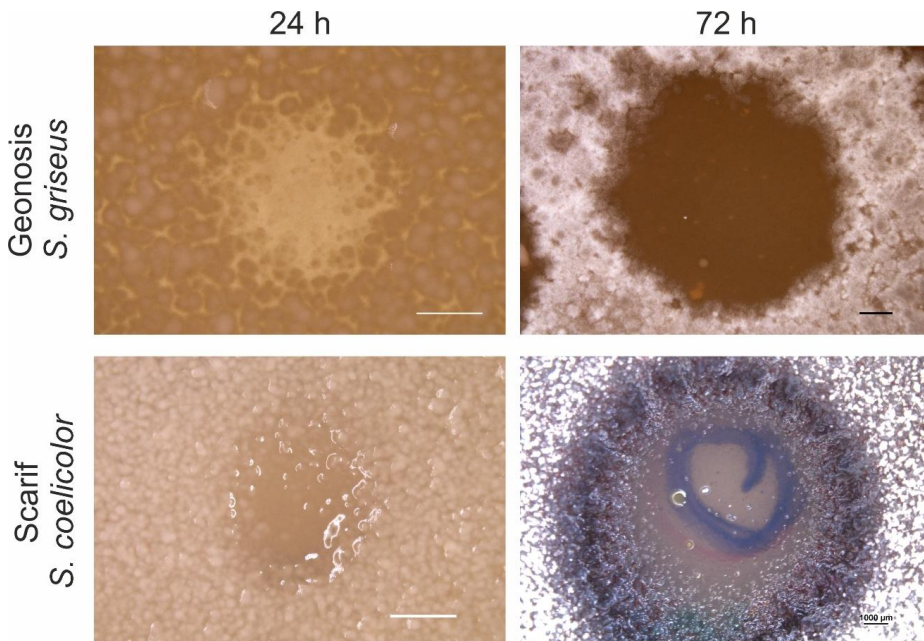
Figure 7: Representative images of development and small molecule production as reaction to phage infection. Two main reactions of *Streptomyces spp*. to phage infection are shown here. On the top with phage Geonosis infecting *S. griseus* enhanced sporulation around the plaque interface 72 hours post infection can be observed. In the bottom row the onset of small molecule production around the plaque interface 72 post infection of Scarif infecting *S. coelicolor* is shown. Molecules which are likely produced here are actinorhodin and undecylprodigiosin, which are known compounds of *S. coelicolor*. The scale bar is 1000 μM, images were taken with the Stereomicroscope.

1.4.3 Integration of small molecule mediated anti-phage defense into the bacterial immune system

Taking all this into account when it comes to phage infection, anti-phage defense mediated by small molecules is a largely understudied topic (Hardy et al., 2023). Given the diversity of phages found in

1. Introduction

the soil and the quantity of small molecules produced by soil dwelling organisms such as *Streptomyces*, it is not surprising that the interaction between phage and host is affected by those small molecules (Clokie, 2011; Zambri et al., 2022). It is important to investigate the role of specialized metabolites in the context of anti-phage defense on both the single-cell level as well as in the context of microbial community interactions in order to integrate the chemical defense into the bacterial immune system (Georjon & Bernheim, 2023). Molecules such as aminoglycosides and anthracyclines show a strong anti-phage potential, hinting towards a yet unknown connection of the specialized metabolism and phage infection. This underlines the ecological relevance of these molecules (Hardy et al., 2023). In contrast to protein or RNA based anti-phage defense systems, protection by secreted small molecules spans both a greater physical range as well as range of phages that are inhibited by those small molecules (Hardy et al., 2023; Luthe et al., 2023b). Therefore, chemical defense adds an additional layer of defense to the network of phage-host interactions (Hardy et al., 2023). In this context, the distribution of antibiotic resistance cassettes via HGT within a population of bacteria strengthens the community wide protection from phage infection mediated by small molecules (Barka et al., 2016; Kever et al., 2024). This not only allows multicellular organisms such as *Streptomyces* to protect offspring spores and young mycelium through division of labour but adds another defense system into the bacterial pan-immune system (Hardy et al., 2023; Zambri et al., 2022)

1.5 Objectives

The general aim of this work is to elucidate anti-phage strategies in *Streptomyces* species with a focus on small molecule mediated anti-phage defense. Investigating and understanding of small molecule mediated anti-phage defense is a crucial step to integrate chemical defense into the context of bacterial immunity.

1. Investigating the anti-phage defense potential of spent media from natural aminoglycoside producing *Streptomyces* strains to understand the ecological relevance of small molecule production in the context of phage infection. The model system *S. venezuelae* and its phage Alderaan were utilized to assess the influence of naturally produced aminoglycosides on phage infection dynamics.

2. Isolation and characterization of novel *Streptomyces* phages to broaden the set of phages that was tested in regard to chemical defense. Increasing diversity of phages that are fully characterized will further deepen the understanding in genomic determinants that might render phages susceptible to small molecules.

3. Screening approaches of known anti-phage small molecules were performed with two sets of phage collections in order to identify pattern of resistance and sensitivity including the identification of sensitivity determinants of the respective phage genomes. 16 *Streptomyces* phages infecting four different species were screened as ecologically closely relevant organisms. Additionally, the BASEL collection as a broad collection of phages infecting the same *E. coli* host, was used for systematic screening approaches as it is important to connect phenotypic observations only to the tested small molecule without interference of host specific factors.

4. Investigation of the effect of daunorubicin as anti-phage small molecule in *E. coli* and the coliphages, as the broadest range of anti-phage defense was observed. Focusing on the mechanism of action of daunorubicin mediated anti-phage defense, experiments were conducted that determine what happens on a molecular level between the compound and the phage infection. Interaction of small molecules with intracellular defense systems and different host backgrounds are of high interest in this work.

1. Introduction

2. Material and Methods

2.1 Materials, equipment and chemicals

All materials, chemicals and laboratory equipment that cannot be considered standard technical equipment or chemical will be specified accordingly in the material and methods section.

2.1.1 Media and antibiotics

Table 1: Media and buffers used in this work

Medium	Component	Concentration
LB medium	Tryptone	10 g/L
	NaCl	10 g/L
	Yeast extract	5 g/L
LB-Agar	Agar	15 g/L
LB-soft Agar	Agar	4 g/L
GYM	Glucose	4 g/L
	Yeast extract	4 g/L
	Malt extract	10 g/L
GYM-Agar	$CaCO_3$	2 g/L
	Agar	15 g/L
GYM-soft Agar	Agar	4 g/L
YEME	Yeast extract	3 g/L
	Malt extract	3 g/L
	Peptone	5 g/L
	Glucose	10 g/L
	Sucrose	340 g/L
YEME-Agar	Agar	15 g/L
SFM-Agar	Mannitol	20 g/L
	Soy flour	20 g/L
	Agar	20 g/L
BHI	Difco^{TM} Brain Heart infusion	37 g/L
BHI-Agar	Agar	15 g/L
TSBY medium	Tryptone soy broth	30 g/L
	Yeast extract	5 g/L
MM medium *(Streptomyces)*	$(NH_4)_2SO_4$	1 g/L
	K_2HPO_4	0.5 g/L
	$MgSO_4 \times 7 H_2O$	0.2 g/L
	$FeSO_4 \times 7 H_2O$	0.01 g/L
	Glucose	10 g/L
2X-YT medium	Tryptone	16 g/L
	Yeast extract	10 g/L
	NaCl	5 g/L
SM-Buffer	Tris-HCl (pH 7.5)	50 mM
	NaCl	100 mM
	$MgSO_4 \times 7 H_2O$	8 mM
TM-Buffer	Tris-HCl (pH 7.5)	50 mM
	$MgCl_2 \times 6 H_2O$	10 mM
PBS-Buffer	NaCl	8 g/L
	KCl	0.2 g/L

	Na$_2$HPO$_4$	1.4 g/L
	KH$_2$PO$_4$	0.2 g/L
ITC-buffer	KH$_2$PO$_4$	11.424 g/L
	K$_2$HPO$_4$	4.682 g/L
	pH 7.3	
qPCR lysis buffer	Tris-HCl (pH 7.0)	10 mM
	NaCl	50 mM
TAE buffer	EDTA disodium salt	1 mM
	Tris	40 mM
	Glacial acetic acid	20 mM
TSS (transformation and storage solution)	PEG 8000	5 g
	1 M MgCL$_2$ x 6 H$_2$O	1.5 mL
	DMSO	2.5 mL
	LB medium	Ad 50 mL
		Filter sterilized

Table 2: antibiotics used in this work

Component	Stock solution	Final concentration	Molecule class
Actinomycin D	20 mM in DMSO	Up to 20 µM *E. coli* Up to 6 µM *Streptomyces*	Peptide antibiotic
Ampicillin	100 mg/mL	100 µg/mL *E. coli*	β-lactam
Apramycin	50 mg/mL in H$_2$O	50 µg/mL *E. coli* 25 µg/mL *Streptomyces*	Aminoglycoside
Bleomycin	20 mM in H$_2$O	20 µM	Glycopeptide antibiotic
Carbenicillin	100 mg/mL	100 µg/mL	β-lactam
Chloramphenicol	34 mg/mL in EtOH	34 µg/mL	Nitrobenzole
Daunorubicin	20 mM in DMSO	Up to 40 µM *E. coli* Up to 6 µM *Streptomyces*	Anthracycline
Echinomycin	1 mg/mL in H$_2$O	50 ng/mL	Peptide antibiotic
Hygromycin B	50 mg/mL in H$_2$O	50 µg/mL	Aminoglycoside
Kanamycin	50 mg/mL in H$_2$O	50 µg/mL	Aminoglycoside
Kasugamycin	50 mg/mL in H$_2$O	100 µg/mL	Aminoglycoside
Nalidixic acid	25 mg/mL in 0.3 M NaOH	20 µg/mL	Quinolone antibiotic
Neomycin	50 mg/mL in H$_2$O	50 µg/mL	Aminoglycoside
Paromomycin	300 mg/mL in H$_2$O	300 µg/mL	Aminoglycoside
Puromycin	9.42 mg/mL in HEPES	20 µM	Nucleoside antibiotic
Spectinomycin	100 mg/mL in H$_2$O	100 µg/mL	Aminoglycoside
Streptomycin	100 mg/mL in H$_2$O	100 µg/mL	Aminoglycoside
Tetracycline	12.5 mg/mL in H2O	12.5 µg/mL	Polyketide antibiotic

2. Material and Methods

2.1.2 Bacterial strains, phages, primers and plasmids

Table 3: Bacterial strains used in this work

Strain	Genotype	Reference/source
Corynebacterium glutamicum MB001	ATCC 13032 with deletions of the prophages ΔCGP1, ΔCGP 2, ΔCGP 3	Our lab collection
Escherichia coli B	WT	DSM 613
E. coli K12 BW25113	F⁻ Δ(*araD-araB*)567, Δ*lacZ4787(::rrnB-3)*, λ⁻, *rph-1*, Δ*(rhaD-rhaB)568, hsdR514*	Maffei et al. 2021
E. coli K12 BW25113 Δ9	*E. coli* K12 BW25113 with deletions of all 9 prophages	Wang et al. 2010
E. coli K12 MG1655	F⁻, λ⁻, *ilvG⁻*, *rfb-50 rph-1*	Maffei et al. 2021
E. coli K12 MG1655 ΔRM	*E. coli* K-12 MG1655 Δ*mrr-hsdRMS-mcrBC* Δ*mcrA*	Maffei et al. 2021
E. coli K12 MG1655 ΔRM pEKEx2.a	*E. coli* K12 MG1655 ΔRM carrying the plasmid pEKEx2.a, Kan^R	This work
E. coli K12 MG1655 ΔRM pEKEx2.b	*E. coli* K12 MG1655 ΔRM carrying the plasmid pEKEx2.b, Hyg^R	This work
E. coli K12 MG1655 ΔRM pEKEx2.d	*E. coli* K12 MG1655 ΔRM carrying the plasmid pEKEx2.d, Apr^R	This work
E. coli K12 MG1655 ΔRM pBR322_ΔP*tet*	*E. coli* K12 MG1655 ΔRM carrying the plasmid pBR322_ΔP*tet,* Amp^R	This work
E. coli K12 MG1655 ΔRM pAH213_EcoKI	*E. coli* K12 MG1655 ΔRM carrying the plasmid pAH213_EcoKI, Amp^R	This work
E. coli K12 MG1655 ΔRM pAH213_EcoCFT_I	*E. coli* K12 MG1655 ΔRM carrying the plasmid pAH213_EcoCFT_I, Amp^R	This work
E. coli K12 MG1655 ΔRM pEcoRI	*E. coli* K12 MG1655 ΔRM carrying the plasmid pEcoRI, Amp^R	This work
E. coli K12 MG1655 ΔRM pEcoRV	*E. coli* K12 MG1655 ΔRM carrying the plasmid pEcoRV, Amp^R	This work
E. coli K12 MG1655 ΔRM pAH213_EcoCFT_II	*E. coli* K12 MG1655 ΔRM carrying the plasmid pAH213_EcoCFT_II, Amp^R	This work
E. coli K12 MG1655 ΔRM pAH213_EcoP1_I	*E. coli* K12 MG1655 ΔRM carrying the plasmid pAH213_EcoP1_I, Amp^R	This work
E. coli K12 MG1655 ΔRM pAH213_Fun/Z	*E. coli* K12 MG1655 ΔRM carrying the plasmid pAH213_Fun/Z, Amp^R	This work
E. coli K12 MG1655 ΔRM pAH213_Old	*E. coli* K12 MG1655 ΔRM carrying the plasmid pAH213_Old, Amp^R	This work
E. coli K12 MG1655 ΔRM pAH213_Tin	*E. coli* K12 MG1655 ΔRM carrying the plasmid pAH213_Tin, Amp^R	This work
E. coli K12 MG1655 ΔRM pTU175_retron_Eco1_p-nativ	*E. coli* K12 MG1655 ΔRM carrying the plasmid pTU175_retron_Eco1_p-nativ, Sp^R	This work
E. coli K12 MG1655 ΔRM pTU175_retron_Eco6_p-nativ	*E. coli* K12 MG1655 ΔRM carrying the plasmid pTU175_retron_Eco6_p-nativ, Sp^R	This work
E. coli LE392	WT	DSM 4230
E. coli DH5α	F⁻ φ80*lacZ*ΔM15 Δ(*lacZYA-argF*)U169 *recA1 endA1 hsdR17(rₖ⁻, mₖ⁺) phoA supE44 λ⁻thi-1 gyrA96 relA1*	Invitrogen
E. coli BL21	F⁻*ompT hsdS_B (r_B⁻, m_B⁻) gal dcm*	NEB

2. Material and Methods

E. coli BL21 (DE3)	F⁻*ompT hsd*S_B (r_B⁻, m_B⁻) *gal dcm* (DE3)	NEB
E. coli BL21 (DE3) pET28a_NgTET	*E. coli* BL21 (DE3) carrying the pET28a_NgTET plasmid expressing the TET enzyme, Kan^R	Pozhydaieva et al. 2024
E. coli BL21 (DE3) pET28a_NgTET_D234A	*E. coli* BL21 (DE3) carrying the pET28a_NgTET_D234A plasmid expressing the inactive TET enzyme, Kan^R	Pozhydaieva et al. 2024
E. coli ET12567 (pUZ8002)	F⁻ *dam⁻13::Tn9 dcm⁻6 hsdM hsdR zjj-202::Tn10 recF143 galK2 galT22 ara-14 lacY1 xyl-5 leuB6 thi-1 tonA31 rpsL136 hisG4 tsx-78 mtl-1 glnV44*	MacNeil et al. 1992
Streptomyces coelicolor A2(3)	WT	Bentley et al., 2002
S. coelicolor A2(3) M145	WT lacking plasmids SCP1 and SCP2	DSM 112524
S. coelicolor A2(3) M145 pIJLK01	*S. coelicolor* A2(3) M145 carrying the plasmid pIJLK01 conferring Hygromycin resistance	Kever et al. 2022
S. coelicolor A2(3) M145 pIJLK04	*S. coelicolor* A2(3) M145 carrying the plasmid pIJLK04 conferring Apramycin resistance	Kever et al. 2022
S. coelicolor A2(3) M145 pIJLK05	*S. coelicolor* A2(3) M145 carrying the plasmid pIJLK05 conferring Spectinomycin resistance	Kever et al. 2022
Streptomyces fradiae	WT	DSM 40063
Streptomyces griseus	WT	DSM 40236
S. griseus pIJLK02	*S. griseus* carrying the plasmid pIJLK02 conferring Kanamycin resistance	This work
S. griseus pIJLK04	*S. griseus* carrying the plasmid pIJLK04 conferring Apramycin resistance	This work
Streptomyces hygroscopicus	WT	DSM 40578
Streptomyces kanamyceticus	WT	DSM 40500
Streptomyces kasugaensis	WT	DSM 40819
S. kasuagensis pIJLK02	*S. kasugaensis* carrying the plasmid pIJLK02 conferring Kanamycin resistance	This work
Streptomyces olivaceus	WT	DSM 41536
S. olivaceus pIJLK04	*S. olivaceus* carrying the plasmid pIJLK04 conferring Apramycin resistance	This work
Streptomyces rimosus	WT	DSM 40260
Streptomyces venezuelae NRRL B-65442	WT	DSM 112328
S. venezuelae NRRL B-65442 pIJLK01	*S. venezuelae* NRRL B-65442 carrying the plasmid pIJLK01 conferring Hygromycin resistance	This work
S. venezuelae NRRL B-65442 pIJLK02	*S. venezuelae* NRRL B-65442 carrying the plasmid pIJLK02 conferring Kanamycin resistance	This work
S. venezuelae NRRL B-65442 pIJLK04	*S. venezuelae* NRRL B-65442 carrying the plasmid pIJLK04 conferring Apramycin resistance	This work

2. Material and Methods

S. venezuelae NRRL B-65442 pIJLK05	*S. venezuelae* NRRL B-65442 carrying the plasmid pIJLK05 conferring Spectinomycin resistance	This work
Streptoalloteichus tenebrarius	WT	DSM 40477
S. tenebrarius ΔaprP	Deletion of *aprP*	Zhang et al. 2021
S. tenebrarius ΔaprQ	Deletion of *aprQ*	Zhang et al. 2021
S. tenebrarius ΔaprU	Deletion of *aprU*	Zhang et al. 2021
S. tenebrarius ΔaprZ	Deletion of *aprZ*	Zhang et al. 2021

Table 4: Phages used in this work

Phage	Host organism	lifestyle	Family	Genus	Genome	Reference
Streptomyces spp. phages						
Abafar	*S. coelicolor*	virulent	*Beephvirinae*	*Manuelvirus*	Linear dsDNA	Rackow et al. 2024
Alderaan	*S. venezuelae*	virulent		*Austintatiousvirus*	Linear dsDNA	Hardy et al. 2020
Ankus	*S. griseus*	virulent	*Stanwilliamsviridae*		Linear dsDNA	Erdrich et al. 2024
Coruscant	*S. venezuelae*	virulent	*Stanwilliamsviridae*	*Coruscantvirus*	Linear dsDNA	Hardy et al. 2020
Dagobah	*S. coelicolor*	temperate		unclassified	Linear dsDNA	Hardy et al. 2020
DekoNeimoidia	*S. griseus*	virulent	*Stanwilliamsviridae*		Linear dsDNA	Erdrich et al. 2024
Endor1	*S. coelicolor*	temperate	*Arquatrovirinae*	*Camvirus*	Linear dsDNA	Hardy et al. 2020
Endor2	*S. coelicolor*	temperate	*Arquatrovirinae*	*Camvirus*	Linear dsDNA	Hardy et al. 2020
Geonosis	*S. griseus*	virulent		*Woodruffvirus*	Linear dsDNA	Rackow et al. 2024
Kamino	*S. kasugaensis*	temperate	*Arquatrovirinae*	*Camvirus*	Linear dsDNA	Rackow et al. 2024
Mandalore	*S. venezuelae*	virulent	*Stanwilliamsviridae*	*Coruscantvirus*	Linear dsDNA	Erdrich et al. 2024
ΦA. Streptomycini III	*S. griseus*	virulent		unclassified	Linear dsDNA	Prauser & Köhler 1965
Φ8238	*S. olivaceus*	temperate		unclassified	Linear dsDNA	DSM 49154
P26	*S. griseus*	virulent		unclassified	Linear dsDNA	Korn et al. 1978
S7	*S. olivaceus*	unknown		unclassified	Linear dsDNA	Prauser 1976
Scarif	*S. coelicolor*	virulent		*Scarifvirus*	Linear dsDNA	Rackow et al. 2024
SV1	*S. venezuelae*	temperate		*Picardvirus*	Linear dsDNA	Smith et al. 2013
Corynebacterium glutamicum phages						

CL31	*C. glutamicum* MB001	temperate		unclassified		Yeh et al. 1985
Escherichia coli phages						
λ	*E. coli* LE392	temperate		*Lambdavirus*	Linear dsDNA	DSM 4499
T4	*E. coli* B	virulent	*Straboviridae*	*Tequatrovirus*	Linear dsDNA	DSM 4505
T4 Δα/β GT	Phage T4 with a deletion of the alpha and beta glycosyltransferase gifted by Marianne De-Paepe					
T5	*E. coli* B	virulent	*Demerecviridae*	*Tequintavirus*	Linear dsDNA	DSM 16353
T6	*E. coli* B	virulent	*Straboviridae*	*Tequatrovirus*	Linear dsDNA	DSM 4622
T7	*E. coli* B	virulent	*Autographviridae*	*Teseptimavirus*	Linear dsDNA	DSM 4623
BASEL collection (69 phages)	*E. coli* MG1655 ΔRM	virulent	See publication			Maffei et al. 2021

Table 5: Primer used in this work.

Nr	Name	Sequence	Function
1	pBR322_insert_seq_fw	AAAATAGGCGTATCACGAGG	Sequencing pBR322 plasmid
2	pBR322_insert_seq_rev	CTCACAACGTTCCAGTAACC	Sequencing pBR322 plasmid
3	T4_alphaGT_fw	GTTTGGGCCTATTCGTAGCG	Check deletions
4	T4_alphaGT_rev	ACGCCTAAATGCCAATCACC	Check deletions
5	T4_betaGT_fw	GCCAGTATAAAGCAGGTTCC	Check deletions
6	T4_betaGT_rev	TCAACTGCTATTCGATGAAC	Check deletions
7	S288_T4_qPCR_fw	AAGCTACTGCTCTACCAGCTGGTATTG	qPCR T4 target gene T4p168
8	S289_T4_qPCR_rv	CGCAGCAATGCTTTGCCAATCAAC	
9	S292_Ecoli qPCR_fw	ACGGAATTTCTCAGCCATGGTCAGAC	qPCR *atpD* housekeeping gene of BL21
10	S293_Ecoli qPCR_rv	GTGTTTGCGGGCGTAGGTGAAC	
11	S177_CL31_clg56_fw	TTGCGGAAGGTCTCGGCA	qPCR CL31 target gene clg56
12	S178_CL31_clg56_rv	AAGTTGGAGCAAGGTCACCG	

Table 6: Plasmids used in this work

Plasmids	Characteristics	Reference
pIJ10257	Hyg[R], integrative plasmid in *Streptomyces,* Cloning vector for conjugal transfer from *E. coli* to *Streptomyces spp.*, constitutive promotor *ermE*, Integration site ΦBTI	Hong et al. 2005
pIJLK01	Hyg[R], derivative of pIJ10257 with additional restriction sites Bst11071 (upstream) and StuI (downstream) of the *aph(7")-Ia* gene allowing exchanging of the antibiotic cassette	Kever et al. 2022
pIJLK02	Kan[R], Derivative of pIJLK01 with *aph(7")-Ia* exchanged for *aphAI* (kanamycin resistance gene)	Kever et al. 2022
pIJLK03	Kasugamycin[R], Derivative of pIJLK01 with *aph(7")-Ia* exchanged for *kac338* (kasugamycin resistance gene)	Kever et al. 2022
pIJLK04	Apr[R], Derivative of pIJLK01 with *aph(7")-Ia* exchanged for *aac(3)IV* (apramycin resistance gene)	Kever et al. 2022
pIJLK05	Sp[R]/Sm[R], Derivative of pIJLK01 with *aph(7")-Ia* exchanged for *aadA* (spectinomycin/streptomycin resistance gene)	Kever et al. 2022
pEKEx2	Kan[R], *C. glutamicum/ E. coli* shuttle vector, P_{tac}, *lacI^q*, pBLI, oriV$_{C.g.}$, pUC18 oriV$_{E.c.}$	Kever et al. 2022
pEKEx2a	Kan[R], derivative of pEKEx2 with additional restriction sites Bst1107I (up-) and NotI (downstream) of the *aphAI* gene, allowing exchange of the antibiotic cassette	Kever et al. 2022
pEKEx2b	Hyg[R], derivative of pEKEx2a, with *aphAI* exchanged for *aph(7")-Ia* (hygromycin resistance gene)	Kever et al. 2022
pEKEx2d	Apr[R], derivative of pEKEx2a, with *aphAI* exchanged for *aac(3)IV* (apramycin resistance gene)	Kever et al. 2022
pUZ8002	Kan[R], RK2 derivative with nontransmissible oriT	Paget et al. 1999
pET28a	Kan[R], expression plasmid with inducible T7 lac promotor, His-Tag	Novagen
pET28a_NgTET	Kan[R], expression of His-tagged NgTET, IPTG inducible	Pozhydaieva et al. 2024
pET28a_NgTET_D234A	Kan[R], expression of His-tagged inactive mutant NgTET_D234A, IPTG inducible	Pozhydaieva et al. 2024
pBR322	Amp[R], Tet[R], oriV, multipurpose cloning vector for *E. coli*	Bolivar et al. 1977
pBR322_ΔP*tet*	Amp[R], Derivative of pBR322, tetracycline resistance cassette deleted, empty vector control	Pleska et al 2016
pAH213_EcoKI	Amp[R], derivative of pBR322 expressing *E. coli* Type I RM system EcoKI of *E. coli* K12	Maffei et al. 2021
pAH213_EcoCFT_I	Amp[R], derivative of pBR322 expressing *E. coli* Type I RM system EcoCFT_I of *E. coli* CFT073	Maffei et al. 2021

pEcoRI	Amp^R, derivative of pBR322 expressing *E. coli* Type II RM system EcoRI	Maffei et al. 2021
pEcoRV	Amp^R, derivative of pBR322 expressing *E. coli* Type II RM system EcoRV	Maffei et al. 2021
pAH213_EcoCFT_II	Amp^R, derivative of pBR322 expressing *E. coli* Type III RM system EcoCFT_II of *E. coli* CFT073	Maffei et al. 2021
pAH213_EcoP1_I	Amp^R, derivative of pBR322 expressing *E. coli* Type III RM system EcoP1_I of *E. coli* phage P1	Maffei et al. 2021
pAH213_Fun/Z	Amp^R, derivative of pBR322 expressing the Fun/Z Abi system of *E. coli* phage P2	Maffei et al. 2021
pAH213_Old	Amp^R, derivative of pBR322 expressing the Old Abi system of *E. coli* phage P2	Maffei et al. 2021
pAH213_Tin	Amp^R, derivative of pBR322 expressing the Tin Abi system of *E. coli* phage P2	Maffei et al. 2021
pTU175_retron_Eco1_p-native	Sp^R, low copy plasmid with pSC101 origin of replication, expression of retron system Ec86 (Eco1) under native promotor and downstream of an arabinose inducible promotor	Millman et al. 2020
pTU175_retron_Eco6_p-native	Sp^R, low copy plasmid with pSC101 origin of replication, expression of retron system Ec48 (Eco6) under native promotor and downstream of an arabinose inducible promotor	Millman et al. 2020

2.2 Bacterial strains and growth conditions

2.2.1 *Streptomyces* growth conditions

Streptomyces liquid cultures were inoculated with spores which were stored at -20 °C in 20 glycerol. *S. coelicolor M145* (Bentley et al., 2002)*, S. griseus, S. kasugaensis* and all variants of those strains were cultivated in YEME medium overnight at 30 °C and 200 rpm. All remaining *Streptomyces* strains were cultivated in GYM medium at the same growth conditions. If required antibiotics were added to the medium with the indicated concentration (Table 2). On solid medium, all *Streptomyces* strains were grown on GYM agar supplemented with the respective antibiotic.

2.2.2 *Streptomyces* spore preparation

Streptomyces species have a complex lifecycle and the spores from this lifecycle are the most convenient form for long-term storage of the strains. Therefore 100 µL of overnight culture of each strain was plated on SFM agar and incubated for 5-7 days at 30 °C. Afterwards the grown bacterial lawn showed the phenotype of sporulation where the surface of the lawn is hydrophobic, and the spores produce the respective pigment, in case of *S. venezuelae* e.g. green. Once this phenotype was observed the plate was flooded with 5 mL sterile ddH$_2$O and the surface was scrubbed with a sterile cotton swab. The liquid was then transferred into a syringe containing sterile cotton and filtered through the cotton to omit big chunks of mycelium. The liquid containing the spores was then

centrifuged for 5 min at 5000 x g, the supernatant discarded and the spores re-suspended in 500 µL 20% glycerol and stored at -20 °C until further usage.

2.2.3 *E. coli* growth conditions

All *E. coli* cultures were grown in LB medium, containing the respective antibiotic in the concentration as described in Table 2. *E. coli* cultures were incubated at 37 °C and 200 rpm. Overnight cultures were inoculated from single colonies which were freshly streaked out on LB agar plates containing the respective antibiotic and incubated overnight at 37 °C.

2.2.4 Micro-cultivation devices

The micro cultivation device that was used in this work was for one the BioLector from Beckmann Coulter (Indianapolis, USA), which is measuring bacterial growth as backscatter. In the BioLector, mainly *Streptomyces* growth experiments were conducted at 30 °C and 1200 rpm shaking frequency. Growth experiments as well as phage infection experiments (described in detail in section 2.3.5) were performed in biological triplicates in 48-well flower plates and the Backscatter light intensity was measured every 15 min over the course of 24 hours (filter module ($e_{xcitation}$/$e_{mission}$, 620 nm/ 620 nm; gain 25). The cultivation was performed in 1 mL of the respective medium and for each individual *Streptomyces* strain with a starting OD_{450} of 0.15. For the cultivation of *E. coli* in the BioLector the temperature was raised to 37 °C, and the cultures were started in 1 mL LB medium with the respective antibiotic with a starting OD_{600} of 0.15. The shaking frequency remained the same for both cultivations.

E. coli cultivation were performed in the Growth Profiler 960 from EnzyScreen (Heemstede, Netherlands) which the preferred micro cultivation device for bacterial cultures with a low cell density. In this micro cultivation device bacterial growth is monitored by taking images from below the plate and calculating the OD equivalent from the respective pixel count in the green, red or blue light based on a calibration curve. *E. coli* cultivations in the Growth Profiler were conducted in 96 well polystyrene plates with a transparent bottom (EnzyScreen, Heemstede, Netherlands) in 300 µL LB medium containing the respective antibiotic. The cultivation was generally started at an OD_{600} of 0.15 and grown at 37 °C with a shaking frequency of 250 rpm and images were taken every 10 minutes.

2.2.5 Harvesting of spent medium

To harvest the spent medium of the aminoglycoside producing *Streptomyces* strains, pre-cultures were started in 4 mL GYM medium inoculated with 5 µL of the spore stock. After overnight cultivation at 30 °C and 120 rpm the pre-culture was used to inoculate 100 mL GYM medium as main culture, starting at an OD_{450} of 0.1. After 24 h, 48 h, and 72 h 25 mL samples were taken from the culture. The supernatant samples were centrifuged for 10 min at 5000 x g and filtered subsequently through a 0.22 µm membrane filter to separate residual mycelium from the supernatant. The supernatant was

divided into 5 mL aliquots and stored at -20 °C until further usage. During the spent medium sampling time points further 100 µL of culture samples were taken to determine the morphology of the culture using microscopy (see section) and ensure that no contamination occurred during the cultivation process.

2.2.6 Cultivation in spent medium

To test whether the spent medium of aminoglycoside producing strains has an impact on bacterial growth or phage infection, liquid infection assays were performed in the BioLector with the previously described cultivation conditions. Here *S. venezuelae* cultures carrying the respective antibiotic-resistance cassette were started overnight from spore stocks in 4 mL GYM medium supplemented with the respective antibiotic. The main culture was then inoculated into a final volume of 1 mL at a starting OD_{450} of 0.15. The main culture contained 20 % of the spent medium harvested at different time points. To compensate for the lacking nutrients of the spent medium 40 µL 5x GYM medium was added to 660 µL 1x GYM medium and finally 100 µL phage lysate or SM buffer were added to the culture for either the phage infection or the control culture. These cultures were grown for at least 24 h in the BioLector and supernatant samples were taken after 0 h, 2 h, 4 h, 6 h, 8 h and 24 h.

2.3 Phage methods

2.3.1 Phage isolation and propagation

Several *Streptomyces* phages that were used in this study were isolated from environmental soil samples. The soil samples were incubated with SM buffer overnight at 4 °C on a shaking plate to resolve phages from soil particles. After overnight incubation the samples were centrifuged for 30 min at 5000 x g to separate the supernatant from the soil particles. Subsequently the supernatant was filtered through sterile 0.22 µm membrane filters to remove residual bacteria from the supernatant. The supernatant containing phages, the so-called lysate, was then enriched overnight on the bacterial host of interest, here several *Streptomyces* species (see Table S1), to amplify potential phages within the lysate. After overnight incubation, the lysate was again separated from residual bacteria by centrifugation and filtration as described previously and the lysate was subsequently spotted in serial dilutions on to the bacterial lawn (described see section 2.3.3). Plaques were observed after overnight incubation at 30 °C.

To purify the phages, yielding in monoclonal phage lysates, plaques were picked and re-streaked twice on double agar overlays (see Section 2.3.3). For the preparation of high titer stocks phage amplification was performed by mixing 100 µL phage sample with 4 mL soft-agar containing the host strain at an OD_{450} of 0.4 and pouring it on a GYM agar plate to obtain near confluent lysis of the bacterial lawn. After overnight incubation of the plates at 30 °C the bacterial lawn should only show

the residual "spider web" pattern that indicates lysed cells. To resolve the phages from the top agar, the plates were flooded with 5 mL SM-buffer and incubated for 1-2 h at room temperature on a shaking plate at 40 rpm. The SM buffer and top-agar were then collected in 50 mL falcon tubes and centrifuged for 15 min at 5000 x g and subsequently filtered through a 0.22 µm membrane filter, to separate the bacteria from the phage lysate. The lysate was then stored either at 4 °C or mixed with 10 % glycerol and stored at -80 °C for long-term storage. The titer of the phage lysate was determined by spotting serial dilutions up to 10^{-8} of the lysate on a double agar overlay containing the respective bacterial host at an OD_{450} of 0.4. Plaques were counted after overnight incubation at 30 °C and the plaques forming units (PFU) per millilitre were calculated from the highest dilution where plaques were still visible.

2.3.2 Liquid phage infections

To obtain greater volumes of phage lysate for later usage, liquid phage amplifications were carried out. Here, 50-100 mL of LB, GYM or YEME medium were inoculated with the respective bacterial host to an OD_{450} or OD_{600} of 0.15 and the phage lysate was added directly to the culture to an MOI (multiplicity of infection) of 0.1 for *E. coli* phages and a PFU/mL of 10^7 for *Streptomyces* phages. The culture is then incubated for 8-16 hours at 30 °C or 37 °C for *Streptomyces* or *E. coli* phages respectively at 120 rpm. After lysis occurred and the culture turned clear, the phage lysate was harvested by centrifugation for 15 min at 5000 x g and subsequent filtration through a sterile 0.22 µm membrane filter to separate the lysate from remaining bacteria. The phage lysate was then stored at 4 °C until further usage.

2.3.3 Double-agar overlay phage infections

Double-agar overlay phage infections were performed in this study to amplify phages on plates to obtain high-titer phage stocks, to determine the titer of lysates by spotting serial dilutions on the top-agar containing the respective host and to observe the plaque morphology and development over time. The general principle of double-agar overlays is based on layering two different agar-agar concentrations in a petri dish to obtain a solid agar layer in the bottom and a viscous layer on top. The bottom agar contains 1.5 % agar agar and is supplemented with the respective antibiotic if necessary. The top-agar (soft agar) contains 0.4 % agar agar and allows for phage lysis due to the higher fluidity of particles due to lower viscosity. For double agar overlay assays we discriminate spot assays and plaque assays. For spot assays the top-agar, containing respective antibiotics in the same concentrations as the bottom layer, 4 mL on round petri dishes and 10 mL on square petri dishes, is mixed with the respective host culture to an OD_{450} or OD_{600} for *Streptomyces spp.* or *E. coli* respectively of 0.4. The top-agar is then poured on the bottom agar and dried in until the top-agar is solid. 2 µL of serial dilutions of phage lysates are then spotted on top of the top-agar and dried in under the sterile

working bench. Spot assays are generally performed to assess phage titer during experiments or of phage stocks. For plaque assays the phage lysate is directly mixed with the bacterial culture and the top-agar to have a higher resolution of phage titer and to obtain single plaques on the bacterial lawn. For high titer preparation of phage stocks the lysate is added to 10^4 to 10^5 PFU/mL to the top-agar. To obtain single plaques and observe morphology and development of plaques the PFU/mL that is added to the top-agar is decreased to 10^2 to 10^3. The double-agar overlay plates are incubated upside-down at 30 °C or 37 °C for *Streptomyces* or *E. coli* phages respectively for 8 to 16 hours. Plaques and spots are subsequently imaged on a light table and the titer is calculated for the used lysate.

2.3.4 Determining the phage host range

For the newly isolated *Streptomyces* phages the host range was determined by using different *Streptomyces* host strains (see Table S1 & Table S2) in the top-agar layer of spot assays. High-titer phage lysates were then serially diluted and spotted on the different host strains to test the infectivity of the respective phages. In this work it was discriminated between clearance of the bacterial lawn and productive infection, where single plaques could be counted on the lawn. For all productive infections, the efficiency of plating (EOP) was calculated by dividing the counted plaques on a foreign host by the counted plaques on the "original" host, which was used for isolation.

2.3.5 Phage infection dynamics

Investigation of infection dynamics was performed in liquid phage infection experiments. The cultivation of liquid infection experiments was performed in the BioLector for *Streptomyces* phages and in the Growth Profiler for *E. coli* phages.

For *Streptomyces* phage infection dynamics the infection experiment was conducted in 48-well flower plates in the BioLector in biological triplicates under the cultivation conditions described in section 2.2.4. For the phage infection, the bacterial culture was inoculated into GYM or YEME medium, including respective antibiotics or spent medium, at an initial OD_{450} of 0.15, and phage lysate was directly added with initial titers ranging from 10^2 to 10^8 PFU/mL. To not only obtain growth curves but also determine phage amplification, supernatant samples were taken every two hours. This supernatant was centrifuged to separate residual bacteria from the phage lysate and was subsequently serially diluted up to 10^{-8} and spotted on double-agar overlays containing the respective host strains.

E. coli phage infection dynamics were generally monitored in the Growth Profiler, since the resolution of growth for less dense growing organisms is better in the Growth Profiler. Here, 300 µL LB medium supplemented with the respective antibiotic (see Table 2) was inoculated with the *E. coli* strain to an OD_{600} of 0.15 and grown in the cultivation condition as described in section 2.2.4. The culture was

either infected with the respective phage directly or infected after 1 hour of growth in the micro cultivation device. To determine the amplification kinetics of *E. coli* phages, supernatant samples were taken every 20 min over the period of at least 2 hours. These supernatant samples were centrifuged to separate the residual bacteria from the supernatant and were subsequently serially diluted and spotted onto the respective bacterial lawn as describe for spot assays. The amount of phage lysate added to the culture was determined by the MOI that was desired in the experiment.

2.3.6 Pre-incubation assay

To determine stability of phage particles of phage Alderaan, λ and CL31 (Yeh, Oreglia, & Sicard, 1985) in medium or spent medium, pre-incubation assays were conducted. Here 50 µL of phage lysate with a high original titer (10^8 PFU/mL or higher) was incubated for 24 hours in 500 µL fresh medium, medium supplemented with antibiotics or $MgCl_2$ or spent medium from aminoglycoside producer strains in 1 mL micro reaction tubes at 30 °C. Spent media were previously pH adjusted to a pH of 7.5 so that the pH of the spent medium was not the accounting factor. Samples were taken during the incubation period after 0h, 6h and 24 h and subsequently diluted and spotted on the host bacterium to avoid further incubation. The phage titer was then determined after incubating the spot assays overnight at 30 °C or 37 °C for phage Alderaan and CL31 or λ respectively and the $\log_{10}$-fold change to T_0 (time point at 0h) was calculated to determine the phage stability and infectivity.

2.3.7 Clean-up of phages using a sucrose gradient

In order to obtain highly purified phages, devoid of all host DNA or metabolites, the phages were cleaned up using a sucrose gradient centrifugation. Therefore, 70 mL of phage lysate were concentrated in the Optima L-80 XP Ultracentrifuge (Beckmann Coulter, Indianapolis, USA) for 2 hours at 100.000 x g and 4 °C using the fixed angle Type 45 Ti Rotor and the 70 mL polycarbonate bottles from Beckmann Coulter. The phage pellet was subsequently dissolved in 1 mL SM buffer and treated with DNase and RNase for 30 minutes at 37 °C to exclude all host DNA and RNA that might stick to the phage particle. After the enzymatic digestion, the phage lysate was loaded on a sucrose gradient that consisted of each 1 mL 5 %, 22 %, 33 % and 45 % sucrose in TM buffer using UltraClear open-top thin wall centrifugation tubes (Beckmann Coulter, Indianapolis, USA) for the SW 28 swinging rotor (Beckmann Coulter, Indianapolis, USA). The sucrose gradient was subsequently centrifuged for 20 minutes at 70.000 x g and 4 °C to separate the phage particles from other metabolites according to the molecular weight. The phage band in the sucrose gradient was then extracted using a syringe and a needle and transferred into a fresh centrifugation tube. To wash the sucrose from the phage particles the centrifugation tube was filled up to three quarters with SM buffer and again centrifuged in the SW 28 swinging rotor for 1 hour at 70.000 x g and 4 °C to pellet the phage particles. After the

centrifugation the supernatant was discarded and the phage pellet was re-suspended in mL SM buffer and stored at 4 °C until further usage.

2.4 Molecular biological methods

2.4.1 PCR, Gibson assembly and plasmid isolation

To construct the plasmids used in this work, see Table 7, different methods were used, which are introduced in the following section.

2.4.1.1 Isolation of Plasmid DNA

Plasmid DNA was extracted from *E. coli* cultures using the GeneJET Plasmid-Miniprep-Kit from ThermoFisher Scientific (Waltham, USA). For plasmid amplification, 5 mL LB medium were inoculated with a single colony and was grown overnight at 37 °C and 170 rpm using the appropriate antibiotic for the respective plasmid of interest. The culture was treated afterwards according to the manufacturer protocol, to confirm the correct isolation of the plasmid, the DNA concentration was measured using a NanoPhotometer (Implen, Munich, Germany).

2.4.1.2 Polymerase chain reaction

Amplification of DNA fragments for Gibson Assembly was performed using the Q5 High-fidelity 2 X Master Mix (New England Biolabs, Ipswich, USA). To confirm positive clones after transformation, colony PCR was performed using the OneTaq Green PCR Master Mix (2X) (Thermo Fisher Scientific, Waltham, USA). The master mixes were used according to the manufacturer's instructions with the respective primers for each amplicon (see Table 5). To check if the correct insert size was amplified the PCR fragments were loaded onto a 1 % agarose gel in 1 X TAE buffer and run for 30 min at 120 V. The Agarose gel was subsequently stained in an Ethidium bromide solution and imaged with UV-light using the Intas GelStick imager (Intas, Göttingen, Germany). For downstream usage of the PCR fragments, the correct sized bands were cut from the gel and purified using the NucleoSpin Gel and PCR Clean-up Mini-Kit (Macherey-Nagel, Düren, Germany) according to the manufacturer protocol.

2.4.1.3 Gibson assembly

The Gibson assembly method was used to fuse several PCR fragments into one background vector. The PCR products were amplified as described above and the Gibson reaction was performed after the gel-clean up. The 15-20 base pair overhanging sequences which were added to the DNA sequence using a specific primer during the PCR led to a specific arrangement of the PCR fragments in the background vector. Furthermore a promotor sequence (J23119), a ribosomal binding site as well as a terminator sequence were added to the gene before cloning into the expression vector (see Table 7). Gene sequences with the acquired mutations, that served as DNA template for the PCR reactions, were purchased from Eurofins Genomics, (Ebersberg, Germany) (see Table 6). The Gibson assembly

reaction (10 µL Gibson assembly master Mix (New England Biolabs, Ipswich, USA), 10 –X µL ddH$_2$O, 0.02-0.5 pmols X µL total amount of DNA fragments, with a ratio of 1:3 vector to insert) was performed in a Thermocycler at 50 °C for 1 hour. 2 µL of the assembled plasmid were subsequently transformed into *E. coli* DH5α competent cells.

2.4.2 Transformation

All plasmids that were constructed in this study (Table 7) were transformed into chemically competent *E. coli* DH5α following the Gibson assembly (Hanahan, 1983). Briefly, for the transformation into *E. coli* strains, competent cells were thawed on ice and 50 µL of the competent cells were transferred into a fresh 2 mL micro reaction tube. 1-3 µL of purified plasmid DNA was added to the cells and gently mixed by flicking the tube several times. The cells were then incubated on ice for 30 minutes, following a heat shock at 42 °C for 30 seconds with subsequent incubation on ice for 5 minutes. Afterwards, 950 µL LB medium were added to the cells and the cells were incubated for 1-2 hours at 1200 rpm and 37 °C. After the incubation, 100 µL of the cells were plated on LB plates containing the respective antibiotics to select for the plasmid of interest. To increase the chance of positive clones a second plate was plated with 100 µL transformed cells after centrifugation for 30 sec. at 16000 rpm, discarding the supernatant and re-suspending the cells in 100 µL LB medium. The plates were then incubated overnight at 37 °C.

2.4.3 Control of correct plasmid assembly

Positive clones after transformation with the Gibson assembled plasmids were validated in a colony PCR to assess whether the insert in the plasmid background had the correct size. If the desired insert size could be observed on an agarose gel after colony PCR, the plasmid was isolated from the *E. coli* strain as described above and 15 µL (50 ng/µL) purified Plasmid was sent for sequencing to Eurofins Genomics (Ebersberg, Germany) with 2 µL (10 µM) respective sequencing primer (see Table 5). Plasmids with a confirmed correct sequence were further transformed or conjugated into the bacterial strain of interest.

2.4.4 TSS transformation

Plasmids that were checked after construction or that were sent from collaboration partners, based on the pBR322 background (Bolivar et al., 1977), were transformed into the *E. coli* strain of interest using TSS (transformation and storage solution) transformation to avoid the need for preparing competent cells for each strain (Chung, Niemela, & Miller, 1989). Here 5 mL LB medium were inoculated with a single colony of the respective background strain and incubated overnight at 37 °C and 170 rpm. The next day the culture was inoculated 1:100 into 5 mL fresh LB medium and grown for 1-2 h at 170 rpm until an OD$_{600}$ of 0.3-0.8 was reached. Next, the culture was cooled for 10 min on ice.

2. Material and Methods

500 µL of the ice colt culture was then mixed with 500 µL TSS buffer by vortexing. 2 µL plasmid was added to the mixture and the tube was inverted once to mix. The mix was then incubated for 45 min on ice and subsequently centrifuged for 4 min at 16000 x g. 800 µL of the supernatant was discarded and the remaining 200 µL were used to re-suspend the pellet. 50 µL of the transformed cells were then plated on LB agar plates containing the respective antibiotic to select for the plasmid of interest and the plates were incubated at 37 °C until colonies were visible.

2.4.5 Conjugation

Streptomyces strains are Gram-positive bacteria and cannot be transformed by preparing chemically competent cells as it is the standard procedure for Gram-negative organisms such as *E. coli*. To transfer the plasmids based on the pIJ10257 vector (Hong, Hutchings, Hill, & Buttner, 2005) into *Streptomyces* strains, conjugation is performed. As conjugating agent the *E. coli* ET12567 strain (MacNeil et al., 1992) carrying the pUZ8002 plasmid (Paget, Chamberlin, Atrih, Foster, & Buttner, 1999) is used as a so-called donor, which does not methylate any carrying DNA and therefore does not interfere with restriction modification systems in the recipient cell. The donor cell is transformed via heat-shock protocol as described in section 2.4.2. A 10 mL LB culture with the respective antibiotics for the plasmids is inoculated from a single colony of the donor strain carrying the plasmid of interest and is grown overnight at 37 °C and 170 rpm. 100 µL of the overnight culture is then transferred into 10 mL fresh LB medium with the respective antibiotics and grown for ~ 4 h at 170 rpm and 37 °C until an OD_{600} of 0.4 is reached. The cells are then washed twice in LB medium to remove the antibiotics and subsequently re-suspended in 1 mL LB medium. While the donor cells are washed 10 µL of *Streptomyces* spore stock (10^8 spores) are added to 500 µL 2 X YT broth and are heat shocked at 50 °C or 10 minutes. After the *Streptomyces* spores cooled down 500 µL of the donor cells are added to the spores and the mix is centrifuged briefly to pellet the donor cells and the spores. The supernatant is discarded and the pellet is re-suspended in the remaining liquid and subsequently serially diluted from 10^{-1} to 10^{-4} in 100 µL ddH$_2$O. The dilutions are then plated on SM agar plates without any antibiotics and incubated for 16-20 hours at 30 °C. After the incubation period, the plates are overlaid with 1 mL water containing 0.5 mg nalidixic acid and the respective antibiotic selecting for the plasmid of interest. The incubation at 30 °C is continued until colony growth is observed. Single colonies are then picked and re-streaked on SM agar plates containing nalidixic acid and the respective selection antibiotic to grow spores. The plates are incubated for 5-7 days at 30 °C until sporulation occurred and the spores are harvested as described in section 2.2.2.

2.4.6 DNA isolation

2.4.6.1 Bacterial DNA isolation

Bacterial genomic DNA was isolated from bacterial cells using the NucleoSpin Microbial DNA Mini-Kit (Macherey-Nagel, Düren, Germany). For both the Gram-positive and Gram-negative organisms used in this work, the manufacturer protocol was followed. Purified microbial DNA was further used as a DNA template for PCR reactions as described in section 2.4.1.

2.4.6.2 Phage genomic DNA isolation

For genome isolation of phages two different methods were used, depending on the quantity and quality that was needed for the downstream processes. Phage DNA that was used as a DNA template in PCR reaction was purified using the Norgen Biotek Corp. Phage DNA isolation kit (Torhold, Canada). The phage DNA isolation kit was used according to the manufacturer protocol, carrying out all additional steps to increase the DNA yields.

Phage DNA that was used for sequencing or TXTL experiments (see Section 2.4.8) was purified using Phenol-Chloroform-Isoamylalcohol. Briefly, 500 µL to 1 mL of concentrated and sucrose-purified phage lysate was enzymatically digested by adding 2 µL DNase I and 2 µL RNase A to the lysate and incubated for 30 min at 37 °C. Subsequently 2 µL (100 µg/mL) Proteinase K was added and incubated at 37 °C for 1 hour. After the enzymatic digestion, an equal volume of ROTI®Phenol/Chloroform/Isoamylalkohol (Carl Roth, Karlsruhe, Germany) (further referred to as PCI) was added to the digested lysate and inverted several times to mix thoroughly. The emulsion was centrifuged for 5 min at 16000 x g to separate the phases. The upper aqueous phase was then transferred into a fresh tube and the PCI step was repeated two more times. After the third PCI step the aqueous phase was again transferred into a fresh tube and was washed three times with pure CHCl$_3$ by inverting several times, centrifugation for 5 min at 16000 x g, and transferring the aqueous phase again into a fresh tube. After the third washing step, the aqueous phase was again transferred into a fresh tube and 0.1 volumes of 3 M sodium acetate and 2.5 volumes of absolute ethanol were added. The suspension was mixed thoroughly and the DNA was precipitated at − 80 °C overnight. After overnight precipitation, the DNA was centrifuged for 2 hours at 4 °C and 16000 x g. The Supernatant was discarded and the DNA pellet air dried. After all the residual ethanol evaporated the DNA pellet was re-suspended in 50 µL ddH$_2$O. DNA concentrations were measured using the NanoPhotometer or the Qbit fluorometric DNA quantification (Thermo Fisher Scientific, Waltham, USA) following the manufacturer's instruction.

2.4.7 RNA isolation

Total RNA was isolated from *E. coli* MG1655 ΔRM after growth for 1 hour in LB medium in presence and absence of 20 μM daunorubicin to later analyse the transcriptome and assess the bacterial reaction of the supplementation of daunorubicin in the medium. Here, pre-cultures were started in triplicates in 5 mL LB medium with and without 20 μM daunorubicin from single colonies and grown over night at 37 °C and 170 rpm. The main cultures were then inoculated into 10 mL fresh LB medium to an OD_{600} of 0.1 and the cultures were grown in presence and absence of 20 μM daunorubicin for 1 hour at 37 °C and 150 rpm before the cells harvested on ice. The culture was transferred into 50 mL falcon tubes filled half with ice and centrifuged for 20 min at 5000 rpm and 4 °C. The cell pellet was re-suspended 1 X DNA/RNA protection reagent from the Monarch total RNA miniprep kit (New England Biolabs, Ipswich, USA) and the cells were lysed using the Precellys®24 Homogeniser (Bertin, Montigny Le Bretonneux, France) 2 x 20 sec at 6500 rpm with 2 minutes on ice between the beating cycles. The RNA isolation was further conducted as described in the manufacturer manual with all additional steps to increase the RNA yield. The RNA quality and concentration was verified using the TapeStation RNA ScreenTape (Agilent, Santa Clara, USA) according to the manufacturer manual. RNA samples which were measured with a RNA Integrity Number equivalent value (RIN^e) =/> 6 were sent for RNA sequencing to Genewiz (Azenta Life Sciences).

2.4.8 TXTL synthesis of phage particles

Cell-free protein synthesis, here called TXTL (transcription-translation), was used to establish and use a cell-free method to synthesize bacteriophages and manipulate said synthesis without the restrictions posed by the bacterial cell. *E. coli* TXTL reactions were performed using the myTXTL Pro Cell-Free expression kit (Arbor Biosciences, Ann Arbor, USA). Synthesis of phages was performed using 9 μL of myTXTL master mix which was incubated on ice with 1 μL GamS Nuclease Inhibitor (75 μM) for 5 min. Subsequently 1.2 μL purified phage DNA (10 nM), daunorubicin at final concentrations of 5 μM, 20 μM or ddH_2O to a final volume of 12 μL were added. The reaction mixture was then incubated for 16 hours at 28 °C in a thermocycler. After incubation, the TXTL mix was serially diluted 10^{-1} to 10^{-8} and was spotted in a double-agar overlay on *E. coli* MG1655 ΔRM to identify successfully synthetized and infective phage particles. The phage synthesis was conducted in biological triplicates. It is important to note that the phage DNA that was used in the TXTL reaction was PCI purified and had three additional Ethanol (70 % v/v) washing steps after overnight precipitation to ensure that no phenol or other residuals from the isolation process entered the *in vitro* synthesis.

2.4.9 Quantitative real-time PCR

Quantification of CL31 phage DNA after spent medium pre-incubation and intra-cellular T4 and T4 nTET (Pozhydaieva et al., 2024) phages was performed using quantitative real-time PCR. Samples

that were taken during liquid infection experiments described in section 2.3.2 at the indicated time points and 3 OD units of cells were harvested by centrifugation for 10 min at 4 °C and 5000 x g followed by two washing steps in PBS buffer before the pellets were stored at -20 °C. For the quantification of intracellular DNA during infection, in presence and absence of 20 µM daunorubicin cells were re-suspended in 500 µL qPCR lysis buffer and lysed using the Precellys®24 Homogeniser at 6000 rpm 3 x for 40 sec with 2 min on ice between the beating cycles. DNA concentrations were then measured after centrifugation for 10 min at 16.000 x g and 4 °C using the nanophotometer and adjusted to 1 ng/µL. For the PCR reaction, 5 µL of the DNA template were mixed with 10 µL 2 x Luna universal qPCR master mix (New England Biolabs, Ipswich, USA) and 1 µL of each forward and reverse qPCR primer (Table 5) and adjusted to a final volume of 20 µL with ddH$_2$O. The qPCR reaction was performed in the qTOWER 2.2 (Analytik Jena, Jena, Germany) in 96-well plates in biological triplicates and technical duplicates. To determine the relative concentration of intracellular phage DNA, the relative expression ratio of the phage target gene (T4p168 coding for the tail protein) compared to the *E. coli* housekeeping gene *atpD* (coding for the F1 sector of membrane-bound ATP synthase, beta subunit) was calculated using the "relative quantification method" function of the qPCRsoft 3.1 software (Analytik Jena, Jena, Germany).

The samples from the pre-incubation assays were prepared slightly different, however the qPCR program as well as the subsequent analysis of phage targeting gene (cgl_56, coding for the minor tail protein) remained the same. Since no host was present in the pre-incubation assay, no host housekeeping gene was targeted in the qPCR. From the CL31 pre-incubation samples 0 h and 24 h post incubation 5 µL sample were directly used as DNA template and the initial denaturation step was increased to 5 min at 95 °C to lyse the phage capsid. The qPCR for the CL31 pre-incubation was performed using biological and technical duplicates.

2.5 Biochemistry methods

2.5.1 Biacore measurements of Phage DNA

Biacore surface plasmon resonance (SPR) measurements were performed to investigate the in vitro interactions between purified phage DNA and the molecules of interest, here apramycin, actinomycin D, and daunorubicin. The phage DNA that was tested with those molecules was of phage Alderaan and phage T4 as well as the T4 nTET variant and the T4 Δα/βGT mutant. The phage DNA was purified using the PCI method to get a high yield of highly pure DNA. As subsequent step for the preparation of the SPR measurement, the pure phage DNA was biotinylated using the Pierce™ Biotin 3' End DNA labelling Kit (Thermo Fisher Scientific, Waltham, USA), so the DNA can be immobilized on the SPR chip. The Biotin 3' End DNA labelling Kit was used according to the manufacturer protocol and the DNA

pellet that was gained at the last step of the protocol was re-suspended in 50 µL ITC buffer. The DNA samples were then sent to the Heermann Lab at the Johannes Gutenberg University in Mainz where the Biacore measurements were conducted. Measurements were performed using the Biacore T200 SPR system (Cytiva, Marlborough, USA) and analysed using the Biacore T200 evaluation software 3.2.1 (Cytiva, Marlborough, USA). SPR measurements were performed in 5 individual runs with decreasing concentrations of the molecules of interest and as technical duplicates on two different chips. Final results of the measurements were then provided by the cooperation partners from the Heermann Lab which are used in this study.

2.5.2 Potassium efflux

Potassium efflux assays were conducted to assess the impact of daunorubicin on the injection of phage DNA into the host cell. It has been described for phage λ (Boulanger & Letellier, 1988; Kronheim et al., 2018) that injection of the genome into the host cell leads to efflux of potassium ions that can be measured using a potassium electrode. Using this method the impact of daunorubicin on the injection of different phage genomes was monitored. Here the phages Bas09, Bas13, Bas20 and λ were used to monitor the efflux of potassium ions in presence and absence of 20 µM daunorubicin. For the potassium efflux assays 5 mL LB medium was inoculated from a single colony of *E. coli* MG1655 ΔRM in presence and absence of 20 µM daunorubicin and incubated overnight at 37 °C and 170 rpm. 50 mL fresh LB medium was inoculated 1:100 from the overnight culture in presence and absence of 20 µM daunorubicin and grown for 1.5-2 hours at 150 rpm and 37 °C. The culture was subsequently harvested by centrifugation for 15 min at 5000 rpm and the pellet was re-suspended in 5 mL SM buffer. The OD_{600} of the cell suspension was then adjusted to 2 and the cells were stored on ice until usage. Directly before usage the cells were incubated at 37 °C for 5 min and 5 mL of the cells at OD_{600} of 2 was mixed with 1:50 Orion ionic strength adjuster (ISA) (Thermo Fisher Scientific, Waltham, USA9. Measurements were started immediately under constant stirring with an Orion potassium ion selective electrode (Thermo Fisher Scientific, Waltham, USA) monitoring the electric potential (mV) every 5 seconds for a total of 60 min at room temperature. If required daunorubicin was added directly to the cells at a concentration of 20 µM. After 5 minutes of measurement, 50 µL of the respective phage lysate was added to a final titer of 10^{10}, achieving a final MOI of 6. As control 50 µL SM buffer was added to the measurement. The measurements were conducted in biological triplicates. It is important to note that the phage lysate used for the potassium efflux assay was cleaned up using a sucrose gradient to avoid the measurement of residual ions from the lysate preparation.

2.6 Microscopy methods

2.6.1 Phase contrast- and Fluorescence-microscopy

Microscopy of spent medium producer cells during the incubation and sampling of spent medium (see section 2.2.5) was performed using a Zeiss Axio Imager M2 (Carl Zeiss, Oberkochen, Germany). Imaging was generally performed using an EC Plan-APOCHROMAT 100x/1.4 Oil Ph3 objective and a Zeiss Axio-Cam MRm/ ICc 3 camera (Carl Zeiss, Oberkochen, Germany). For each time point of sampling 2 µL of sample were pipetted on a 1 % agarose pad and imaged using phase contrast to ensure no contamination occurred during cultivation or sampling of the spent medium.

2.6.2 Transmission electron microscopy

Visualization of phage particles was conducted using transmission electron microscopy (TEM). Here, 5 µL of pure high titer phage lysate was placed on a glow-discharged (15 mA, 30 s) carbon-coated copper grid (CF300-CU, carbon film 300 mesh copper). Staining of the phage particles on the copper grid was performed in 2 % (wt/v) uranyl acetate for 5 min and two subsequent washing steps in ddH$_2$O. The stained grids containing the phages Geonosis and Kamino were then air-dried and imaged using a TEM Talos L120c (Thermo Scientific, Dreieich, Germany) at an acceleration of 120 kV.

Grids containing phage particles from Abafar and Scarif were visualized using a Zeiss EM 910 or Zeiss Libra 120 Plus transmission electron microscope (Carl Zeiss, Oberkochen, Germany) at an acceleration of 80 kV/ 120 kV using a calibrated magnification. Those phages were attached on 300 mesh copper grids with a mica-floated carbon film.

2.6.3 Stereomicroscopy

Observation of the plaque morphology and development of phages characterized in this work, namely Abafar, Geonosis, Kamino, and Scarif, was performed using a Nikon SMZ18 stereomicroscope with a NIS-Elements AR 5.3 software (Nikon, Minato, Japan). Plaque assays on double-agar overlays (see section 2.3.3) using a phage titer of 10^2 to 10^3 PFU/mL were incubated over a period of 72 hours at 30 °C. Images of single plaques were taken after 24 h, 48 h and 72 h to monitor the morphology and development of the plaques. The area of the plaques was determined using the auto-detect ROI (region of interest) tool in the NIS-elements software which then calculated automatically the area of the ROI.

2.7 Computational methods

2.7.1 DNA seq, genome assembly and annotation

Whole genome sequencing of isolated phage genomes was performed by Genewiz Germany, using an Illumina NovaSeq platform with a read length of 2 x 150 bp. The NEBNext Ultra II DNA Library Prep Kit

was used to sequence the whole genome of phages on an Illumina MiSeq platform with paired reads with a length of 15 to 150 base pairs. Raw sequencing reads were checked for quality using FASTQC v.0.11.9 (http://www.bioinformatics.babraham.ac.uk/projects/fastqc/). Trimming of the reads as well as clean-up of low quality reads and adapter sequences was performed using the fastp v.0.23.2 program (Chen, Zhou, Chen, & Gu, 2018). As next step the whole genome *de novo* assembly was performed using the Shovill pipeline v.1.1.0 (https://github.com/tseemann/shovill) using the SPAdes genome assembler v.3.15.5 (Bankevich et al., 2012). Improvement and curation of the assembled genomes was further conducted using the Pilon version 1.24 (Walker et al., 2014) and the genomic terminal ends were identified using the PhageTerm online galaxy platform (Garneau, Depardieu, Fortier, Bikard, & Monot, 2017).

Annotation of the *de novo* assembled genomes was performed using the Prokka 1.8 tool using different databases (Markov model profiles databases, including Pfam and TIGRFAMs). Genome sequences were additionally searched using the hmmscan from the HMMER 3.1 package (Seemann, 2014) and compared to the PHROG database (Terzian et al., 2021). Taxonomic classification of the newly isolated phages was determined based on the identity level to close related phages using NCBI BLASTn (NCBI, 2023) search and ordered according to the latest virus taxonomy release (International Committee on Taxonomy of Viruses ICTV, 2023). The annotated phage genomes were finally deposited at the NCBI database for public search and use with following GenBank accession numbers: Abafar (PP750865), Geonosis (PP750866), Kamino (PP750867), and Scarif (PP750868).

2.7.2 RNA seq analysis

Standard total RNA sequencing with rRNA depletion was performed using an Illumina sequencing platform with a sequence coverage of 2 x 150 bp length and library preparation was conducted by Genewiz Germany. The sequencing results were subsequently analysed using the CLC genomics workbench v.20 (Qiagen, Hilden, Germany). Beginning with quality control of the reads as well as subsequent trimming of adapter sequences and low quality reads as well as ambiguous nucleotides. As reference the genome of *E. coli* K12 MG1655 (U00096.3) was used for mapping of the reads. The Transcripts per million (TPM) were calculated using the "RNA-seq Analysis" tool of the CLC genomics workbench (mismatch cost 2; insertion cost 3; length fraction 0.9; similarity fraction 0.9; strand specificity both; maximum number of hits for a read 10) . Differential expression of genes was determined using the "Differential expression in Two Groups" tool in CLC genomics workbench combining triplicates for comparing samples grown in presence and absence of 20 µM daunorubicin with an FDR p-value of ≤ 0.05. A heat map of differentially expressed genes presenting the annotated TPM was visualized using GraphPad Prism 9.0.0 as well as a volcano plot visualising the expression of

samples in presence of daunorubicin compared to those in absence of daunorubicin showing the -log(false discovery rate) value against the $\log_2$-fold change of expression.

2.7.3 PADLOC analysis of defense systems

Analysis of the defense system repertoire of bacterial host strains was performed using the PADLOC (Prokaryotic Antiviral Defence LOCator) tool v2.0.0 (https://padloc.otago.ac.nz/padloc/) (Payne et al., 2022). In order to compare the defense system repertoire the genomes of *E. coli* strains K12 MG1655 (U00096.3), K12 BW25113 (CP009273), BL21 (DE3) (CP001509) and B (NZ_CP014268) were analysed to further understand the infection dynamics observed in infection experiments.

2.7.4 Fiji analysis of microscopy images

The analysis of TEM microscopy images for Tail length as well as capsid width and length was performed using the Fiji is just ImageJ (Fiji) (Schindelin et al., 2012; Schindelin, Rueden, Hiner, & Eliceiri, 2015) software. The length of tail and capsid as well as capsid width was measured by manually drawing a segmented line with a width of 7 pixels (pixel size = 64.5 nm) along the tail or capsid. The length of the ROI (region of interest) was then measured in Fiji for every marked phage particle. Average length and width as well as the according standard deviation was calculated for each phage and visualized using GraphPad Prism 9.0.0.

2. Material and Methods

3. Results

3.1 Anti-phage properties of spent medium from aminoglycoside producing *Streptomyces spp.*

In previous studies, Kever and colleagues could show that spent medium of the apramycin producer *Streptoalloteichus tenebrarius* was sufficient to prevent phage infection from phage Alderaan on *S. venezuelae* (Kever et al., 2022). In this work further aminoglycoside producing *Streptomyces* strains were tested for their impact on phage infection. As model system for phage infections *S. venezuelae* and its lytic phage Alderaan were used throughout the experiments.

3.1.1 Anti-bacterial effect of spent medium on *S. venezuelae*

Streptomyces spp. produce a variety of specialized metabolites which are secreted into their environment and have different functions, such as anti-bacterial, anti-fungal or anti-viral properties. In order to assess whether the harvested spent medium (SM) of the different aminoglycoside producer strains actually has anti-bacterial potential, a submerged culture of *S. venezuelae* was supplemented with 20 % of SM harvested after 1 day, 2 days or 3 days of incubation. Producer strains and the main aminoglycoside that is supposed to be produced can be found in Table 7, including the antibiotic resistance gene that is used in liquid infection experiments. Over the course of 72 hours the producer strains have been phenotypically monitored using light microscopy, representative images of production strains are shown in supplementary Figure S1.

Table 7: Producer strains for spent medium assays. Listed are the main aminoglycosides produced by the respective strain as well as the antibiotic resistance gene that was used in *S. venezuelae* in further spent medium experiments

Producer strain	Aminoglycoside produced	Antibiotic resistance gene
Streptoalloteichus tenebrarius	Apramycin	*aac(3)IV*
S. kanamyceticus	Kanamycin	*aphAI*
S. hygroscopicus	Hygromycin	*aph(7")-Ia*
S. griseus	Streptomycin	*aadA*
S. rimosus	Paromomycin	*aphH**
S. spectabilis	Spectinomycin	*aadA*
S. fradiae (not shown here)	Neomycin	*aphAI*

*not used in further experiments

3. Results

The SM of *S. tenebrarius, S. kanamyceticus, S. hygroscopicus, S. griseus, S. rimosus* and *S. spectabilis* was tested for antibacterial effects by measuring the OD_{450} over a cultivation period of 24 hours. These strains mainly produce the aminoglycosides apramycin, kanamycin, hygromycin, streptomycin, paramomycin and spectinomycin respectively, among other specialized metabolites. The wild type *S. venezuelae* was grown in fresh GYM medium as control as well as in GYM medium supplemented with 20 % SM of all producer strains separately. It can be observed in Figure 8 that the SM of the producer strains had varying effects on *S. venezuelae.* Spent media harvested from *S. tenebrarius, S. griseus* and *S. spectabilis* had growth repressing effects on *S venezuelae,* regardless of the SM harvesting time, showing OD_{450} values between 0 and 2.9, which stands in contrast to an OD_{450} of 16.5 after 24 hour growth in fresh GYM medium (in black). Contrarily, SM of *S. kanamyceticus* and *S. hygroscopicus* only had minor or no effects on the growth of *S. venezuelae*, irrespective of the time of harvest, as the culture reaches OD_{450} values between 6.4 and 18.9 in presence of the SM. For the SM of *S. rimosus* a gradual effect on the growth of *S. venezuelae* can be observed, SM sampled after 1 day shows no growth defect (OD_{450}=17.7). However, SM sampled after 2 and 3 days shows a strong growth defect with an even stronger effect from 3 days old SM reaching OD_{450} values of 2.16 and 0.33 respectively. The effect of SM on *S. venezuelae* was tested in unicates to get an idea on the production of specialized metabolites for further experiments with the SM.
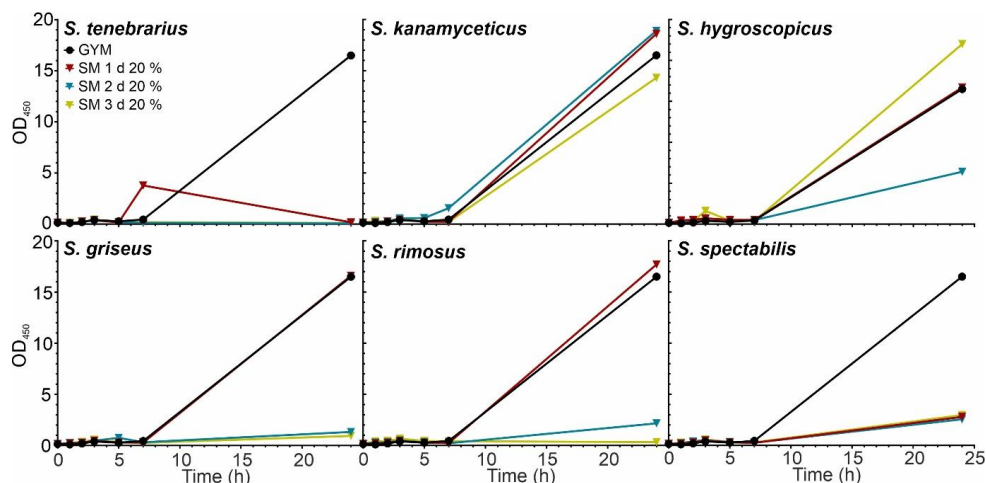
Figure 8*: **Anti-bacterial effect of *Streptomyces* spent medium.** Spent medium (SM) of the aminoglycoside producer strains *S. tenebrarius, S. kanamyceticus, S. hygroscopicus, S. griseus, S. rimosus* and *S. spectabilis* (from top left to bottom right) sampled after 1 (red), 2 (turquoise) and 3 days (yellow) of cultivation is tested for antibacterial properties by supplementing 20 % of the cultivation medium of *S. venezuelae* with the respective SM. Growth of *S. venezuelae* is compared to growth in fresh GYM medium (black). n=1

3. Results

3.1.2 Spent medium of different aminoglycoside producing *Streptomyces* strains shows varying degrees of anti-phage defense

Anti-phage defense properties of the SM of aminoglycoside producer strains was tested using liquid infection assays in the BioLector with sampling of supernatant every two hours to assess infection dynamics as well as phage amplification kinetics. In Figure 9, the anti-phage effect of SM from *S. tenebrarius, S. griseus, S. kanamyceticus* and *S. fradiae* is shown. The bar graph depicts the $\log_{10}$-fold change of phage particles in the colours corresponding to the growth curves. For the infection assays shown here, *S. venezuelae* strains carrying a resistance cassette according to the main aminoglycoside produced (Table 7) by each producer strain were cultured and infected with phage Alderaan at a PFU/mL of 10^7. SM harvested from *S. tenebrarius* shows a similar growth of *S. venezuelae* in pure GYM medium as well as 1-day-old SM, for both infected and uninfected cultures. In addition, the phage titer develops similarly for both conditions showing an increase in phage particles by about 1.5 $\log_{10}$-fold 24 hours post infection. 2-day-old SM shows a strong growth defect on infected and uninfected cultures which is also resembled in the phage titer, which decreases two $\log_{10}$ levels 24 hours post infection. Growth curves of the infection assay with SM of *S. griseus* showed the expected phenotype for the control culture in fresh GYM medium, where the culture in absence of phage particles grew exponentially after 2 hours of lag phase. In presence of phage Alderaan the culture collapsed after about 8 hours post infection and an increase in titer was measured of about 1.5 $\log_{10}$-fold. The growth curves of the infected and uninfected samples supplemented with 1- and 2-day-old SM showed overlapping growth which indicates that no culture collapses resulted in the phage infection. This is also represented in the development of the phage titer, which decreased one $\log_{10}$-fold for both 1- and 2-day-old SM. It is, however, apparent that 2-day-old SM had a stronger growth defect compared to 1-day-old SM as the culture had a longer lag phase and reached an overall lower backscatter value. In the third row of Figure 9, the infection assay supplemented with SM from *S. kanamyceticus* is shown. In contrast to the other two graphs, the infected and uninfected lines showed a similar growth phenotype, irrespective of the age of the SM used to supplement the cultivation. Here, no anti-phage phenotype of the SM could be observed in the infected cultures as the cultures collapsed around five to eight hours post infection. The lack of anti-phage properties of *S. kanamyceticus* SM was also visible in the phage titer development, where the final phage titer for all three conditions increased up to 2 $\log_{10}$ folds. It is important to notice that the amplification of the phages seemed to be impaired somehow by the SM as the increase in phage titer was only visible after six to eight hours post infection for 1- and 2-day-old SM respectively but largely the phage infection was not completely inhibited by the SM of *S. kanamyceticus.* In the bottom row the infection assay supplemented with SM from *S. fradiae* is shown. In the growth curve it can be observed that all growth curves supplemented with SM

as well as the uninfected culture completely overlap until about 14 hours post infection and showed normal growth behaviour without signs of phage infection. The infected culture in fresh GYM medium showed complete culture collapse, indicating successful phage infection. Successful phage infection
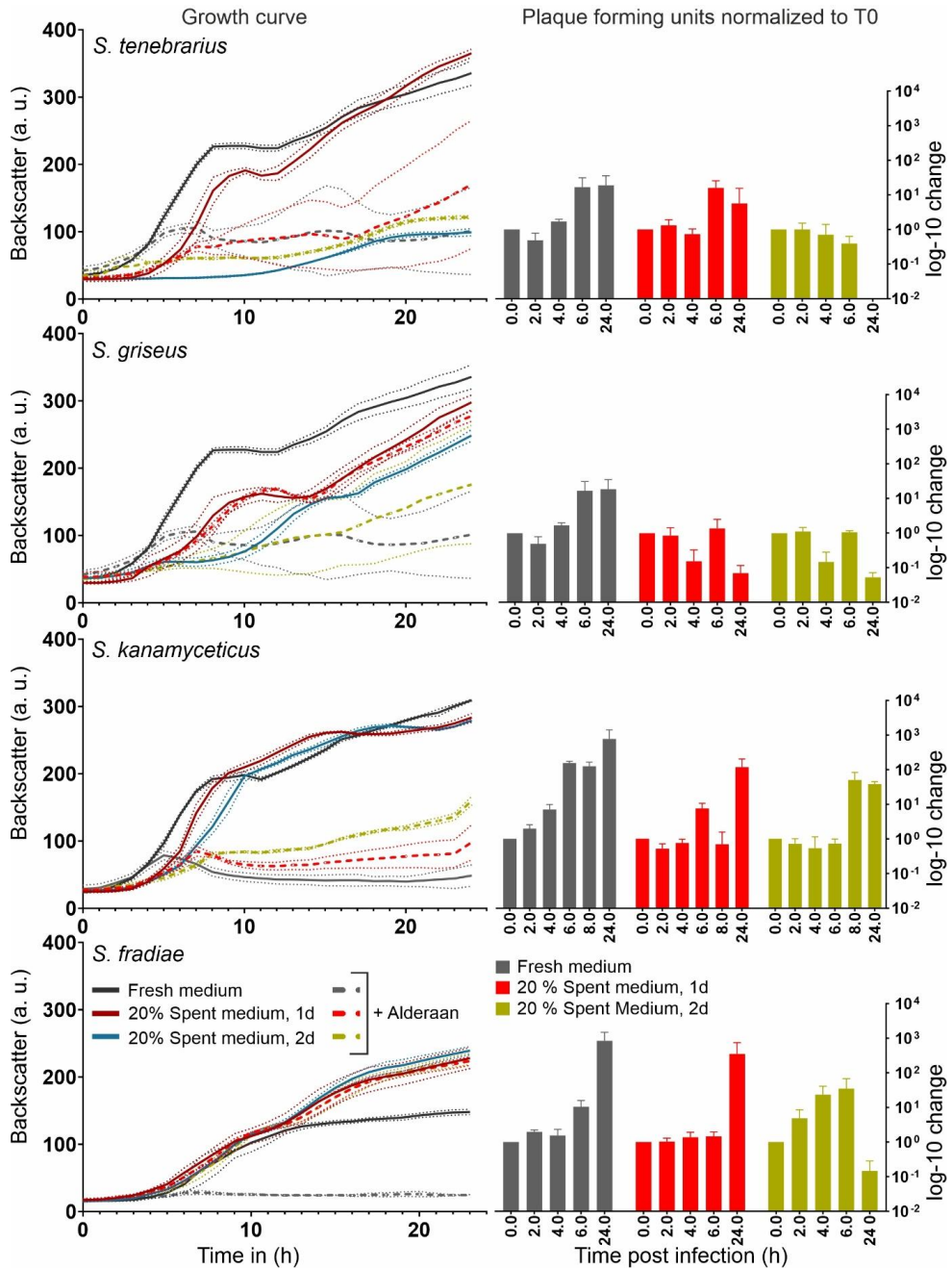
Figure 9: Effect of spent medium of Alderaan infection of *S. venezuelae*. Liquid phage infection assays of phage Alderaan infecting *S. venezuelae* supplemented with 20 % spent medium harvested after 1 or two days of cultivation. On the left growth curves are shown and on the right the corresponding plaque forming units normalized to the T_0. In black is the uninfected culture in fresh GYM medium and in grey dashed lines the infected culture in fresh gym medium, in dark red is the uninfected culture supplemented with 20 % 1-day-old SM and in the bright red dashed line the corresponding infected culture. The turquoise solid line represents the uninfected culture supplemented with 20 % 2-day-old SM and in yellow dashed, the corresponding infected culture. The bar plot colours correspond to the infected cultures with the respective supplement in the medium (grey = GYM, red = 1 d SM, yellow = 2 d SM). The culture was inoculated at an $OD_{450}= 0.15$ and infected with Alderaan at 10^7 PFU/mL. n=3 independent biological replicates, dotted lines in the growth curves and error bars in the bar plot show the standard deviation.

and amplification was also resembled in the phage titer development, which increased about 3 $\log_{10}$-folds in fresh medium. Surprisingly, the phage titer of the culture supplemented with 1-day-old SM also showed an increase of phage titer of about 3 $\log_{10}$-folds, but only after 24 hours post infection, before that no change in phage titer was detected. For the culture supplemented with 2-day-old SM an initial increase of phage titer was observed between two to six hours post infection but the final phage titer 24 hours post infection decreased about 1 $\log_{10}$-fold compared to the initial phage titer at T_0. Generally speaking, varying degrees of anti-phage properties of SM were observed here, with 2-day-old SM of *S. tenebrarius* showing the strongest anti-phage defense properties, which was already shown previously (Kever et al., 2022). Furthermore, spent medium of *S. griseus* and 2-day-old SM of *S. fradiae* showed anti-phage defense properties, decreasing the final phage titer 24 hours post infection. Only for SM of *S. kanamyceticus* no decrease in the final phage titer was observed, however a decrease in amplification speed was observed here.

3.1.3 Cultivation medium shows an impact on specialized metabolite production in *S. tenebrarius*

In previous studies, it was shown that the medium composition has a great effect on the production of specialized metabolites during the cultivation (Zhang, Chi, Wu, Deng, & Yu, 2021). In this work, two different cultivation media were compared regarding production of antiphage molecules. Here, the apramycin producer *S. tenebrarius* as well as two mutants with mutations in the apramycin synthesis pathway, *S. tenebrarius* Δ*aprP* and *S. tenebrarius* Δ*aprQ,* were cultivated in GYM medium as well as minimal medium (MM) and the resulting SM after 3 days of cultivation was tested for the anti-phage properties. The minimal medium used here had a defined composition of 0.1 % $(NH_4)_2SO_4$, 0.05 % K_2HPO_4, 0.02 % $MgSO_4$, 0.001 % $FeSO_4$ and 1 % glucose which is a strong reduction of the C-source and a more defined composition of inorganic salts compared to GYM medium. It was previously used to identify the self-resistance mechanism of the apramycin producer *S. tenebrarius* (Zhang et al., 2021). In Figure 10 an abbreviated version of the apramycin synthesis pathway is depicted with the important enzymatic steps that are disrupted by the deletions of *aprP* (encoding a deacetylase) and *aprQ* (encoding a FAD-dependent dehydrogenase)*.* The mutant strains *S. tenebrarius* Δ*aprQ* and

S. tenebrarius Δ*aprP* are expected to only produce the intermediates lividamine and 7'-N-acytelated,5-O-phosphorylated demethylaprosamine respectively.
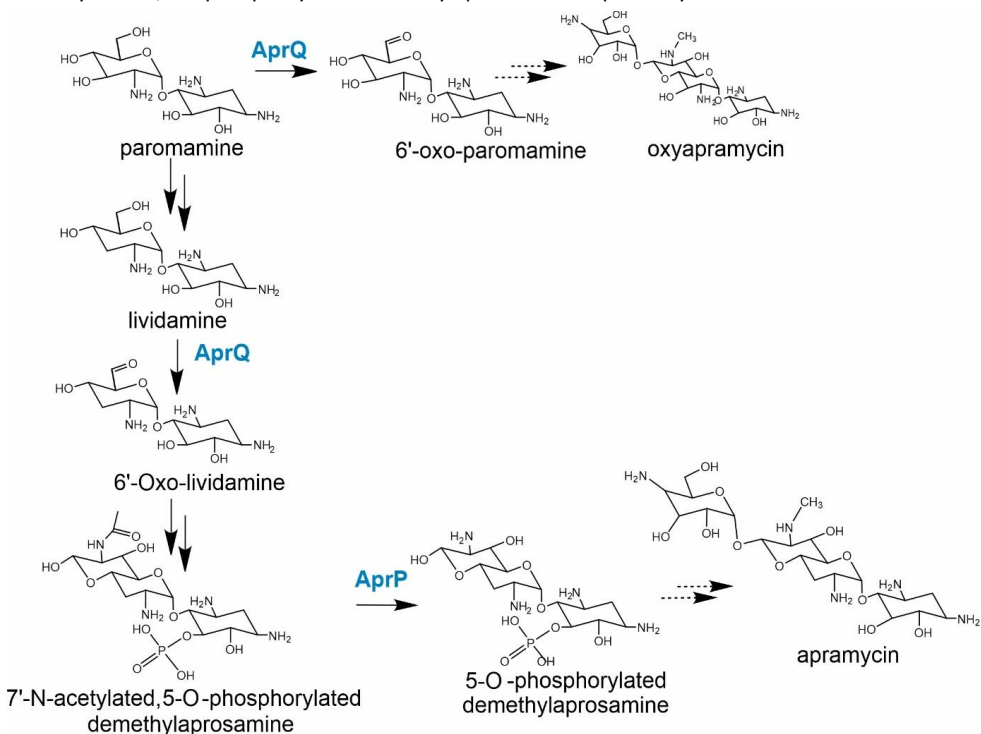
Figure 10: Apramycin synthesis pathway showing the steps inhibited by respective mutations. The apramycin synthesis pathway is shown in an abbreviated form, showing important steps in the pathway that are impaired in the mutants tested here. Starting from the molecule paromamine the enzyme encoded by *aprQ* dehydrogenizes the molecule either to 6'-oxo-paromamine which finally forms oxyapramycin or the enzymes dehydrogenizes lividamine to 6-oxo-Lividamine. The enzyme encoded by *aprP* hydrolyses the N-7'-acetyl group from the previous intermediate to 5-O-physphorylated demthylaprosamine. Mutant strains of *S. tenebrarius* Δ*aprP* and Δ*aprQ* are expected to produce the intermediates 7'-N-acytelated,5-O-phosphorylated demthylaprosamine and lividamine respectively.

Similarly to the test of SM of different aminoglycoside producer strains, liquid infection experiments of phage Alderaan infecting *S. venezuelae* pIJLK04 at an initial titer of 10^8 was supplemented with 20 % of SM (adjusted to pH 7.5). In Figure 11 the results of the liquid infection assays supplemented with 20 % SM are depicted. In the top row, SM of the *S. tenebrarius* wild type is shown. For the wild type no distinct difference in the culture growth was observed, both SM in GYM and MM showed

overlapping curves for infected and uninfected samples, indicating inhibition of phage infection. For
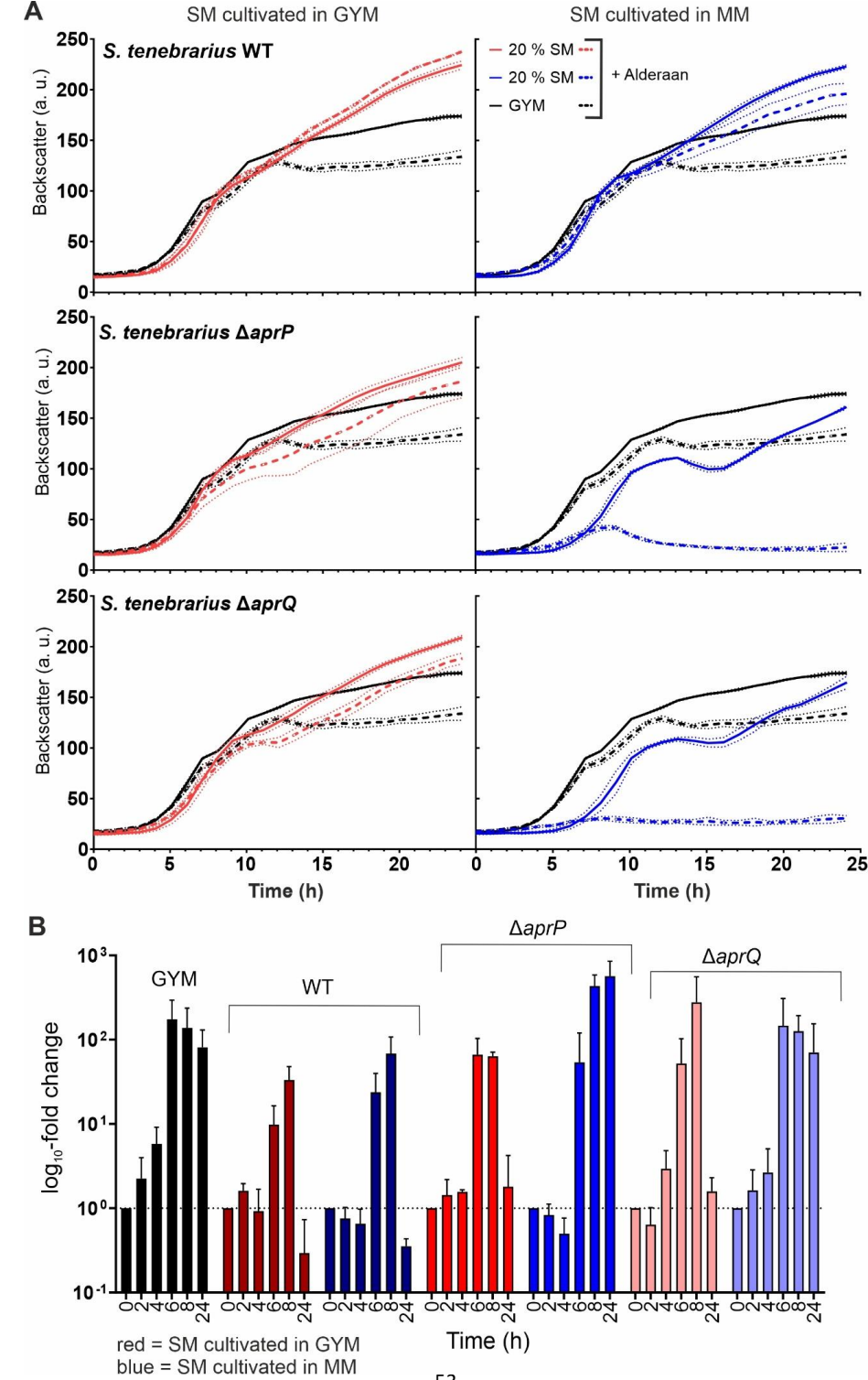
Figure 11: Comparison of cultivation media for the acquisition of spent medium from *S. tenebrarius* and two mutants. A) growth curves of *S. venezuelae* infected (dashed line) and uninfected (solid line) with phage Alderaan in presence (red/blue) and absence (black) of 20 % spent medium which was cultivated in either GYM (red) or Minimal medium (blue). n= 3 independent biological replicates, dotted lines in the corresponding colour show the standard deviation. From top to bottom SM of *S. tenebrarius* wild type, *S. tenebrarius ΔaprP* and *S. tenebrarius ΔaprQ* are shown. B) $\log_{10}$-fold change of the phage titer normalized to T_0 for phage Alderaan infections in GYM, SM of the wild type, SM of *ΔaprP* and SM of *ΔaprQ* from left to right respectively. Red coloured bars indicate SM cultivated in GYM, blue coloured bars indicate SM cultivated in MM. n=3 independent biological replicates, error bars show standard deviation, dotted black line at 10^0 indicates the starting titer of each sample.

the control growth curves only a minor growth defect in the infected culture was observed, however phage amplification was detected in the increase of the phage titer of about 2 $\log_{10}$-folds. For both mutants tested in this experiment clear differences in the growth curves were determined. Both *ΔaprP* and *ΔaprQ* showed inhibitory effects on phage infection when cultivated in GYM medium however no such effect was observed in SM harvested from MM, where a complete culture collapse was observed for both mutant spent media tested here. This trend was also represented in the $\log_{10}$-fold change of the phage titer, where the phage titer of GYM cultivated SM 24 hours post infection was similar to the starting titer or even decreased in the case of the wild type SM. In contrast to this, the phage titer of infection assays supplemented with SM cultivated in MM increased over the course of the infection assay up to nearly 3 $\log_{10}$-folds for *ΔaprP* SM and 2 $\log_{10}$-folds for *ΔaprQ* spent medium. Only the wild type SM cultivated in minimal medium showed a similar titer development as the spent medium cultivated in GYM medium. This assay showed that the cultivation medium had a strong effect on the specialized metabolites that were produced during cultivation, thus had an impact on the anti-phage properties of the respective SM.

3.1.4 Anti-phage molecules do not act via triggering the stringent response

Kever and colleagues have described the inhibitory effect of apramycin, an aminoglycoside antibiotic, on early stages of phage infection in detail in 2022. However, the exact mechanism of action of apramycin remains yet unknown (Kever et al., 2022). One hypothesis that was formulated during the investigation of the apramycin effect was that the combination of apramycin and phage infection might trigger the stringent response in the host and thereby leading to abortive infections, finally inhibiting the phage infection. To investigate this hypothesis, liquid phage infection assays were performed where the stringent response was triggered using serine hydroxamate (SHX), which was described previously to increase intracellular (p)ppGpp in *Streptomyces* strains (Strauch, Takano, Baylts, & Bibb, 1991). Different SHX concentrations, ranging from 1 to 25 mM were tested and compared to liquid infection assays supplemented with 10 µg/mL apramycin, monitoring the bacterial growth as well as the phage titer development. In all of the growth curves with SHX supplemented cultivations, it was observed that phage infection led to a culture collapse, showing a similar growth curve as the infected sample in GYM medium only, indicating that SHX does indeed not lead to

inhibition of phage infection. In the infection experiment with 25 mM SHX (orange) even the uninfected culture showed growth defects, indicating that the ppGpp levels were very high, which led to slower growth or even cell death. The control assay supplemented with 10 µg/mL apramycin showed the expected phenotype in the bacterial growth, where the infected and uninfected growth curve in presence of apramycin overlap and showed no sign of phage infection, whereas the infected sample in absence of apramycin showed the expected culture collapse. The lack of inhibitory effect on phage infection of SHX was also visible in the development of the phage titer (Figure 12F), where an increase of phage titer was observed for all SHX supplemented cultures and only in the apramycin supplemented culture a decrease of 1 $\log_{10}$-fold was observed. Based on these findings we could deduce that apramycin does not trigger a stringent response in *S. venezuelae* when present during infections with phage Alderaan. Considering these results, we can reject the hypothesis that the induction of the stringent response by apramycin treatment is the underlying reason for its anti-phage properties.
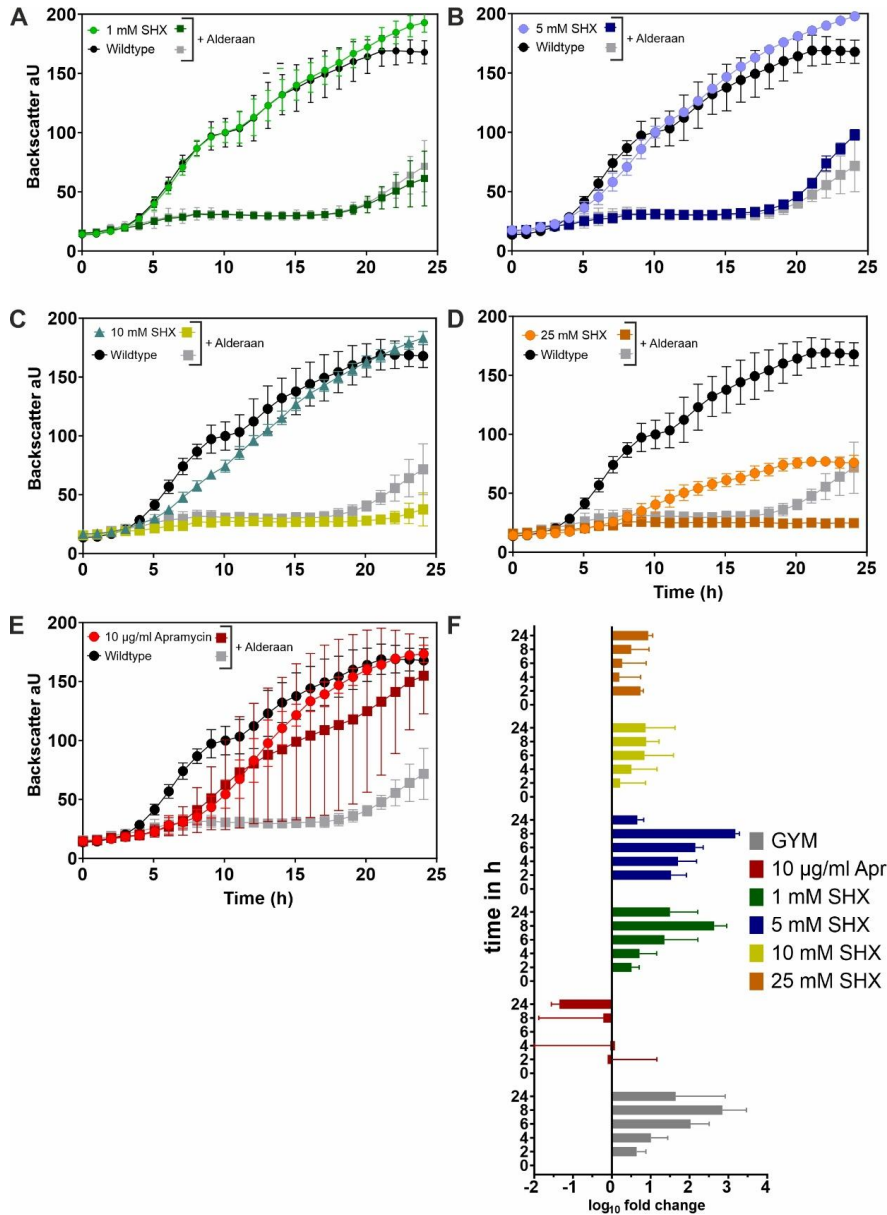
Figure 12: Comparison of apramycin mediated chemical defense with SHX triggered stringent response. Growth curves of liquid infection experiments of Phage Alderaan infecting *S. venezuelae* in presence and absence of different concentrations of serine-hydroxamate (SHX) and apramycin are shown here. A) *S. venezuelae* growth curves 1 mM SHX supplemented medium in green and GYM medium in black, infected curves are shown in dark green when supplemented with 1 mM SHX and grey in GYM. This colour scheme is true for all growth curves, bright colour in absence of phage and dark colours in presence of Alderaan at 10^8 PFU/mL. B) 5 mM SHX in shades of blue, C) 10 mM SHX in turquoise (uninfected) and yellow (infected), D) 25 mM SHX in orange and E) 10 µg/mL Apramycin in shades of red. F) Change of phage titer as log_{10}-fold change normalized to the phage titer at T_0 for GYM (grey), 10 µg/mL apramycin (red), 1 mM SHX (green), 5 mM SHX (blue), 10 mM SHX (yellow) and 25 mM SHX (orange). n= 3 independent biological replicates, error bars indicate the standard deviation for both the growth curves and the phage titer.

3. Results

3.1.5 Impact of spent medium on free phage particles from Alderaan, CL31 and λ

In previous experiments, it was shown that the effect of naturally produced aminoglycosides on phage infection varies significantly regarding the producer strain as well as the cultivation medium that was used to generate the SM. Furthermore, one possible mode of action, abortive infection triggered by ppGpp, was excluded by the experiment described in the last section. *Streptomyces* are naturally found in soil, which represents a highly structured environment, and are known to secrete the specialized metabolites that are produced. One hypothesis that was postulated was that secreted small molecules produced by *Streptomyces* might be able to inactivate free phage particles (Kieser et al., 2000; Zambri et al., 2022). To further investigate the mode of action of naturally produced aminoglycosides, the extracellular effect of SM on different phage particles was tested. Three different phages infecting three distinct host bacteria, namely phage Alderaan infecting *S. venezuelae,* CL31 infecting *C. glutamicum* MB001 and λ infecting *E. coli* LE392 were tested in different SM from aminoglycoside producing *Streptomyces* strains. Spent medium of the strains *S. tenebrarius, S. kanamyceticus, S. hygroscopicus, S. griseus, S. rimosus* and *S. spectabilis* cultivated in GYM medium and harvested after 1 day, 2 days and 3 days of cultivation were used in pre-incubation assays (Figure 13). Furthermore, GYM medium with a defined pH of 6.5, 7.5, and 8.5 were used as controls in the pre-incubation assays (Figure 13). For phage Alderaan infecting *S. venezuelae* only minor effects of the SM could be observed. For 3-day-old SM of *S. tenebrarius, S. kanamyceticus* and *S. griseus* a reduction in phage titer of 0.5 to nearly 1 $\log_{10}$-fold was observed. SM of *S. rimosus* and *S. spectabilis* showed a similar effect for both 2- and 3-day-old SM. This reduction however is not significant and varies in the normal range of pipetting and dilution errors. Phage λ infecting *E. coli* LE392 was affected in a similar strength, by SM from nearly all aminoglycoside-producing strains. λ showed a variation in phage titer of 0.5 to 1 $\log_{10}$-fold compared to the titer at T_0. Again, no significant reduction in the titer was observed. In contrast to this, CL31 infecting *C. glutamicum* MB001 showed a strong reduction in phage titer when incubated with SM from *S. tenebrarius*. In the *S. tenebrarius* SM no more plaques could be observed after 6 hours of incubation for both 2- and 3-day-old SM and after 24 hours of incubation in 1-day-old SM, indicating an extracellular anti-phage effect for this combination of phage and SM. None of the other tested SM showed any significant reduction in titer with CL31. The dotted line at 10^0

indicates the starting titer measured at T_0 of the pre-incubation experiment, which was conducted
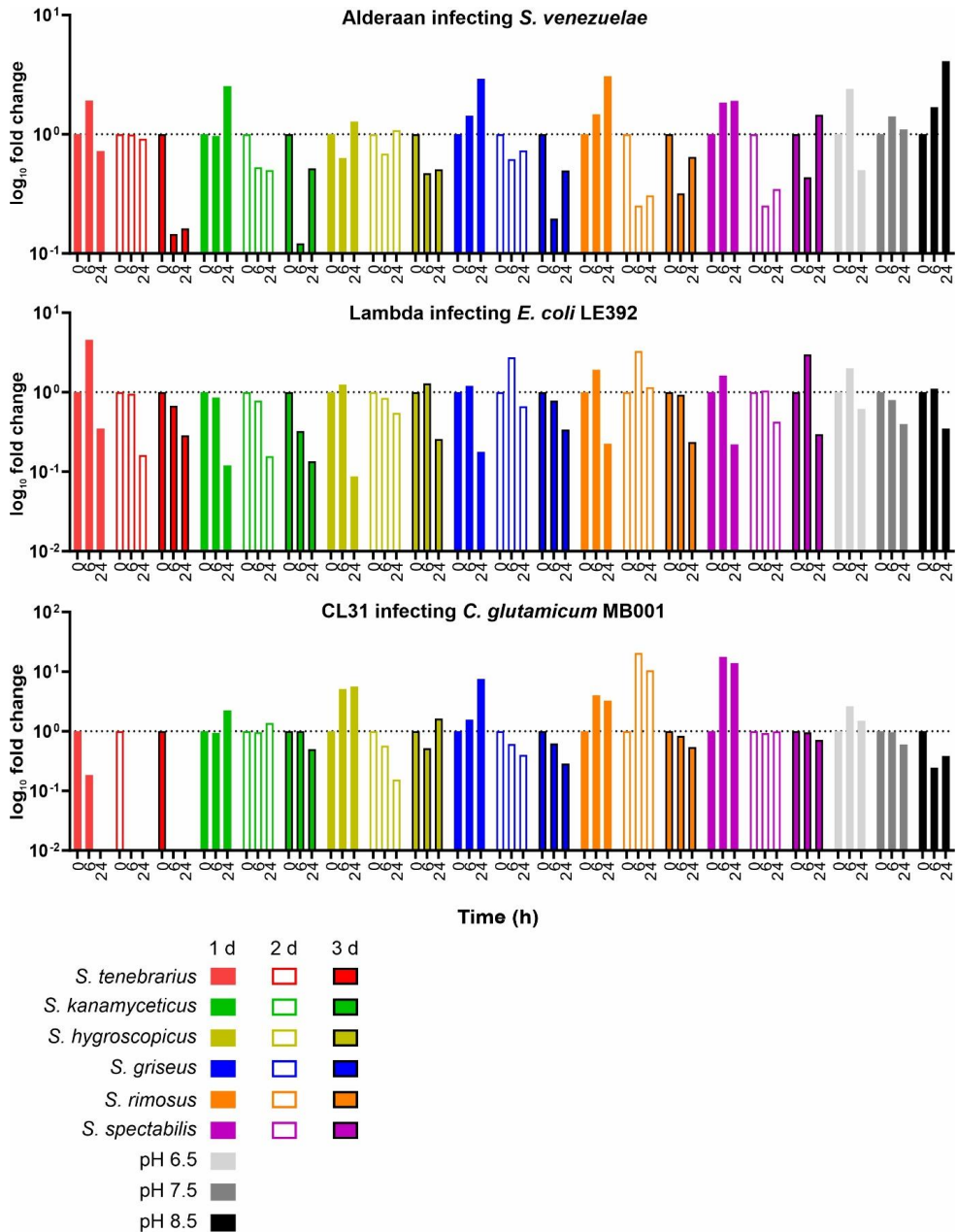
Figure 13: Inactivation of free phage particles by *Streptomyces* spent medium. Log$_{10}$-fold change of phage titer normalized to T_0 is depicted for the phages Alderaan, λ and CL31 (top to bottom) after incubation in different spent media. The dotted black line represents the phage titer at T_0. Spent medium of *S. tenebrarius* (red), *S. kanamyceticus* (green), *S. hygroscopicus* (yellow), *S. griseus* (blue), *S. rimosus* (orange) and *S. spectabilis* (purple) were harvested after 1 (fully coloured), 2 (coloured outline) and 3 days (black outline filled with colour) and phage particles were incubated over a course of 24 hours. GYM medium with pH of 6.5 (light grey), 7.5 (dark grey) and 8.5 (black) were used as control. The change in tire is shown for 0 h, 6 h and 24 h of incubation. n = 2 independent biological replicates.

with biological duplicates.

3.1.6 Extracellular anti-phage effect of *S. tenebrarius* spent medium on phage CL31

After observing that *S. tenebrarius* SM did indeed have an extracellular effect on the infectivity of CL31 after pre-incubation for 6 hours, the next step was to investigate what happened to the phage particle so that it did lose its ability to infect the host cell. In order to distinguish, whether it is solely the produced apramycin in the SM or another component produced by *S. tenebrarius*, two mutants of the apramycin synthesis pathway were included in the pre-incubation assay, Δ*aprP* and Δ*aprQ* (Zhang et al., 2021). The pre-incubation assay was repeated with CL31, incubated in SM of the three *S. tenebrarius* strains harvested after 1, 2 and 3 days of cultivation, as well as GYM medium supplemented with 50 µg/mL apramycin, GYM medium supplemented with 5 mM $MgCl_2$, and pure GYM medium as control. This time the pre-incubation assay was coupled to a quantitative real-time PCR to determine the CL31 DNA concentration during the incubation period. Furthermore, samples of the CL31 24 h incubation in 3-day-old wild type SM and GYM medium were used for transmission electron microscopy (TEM) analysis to monitor the integrity of the phage particle. In Figure 14A the phage titer as well as the phage DNA concentration is shown for 0 h and 24 h of incubation in SM. The previously observed phenotype of strong phage titer reduction after incubation in *S. tenebrarius* wild SM was reproduced here with titer reductions of 10^3 in 1 day old SM and 10^8 in 2- and 3-day old SM. The reduction in CL31 DNA concentration was less than the plaque forming units indicated by the black circles. However, a reduction of at least 2 $\log_{10}$-folds was determined. For incubation in SM of the apramycin-production deficient strains, only minor reductions in the phage titer were observed, of 10^1 for Δ*aprP* and Δ*aprQ* regardless of the time point of SM sampling. Furthermore, the phage DNA concentration correlated with the phage titer, which showed only minor effects of these SM on the infectivity of CL31 particles. The control treatment of apramycin supplemented GYM medium showed no reduction in titer or DNA concentration. In the two control treatments with 5 mM $MgCl_2$ and pure GYM medium the phage titer decreased about 3 $\log_{10}$-folds, however the DNA concentration remained stable. Phage particles incubated in 3-day-old wild type SM were visualized using a TEM to investigate the particle integrity. Figure 14B shows CL31 incubated for 0 hours in 3-day-old SM with a magnification of 92k. Figure 14C and D CL31 incubated for 24 h in 3-day old SM was imaged with a magnification of 45k and 92k respectively, and Figure 14E shows the control CL31 incubated for 24 h in pure GYM medium at a magnification of 92k. In the TEM images it is clearly visible that phage particles were degraded after 24 h incubation in the 3-day-old SM, as phage capsids are disconnected from the tails and the phage tails clump together in bundles. No such disruption can be observed in the control incubation in GYM medium (Figure 14E), where intact phage particles with DNA filled capsids can be found, similar to the starting point of the incubation in SM (Figure 14B). Overall, these

results confirm that only SM of the *S. tenebrarius* wild type has an extracellular anti-phage effect on phage CL31, in this particular case by disrupting the phage particle integrity.
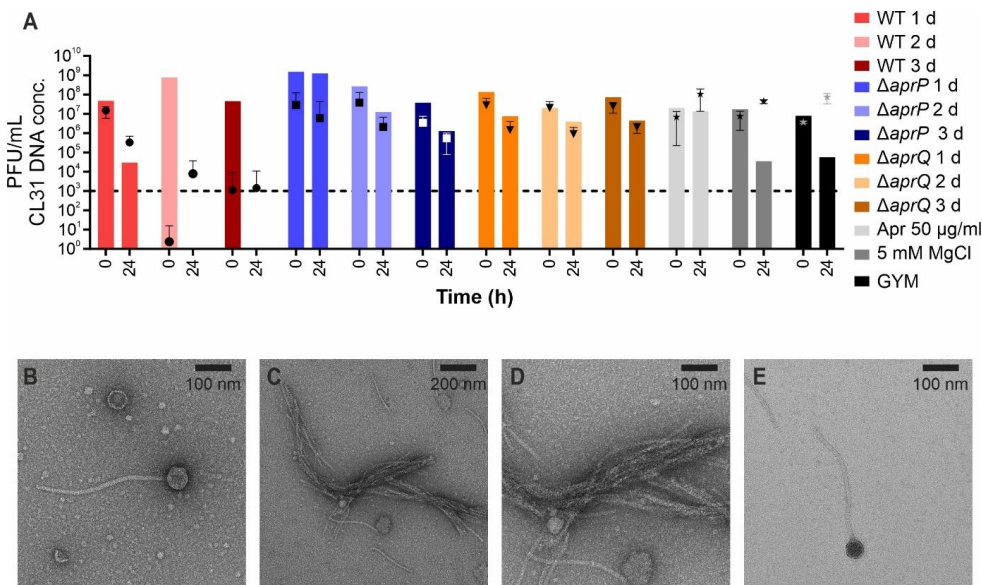
Figure 14: Effect of *S. tenebrarius* spent medium on CL31 phage particle integrity. A) Phage titer in PFU/mL and DNA concentration of CL31 are depicted in a bar graph where the coloured bar represents the phage titer in PFU/mL and the symbol with error bars the DNA concentration measured with the qPCR at the respective time point post incubation in the different spent media. Spent medium of *S. tenebrarius* wild type (red) and the two mutants Δ*aprP* (blue) and Δ*aprQ* (orange) were tested when harvested after 1 (bright colour), 2 (light colour) or 3-days (dark colour) of cultivation. As control GYM medium supplemented with 50 µg/mL Apramycin (light grey), 5 mM $MgCl_2$ (dark grey) or pure (black) were tested. Time of sampling is shown on the x-axis in hours, n= 2 independent biological replicates and 2 technical replicates for the qPCR. B) TEM image of CL31 incubated in 3 d *S. tenebrarius* WT SM for 0h, 92 k magnification, C) TEM image of CL31 incubated in 3 d *S. tenebrarius* WT SM for 24 h at a 45 k magnification. D) Zoom in of image C with 92 k magnification, E) TEM image of CL31 incubated in pure GYM medium for 24 h at 92 k magnification.

3.2 Isolation and characterization of new *Streptomyces* phages

Phage research in *Streptomyces spp.* has long focused on the development of new genetic tools and the usage of this knowledge to construct new integrative plasmids or identify RM systems (Jensen et al., 1998; Smith, Burns, Wilson, & Gregory, 1999; Smith et al., 2013). In recent years the focus of phage biology shifted more to the interaction between phage and host bacteria and is enhanced with increased diversity of phages that are isolated, characterized and readily available (Hardy et al., 2020; Hatfull, 2015). In order to broaden our understanding of *Streptomyces* interaction with phages the isolation of new phages is a prerequisite. In this part of the work four novel phages infecting three different *Streptomyces* species were isolated, fully characterized and subsequently deposited for public use at the DSMZ (German Collection of Microorganisms and Cell Cultures).

Results that are shown in this section have been part of the master thesis of Isabelle Mohnen which was supervised as part of this doctoral thesis and are published as "Isolation and characterization of

the new *Streptomyces* phages Kamino, Geonosis, Abafar and Scarif infecting a broad range of host species" in Microbiology Spectrum by Rackow et al (Rackow et al., 2024).

3.2.1 Bacteriophage isolation and morphology

Four novel phages infecting different *Streptomyces* species were isolated from soil. Phage Kamino was isolated on *S. kasugaensi*s as host, Geonosis on *S. griseus*, as well as Abafar and Scarif on *S. coelicolor* as isolation host. Phage Kamino forms small, turbid plaques (Figure 15A) with a plaque area of approximately 0.3 mm^2; the plaque size is relatively constant over 48 hours of incubation (Figure 15B). Phage Geonosis forms round and clear plaques with sharp edges (Figure 15A) and a plaque area of approximately 4 mm^2 after 24 h of incubation, which increases up to 38 mm^2 on average after 72 hours of incubation (Figure 15B). The *S. coelicolor* infecting phages Abafar and Scarif show an overall similar plaque size as Geonosis with average plaque areas of 4.2 and 4.0 mm^2, respectively, after 24 hours incubation. Abafar and Scarif also show an increase in plaque area over the course of 72 hours up to an average plaque area of 17 and 21 mm^2 (Figure 15B). Additionally, around the plaques of Abafar and Scarif enhanced production of actinorhodin and undecylprodigiosin was observed by the

formation of coloured halos around the plaques (Figure S3), which has been described in previous studies reporting *S. coelicolor* phages (Hardy et al., 2020; Kronheim et al., 2023) (Figure 15A).
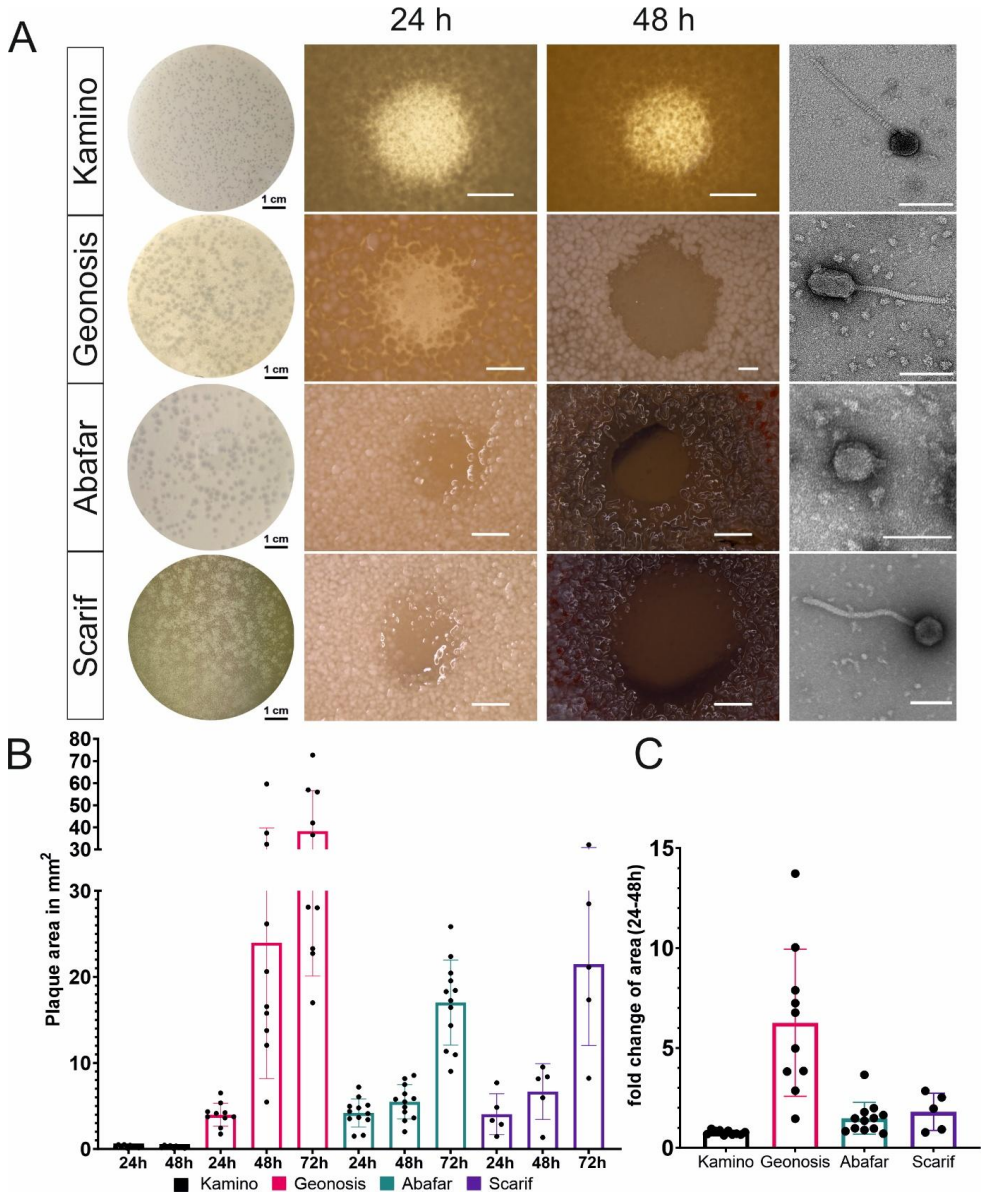
Figure 15: Morphological comparison of plaques and virions. A) Plaque and TEM images of the tested phages with an overview image of a plate with plaques 24 h post infection, a plaque close up image 24 h and 48 h post infection and a TEM image of the virion from left to right respectively for the phages Kamino, Geonosis, Abafar and Scarif from top to bottom. The scale bar for the overview images is 1 cm in length, for plaque close ups the scale bar is 1000 µm and for TEM images 100 nm. B) Comparison of the development of plaque area over time of 24-72 hours post infection with plaque area shown in mm^2 for the phages Kamino (black, n= 10) Geonosis (pink, n= 10), Abafar (turquoise, n= 12) and Scarif (purple, n= 5). C) Fold change of plaque area between 24 h and 48 h post infection for all four phages in the same colour as graph B.

3. Results

TEM imaging of the phage particles revealed that phages Kamino, Geonosis and Scarif belong to the morphotype siphovirus with Kamino and Scarif showing an icosahedral capsid and Geonosis an elongated head (B3 morphotype). All three display a long, non-contractile tail, whereas phage Abafar features a podoviral morphotype, showing an icosahedral capsid with a very short tail (Figure 15A right column). Details on capsid and tail length are provided in Table 8.

Table 8: Morphological comparison of virions

Phage	Tail length [nm]	Capsid length [nm]	Capsid diameter [nm]
Kamino (n=13)	223.4 (+/- 7.1)	63.5 (+/- 2)	61.5 (+/- 1.4)
Geonosis (n=15)	176.5 (+/- 4.4)	88.6 (+/- 4.8)	53.8 (+/-3.0)
Abafar (n=30)	16 (+/- 2)	60 (+/- 3)	61 (+/- 2)
Scarif (n=30)	254 (+/- 10)	69 (+/- 4)	65 (+/- 3)

3.2.2 Infection curves of bacteriophages

In order to assess phage infection dynamics, phage infections in liquid cultures on the original host strain were performed. As it is not suitable to perform one-step growth curves with *Streptomyces* spp. due to the multicellular development, the host strains were cultivated in microtiter plates in presence of different phage titers. Cell growth was monitored by backscatter measurements in 15 minutes intervals over the course of 24 hours and phage propagation was determined by taking samples from the culture supernatants every 2 hours to determine the titer of infectious phage particles at the respective time (Figure 16). Infections with phage Kamino and phage Geonosis lead to a complete culture collapse of their respective hosts, *S. kasugaensis* and *S. griseus,* with a starting titer as low as 10^2 PFU/mL. The titer of Kamino and Geonosis increased steadily and reached final titers of 10^6 to 10^9 PFU/mL for Kamino and 10^{10} to 10^{11} PFU/mL for Geonosis. On high titers (10^7), however, little to no amplification was observed for phage Kamino. In contrast, phages Abafar and Scarif showed little to no growth defect in their host strain. Amplification of Abafar and Scarif could only be observed in spot assays, determining the phage titer over time. In case of phage Abafar, amplification in liquid was first observed for a starting titer of 10^4 PFU/mL and for phage Scarif at a starting titer of 10^5 PFU/mL, which indicates a probably lower burst size and decreased infectivity compared to Geonosis and Kamino. While the final titer determined for phages Kamino and Geonosis appeared independent from the starting titer, final titers drastically increased for Abafar and Scarif, when infection was initiated with higher starting titers. Under the specified conditions, Abafar achieved final titers of 10^6 to 10^{12} PFU/mL 24 h post infection while Scarif achieved titers between 10^4 to 10^6 PFU/mL. Altogether, the four

phages are able to propagate in liquid cultures to different extents. Abafar and Scarif however reached higher titers when the lysate is prepared on plates. For phage Abafar and Scarif it can also be observed that the phage titer in the spot assay does not necessarily correlate with the added phages. This
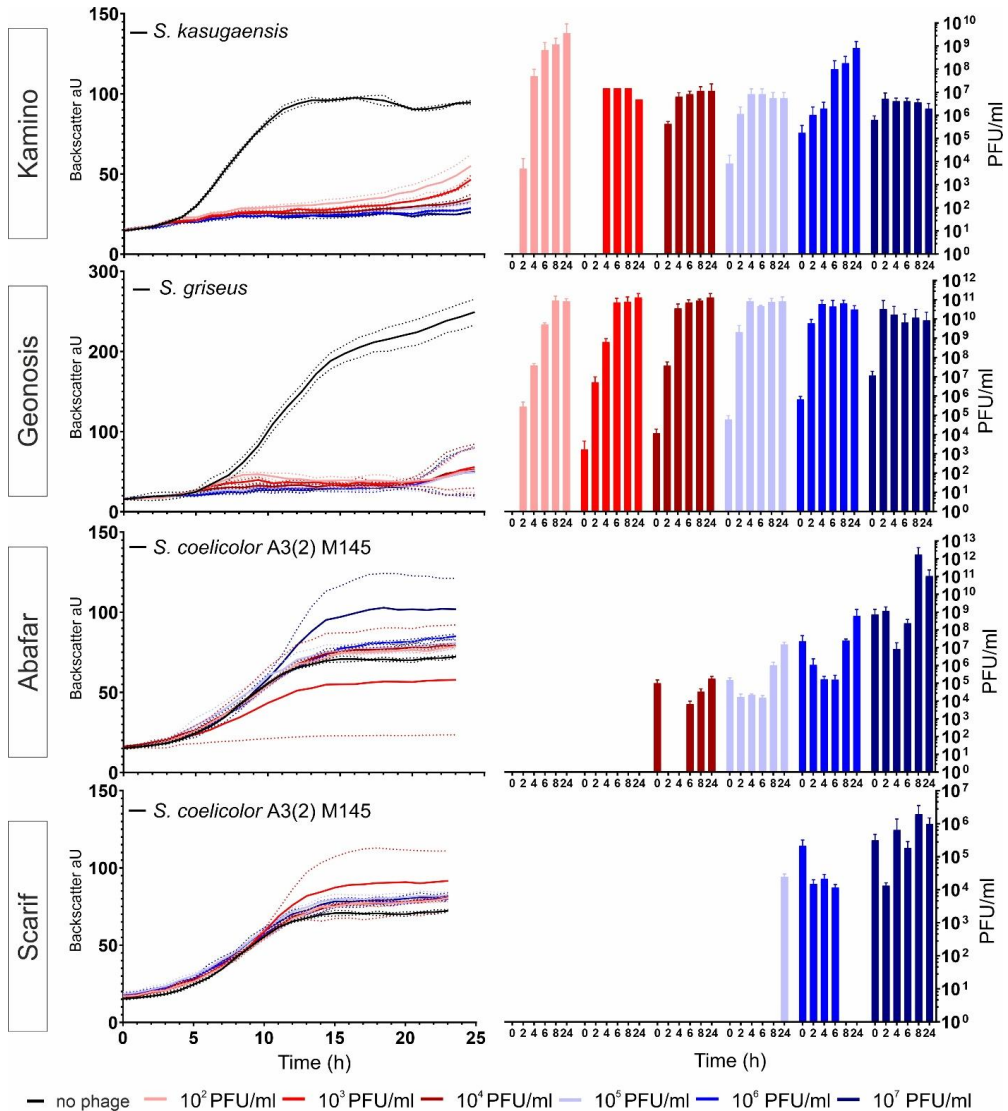
Figure 16: Infection curves of the four phages on their isolation host *S. kasugaensis* infected by Kamino, *S. griseus* infected by Geonosis and *S. coelicolor* A3(2) M145 infected by Abafar and Scarif. *S. kasugaensis* and *S. griseus* were inoculated to GYM medium and *S. coelicolor* was grown in YEME medium. All strains were cultivated in microtiter plates and infected with increasing titers of the respective phages. In the left panel, the backscatter is plotted against time to visualize growth of the bacterial culture. In the right panel phage titer at different time points throughout the infection (2/4/6/8 and 24 h) are shown. The colours of the growth curves and the bar plots for the phage titer correlate to the same initial infection titer between 10^2 to 10^7 PFU/mL, the black curve indicates growth of the host bacterium in absence of phages. n= 3 independent biological replicates. Dotted lines or error bars in the respective colours indicates the standard deviation. (Graph adapted from Rackow et al. 2024)

phenomenon might be explained by the complex growth of the host bacterium *S. coelicolor.* We hypothesise that the mycelial structures of the host might trap free phages without being infected and thereby lowering the phage titer in the supernatant.

3.2.3 Host Range of phage isolates

One physiological trait that is important to consider when using or studying phages is the range of bacterial hosts they are able to infect. In this study, we determined the host ranges of the novel phage isolates by spotting serial dilutions of the phages on lawns of >40 different *Streptomyces* species (Table S2). A distinction must be made between the simple lysis of bacteria and the ability to cause a productive infection, because only the latter leads to the formation of individual plaques (Figure 17). From the four phages described in this study, phage Kamino has the broadest host range with lawn clearance on 22 *Streptomyces* spp. and productive infections on 15 different species among the 45 species tested (Table S2, Figure 17). The efficiency of plating (EOP) refers to the ratio of plaques formed on the host used for isolation compared to another host species. While phage Kamino is able to infect a wide variety of host strains, the EOP ranges from 0.002 % on *S. olivaceus* up to 5000 % on *S. afghaniensis* (Table 9). The phages Abafar and Scarif have the same range of productive infections with 7 different species but differ in their lawn clearance, where Abafar shows clearance on 12 species and Scarif only on 10 (Figure 17). Phage Abafar displays an EOP lower than 100 % on the alternative hosts. Scarif however, reaches EOP's up to 8000 % on *S. afghaniensis* (Table 9). In contrast to these broad host-range phages, phage Geonosis is only able to infect two different *Streptomyces* species, its isolation host *S. griseus* and one additional host, *S. olivaceus* with an EOP of 0.15 %, which classifies
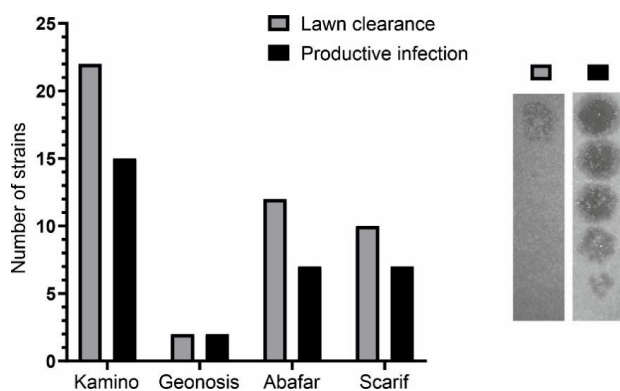
Figure 17: Distribution of productive infection (black) versus lawn clearance (grey). On the right are exemplary images of lawn clearance and productive infection of phage Scarif on *S. coelicolor*.

Geonosis as a narrow host-range phage in this context (Table 9, Figure 17). Out of the 45 tested *Streptomyces* species, 15 have previously been phylogenetically analysed (Nouioui et al., 2018) and no pattern of phylogenetic relatedness and host range could be observed. Furthermore an analysis of

the defense system repertoire of several of the tested strains was performed using PADLOC (Table S4) and also here no distinct pattern of defense systems could be detected which would render the host more resistant to phage infection by the here described broad host range phages (Nouioui et al., 2018).

Table 9: Host range of the *Streptomyces* phages Kamino, Geonosis, Abafar and Scarif with Efficiency of plating in %. Underlined numbers indicate the isolation host and bold numbers indicate productive infection.

	Kamino	Geonosis	Abafar	Scarif
Streptomyces afghaniensis	**5000**	0	**16.67**	**8000**
Streptomyces coelicolor A3(2) (host)	**6.36**	0	<u>100</u>	<u>100</u>
Streptomyces antibioticus	0	0	**2**	0
Streptomyces celluloflavus	0	0	0	**2**
Streptomyces chartreusis	0	0	0	**2**
Streptomyces fradiae	**139.39**	0	0	0
Streptomyces griseorubens	0	0	**33.33**	**2000**
Streptomyces griseus (host)	**0.07**	<u>100</u>	0	0
Streptomyces hygroscopicus	**0.15**	0	0	0
Streptomyces kanamyceticus	**0.04**	0	0	0
Streptomyces kasugaensis (host)	<u>100</u>	0	0	0
Streptomyces longispororuber	**12.5**	0	0	0
Streptomyces luridus	**2500**	0	**16.67**	**800**
Streptomyces niveus	**37.5**	0	**16.67**	0
Streptomyces nodosus	0	0	0	**0.2**
Streptomyces olivaceus	**0.006**	**0.15**	0	0
Streptomyces purpurascens	**2500**	0	**33.33**	0
Streptomyces rimosus	**0.05**	0	0	0
Streptomyces venezuelae	**0.02**	0	0	0
Streptomyces viridosporus	**1250**	0	0	0

3.2.4 Comparison of genomes

Phage DNA of all four phages was isolated and sequenced using Illumina short read sequencing. Reads were assembled and contigs were annotated using Prokka with implemented PHROG analysis (Table 10). Prediction of the phage lifestyle was performed with the machine-learning tool PhageAI (Tynecki et al., 2020) with 93.8 % confidence for a temperate lifestyle of Kamino and 93.5 %, 95.0 % and 73.6 % confidence for Geonosis, Abafar and Scarif having a virulent lifestyle, respectively.

Table 10: Summary of genomic features of the four *Streptomyces* phages.

Phage name	Host	Genome size (bp)	GC content (%)	Number of ORFs	CDS coding density (%)	Lifestyle prediction	Taxonomy
Kamino	*Streptomyces kasugaensis* DSM 40819	49,381	65.4	73	92.5	temperate	*Caudoviricetes Arquatrovirinae Camvirus,* "Camvirus kamino"
Geonosis	*Streptomyces griseus* DSM 40236	57,039	68.9	69	90.2	virulent	*Caudoviricetes,* "Woodruffvirus geonosis"
Abafar	*Streptomyces coelicolor* A3(2) DSM 112524	43,704	60.2	58	85.8	virulent	*Caudoviricetes, Beephvirinae, Manuelvirus,* "Manuelvirus abafar"
Scarif	*Streptomyces coelicolor* A3(2) DSM 112524	55,306	59.1	83	93.3	virulent	*Caudoviricetes,* "Scarifvirus", "Scarifvirus scarif"

The genome of phage Abafar consists of 43,704 bp (GC% 60.2) with 58 predicted open reading frames (ORF) and 15 genes for tRNAs (Figure 18), 27 of the 58 ORF's are annotated genes (46 %). BLASTn analysis against NCBI database for viruses (taxid: 10239) identified four closely related phages, classified members of the genus *Manuelvirus*. All of them share a similar genome organization with functional gene clusters for packaging, and structural proteins with an embedded gene for a putative endolysin between the genes encoding the terminase large subunit and a portal protein (Figure S4). The cluster for replication contains conserved genes coding for a primase, a helicase and different

nucleases. No genes related to lysogeny were identified, which is in line with the prediction of Abafar being virulent.
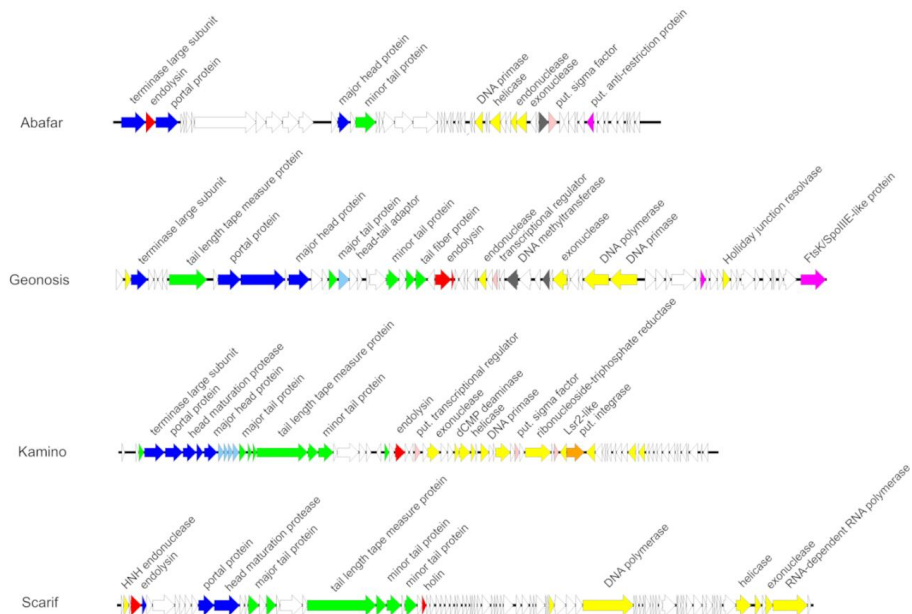
Figure 18: Annotated genomes of phages Abafar, Geonosis, Kamino and Scarif. Phage Abafar encodes 58 ORF's, Geonosis 69 ORF's, Kamino 91 ORF's and Scarif 83 ORF's which are indicated by differently coloured arrows. Colouring is based on the PHROG colour code for functional clusters (Terzian et al., 2021) (orange: integration and excision; blue: head and packaging; purple: transcription; light blue: connector; green: tail; red: lysis; yellow: DNA, RNA and nucleotide metabolism; pink: moron, auxiliary metabolic gene and host takeover; dark grey: other).

Phage Geonosis has a genome size of 57,039 bp with an average GC content of 68.3 % comprising 69 ORFs but no tRNA genes (Figure 18), 24 of the ORF's are annotated genes (34.7 %). Comparison with other related Woodruffviruses like phage YDN12 (Donegan-Quick et al., 2017) revealed a similar genome organization with gene clusters for packaging, structural head and tail proteins, lysis comprising endolysin and holin genes and replication containing characteristic genes for an endonuclease, a DNA methyltransferase, an exonuclease, a DNA polymerase and a DNA primase (Figure S5). Furthermore, phage Geonosis also harbours genes for a putative Holliday junction resolvase and an FtsK-like protein, respectively, that might also be used during replication.

Phage Kamino features a genome size of 49,381 bp with an average GC content of 65.4 % harbouring 73 ORFs, of which 33 ORF's are annotated genes (45.2%), but no tRNA genes were found (Figure 18). BLASTn analysis identified related phages of the genus *Camvirus* like Endor1 (Hardy et al., 2020), phiCAM (Monson & Salmond, 2012), Verabelle or Vanseggelen (Ongenae et al., 2023). All of them

share the same genome organization with characteristic gene clusters for structure, replication and lysis (Figure S6). In contrast to the other three isolated phages, phage Kamino harbors a gene for a serine integrase (Kamino_00049) and additional genes putatively involved in transcriptional regulation (Kamino_00029, Kamino_00043 and Kamino_00046), which is in line with the AI prediction of a temperate lifestyle.

Genomic analysis of phage Scarif revealed a genome size of 55,306 bp (GC%: 59.1) with 89 predicted ORFs, of which 18 are annotated (20.2 %), organized in characteristic clusters for replication including genes for a DNA polymerase, a helicase, an exonuclease or an RNA-dependent RNA polymerase and for head and tail structure comprising genes for a portal protein, minor and major tail proteins and a tail length tape measure protein (Figure 18). Given that this protein determines the tail length of the phage and assuming a tail length of 1.5 Å per amino acid residue, the calculated length (~274 nm) fits to range of the size which was measured via electron microscopy (Katsura & Hendrix, 1984). Generally, phage Scarif shares this genomic organization with phages belonging to the genus *Rimavirus* (Figure S7).

VIRIDIC analysis (Suppl. Table 3**)** (Moraru, Varsani, & Kropinski, 2020) identified phages Abafar, Geonosis and Kamino as putative new species within the genera *Manuelvirus*, *Woodruffvirus* and *Camvirus*, respectively, according to the ICTV rules with 95 % and 70 % nucleotide sequence identity over the length of the genome as species and genus demarcation criteria, respectively (Adriaenssens & Brister, 2017; Krupovic et al., 2021). In contrast, based on this analysis, phage Scarif forms a new genus that we suggest to call "Scarifvirus".

3.3 Screening of potential anti-phage defense small molecules

In the following chapter of this work, the screening of potential anti-phage defense small molecules is shown. For individual phages an inhibitory effect of small molecules has been reported (Kever et al., 2022; Kronheim et al., 2018), chemical defense however has not been investigated in a systematically comparative study. In order to identify whether chemical defense is dependent on phage specific features or rather on the host bacterium used, screenings were performed which systematically tested the effect of small molecules on the phage infection of two distinct collections of phages. On the one hand, 16 *Streptomyces* phages were used, infecting different *Streptomyces* species. On the other hand, the *E. coli* BASEL (BActeriophage SElection for your Laboratory) (Maffei et al., 2021) collection, consisting of 69 phages all infecting the same *E. coli* strain. These collections of phages were screened on different small molecules, which are known to harbour anti-phage defense properties in order to elucidate a possible pattern of the respective defense mechanism and understand more of the mechanism of action.

3. Results

3.3.1 Screening of *Streptomyces* phages on small antiphage molecules

Investigation of chemical defense mechanism on ecologically relevant *Streptomyces* phages, since the antiphage molecules reported so far are produced by *Streptomyces spp.,* was conducted by screenings on double-agar overlays with increasing concentrations of the small molecule of interest, visualized in Figure 19A. The small molecules of interest here were apramycin, an aminoglycoside antibiotic produced by *S. tenebrarius*; actinomycin D, a peptide antibiotic produced by *Streptomyces galbus;* and daunorubicin, an anthracycline produced by *Streptomyces peucetius* (Figure 19B). Since the mechanism of action of these small molecules for bacterial and eukaryotic cells is known, apramycin is classified as a 16S rRNA targeting translational inhibitor and actinomycin D as well as daunorubicin are described as DNA intercalating agents. It is important to note, that the screening on apramycin was performed on host strains carrying an antibiotic resistance plasmid (pIJLK04, see Table 3) whereas screening on actinomycin D and daunorubicin was performed on wild type strains, as no resistance cassettes are readily transformable for those molecules. For daunorubicin the self-resistance mechanism of the producer strain *S. peucetius, drrABC* is known and described, however it was not possible to introduce and express this resistance mechanism into the host strains used here (Kaur & Russell, 1998; Prija & Prasad, 2017; Stutzman-Engwall & Hutchinson, 1989). In order to understand phage sensitivity determinants on those small molecules, 16 *Streptomyces* phages infecting four different *Streptomyces* species were screened in double-agar overlay spot assays. Specifically the phages included Alderaan, Coruscant, Mandalor, and SV1 infecting *S. venezuelae,* ΦA.Streptomycini III (Prauser & Köhler, 1965), P26 (Korn, Weingärtner, & Kutzner, 1978), Ankus, DekoNeimoidia, and Geonosis infecting *S. griseus,* Dagobah, Endor I, Abafar, Scarif, and Kamino infecting *S. coelicolor* M145 as well as S7 (Prauser, 1976), and Φ8238 infecting *S. olivaceus.* The heat map in Figure 19C shows the change in phage titer as reaction to increasing small molecule concentrations normalized to the phage titer on pure GYM-agar plates in $\log_{10}$-folds, grey areas in the heat map indicate a lack of bacterial growth. For apramycin, all *S. venezuelae* infecting phages showed a reduction in titer with increasing concentrations, Alderaan and SV1 a reduction in titer of up to 10^8 at a concentration of 25 µg/mL (see Figure 19C). Coruscant and Mandalor showed a slightly less strong phenotype with reductions of 10^5 and 10^4 respectively at a concentration of 50 ng/µL (see Figure 19B). The remaining phages that showed plaques on apramycin up to a concentration of 25 µg/mL exhibited only a minor reduction in titer. Specifically, ΦA. Streptomycini III and P26 had a reduction in titer of 10^1, Geonosis titer was not reduced, and Abafar, Scarif and Kamino showed a titer reduction of 10^3, 10^2 and 10^1 respectively (Figure 19B). On actinomycin D all phages except for Scarif and Kamino had a reduced titer on the highest concentration of 6 µM. The strongest reduction in titer was observed for the phages DekoNeimoidia, S7 and Φ8238 with a reduction of 10^5 to 10^6. All remaining phages showed a titer

reduction of at least 10^1 (Dagobah and P26) up to 10^4 (SV1 and Ankus), indicating a broad anti-phage defense effect of actinomycin D on the *Streptomyces* phages tested here. A similar phenotype can be observed for the phages screened on daunorubicin. Here, all phages, except for ΦA. Streptomycini III and P26, showed a reduction in titer on the highest concentration of daunorubicin they were screened on. The strongest reduction in titer was observed for Mandalore with a reduction in titer of 10^5 at a concentration of 6 µM, the remaining phages that showed plaques at 6 µM showed a reduction in titer of 10^1 to 10^4. Phages that only showed plaques on 1 µM daunorubicin were reduced in titer by 10^1 to 10^3. Similar to actinomycin D, daunorubicin seems to present a broad anti-phage defense spectrum with a comparably less strong effect on the single phage as apramycin on the *S. venezuelae* phages. Representative images of the spot assay of *S. venezuelae* phages are shown in Figure S8 depicting the reduction in phage titer for all anti-phage molecules shown here. Generally speaking,

the screening of anti-phage defense small molecules showed a phage specific sensitivity towards small molecules, as there was no distinct pattern to be observed.
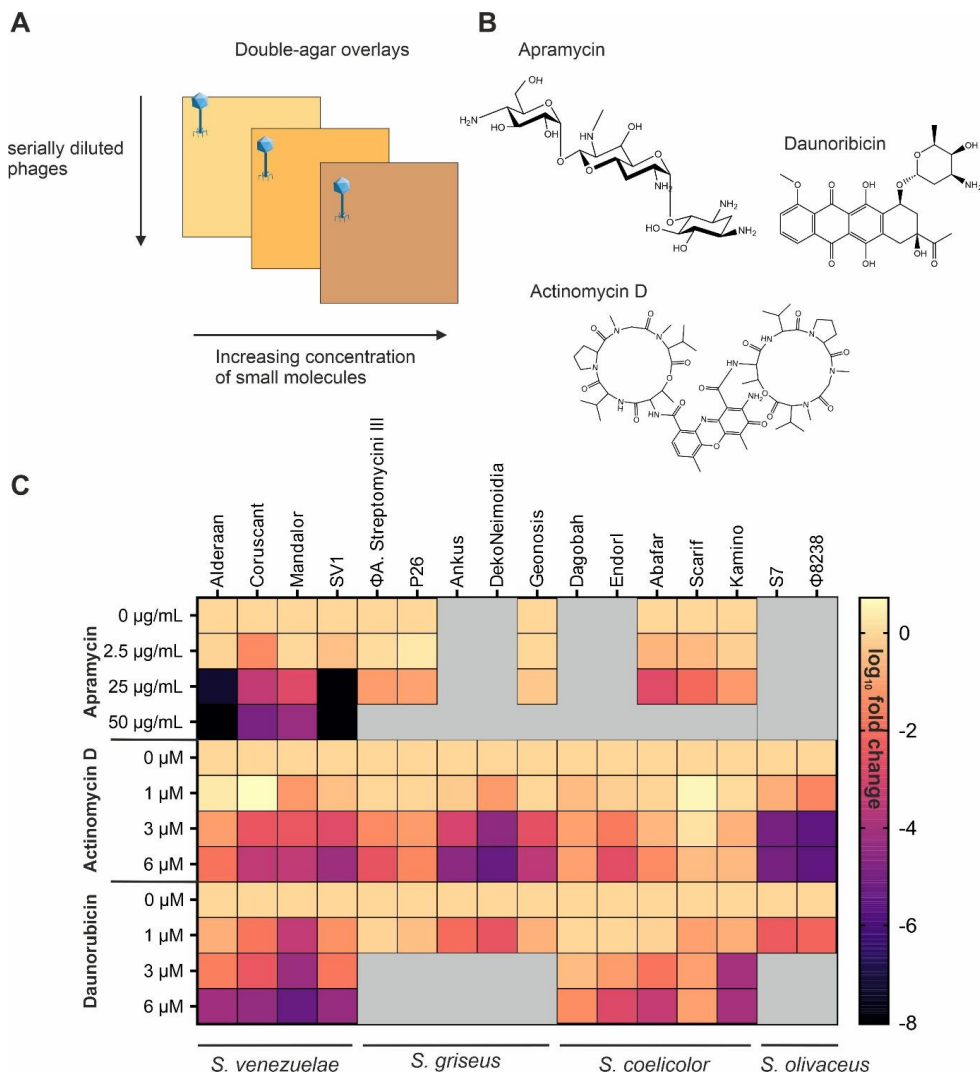
Figure 19: Screening of *Streptomyces* phages on small molecules known to mediate anti-phage defense. A) A general scheme of the screening experiment of double-agar overlay spot assays with increasing concentrations of small molecules and decreasing concentrations of phages. B) Chemical structure of small molecules used in this experiment, apramycin (an aminoglycoside), daunorubicin (an anthracycline), and actinomycin D (a peptide antibiotic), the chemical structure was drawn with ChemDraw 22.2.0. C) Heat map depicting the $\log_{10}$-fold change in phage titer normalized to the titer at concentration 0. On the left side, the rows of the heat map are described with the respective molecule and concentration, on top, the columns are named with the respective phage tested and on the bottom is the respective host strain the phage was infecting during the experiment. The legend on the right shows the colour code for the change in phage titer as $\log_{10}$-fold change. n = 2 independent biological replicates. Experiments were performed on GYM double-agar overlay plates with the same concentration of small molecules in both layers of agar.

3. Results

3.3.2 Screening of BASEL collection on small antiphage molecules

To identify phage sensitivity determinants to anti-phage defense small molecules a more sophisticated phage collection was additionally screened on previously known anti-phage small molecules. The BASEL phage collection was used here to increase the diversity of phages tested on the small molecules while simplifying the bacterial background by using the *E. coli* K12 MG1655 ΔRM strain, which is devoid of all restriction-modification systems, as well as the PifA and RexAB Abi systems, as well as the O-antigen glycan barrier (Maffei et al., 2021). This strain allows to directly identify the effect of small molecules on phage infection without interference of the native bacterial immune system. The molecules screened here are apramycin and kanamycin as representatives of aminoglycoside antibiotics and actinomycin D and daunorubicin as DNA intercalating agents. The screening was performed in the same way as described before and the heat map in Figure 20 shows the logarithmic reduction in phage titer as a response to the small molecule. Furthermore, the distribution of the GC-content in % as well as the genome size in bp is depicted in Figure 20 to better correlate these phage traits to the phenotype observed on the respective small molecule. Screening the aminoglycosides apramycin and kanamycin on the BASEL collection did not result in any significant titer reduction, only the control phage λ, showed a reduction of 10^2 and 10^3 on apramycin and kanamycin respectively, which was expected as λ was shown to be sensitive to those aminoglycosides in previous studies (Kever et al., 2022). None of the other tested phages showed such a phenotype. It is important to notice here, that the phages Bas03, Bas05 and Bas07 were not able to show plaques on the *E. coli* MG1655 ΔRM strains carrying the resistance plasmids pEKEX2.a and pEKEX2.d for kanamycin and apramycin resistance respectively (see Table 6). The screening on actinomycin D however revealed single phages that seem to be sensitive towards the anti-phage effect of this small molecule. In the screening the phages Bas14, Bas17, Bas19-Bas23, Bas25, Bas26, Bas31, Bas45, Bas60 and λ showed a reduction in titer of at least 10^1 up to 10^6 at a concentration of 20 μM actinomycin D (Figure 20). Most of the phages that showed sensitivity towards actinomycin D have a siphovirus morphotype and 9 of the 13 sensitive phages belong to the family of *Siphoviridae*. The strongest reduction in titer was observed for the phages Bas22 and Bas25 with a reduction of ~10^6, which is 3 $\log_{10}$-folds more compared to the positive control phage λ, which was previously described to be sensitive to actinomycin D (Kronheim et al., 2018). The genome size of sensitive phages ranges from 43 kbp (Bas14) to 170 kbp (Bas45) and the GC content ranges between 35.6 % (Bas45) and 54.6 % (Bas17), covering basically the complete range of both genetic traits (Figure 20, Section 6.4 Supplementary material). For daunorubicin the screening revealed a very pronounced anti-phage defense pattern. Here complete families of phages were either sensitive to the small molecule or showed complete resistance with only two exceptions to this pattern, namely Bas18 (sensitive, genus

3. Results

Dhillonvirus) and Bas24 (resistant, genus *Seuratvirus*). Otherwise, the family of *Drexlerviridae,* the subfamily of *Queuovirinae*, the family of *Demerecviridae* as well as the *Vequintavirinae,* unclassified *Myoviridae* and *Schitoviridae* showed sensitivity towards daunorubicin. The genus *Dhillonvirus,* subfamily *Tevenvirinae* and the family of *Autographviridae* however were resistant to the anti-phage effect of daunorubicin. Reduction of phage titer was observed here starting at daunorubicin concentrations as low as 1 µM for e.g. Bas01, Bas03 or Bas32. At the highest concentration of 20 µM the reduction in phage titer ranged from 10^3 to 10^8, which was the complete inhibition of phage infection (Figure 20). Resistant phage families either have a rather small genome (39-44 kbp) with relatively high GC content (50-55 %) (*Dhillonvirus* and *Autographviridae*) or a large genome (164-170 kbp) with a relatively low GC content (35-37 %) (*Tevenvirinae),* however neither genome size nor GC-content seem to correlate with daunorubicin resistance or sensitivity. Taxonomic classifications for the phages stated here are based on the original publication of the BASEL collection (Maffei et al., 2021) (Figure 3). Overall, these results suggest that daunorubicin has a broad anti-phage defense
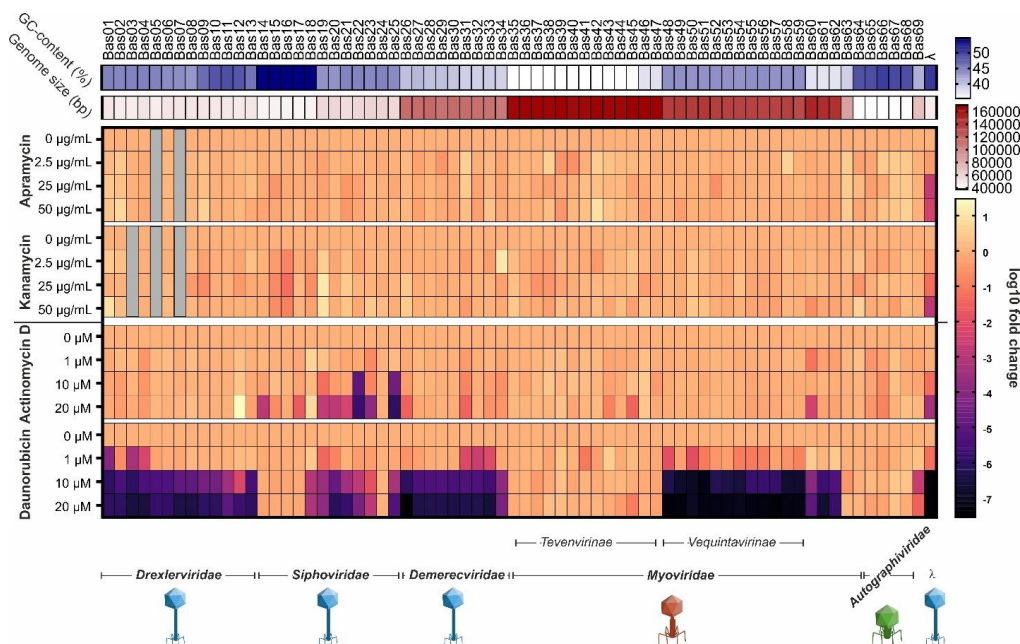
Figure 20: Screening of the BASEL phage collection on small molecules that are known to mediate anti-phage defense. Heat map of the chemical defense screening of the BASEL collection. On top of the columns the respective name of each phage is shown. The first row in shades of blue depict the GC content of each phage in % in a range from 35 to 55 % (legend on the right). The second row, in shades of red represents the genome size in base pairs (bp) in a range of 37000 bp to 170000 bp, the colour code is defined in the legend to the right. The following 16 rows show the change in phage titer normalized to the titer on concentration 0 as a log_{10}-fold change, legend on the right depicts the colour code to the responding decrease or increase in titer. Four rows for each Apramycin, Kanamycin, Actinomycin D and Daunorubicin with increasing concentrations (top to bottom) are shown and show the phage reaction to each small molecule. Below the heat map, the corresponding phage families and subfamilies are shown as well as a scheme of the respective morphotype of phage. n = 2 independent biological replicates. Experiments were performed on LB double-agar overlay plates with the same concentration of small molecules in both agar layers.

effect and that sensitivity towards small molecules is specific to the phage. In comparison of all four tested small molecules daunorubicin poses the most interesting pattern, leading to further in depth investigation on the mechanism of action in the following sections of this work.

3.4 Investigating the mode of action of daunorubicin mediated chemical defense

In the following chapter of this work, the focus is on the elucidation of the mechanism of action of the anti-phage small molecule daunorubicin. Results that are shown in this chapter were generated using different *E. coli* strains as well as a selection of phages from the BASEL collection and thoroughly studied model phages such as T4 and T7 (Maffei et al., 2021). The aim was to understand which step of phage infection is inhibited by daunorubicin and what role the genetic background of the host strain poses in the anti-phage defense of small molecules. Experiments of this section were performed in close collaboration with Dr. Larissa Kever, if experiments were conducted by Dr. Kever it will be indicated in the Figure description.

3.4.1 Transcriptome analysis of *E. coli* MG1655 ΔRM under daunorubicin pressure

Although the main host strain *E. coli* MG1655 ΔRM (Maffei et al., 2021) which was used in the investigation of daunorubicin's anti-phage defense, is expected to lack all intra-cellular anti-phage defense systems, it was essential to examine the bacterial response to the small molecule itself. In order to analyse transcriptomic changes as reaction to daunorubicin pressure, three independent biological replicates of *E. coli* MG1655 ΔRM were cultivated in presence and absence of 20 μM daunorubicin for one hour, which resembles the cultivation time in infection experiments before the phage is added to the culture. In the RNA-seq data of this cultivation, 88 genes were identified that were significantly up or downregulated when compared to the gene expression in absence of daunorubicin (FDR p-value ≤0.05) (Figure 21A). Among these 88 genes (suppl. Table S5), 39 genes were identified to be related to enzymatic pathways or transport of molecules, including the nitrogen metabolism, methane metabolism, galactose metabolism and genes associated with metabolism in diverse environments (Figure 21B). 26 of the differentially expressed genes are related to ribosomal RNA or non-coding RNA, 7 genes were related to DNA regulation or synthesis and 16 genes were clustered as "other" (Figure 21B). The differential expression of the genes is visualized in a heat map depicting the transcripts per million (TPM) for each replicate individually as well as the $\log_2$-fold change (Figure 21B). The overall expression pattern of up- and downregulated genes is plotted in a volcano-plot were expression of cultures grown in presence is compared to cultures in absence of daunorubicin (Figure 21A), red coloured dots indicate significant differential expression. It is striking to observe that RNA-related and metabolism genes are the biggest groups (~74 %) of genes that are up- or down-regulated as daunorubicin is known to intercalate into DNA, while DNA regulatory genes only make up about 8 % of the significantly differentially expressed genes. The strongest positive

3. Results

log$_2$-fold change is for the genes *insD7* (11.4), encoding for a putative transposase from the Qin prophage, as well as *rrfB* (9.5) and *rrfE* (9.5) encoding two 5S ribosomal RNA's respectively. The strongest downregulated genes are *rrfG* (-5.3), *matA* (-5.2) and *rrfD* (-4.8) encoding for two 5S ribosomal RNA's (*rrf)* and a DNA-binding transcriptional dual regulator (suppl. Table S5). Overall, the transcriptome data suggests that the culture remains fully viable in presence of the anthracycline antibiotic. However, further transcriptome data of infected cells in presence and absence of daunorubicin are needed to complete the understanding for the anti-phage defense conferred by daunorubicin.

A

MG1655 ΔRM with daunorubicin vs. without daunorubicin

B
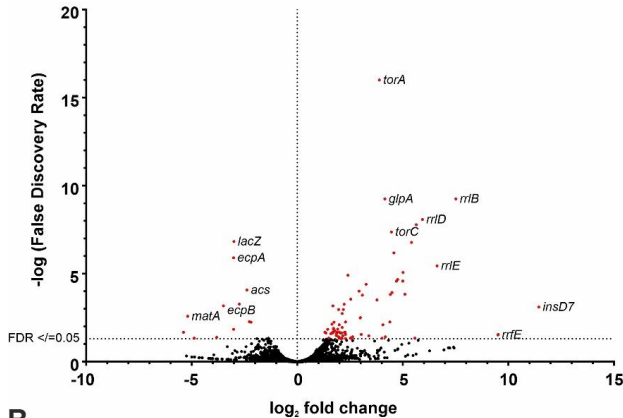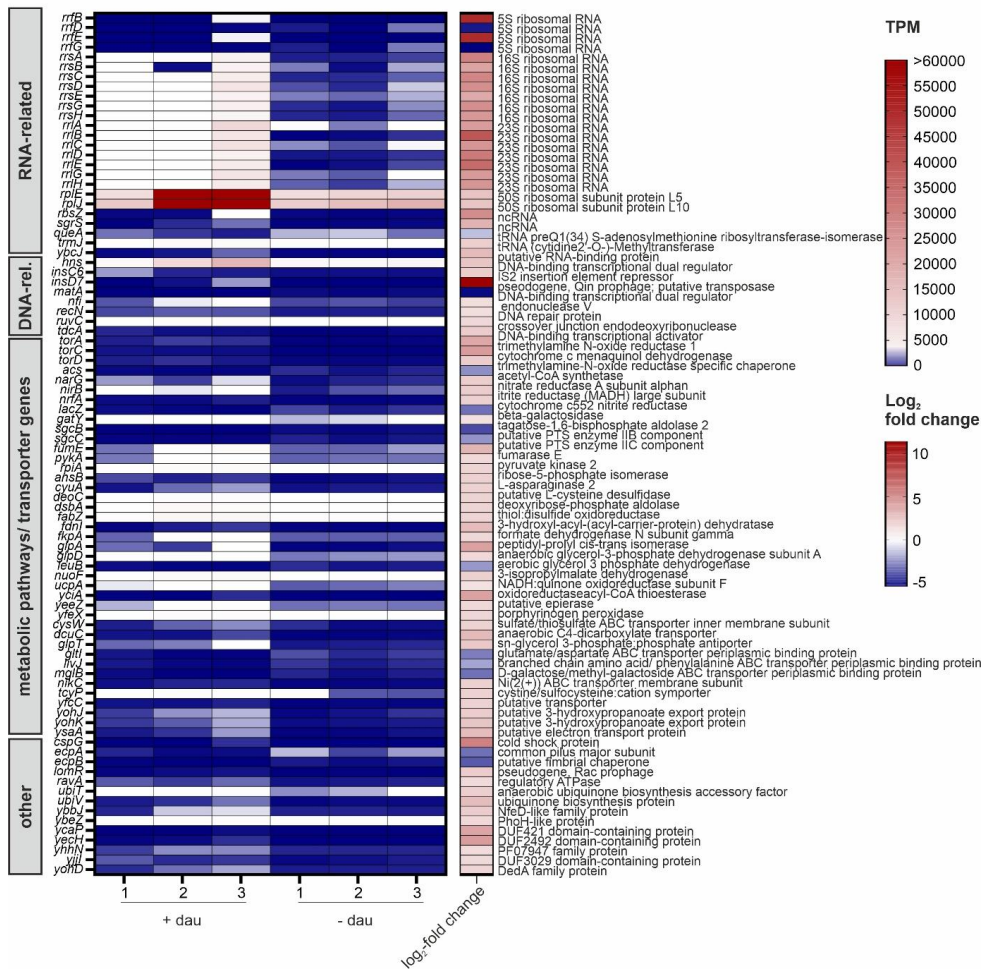
Figure 21: Transcriptome analysis of *E. coli* MG1655 ΔRM in presence and absence of daunorubicin. A) Volcano-plot of the expression pattern of *E. coli* MG1655 ΔRM showing the change in expression comparing with and without the addition of daunorubicin. On the y-axis, the negative logarithm of the false discovery rate (FDR) is depicted and on the x-axis, the $\log_2$-fold change. Each dot in the plot represents one gene, black dots are genes that are not significantly different in their expression in presence and absence of daunorubicin, and red dots are significantly differentially expressed with p-value of FDR ≤0.05. n = 3 independent biological replicates. B) Heat map of the significantly differently expressed genes, showing the transcripts per million (TPM) for each replicate (as defined below) of each gene and the $\log_2$-fold change of the respective gene when comparing the expression in presence and absence of the compound. The legends for TPM and $\log_2$-fold change are shown on the right. The names of the genes in the heat map are written on the left of each row. Genes are grouped based on their predicted or known function. The annotated function of each gene is shown on the right side of the heat map.

3.4.2 Investigation of the DNA injection of daunorubicin sensitive phages in presence and absence of the anti-phage defense small molecule

With the aim to arrow down when and where the inhibition of phage infection by daunorubicin is taking place, potassium efflux assays of *E. coli* MG1655 ΔRM infected with daunorubicin sensitive phages were conducted to determine whether the DNA injection was already impaired upon daunorubicin pressure. Previous studies described successful injection of the phage λ genome coinciding with a measurable efflux of potassium ions (Kronheim et al., 2018). It is important to notice that this behaviour was shown for single phages such as λ, T4 and T5, but not necessarily applies for all phages (Boulanger & Letellier, 1992; Keweloh & Bakker, 1984; Thompson & Wiberg, 1978). Using this technique and phage λ as a positive control, three daunorubicin sensitive phages, Bas09, Bas13, and Bas20, were tested regarding a potential potassium efflux in presence and absence of daunorubicin. The potassium efflux assays were conducted by infecting an *E. coli* MG1655 ΔRM culture at an OD_{600} of 2 with an MOI of ~6. For the Potassium efflux assays highly purified phage lysates were used (see Section 2.3.7) to ensure that no remnants of lysed cells or medium were transferred into the potassium measurement. Furthermore, growth analysis and spot assay analysis were conducted using the same conditions as in the potassium efflux assay. The liquid infection assays were performed to validate the efficiency of daunorubicin in the conditions tested and can give insights into the mechanism of action, such as abortive infections. The potassium efflux assays as well as the corresponding liquid infection experiments were performed with three independent biological replicates. Bas09 showed a similar increase of potassium efflux in presence and absence of daunorubicin with a total increase of ~ +16 mV after the addition of phages (Figure 22A) . The phages Bas13, Bas20 and λ showed an increased efflux of potassium ions upon daunorubicin pressure compared to daunorubicin free conditions with a total increase of +18 mV, +17 mV and +15 mV respectively (Figure 22 B, C & D). In absence of daunorubicin Bas13, Bas20 and λ had a considerably lower measurable efflux of potassium ions of ~ +1.5 mV, 2 mV and 4 mV respectively (Figure 22 B, C & D). The potassium efflux measured for λ did not align with data presented in the publication of Kronheim and colleagues. However in the previous study the mM concentration of Potassium ions was measured, whereas in this work the change in voltage of the medium was assessed. Furthermore, a different host strain was used by Kronheim and colleagues to assess the potassium efflux of λ, which

might explain the difference (Kronheim et al., 2018). Measuring the control of *E. coli* MG1655 ΔRM at an OD_{600} of 2 with the addition of an equal volume of SM buffer instead of clean phage lysate showed no increase in measurable mV which suggests that the measured efflux of potassium ions can be attributed to phage infection (Figure 22E). In the growth curves of the corresponding liquid infection experiment a successful phage infection could be determined for all phages tested, as the infected culture in absence of daunorubicin showed a culture collapse (Figure 22). In presence of daunorubicin however different phenotypes were observed, as for Bas13 infected cultures with daunorubicin showed a restored growth with a slightly lower OD_{600}, however, a growth increase could be observed (Figure 22B). For the cultures infected with Bas09, Bas20 and λ in presence of daunorubicin no bacterial growth was measured during the time of cultivation, suggesting an abortive infection phenotype of anti-phage defense (Figure 22 A, C & D). Uninfected cultures of *E. coli* MG1655 ΔRM showed no growth difference in presence or absence of daunorubicin (Figure 22). The corresponding plaque assay showed no significant changes in the phage titer over the course of 60 minutes, which can be explained by either the limited time for amplification or an abortive infection mechanism (Figure 22F). The results of the assay showed that none of the tested phages were inhibited in the injection of their genome by the presence of daunorubicin. These results strengthen the hypothesis of an anti-phage defense mechanism after the injection of the genome but likely before transcription of phage proteins, which was already postulated for chemical defense in previous studies (Kever et al., 2022; Kronheim et al., 2018).

Potassium efflux · Infection curves

A) Bas09
B) Bas13
C) Bas20
D) λ
E) Control
F)
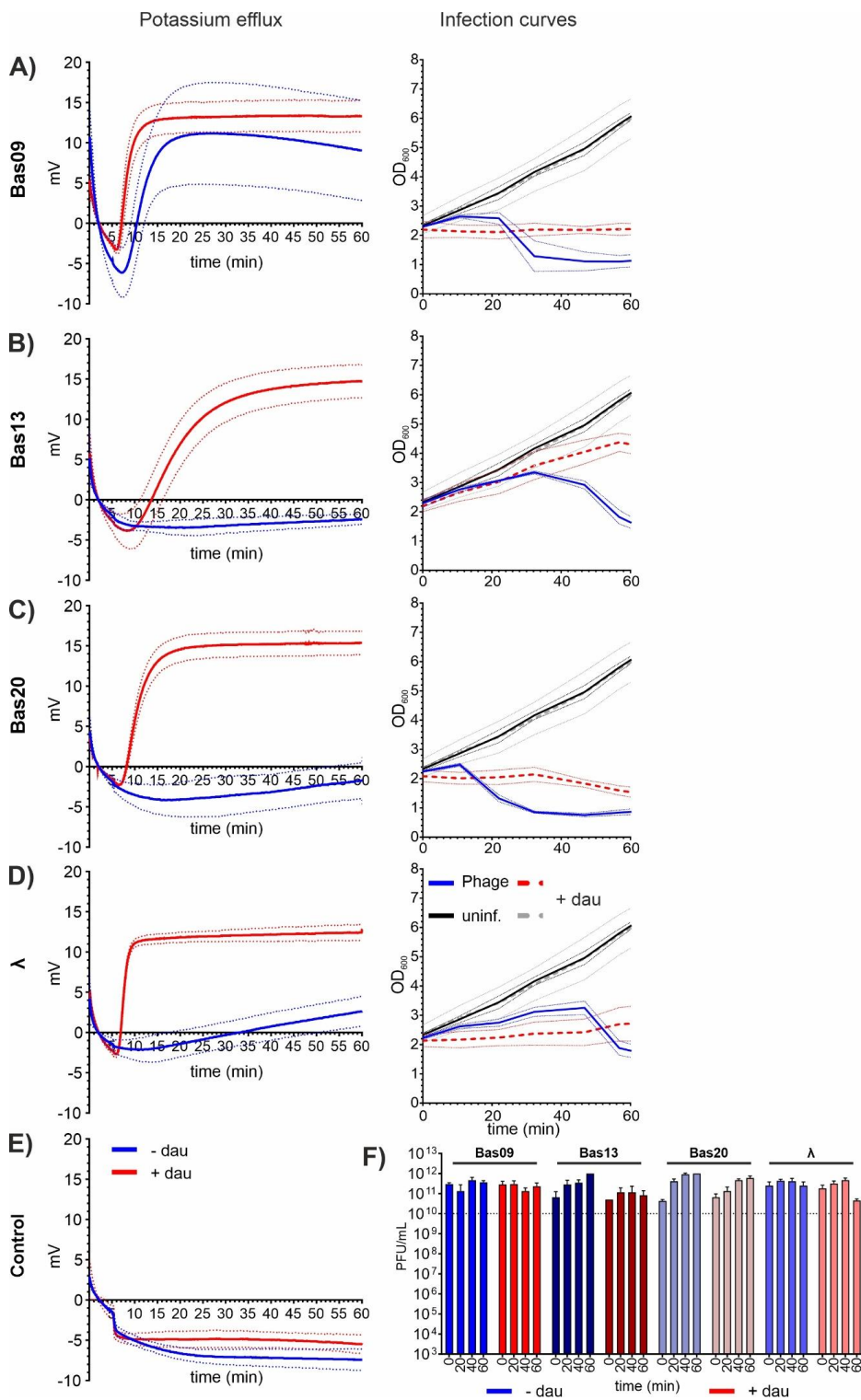
Figure 22: Testing the injection of phage DNA into the host cell under daunorubicin pressure using potassium efflux assays. Successful phage DNA injection can be monitored by measuring the efflux of potassium ions, which is shown in the left of the panel, where the y-axis depicts the voltage in mV. On the x-axis, the time in minutes is shown. In the left panel blue lines indicate the voltage measured in absence of daunorubicin and red lines the voltage in presence of daunorubicin. On the right panel, growth curves of the liquid phage infections with the same conditions are shown where black is the uninfected host, red the host infected by the respective phage in presence of daunorubicin and in blue infection in absence of daunorubicin. For the growth curves, the y-axis shows the OD_{600} and the x-axis the time in minutes. From top to bottom the phages Bas09, Bas31, Bas20 and λ are shown, the bottom row shows on the left the potassium efflux of the host in absence of phage and on the right the corresponding phage titer is shown. The bottom right graph shows on the y-axis PFU/mL and on the x-axis the time in minutes with the titer for Bas09 in bright colours, Bas13 in dark colours, Bas20 in pastel colours and λ in light colours with shades of blue for –dau and shades of red for +dau. n= 3 independent biological replicates, standard deviation is depicted as dotted line in the responding colour for potassium efflux and growth profiler data and as error bars for the phage titer.

3.4.3 Modification of the phage genome plays an important role in the resistance to nucleic-acid targeting defense systems

Sensitivity and resistance towards chemical defense conferred by daunorubicin appears to be a phage specific trait, which could be attributed to the modification of the respective phage DNA. The model phage T4 belongs to the subfamily of *Tevenvirinae* which has been resistant towards the anti-phage properties of daunorubicin (Figure 20). The *Tevenvirinae* including T4 are known to hypermodify their genetic material by adding sugar moieties to certain bases, e.g. in T4 all cytosines are glycosylhydroxymethylated (Hattman, 2009; Luria & Human, 1952). With a system provided by collaboration partners of the Max-Planck-Institute for terrestrial microbiology in Marburg, it was possible to transiently reduce the glycosylation of the cytosines down to ~ 50 %. This was achieved by using the ten-eleven translocation (TET) methylcytosine dioxygenase from *Nalgeria gruberi,* by an iterative oxidation followed by decarboxylation of the hydroxymethyl group of the cytosine (Figure 23A) (Pozhydaieva et al., 2024). Furthermore, T4 as a model phage is already widely used and certain mutant lines are already established, including a Δα/β-glycosyltransferase mutant. This mutant is restricted to hydroxymethylated cytosines and is not able to glycosylate its DNA at all, which was kindly provided by collaboration partners from the Micalis Institute, Paris. In this study the differently modified T4 variants were used to determine whether the DNA modification is indeed the source of the phage resistance towards chemical defense. The growth curves of the liquid infection experiment are depicted in Figure 23B and the respective titer development is shown as bar plot in Figure 23C. Liquid phage infections were performed with different concentrations of daunorubicin supplemented in the culture using the BioLector for growth monitoring (Figure 23B). The phages T4 wild type and the Δα/β-glycosyltransferase mutant were infecting the *E. coli* MG1655 ΔRM strain. The NgTET treated T4 (called T4_nTET) infected *E. coli* BL21 (DE3) carrying the NgTET plasmid as well as an inactive variant of NgTET (NgTET_D234A) as negative control (Figure 23, Table 6). Since the BioLector is not the best device to monitor growth of less dense growing bacteria such as *E. coli,* further experiments should be performed using the EnzyScreen growth profiler (Figure 23B). In the growth curves no real difference of host growth, phage infected growth in absence of daunorubicin or in presence of 20 µM

or 40 µM daunorubicin could be observed. The progression of phage titer in this case provided significantly more detailed insights. E.g. for the wild type T4, no difference in phage amplification could be observed for either daunorubicin condition, as the titer in presence and absence of daunorubicin reached the same titer of 10^{12} PFU/mL after 100 min post infection (Figure 23C). For the T4 Δα/β-GT the amplification of phage particles seemed to be impaired by daunorubicin. The titer in presence of daunorubicin 60 min post infection only reached 10^5 compared to the titer in absence of daunorubicin at 10^6, however, the end titer at 18 hours post infection was the same of approximately 5 x 10^{11} (Figure 23C). Overall, the amplification of the mutant T4 was slower compared to the wild type T4. However, this was expected, as the mutant phage lacks a part of its genetic material. The NgTET treated T4 phages infecting *E. coli* BL21 carrying the respective NgTET plasmids showed a more pronounced inhibitory effect of daunorubicin, as the amplification of phage titer in presence of daunorubicin significantly differed from the amplification in absence of daunorubicin. Here both conditions, on the active and inactive NgTET enzyme showed a standard amplification pattern in absence of daunorubicin, reaching final titers of about 10^{12} PFU/mL, which was comparable to the T4 wild type (Figure 23C). In presence of daunorubicin no increase in titer in the first 120 minutes post infection could be observed for the T4_nTET variant, were the titer stayed constant a 10^5 PFU/mL and a final titer of approximately 5 x 10^8 was determined at 18 hours post infection (Figure 23C). A similar phenotype was depicted for the T4_nTET_D234A variant, which only showed a minor increase when treated with 20 µM daunorubicin in the first 120 min post infection from 10^5 to 10^6 and no increase in titer over the time span in presence of 40 µM daunorubicin was observed. The final titers at 18 hours post infection were similar to the nTET variant, reaching titers of 10^9 and approximately 5 x 10^9 in presence of 20 µM and 40 µM daunorubicin respectively (Figure 23C). At first observation these results support the hypothesis, that DNA modifications might indeed be responsible for the resistance to chemical anti-phage defense systems. However, it must be taken into account, that two different host strains were used for the liquid infection experiments. To draw conclusions on the resistance of T4 which are actually comparable it was necessary to perform comparative experiments of the T4

variants on the same host background as the degree of phage sensitivity towards daunorubicin was shown to depend on the host background (Kronheim et al., 2018).
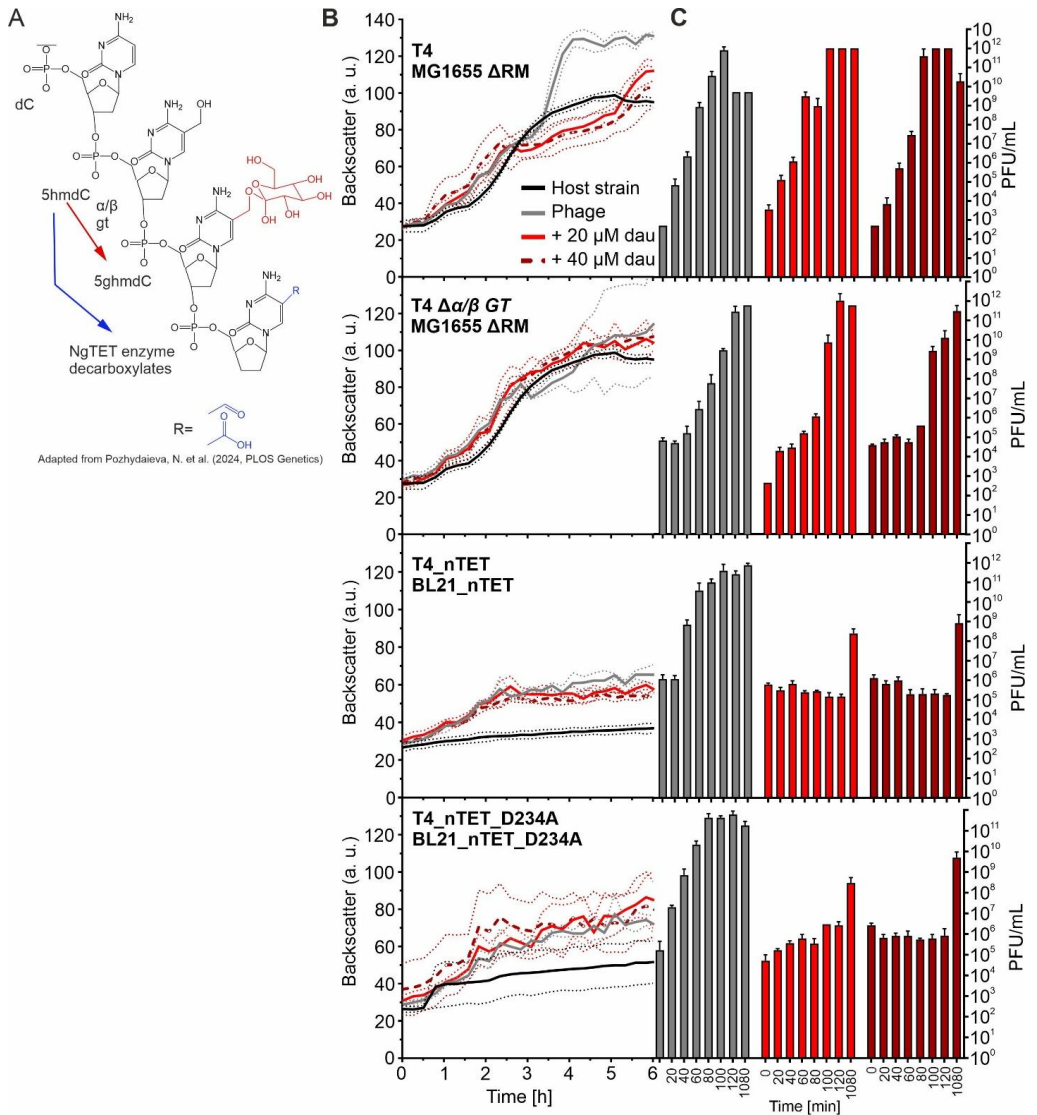
Figure 23: Testing T4 phage variants on different concentrations of daunorubicin to understand the significance of genomic modifications in the context of chemical defense. A) Scheme of cytosine modifications mediated by T4 in the wild type (red arrow) and the manipulation of the modification using the NgTET enzyme (blue). Scheme adapted from Pozhydaieva, N. et al (2024, PLOS Genetics). B) Growth curves of liquid infection assays of T4 wild type, T4 Δα/βGT, T4_nTET and T4_nTET_D234A (top to bottom), where the uninfected host is shown in black, the infection in absence of daunorubicin in grey, 20 µM daunorubicin in bright red and 40 µM daunorubicin in dark red. The y-axis shows the backscatter in arbitrary units and the x-axis the time in hours. n = 3 independent biological replicates, dotted lines in the corresponding colour show the standard deviation. C) Phage titer of the liquid infection in corresponding colours, grey (no small molecule), red (20 µM dau) and dark red (40 µM dau). The y-axis shows PFU/mL and the x-axis time in minutes. n= 3 independent biological replicates with error bars indicating the standard deviation.

3.4.4 Comparison of T4 variants on different *E. coli* host strains to determine whether the anti-phage defense properties of daunorubicin are independent on host genetics

Previous results in this work indicate that phage genome modifications might have an influence on the resistance towards chemical anti-phage defense. These results are in line with resistance towards other nucleic-acid targeting anti-phage defense systems such as CRISPR-Cas or Restriction-Modification (Bryson et al., 2015; Vlot et al., 2017; S. Wang et al., 2023). However, the different host strains might also impact the resistance or sensitivity towards daunorubicin. Therefore, T4 wild type and the NgTET treated variant were compared on different host strains in liquid infection experiments and double-agar overlay spot assays to determine the phage amplification kinetics. The *E. coli* host strains that were used here are *E. coli* K12 MG1655, *E. coli* K12 MG1655 ΔRM, *E. coli* BL21, *E. coli* BL21 (DE3) and *E. coli* BL21 ΔRM type IV. The ΔRM type IV host strain was chosen to be included in this experiments as T4 is known to be susceptible to type IV RM systems, which targets modified DNA (Bair & Black, 2007). Furthermore, MG1655 ΔRM is devoid of all RM systems, as described before (Maffei et al., 2021), BL21 (DE3) carries an additional prophage region, where no further defense systems could be identified. Analysis of the anti-phage defense systems in the BL21 and K12 wild type host strains using the PADLOC pipeline revealed a different composition of defense systems comparing the K12 derivatives with the BL21 derivatives (see Table 11). The full PADLOC analysis is in the supplementary Tables S6 for *E. coli* K12 MG1655, S7 for *E. coli* B and S8 for *E. coli* BL21 (DE3). The difference between the wild type hosts MG1655 and BL21 lies in the retron system of BL21, whereas MG1655 is equipped with additional defense, namely Lit, Hachiman, VSPR and PCD_02.

Table 11: Comparison of defense systems of *E. coli* K12 MG1655 and *E. coli* BL21 using PADLOC analysis.

System	MG1655	BL21
RM	RM type I	RM type I
	RM type IV	RM type IV
CRISPR	CRISPR array001	CRISPR array001
	CRISPR array002	CRISPR array002
Retron	-	Retron Eco1 (EC86)
Other	Lit, Hachiman_type_I, VSPR, PDC_S07, PDC_S12, PCD_02, PDC_04 & PDC_S13	PDC_S07, PDC_S12, PDC_04 & PDC_S13

In Figure 24 the growth curves as well as the phage titer on the different host strains are shown. For the infection of the two K12 derivatives no anti-phage effect of daunorubicin could be observed for neither of the T4 variants. Infected cultures collapsed regardless of the presence of daunorubicin and the phage titer increased in the same pace for both conditions with and without 20 µM daunorubicin (Figure 24 A&B). In contrast to this, for all BL21 derivatives a restored growth could be observed in

presence of daunorubicin, again showing only minor differences when comparing the two T4 variants (Figure 24 C, D & E). On all BL21 derivatives, regardless on the presence of the DE3 prophage or the absence of the type IV RM system, both T4 wild type and NgTET treated T4 did not lead to a culture collapse in presence of daunorubicin and the phage titer did not increase in the same way as in absence of daunorubicin. Both phages reached final titers of 10^{11} in absence of daunorubicin, whereas the titers stagnated at 10^6 in presence of the anti-phage molecule. Since on the K12 derivatives no difference in phage titer was observed between the two T4 variants, only the T4 wild type is shown. On the BL21 derivatives slight differences in the infectivity and the phage amplification could be observed. On all BL21 derivatives the T4_nTET variant led to a stronger growth defect in absence of daunorubicin compared to the wild type, however the amplification of phage particles was comparable for both phages in both conditions (Figure 24 C, D & E). Concerning these results, we speculated that phage DNA modification is not the main source of resistance and that the anti-phage defense provided by daunorubicin is a more complex mechanism that actually interacts with intracellular defense systems of the host.
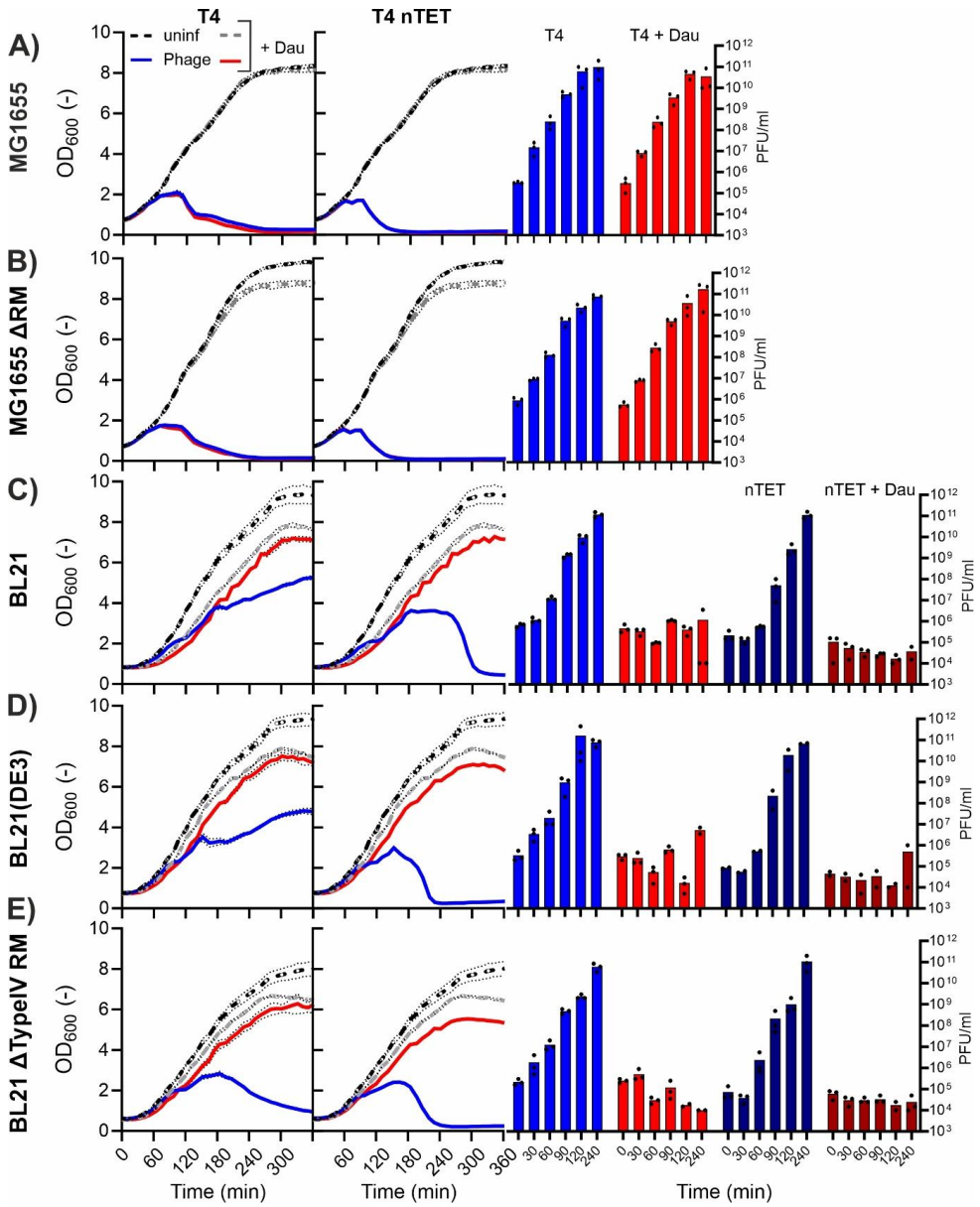
Figure 24: Comparison of T4 wild type and T4_nTET on different host strains under daunorubicin pressure. T4 wild type (first column) and T4_nTET (second column) liquid infection growth curves on the *E. coli* strains A) MG1655, B) MG1655 ΔRM, C) BL21, D) BL21 (DE3) and E) BL21 Δ type IV RM are shown where the black curve is the uninfected host in absence of daunorubicin and the grey curve in presence of daunorubicin. In blue the infected host in absence of daunorubicin is shown and in red the infected host in presence of daunorubicin. The y-axis shows OD_{600} and the x-axis the time in minutes. n = 3 independent biological replicates with dotted lines in the respective colour indicating the standard deviation, for the red line SD is indicated in black dotted lines.. The third column shows the respective phage titer over time in blue for T4 wild type - dau and red + dau, dark blue for T4_nTET - dau and dark red + dau. The y-axis shows phage titer in PFU/mL and the x-axis time in minutes. n= 3 independent biological replicates which are indicated with the black dots in the respective bar. Experiments were conducted by Dr. Larissa Kever.

3.4.5 Investigating the effect of daunorubicin on phage DNA replication during infection of *E. coli* BL21

So far it was apparent that the host strain is an accounting factor for the efficiency of the daunorubicin mediated anti-phage defense, a next step was to compare the phage DNA replication of an NgTET treated T4 with the wild type. T4_nTET and T4 wild type DNA replication was determined using qPCR while infecting *E. coli* BL21 with the nTET or inactive nTET plasmid respectively under daunorubicin pressure (Figure 25A). Using this technique, not only phenotypic results of the phage infection could be measured but also the intracellular replication of the phage genome, hinting towards successful replication or the inhibition thereof. In Figure 25A the replication of T4 and T4_nTET DNA in presence and absence of 20 µM daunorubicin is shown. For T4 wild type (Figure 25A), a continuous increase of phage DNA/host DNA was observed, indicating active DNA replication in absence of daunorubicin. In presence of daunorubicin an increase of phage DNA over host DNA was observed until 20 minutes post infection followed by a decrease of phage DNA over host DNA. This indicated the injection process within the first 20 minutes, followed by no replication of phage DNA or even a degradation of phage DNA, while the host grew and replicated normally. T4_nTET DNA replication in absence of daunorubicin showed a similar trend of steadily increasing over time, which indicated active DNA replication. In presence of daunorubicin, the T4_nTET DNA increased up to 30 minutes and stayed at a constant level until 90 minutes post infection where a slight decrease of phage DNA over host DNA was observed. Again, the first 20 to 30 minutes indicated successful infection and thereby injection of the phage genome but no following DNA replication. These results also indicated that T4_nTET DNA is less strongly degraded over time as the intracellular phage DNA remains at overall higher levels for T4_nTETcompared to T4 wild type (Figure 25B). The double-agar overlay spot assay (Figure 25C) supports the DNA replication data of the qPCR. A steady increase in phage titer from 10^6 to 10^9 for T4 wild type and 10^7 to 10^9 for T4_nTET was shown in absence of daunorubicin and no change in phage titer for T4_nTET or even a slight decrease for T4 wild type was measured. These results indicate that indeed replication of phage DNA is impaired in the presence of daunorubicin, which once more strengthens the hypothesis that was already formulated in different publications for chemical defense

systems (Kever et al., 2022; Kronheim et al., 2018). A direct mechanism of action however remains elusive.
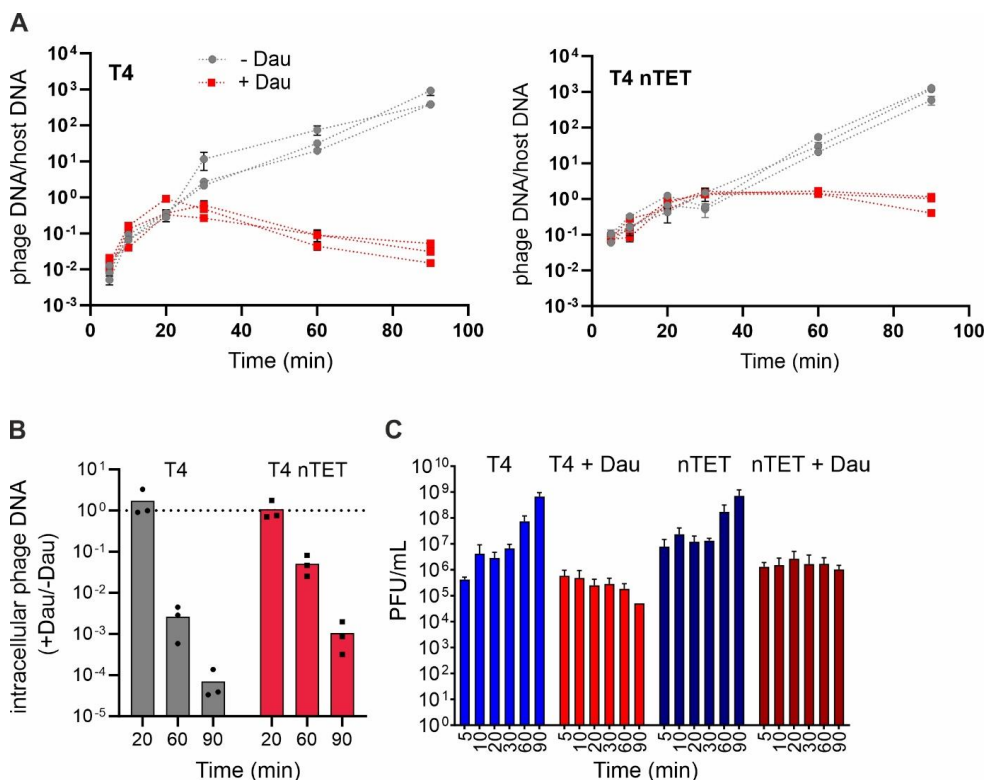
Figure 25: Investigation of the direct impact of daunorubicin on the phage amplification of T4 and T4_nTET. A) qPCR results of T4 wild type (left) and T4_nTET (right) infections of *E. coli* BL21 in presence (red) and absence (grey) of daunorubicin. The y-axis shows the concentration of phage DNA over host DNA and the x-axis shows time in minutes. n=3 independent biological replicates which are each depicted with a single line, standard deviation is shown with error bars. qPCR measurements were conducted by Dr. Larissa Kever B) Calculation of total intracellular phage DNA when comparing +daunorubicin and – daunorubicin conditions, for T4 (grey) and T4_nTET (red) where the dotted line represents the intracellular phage DNA concentration 20 min post infection. Y-axis depicts intracellular phage DNA (+dau/-dau) and the x-axis the time in minutes. n= 3 independent biological replicates which are indicated as black dots. C) Development of phage titer corresponding to the qPCR data of T4 with (red) and without (blue) daunorubicin as well as T4_nTET with (dark red) and without (dark blue) daunorubicin. The y-axis depicts the phage titer in PFU/mL and the x-axis the time in minutes. n= 3 independent biological replicates with error bars indicating the standard deviation.

3.4.6 Surface plasmon resonance measurements show on/off binding kinetics of anti-phage molecules to phage DNA

In order to understand the mode of action of the anti-phage small molecules tested in the big screenings, surface plasmon resonance (SPR) measurements using a T200 Biacore system were performed to assess the binding of daunorubicin, actinomycin D and apramycin to differently modified DNA's (T4 wild type, T4_nTET and T4Δα/βGT*)*. Biacore measurements were performed by collaboration partners from the Johannes Gutenberg Universität Mainz. Increasing concentrations of the molecules with anti-phage activity were washed over the surface-bound DNA to assess binding

kinetics and also the mode of binding. The phage DNA that was used here was prepared as described in Section 2.4.6 and 2.5.1 to bind the DNA to the SPR chip surface. In the SPR measurements no difference of the small molecules to either of the modified DNA samples could be measured, showing that the DNA modification does not influence small molecule binding to the DNA directly (suppl. Figure S9). Furthermore, no covalent binding of daunorubicin, actinomycin D or apramycin to the DNA was shown. For daunorubicin a rather loose association to the DNA comparable to an "on/off"-status could be determined, as the molecule association and dissociation kinetics were the same (see suppl. Figure S9). For actinomycin D a similar phenotype was observed where association as dissociation of the small molecule to either DNA was comparatively fast. The association of actinomycin D to the purified phage DNA was overall lower compared to the association of daunorubicin as the response units (RU) increased only to a maximum of 10, whereas RU of daunorubicin reached up to ~ 120. A similar phenotype was observed for apramycin, with an "on/off" phenotype at low RU on either of the purified phage DNAs. These results indicate that the interaction of the small molecules is independent of presence or absence of DNA modification but also show that in these *in vitro* conditions no intercalation of the molecules into the DNA double-helix occurred.

3.4.7 Infection kinetics influence the strength of chemical defense

Infection kinetics of phages in presence and absence of an anti-phage defense system can reveal information about the mechanism of action of the chemical defense system, such as abortive infection. In this study, 8 phages of the BASEL collection, Bas01, Bas13, Bas20, Bas24, Bas30, Bas41, Bas55, and Bas69, as well as λ and T4 were selected for liquid infection kinetic experiments. The host culture of *E. coli* MG1655 ΔRM was infected with MOI's of 0.1, 1 and 10 of each phage and the growth was monitored (Figure 26). Infection kinetics were determined in presence and absence of 20 µM daunorubicin to assess if daunorubicin restored growth at all different MOI's or led to a complete culture collapse in presence of high MOI, which would indicate an abortive infection mechanism. The phages Bas01, Bas13, Bas20, Bas24, Bas30, Bas41, Bas55, and Bas69 represent different phage families from the Basel collection and are - except for Bas24 and Bas41 - sensitive towards daunorubicin (see Figure 20). Phage λ represents a sensitive model phage whereas T4 is the resistant counterpart. In absence of the small molecule all phages except for Bas69 show an infection phenotype responding to the initial phage titer, meaning the higher the MOI, the faster a culture collapse can be observed. For the phages Bas01, Bas13, Bas20, Bas30, and λ a restoration of the growth comparable to the growth in absence of phage can be observed when 20 µM daunorubicin is added to the culture, irrespective of the MOI added. Two of the three phages that were known to be resistant, Bas41 and T4 show overlapping growth curves of the respective MOI in presence and absence of daunorubicin, indicating that the small molecule does indeed not interfere with successful infection (Figure 26).

3. Results

Similarly, the kinetics of the culture collapse correlate with the MOI, showing the expected phenotype. For the phages Bas24 and Bas55 an intermediate phenotype can be observed. Bas55 has been previously identified as sensitive and Bas24 as resistant (see Figure 20). In the infection experiments presented in Figure 26, the culture growth can be recovered by daunorubicin when Bas24 infects with an MOI of 0.1, the culture reached an OD_{600} of about 12.5 which is similar to the uninfected control presence of daunorubicin at 400 min post infection. At an MOI of 1 however, still a strong growth defect can be observed until about 200 min post infection and at an MOI of 10 a culture collapse comparable to the MOI 0.1 infected culture in absence of daunorubicin can be observed even in presence of daunorubicin. For Bas55 a similar phenotype can be observed, as at an MOI of 0.1

daunorubicin can restore growth to a certain degree, where the infected culture reaches an OD_{600} of 10 compared to the uninfected culture in presence of daunorubicin which grew to an OD_{600} of 12. However, at MOI of 1 and 10 the growth curves overlap with those in absence of daunorubicin. Phage titer development is depicted in supplementary Figure S10. These results suggest that the mechanism of action of daunorubicin might not only be intracellular but could also differ for different phages, underlining that sensitivity to chemical anti-phage defense is specific to the phage. It is important to notice that for the phages Bas20 and λ, already abortive infections mechanism were shown in Figure 22, therefore abortive infection as mode of action should not be excluded, even though the growth curves depicted in Figure 26 do not indicate this.
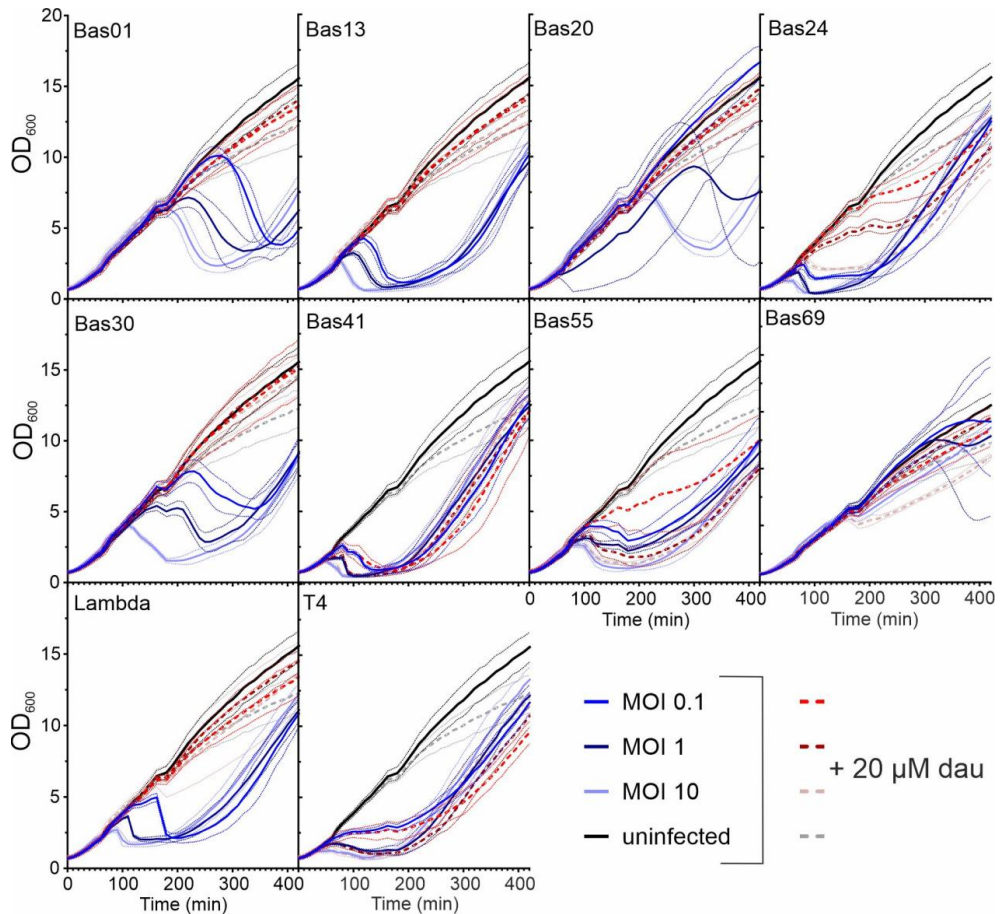
Figure 26: Infection kinetics of a selection of phages at different MOI under daunorubicin pressure. Shown from top left to bottom right are growth curves of liquid infection experiments with the phages Bas01, Bas13, Bas20, Bas24, Bas30, Bas41, Bas55, Bas69,λ and T4 respectively. The growth curves show for each phage an uninfected culture in w/o daunorubicin (black solid line) and with daunorubicin (grey dashed line. MOI of 0.1 is shown in bright blue (w/o dau) and bright red dashed line (with dau), MOI 1 is dark blue in absence of daunorubicin and dark red dashed line in presence of daunorubicin and MOI 10 is light blue in absence of the small molecule and light red dashed line in presence of 20 µ daunorubicin. For all 10 graphs the y-axis shows the OD_{600} and the x-axis time in minutes. n=3 independent biological replicates with dotted lines in the respective colour indicating the standard deviation.

3.4.8 Manipulation of *in vitro* synthesis of infective phage particles with daunorubicin

In a comparable approach, in the context of the master thesis of Sümeyye Celen (2024), which was supervised as part of this doctoral project, TXTL synthesis of infective phage particles was conducted. As a further means to identify the mode of action of daunorubicin anti-phage properties synthesis of infective phage particles *in vitro* using a TXTL system and challenging the synthesis with the addition of daunorubicin was performed. TXTL systems are cell free expression platforms that neither have a cell membrane, nor are restricted by toxicity or other cell growth restricting factors (Figure 27A). In context with daunorubicin, the TXTL system allows to narrow down the mechanism of action in absence of other cellular factors, such as cell suicide factors through abortive infection mechanism. In this study the myTXTL kit (Arbor Biosciences) was used to synthetize the phages T7 and Bas09 in presence of daunorubicin. For the synthesis highly pure phage DNA was added to the myTXTL Pro Cell-Free expression master mix and the reaction was supplemented with either water, 5 µM or 20 µM daunorubicin. After incubation at 28 °C for 16 hours the reaction was serially diluted and spotted to determine the successfully synthetized infective particles. In Figure 27B the phage titer that was achieved in this synthesis is shown, where phage T7 reaches a titer of ~ 5×10^7 PFU/mL in the normal reaction without daunorubicin and a similar titer with 5 µM daunorubicin (Figure 27B). In presence of 20 µM daunorubicin the final titer decreases to ~ 5×10^4 PFU/mL, which indicates an inhibitory effect of daunorubicin with rising concentration, hampering cell free phage synthesis. Bas09 in contrast was not negatively impacted by the presence of daunorubicin in the TXTL reaction, reaching a titer of 10^8 PFU/mL in absence of daunorubicin and even a slightly higher titer of 10^9 PFU/mL in presence of both concentrations of daunorubicin (Figure 27B). This change in titer was also observable in the spot assay images of Figure 27C. These results differ significantly from the *in vivo* effects observed in Bas09 infections, suggesting that the genomic features of Bas09 are unlikely to be the underlying cause of daunorubicin's anti-phage effect. Furthermore, considering that self-toxicity is omitted in the TXTL system, the phenotypes observed here, strengthen the hypothesis of a daunorubicin induced abortive infection mechanism.
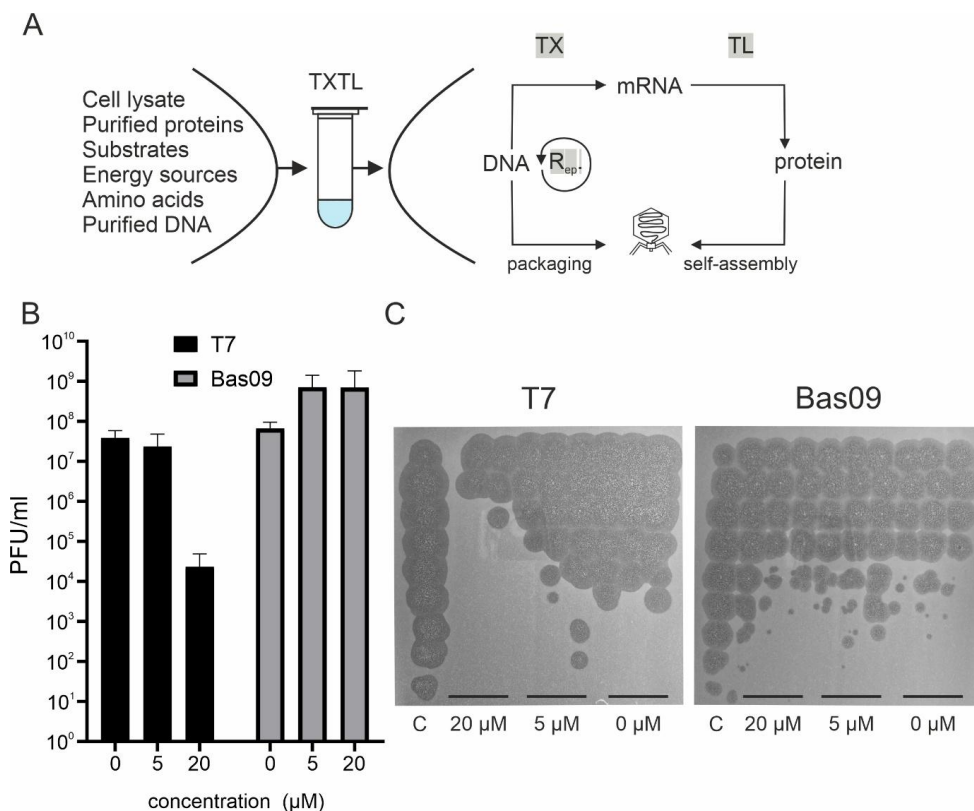
Figure 27: Using cell free expression systems as means to elaborate the mechanism of action of daunorubicin mediated chemical defense. A) Schematic overview how a TXTL expression system is working, which ingredients are present in the reaction and which cellular reactions are imitated, scheme adapted from Shin et al. 2012. B) Titer of infective phage particles produced in the myTXTL master mix in presence of 0 µM, 5 µM or 20 µM daunorubicin of T7 (black) and Bas09 (grey). The y-axis shows phage titer in PFU/mL and the x-axis the daunorubicin concentration in µM. n=3 independent biological replicates, error bars indicate standard deviation. C) Images of spot assays of T7 and Bas09 after TXTL synthesis of *E. coli* MG1655 ΔRM. C is the positive control of phage lysate. From left to right three lanes of spots correspond to synthesis with each concentration 20 µM, 5 µM and 0 µM daunorubicin after TXTL synthesis. n=3 independent biological replicates.

3.5 Investigation of synergism between intracellular defense systems and chemical defense

As it was already shown in Figure 24 for T4 and NgTET treated T4, the host strain used for infection influences the anti-phage defense properties of daunorubicin. One possible explanation for the differences observed are synergistic effects of intracellular defense systems and chemical defense. A difference in daunorubicin uptake however could also play a role in the distinct phenotypes observed on the two different *E. coli* strains. In order to understand if the synergy between chemical defense and intracellular defense systems is taking place, different plasmid based defense systems were combined with daunorubicin in order to determine the combined effects and gauge which combinations act synergistically. In this chapter experiments were conducted in collaboration with Dr. Larissa Kever, indicated in the Figure description.

3.5.1 Synergy of daunorubicin mediated chemical defense with plasmid based intracellular defense systems is a sweet spot

In order to investigate which combination of intracellular defense system and daunorubicin concentration might act synergistically, double-agar overlay spot assays were performed on the *E. coli* MG1655 ΔRM host carrying different plasmid-based defense systems (Table 6) by adding increasing concentrations of daunorubicin. Phages from the BASEL collection that were previously identified as sensitive (Figure 20) were tested in this double-agar overlay spot assay. The intracellular defense systems that were selected for this assay, except for the two retron systems, were previously also tested on the BASEL phages (Maffei et al., 2021), therefore the reaction of each phage to single systems was already known. For example Bas09 was shown to be sensitive to both type II and type III RM systems (Maffei et al., 2021). Systems that were tested belong to the classes of type I, type II and type III restriction modification systems as well as three different abortive infection systems and two distinct retron systems (see Table 12).

Table 12: Intracellular defense systems that were reintroduced into *E. coli* MG1655 ΔRM on a plasmid for screening purposes (information about target and mechanism of action based on (Maffei et al., 2021; Millman et al., 2020).

Name	Type	Target	Mechanism of action
EcoKI	Type I RM	AAC[N$_6$]GTGC TTG[N$_6$]CACG	Unmodified target sequence triggers cleavage of DNA (often far away from target sequence)
EcoCFT_I	Type I RM	GAG[N$_7$]GTCA CTC[N$_7$]CAGT	
EcoRI	Type II RM	GAATTC CTTAAG -> sticky ends	Unmodified DNA target sequence triggers immediate DNA cleavage
EcoRV	Type II RM	GATATC CTATAG-> blunt ends	
EcoCFT_II	Type III RM	CACAG GTGTC	Pair of unmodified target sequences in head to head direction triggers cleavage in between the two sequences
EcoP1_I	Type III RM	AGACC TCTGG	
Fun/Z	Abortive infection	Molecular mechanism unknown	
Old	Abortive infection	Putative sensing of dysfunctional or absence of *ExoV*, degradation of tRNA as presumed killing mechanism	

Tin	Abortive infection	Poisoning of phage encoded replicative ssDNA-binding protein, especially *Tevenvirinae*
Retron_Eco1/EC86	Retron system	Mechanism of action unknown
Retro_Eco6/EC48	Retron system	Guarding of RecBCD complex, inhibition of RecBCD triggers retron, leading to abortive infection

In the screening of synergism between intracellular defense systems and chemical defense (Figure 28A) three distinct phenotypes can be observed: Either there is no interaction (EQ3), an additive effect of intracellular and chemical defense systems (EQ2) or a synergism (EQ1) that is expressed in the epistatic coefficient (EQ4). These effects are calculated based on the efficiency of plating (EOP) that is counted in the double-agar overlay spot assays and the interactions are defined as follows (Wu et al., 2024):

$$\text{synergy} = |\log_{10}(EOP_{system1+system2})| > |\log_{10}(EOP_{system1})| + |\log_{10}(EOP_{system2})| + 1 \text{ EQ1}$$

$$\text{additive} = [|\log_{10}(EOP_{system1})| + |\log_{10}(EOP_{system2})|] < |\log_{10}(EOP_{system1+system2})| < |\log_{10}(EOP_{system1})| + |\log_{10}(EOP_{system2})| + 1 \text{ EQ2}$$

$$\text{null} = |\log_{10}(EOP_{system1+system2})| < |\log_{10}(EOP_{system1})| + |\log_{10}(EOP_{system2})| \text{ EQ3}$$

The epistatic coefficient is then calculated as

$$|\log_{10}(EOP_{system1+system2})| - |\log_{10}(EOP_{system1})| - |\log_{10}(EOP_{system2})| \text{ EQ4}$$

indicating the strength of the interactions (Wu et al., 2024). In Figure 28A the heat map of the resulting epistatic coefficient is shown for the conditions of 1 µM and 5 µM daunorubicin. In the direct comparison of the two heat maps it is noticeable that the concentration of daunorubicin is crucial for the kind of interaction that was determined. For example, the Old abi system with 1 µM daunorubicin showed synergy on the phages Bas01-Bas11 (Figure 28A). In combination with 5 µM daunorubicin Old mediated defense did not show synergism for Bas01 and Bas07, however synergism was determined for the phages Bas03, Bas05, Bas09, Bas11, Bas13, Bas24 and Bas34 (Figure 28A). These results indicate that synergism of chemical defense with an intracellular defense system seems to be a "sweet-spot", where one system should not overpower the other in order to increase the overall efficiency of anti-phage defense. This "sweet-spot" phenotype could be observed for several defense systems, where no interaction is determined on 1 µM daunorubicin, synergistic effects were present on 5 µM daunorubicin (Figure 28A). In contrast to this, for the retron system Eco6 neither synergistic nor additive effects in combination with 5 µM daunorubicin could be calculated, therefore it is not shown at 5 µM. To further investigate the relation between daunorubicin concentration and defense

systems liquid infection assays of Bas09 on selected defense systems were performed, i.e. EcoCFT_II and Old. In Figure 28A it can already be observed that the synergy with EcoCFT_II seems to be dependent on the daunorubicin concentration as no synergy was determined at 1 µM daunorubicin but on 5 µM. Furthermore, the concentration of phage particles for infection was investigated by infecting with different MOI ranging from 0.01 to 5. In Figure 28B the growth curves of these infection experiments are shown. In the absence of daunorubicin (Figure 28B), the control culture collapsed upon infection with Bas09. The timing of the collapse correlates to the MOI used for infection—higher MOIs led to a more rapid culture collapse. A similar phenotype could be observed on EcoCFT_II, even though the culture collapsed a bit slower compared to the control, which is due to the active type II RM system. For the Old defense system a rescue phenotype of growth could be observed at an MOI of 0.01 but for higher MOI the culture collapsed in a similar fashion as for EcoCFT_II and the control, correlating to MOI. In presence of daunorubicin (Figure 28B), the control showed a delayed culture collapse which correlated in timing with the MOI used for infection. On EcoCFT_II, infection with low MOIs of 0.01 and 0.1 allowed a complete rescue in growth in presence of daunorubicin. For an MOI 1 the culture growth was slower but not completely impaired and for an MOI of 5 no growth was observed. A similar phenotype could be observed on the Old defense system in presence of daunorubicin with a rescued culture growth at low MOI's of 0.01 and 0.1, a slowed growth of the culture infected with an MOI of 1 and no growth at all at an MOI of 5. In Figure 28C the corresponding $\log_{10}$-fold change in phage titer is shown, which correlated with the defense phenotype observed in the growth curves. In absence of daunorubicin the phage titer overall increased except for the infection of the Old system with an MOI of 0.01. In presence of daunorubicin an increase in phage titer could only be observed on the control plasmid whereas on the tested defense systems the phage titer decreased or did not change in case of MOI 5 on both systems. These results showed that synergy between intra- and extracellular defense systems exists but is a matter of several factors that influence this delicate balance. Such factors are the concentration of the small molecule, the concentration of infective phage particles and the effectivity of the intracellular systems on the phage. Infections with higher MOI in presence of daunorubicin led to a complete growth arrest of the culture, which indicates

an abortive infection mechanism of daunorubicin, as this phenotype was also observed in the control culture.

A)

Figure A: Heatmaps showing Epistatic coefficient for 1 μM Daunorubicin and 5 μM Daunorubicin across enzymes (EcoKI, EcoCFT_I, EcoRI, EcoRV, EcoCFT_II, EcoP1_I, Fun/Z, Old, Tin, Eco1, Eco6) versus strains (Bas01, Bas03, Bas05, Bas07, Bas09, Bas11, Bas13, Bas20, Bas24, Bas30, Bas34). Legend: Null (white), Additive (grey), Epistatic coefficient (red scale from 1.0 to 7.5).

B) Control, CFT_II, Old growth curves (OD$_{600}$ vs Time (min)) for − dau and + dau 2.5 μM conditions. Legends: uninf, MOI 0.01, MOI 0.1, MOI 1.0, MOI 5.

C) − dau and + dau, 2.5 μM bar charts of log$_{10}$ fold change for Control, CFTII, Old.

3. Results

Figure 28: Synergetic effects of daunorubicin mediated chemical defense with intracellular defense systems. A) Heat map of synergy screening on plate with 1 µM (left) and 5 µM (right) daunorubicin. Tested were the phages Bas01, Bas03, Bas05, Bas07, Bas09, Bas11, Bas13, Bas20, Bas24, Bas30 and Bas34 (top to bottom) were tested on the defense systems in Table 12. Shades of red indicate synergistic effects shown as epistatic coefficient, grey indicates an additive effect, white shows no effect. The rows are named with the respective phage and the columns with the tested system below. n= 3 independent biological replicates. B) Growth curves of synergy assays with Bas09 on the empty plasmid control (left), EcoCFT_II (middle) and Old (right) with different MOIs, 0.01 (light colour), 0.1 (bright colour), 1.0 (dark colour) and 5 (pastel colour) with (shades of red) and without (shades of blue) 2.5 µM daunorubicin. The y-axis shows OD_{600} equivalents and the x-axis the time in minutes. n= 3 independent biological replicate, dotted lines indicate the standard deviation. C) Log_{10}-fold change of phage titer corresponding to the growth curves of B). Left shows the titer change in absence of daunorubicin and right the change in titer in presence of 2.5 µM daunorubicin. Colours correspond to those in B), with increasing MOI from left to right. Y-axis shows the log_{10}-fold change normalized to the staring titer at T_0. n= 3 biological replicates with black dots indicating the single replicates. Dr. Larissa Kever conducted Bas09 liquid synergy assays (B&C).

4. Discussion

The bacterial immune system is a complex network of defense systems, which work in concert with one another and thereby build an intricate layered framework to defend the bacterial cell from phage infection. Previous studies primarily focused on intracellular systems which mediated anti-phage defense with proteins or RNA (Georjon & Bernheim, 2023). This work however concentrates on the anti-phage defense mediated by secreted small molecules produced by *Streptomyces spp.* and how this chemical defense interacts with the remaining defense systems. Lately many similarities between the prokaryotic and eukaryotic immune system have been identified in the research field of anti-phage defense systems (Wein & Sorek, 2022). Therefore, chemical defense poses a potentially interesting system for similar mechanism of action in prokaryotes and eukaryotes. The aim of this work was to elucidate the anti-phage defense systems of *Streptomyces spp.,* especially the chemical defense, and how chemical defense provided by *Streptomyces* acts in model organism phage-host pairs such as *E. coli* and coliphages.

4.1 The effect of spent medium of aminoglycoside producing strains on phage infection

In the following chapter, the effect of chemical defense in the natural context will be discussed. Chemical defense mediated by different aminoglycosides produced by their respective producer strain in spent media resembles an ecologically relevant setting. Naturally, a producing organism secretes the small molecule, which diffuses through the environment and thereby leads to defense (or the lack thereof) for other microorganisms in the community. Liquid infection assays were performed with phage Alderaan and *S. venezuelae,* as this phage-host pair is closely related to the producing strains and could inhabit the same ecological niche as the producer strain. With the focus of the apramycin producing strain, *S. tenebrarius,* different factors were tested that might influence the potency of the spent medium. Furthermore the mechanism of action of chemical defense mediated by apramycin was compared to the stringent response as anti-phage defense mechanism and the extracellular effect of spent media on different phage particles was investigated. As the mechanism of action, for apramycin mediated phage inhibition remained elusive, there are different hypotheses, how aminoglycosides provide anti-phage defense. On the one hand an extracellular inhibition of phage particles could be possible, where the aminoglycoside prevents the phage particle from injecting its genome into the cell and thereby inhibiting phage infection completely. On the other hand an intracellular mechanism might be possible where both the aminoglycoside as well as the phage DNA enter the cell and the aminoglycoside deters the replication of phage DNA through the inhibition of either the DNA circularization or the onset of DNA replication.

4. Discussion

4.1.1 Spent medium of different producer strains show varying degrees of anti-phage defense

Spent medium of different aminoglycoside producing strains was first tested on *S. venezuelae* wild type cultures to estimate the anti-bacterial potential of the spent medium. Different anti-bacterial and anti-phage effects of the SM could be observed with differences regarding the producer strain as well as the time of harvest of the SM. Results of *S. tenebrarius* SM are in line with the results published by Kever and colleagues in 2022, who already showed that spent medium of *S. tenebrarius* is sufficient to inhibit Alderaan infections (Kever et al., 2022). The effect of the streptomycin producer *S. griseus* is consistent with expectations. Streptomycin was one of the first observations of chemical anti-phage defense (Hardy et al., 2023), establishing that the effect observed with the apramycin producer is not an individual case. For SM from the kanamycin producer no significant effect on the phage infection could be shown (Figure 9) which is in line with the antibacterial potency tested in Figure 8, as neither the culture collapse due to the phage infection is inhibited, nor the phage amplification. This could be explained by the complex regulation of the production of specialized metabolites in *Streptomyces spp*. and it might be that the cultivation conditions in which the spent medium was harvested were not suitable for the production of kanamycin (Bibb, 2013; Kieser et al., 2000). However, metabolite analysis of the spent medium would be needed to further elucidate what was produced and which composition of small molecules is present in the spent medium (Samain, Dupin, Delrieu, & Inchauspe, 1987). Liquid infections with *S. fradiae* spent medium showed a markedly atypical phenotype, where no growth defect due to phage infection could be observed in presence of the SM, but the phage amplification was not completely impaired, as an increase in phage particles was observed (Figure 9). To identify the source of this phenotype, microscopic images of the infected culture would be needed to determine whether the culture is indeed protected from infection by the SM or whether the culture is just more dispersed due to partial lysis and therefore no growth defect can be detected. Spent medium from *S. hygroscopicus* and *S. spectabilis* (Suppl. Figure S2) do not fit into the phenotypes described above. Overall there are different reasons why some spent media show no anti-phage effect, whereas others do. On the one hand, the molecule of interest might not have been produced by the aminoglycoside producing strain in the timeframe of cultivation in which the spent medium was harvested (Forge & Schacht, 2000). This could be either due to non-favourable conditions for expression of the BGC or a too short time frame of cultivation (Hopwood, 2007). On the other hand, the produced aminoglycosides all have different functional groups, which might explain the different potency of inhibition (Krause, Serio, Kane, & Connolly, 2016). Furthermore, the host strain carried antibiotic resistance cassettes encoding for aminoglycoside modifying enzymes (AME's) during the liquid infection assays which alter the respective functional group of the aminoglycoside, which attacks the 16S rRNA of the small ribosomal subunit (Garneau-Tsodikova & Labby, 2016). It its highly

unlikely that this alteration could already lessen or diminish the anti-phage effect of the small molecule in some cases, as Kever and colleagues could show that *in vitro* acetylation of apramycin did not diminish the anti-phage effect but only the antibacterial effect of the aminoglycoside (Kever et al., 2022). During the comparison of media for apramycin production, the intricate regulation of specialized metabolite biosynthesis became more evident, as distinct variations in the protective effect of different spent media was observed (Figure 11). This again underscores the importance of the correct conditions for the production of specialized metabolites and a functioning analytic platform to confirm the composition and concentration of the respective spent media (Krause et al., 2016; Zhang et al., 2021) Summing up, the tested spent media showed the potency of aminoglycosides in a naturally produced setting to act as anti-phage defense mechanism, also in a community wide protection (Kever et al., 2024). Chemical defense mediated by naturally produced small molecules is a system underlying the complex regulatory network of *Streptomyces* BGC's, showing the importance of this defense system in the life-cycle of *Streptomyces*, as the metabolic burden would be too high to justify a redundant system (Hardy et al., 2023). The strength of these results is however impaired due to the lack of HPLC or LC/MS analysis of the respective spent media, as it could not be determined exactly which small molecules were produced and in which concentrations. For future investigations of spent media, an established method for e.g. a triple quadrupole LC/MS/MS to measure metabolite concentration and composition is definitely required.

4.1.2 Chemical defense does not trigger the stringent response as mechanism of action

Chemical anti-phage defense mediated by apramycin has been described in detail by Kever and colleagues, where the timeframe of inhibition could be narrowed down to the early stages of phage infection, a distinct mechanism of action however was not identified (Kever et al., 2022). As *Streptomyces* are not easily genetically manipulated and multicellular development complicates different "classical" phage methods, the idea was to rule out certain mechanisms of action, such as activation of the stringent response in the presence of apramycin (Kieser et al., 2000; Smith et al., 2013; Strauch et al., 1991). Stringent response is the (p)ppGpp (guanosine 5'-diphosphate-3'-diphosphate) mediated change in cellular expression pattern where transcription rates of stable RNA genes will be reduced and e.g. expression of amino acid BGC's will be increased (Strauch et al., 1991). Overall, it is described as a generic stress response with various triggers which is supposed to ensure the viability of the population throughout the stress, in this case the phage infection (Rostøl & Marraffini, 2019; Tabib-Salazar et al., 2018; N. Tal et al., 2022). For T7 infection in *E. coli* an accumulation of (p)ppGpp as a response to phage infection was described as well as a protein produced by T7, Gp5.7, which counteracts this antagonizing effect of (p)ppGpp (Tabib-Salazar et al., 2018). In other cases the presence of (p)ppGpp has been described to be necessary for successful

phage amplification of phage Mu (North, Kirtland, & Nakai, 2007) or can influence the lytic/lysogeny decision of temperate phages such as λ (Slomińska, Neubauer, & Wegrzyn, 1999). In this work the effect of the SHX-induced stringent response (Strauch et al., 1991) as anti-phage defense is directly compared to apramycin mediated chemical defense (Kever et al., 2022) in the model system Alderaan infecting *S. venezuelae*. In Figure 11 it is clearly visible that the phenotype elicited by the two distinct systems is very different. While apramycin mediated chemical defense leads to an inhibition in phage infection, visible in the culture growth and the decrease in phage titer over time, the stringent response triggered by different concentrations of SHX does not affect Alderaan infection (Figure 12). Considering these results, it is clear that chemical defense mediated by apramycin displays an individual kind of anti-phage defense which is distinct from the ppGpp mediated stringent response.

4.1.3 Phage CL31 is susceptible to spent medium of *S. tenebrarius*

In a similar fashion to the stringent response experiments, pre-incubation of phage particles in different SM was supposed to rule out or identify whether an extracellular effect of SM on phage particles was present. While Kever and colleagues could show for phage λ that genome injection was still successful in presence of apramycin, this was not possible for the *Streptomyces* phages (Kever et al., 2022). Therefore, the hypothesis of an intracellular effect of aminoglycosides was rather speculative and an extracellular effect, especially of SM, cannot be ruled out completely (Hardy et al., 2023; Kever et al., 2022). In this work the extracellular effect of different SM was tested in absence of host cells to determine whether the chemical defense mediated by *Streptomyces* SM relies on an intracellular or extracellular mechanism of action. Three different phages infecting bacteria of three distinct genera were used for this pre-incubation assay to estimate whether the mechanism of action observed for *Streptomyces* SM mediated chemical defense might differ regarding the host organism. For phage Alderaan and λ no significant effect of the SM on the infectivity of the phage particles was observed, however infectivity of CL31 particles was strongly impaired by *S. tenebrarius* SM (Figure 13). It seems likely that this effect is connected to the apramycin synthesis pathway since the mutants of the apramycin synthesis Δ*aprQ* and Δ*aprP* led only to a non-significant reduction in infectivity (Figure 14). One possible explanation is the secretion of a protease in concert with the later steps of the apramycin synthesis, which subsequently acts on the phage particle in a highly specific manner (Zhang et al., 2021). It is noteworthy that only the CL31 phage particle is affected by the SM and not the other two phages, even though they share the same morphotype. A specificity towards the CL31 proteins would explain why the putative protease in the SM only affects CL31 particles but neither Alderaan nor λ. Here again analysis of the composition and concentration of the *S. tenebrarius* wild type spent medium would be crucial to decipher which component leads to the distortion of CL31 particles, which was not possible during the duration of this study. For further investigations in this direction of

extracellular anti-phage defense it would be possible to include protease inhibitors in the pre-incubation assay to determine whether the effect is exerted by a protease or a different metabolite.

For all spent medium experiments it would be necessary to establish a running analytic method to determine the composition and concentration of the respective spent media before they are used in any experiment. The idea of spent media assays however should be followed up on as this underlines the ecological context and relevance of chemical defense mediated by *Streptomyces* spent medium. Furthermore, all results from this first chapter indicate that chemical defense might be both specific to the phage and variable between host organism regarding uptake of metabolites and availability of resistance genes (Kever et al., 2024; Luthe et al., 2023b). For *Streptomyces* phages an intracellular mechanism in the host cell seems most likely, as extracellular inactivation of Alderaan was not observed. If the mechanism of action acts within the confines of the intracellular space or rather acts as a blockage of the injection of the phage genome remains to be determined for *Streptomyces* phages (Kever et al., 2022). It would also be important to include more *Streptomyces* phages in the investigation approach, as a broader range of phages might reveal phage specific sensitivity determinants. Coliphages such as λ are likely inhibited after the injection of the genome into the host cell, which was already shown by Kever and colleagues (2022).

4.2 Isolation and characterization of novel *Streptomyces* phages

The discussion in this part has already been published in Rackow et al. 2024 (Microbiology Spectrum).

In this study, we present the isolation and characterization of four novel *Streptomyces* phages. Phage Kamino was isolated on *S. kasugaensis,* Geonosis was isolated on *S. griseus* and Abafar and Scarif were isolated on *S. coelicolor.* Phage Kamino is predicted to be a temperate phage, carrying a serine integrase on its genome, whereas Geonosis, Abafar and Scarif are predicted to be strictly virulent. Three of the four phages described in this study have a broad host range with productive infections on 7 to 15 different *Streptomyces* species (out of 45 different strains tested). Out of the 45 strains tested for host range, 15 were previously analysed for their phylogeny (Nouioui et al., 2018), however no phylogenetic pattern can be observed within the infection pattern. Similar to this, the defense mechanism distribution of the tested strains (Table S4) analysed by PADLOC does not show a significant pattern (Payne et al., 2022). In particular for the strains infected by phage Kamino we could find only one defense system that was present in all strains, the system PD-T4-6 (Vassallo, Doering, Littlehale, Teodoro, & Laub, 2022). These strains however all are lacking several systems, such as the Ssp (Shiwei Wang et al., 2021; Xiong et al., 2020) or DnD (Tong et al., 2018) defense systems as well as the Cas-type I-B system (Makarova et al., 2020), which are among others present in several strains

which are resistant to Kamino. We hypothesize that the host range pattern is therefore rather influenced by receptor availability and cell surface structures than by phylogenetic similarities.

Of the phages reported in this study, Kamino and Geonosis amplify well in liquid cultures (Figure 16). In particular, Kamino showed highly efficient infection of *S. kasugaensis* already at very low starting titers (10^2 PFU/ml). In contrast to this, Abafar and Scarif show little amplification in liquid infections and no effect on the growth of their host organism *S. coelicolor* A3 (2) M145. This is, in fact, not an unusual feature of phages infecting *Streptomyces* and has been reported previously (Hardy et al., 2020; Ongenae et al., 2023). This phenotype could be a phage specific feature, as it was also described by Hardy et al. (Hardy et al., 2020) in the characterization of 5 novel *Streptomyces* phages, where for example phage Dagobah infecting *S. coelicolor* A3(2) M145 does not show a culture collapse despite showing amplification in phage titer, similar to phage Coruscant infecting *S. venezuelae*, described in the same publication.

When compared to the recently reported *Streptomyces* phages Vanseggelen and Verabelle, which also infect several different species (Ongenae et al., 2023) (Figure S6), two major differences were detected in the genome of phage Kamino (Hardy et al., 2020). First, the gene for the integrase (Kamino_00049) shows no similarity at the nucleotide level to the integrase genes in Vanseggelen and Verabelle, secondly the gene annotated as a putative tail fibre in Verabelle and Vanseggelen, respectively, also reveals only weak similarities to its homolog in Kamino (Kamino_00020). However, the differences in their tail fibres compared to their otherwise conserved genome structure might explain their different host range behaviour as those structures are major players in virus-host interactions (Hardy et al., 2020). Moreover, broad host range phages like Kamino, equipped with a serine integrase for a temperate lifestyle, can serve as powerful tools for genetic manipulation across various strains (Montaño et al., 2022; Smith et al., 1999). In this context, novel integrative plasmids could be engineered utilizing the *attP* site of Kamino, expanding the repertoire of genetically modifiable *Streptomyces* strains.

Little is known so far about the characteristic phage traits of different morphotypes in phages infecting actinobacteria (Hatfull, 2020; Podgorski et al., 2020). In line with our findings, the majority of described *Streptomyces* phages belong to the morphotype of siphoviruses. Phage Abafar isolated in this study, however, might be a good example to study the differences in infection dynamics and adsorption of podoviruses. Genomic analysis of phage Abafar revealed that - in contrast to the three siphoviruses of this study - its genome contains 15 tRNA genes. Those phage-encoded tRNAs are considered to be used to evade host defense mechanisms that directly target tRNAs (Burman et al., 2024; van den Berg, van der Steen, Costa, & Brouns, 2023). Furthermore, we detected a gene

(Abafar_00064) with an incomplete conserved domain that shows similarities to an ArdA-like anti-restriction protein. BLASTp analysis of the predicted amino acid sequence identified homologous proteins only in other podoviruses infecting *Streptomyces* species.

To gain deeper insights into the determinants of phage-host interactions, particularly in relation to sensitivity to anti-phage defense systems - including those involving small molecules -, the comparative analysis of a diverse set of phages is required. In fact, systematic phage collections proved highly valuable in assessing the efficacy of diverse defense systems against a wide spectrum of phages infecting a particular host or genus (Maffei et al., 2021). Broad host range phages further provide the opportunity to determine context dependency by comparing the effect of a given defense system/anti-phage molecule across different host species. Beyond the study of bacterial immune systems and phage-encoded counter-defenses, the application of phages has also provided new insights into cell envelope biosynthesis and structure through the screening and analysis of phage-resistant bacterial strains (Hünnefeld et al., 2021; Kever et al., 2022; McKitterick & Bernhardt, 2022). Expanding the phage universe by providing new isolates to the scientific community is therefore valuable across multiple research areas within phage-host biology.

4.3 Screening efforts to identify more anti-phage small molecules

Screenings of small molecules which mediate chemical defense were primarily performed to identify sensitivity determinants in phages, that might explain the phenotype observed. In this context, an extensive library of phages, preferably infecting the same host strain, that differ in their genomic composition is of high value, as it allows to make direct comparisons in their response to chemical defense and probably draw conclusions based on their genomic makeup. This requires a complete characterization of the phage library, which is rarely found for *Streptomyces* phages (Rackow et al., 2024), however for coliphages there is an already described sophisticated library at hand, the BASEL collection, which was then used as tool to increase the screening capacity and significance (Maffei et al., 2021).

4.3.1 Screening of *Streptomyces* phages

The *Streptomyces* phages that were used in the screening of chemical defense mediating small molecules infect four different species and were mostly isolated and characterized in our own lab. Eleven out of the 16 phages used for screening were isolated in the Frunzke lab (Erdrich et al., 2024; Hardy et al., 2020; Rackow et al., 2024) and were thoroughly described regarding their genomic content, morphology and liquid infection dynamics. The phages used in this study are highly diverse concerning their GC content, ranging from 48 % to 73 %, their genome size between 34 kbp and 127 kbp as well as their lifestyle including both virulent and temperate lifestyles (Erdrich et al., 2024; Hardy

et al., 2020; Rackow et al., 2024). This collection of phages represents a good diversity of phage traits found in *Streptomyces* phages, which might determine sensitivity or resistance to chemical defense. In this case however no correlation of the genetic make-up of phages and efficiency of chemical defense could be drawn, most of the phages showed sensitivity towards the tested compounds (Figure 19C). For the screening of the *Streptomyces* species used in this study only one antibiotic resistance cassette was available, the *aac(3)IV* gene, expressed on the pIJLK04 plasmid (Table 6) which acetylates apramycin (Garneau-Tsodikova & Labby, 2016). It has to be noted that some phages still could not be tested on apramycin, as the host strain did not grow sufficiently despite the antibiotic resistance cassette. Neither for actinomycin D nor for daunorubicin it was possible to introduce a resistance cassette into the host strains, therefore the used concentrations are considerably lower and some phages could not be tested on higher daunorubicin concentrations, as the host did not grow (Figure 19C). One major drawback in the screening with *Streptomyces* phages however is, that only wild type host strains (equipped with a resistance cassette) were used. This means that different defense systems were present in each host and could interfere with the strength of the chemical defense (Tesson & Bernheim, 2023; Wu et al., 2024). Overall, most of the phages showed a decrease in titer on all of the tested compounds. This indicates the broad range of chemical defense as well as the ecological relevance of this anti-phage defense mechanism, as all species inhabit a similar ecological niche and could possibly be found in the same environment (Hardy et al., 2023; Hopwood, 2007; Zambri et al., 2022). It might be that the phage inhibitory effect observed in the screening is a result of synergistic effects between the small molecule and intracellular defense systems, therefore a defense deficient host strain in absence of any intracellular defense systems would be preferable. This would allow to compare the phage sensitivity to the tested compound and not the combination of the compound with a variation of defense systems (Section 4.5) (Baltz, 1998; Maffei et al., 2021; Smith et al., 2013). Genetic manipulation of *Streptomyces* strains is however not as simple as it is for model organism such as *E. coli* or *C. glutamicum* (Kieser et al., 2000). In this line of thought, it would be also interesting to test the chemical defense on broad host range phages isolated in this study on different hosts. Here more insights in the interplay between the host's genetic background and the chemical defense could be gained. Furthermore, a more systematic screening for chemical defense using the BASEL collection was performed, as the host strain of this collection is devoid of intracellular defense systems (Maffei et al., 2021). All phages from the collection infect the same host, *E. coli* MG1655 ΔRM, allowing for the testing of the effect of small molecules without the interference of other systems, thereby minimizing the variables in the screening significantly (Maffei et al., 2021).

4.3.2 Screening the BASEL collection

Screening of small molecule mediated chemical defense with the BASEL collection was performed to increase the depth of the screening, including a broader diversity of phage families that infect the same host strain (Maffei et al., 2021). The screening host *E. coli* K12 MG1655 ΔRM is a model organism which is fully described in both genomic make up as well as physiological behaviour, which was additionally modified to be devoid of all anti-phage defense systems that might interfere with the chemical defense (Maffei et al., 2021; Mee-Jung & Sang Yup, 2012; Vassallo et al., 2022; S. Wang et al., 2023). Screening of the BASEL collection revealed that aminoglycoside antibiotics have little to no inhibitory effect on coliphages as only the positive control phage λ was inhibited by apramycin or kanamycin. DNA intercalating agents such as actinomycin D and daunorubicin however show a strong, broad range anti-phage defense effect with the latter being a potent chemical defense agent inhibiting whole phage families such as the *Drexlerviridae, Demerecviridae* or *Vequintavirinae* (Figure 20). This screening led to the focus for the remainder of this work on daunorubicin as potent anti-phage defense small molecule, which was already described to exert a broad range anti-phage defense (Kronheim et al., 2018). Phages that showed sensitivity towards actinomycin D were with three exceptions also susceptible to daunorubicin, which could imply a similar mechanism of action of both small molecules on those phages (Figure 20). Bas14, Bas17 and Bas45 are the exceptions which show sensitivity to actinomycin D but not to daunorubicin, this is however not to be explained by any similarities in genome length or GC content. The two *Dhillonviruses* and the *Tequatrovirus* have very little in common, as the first two phages have a genome size of ~ 43 kbp and a GC content of 54 % whereas the latter has a genome size of 170 kbp and a GC content of 35 % (Kronheim et al., 2018). This lack of similarity holds true for all phages which are susceptible to actinomycin D, which spans the whole range of virion morphology, genome size and GC content. So no direct conclusions can be drawn regarding phage sensitivity determinants towards actinomycin D (Kronheim et al., 2018). For daunorubicin, a similar pattern is observed, with a wide range of characteristics among sensitive phages. However, resistant groups stand out to daunorubicin-mediated chemical defense. The *Tevenvirinae* are among others one family of phages known for their highly modified DNA (Maffei et al., 2021; Tong et al., 2018; Shuangshuang Wang et al., 2022). A hypothesis which was postulated upon this observation was that the addition of the sugar moiety to the cytosines of the phage DNA might block intercalation of the anti-phage molecule and therefore provide resistance. For the phages of the genus *Dhillonvirus* such genomic modification is not described, however they are considerably smaller in the genome size with 43-46 kbp and have a significantly higher GC content of ~55 % when comparing to the *Tevenvirinae* (Maffei et al., 2021). Bas18 of the genus *Dhillonvirus* is an outlier in the sensitivity to daunorubicin, as in contrast to the other phages of this genus, Bas18 is indeed inhibited by the small

molecule, however no indicating factor could be identified when comparing the genomes of these phages (Figure 20, Section 6.4, suppl. material) (Maffei et al., 2021). It is possible that the small genome size allows for faster replication of the phages in this genus, which might be another strategy to avoid the inhibition of the infection by daunorubicin. The last distinct group of phages that is resistant to daunorubicin are the *Studiervirinae* which are closely related to T3 and T7 (Figure 20) (Maffei et al., 2021). Furthermore, for these phages no distinct genomic modification is known which might resemble the features of the *Tevenvirinae*. However, for the *Studiervirinae* it is well known that those phages carry their own RNA polymerases, which are also biotechnologically used, and which might here play a role in the resistance towards chemical defense (Maffei et al., 2021; Savalia, Robins, Nechaev, Molineux, & Severinov, 2010). It is a possible mechanism of action, that daunorubicin works in concert with host factors which are often blocked by T7-like phages after the early expression phase, which could explain the resistance observed here (Tabib-Salazar et al., 2018). These findings in the BASEL screening led the direction of this work to the in depth study of chemical defense mediated by daunorubicin in order to understand the mechanism of action which remained elusive despite intensive research in this topic (Hardy et al., 2023; Kever et al., 2022; Kronheim et al., 2018). Regarding the results of the screening no distinct mechanism of action or phage genomic sensitivity determinants can be identified. However, different hypothetical mechanism were postulated, ranging from dsDNA breaks due to intercalation into the DNA, via abortive infection mechanism triggered by daunorubicin to a hindrance of phage DNA replication by the blockage of the DNA polymerases.

4.4 Uncovering the mechanism of action of daunorubicin mediated chemical defense

Since daunorubicin presented to be the most potent anti-phage defense mediating small molecule, this study further focused on daunorubicin mediated chemical defense. Different hypothesis about the mode of action of daunorubicin were postulated over the course of this study. One possible mode of action is the alteration of the host metabolism which in turn leads to a blockage of the phage infection from an early stage of infection. Another possible mode of action is the blockage of the phage entry into the host cell by inhibiting the genome injection. If daunorubicin acts intracellularly, different scenarios for the mode of action were hypothesized. For example a similar mode of action of daunorubicin that was shown for eukaryotic and prokaryotic DNA could be possible, where daunorubicin intercalates into the DNA and thereby leads to dsDNA breaks. For doxorubicin, a closely related molecule to daunorubicin, a two-step intercalation mechanism is described, the AT rich minor groove is bound first, followed by the intercalation of the aromatic rings into GC-rich regions of the DNA double-helix (Pérez-Arnaiz, Busto, Leal, & García, 2014). Furthermore, it is possible that daunorubicin deters the DNA-protein complex formation of the DNA polymerase with the DNA, thus inhibiting DNA replication. It is also possible that daunorubicin acts in concert with downstream

defense systems such as RM systems by slowing down the phage replication machinery and thereby allowing the intracellular system to act sufficiently to stop the phage infection. And lastly it was hypothetised that the combination of daunorubicin and phage infection lead to an abortive infection which could be caused by the increased influx of the small molecule due to the cell wall perforation of the host during the injection of the genome. This could lead to a disbalance in the cytosolic space and subsequently lead to cell death. In the following chapter the experiments conducted will be set into perspective and it will be discussed which of the postulated hypothesis (Figure 29) is the most likely explanation for the phenotypes that were observed.
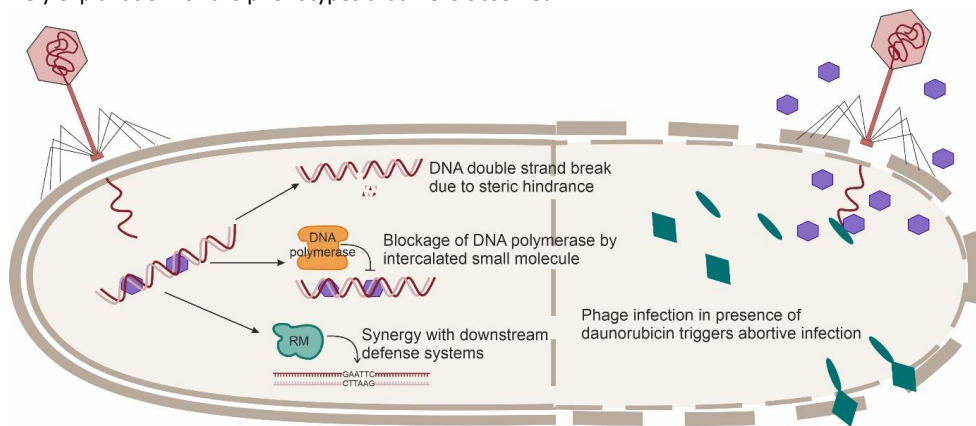
Figure 29: Hypothetical mode of action of daunorubicin mediated chemical defense. In this scheme the different possible modes of action of daunorubicin mediated anti-phage defense in the intracellular context are shown. On the left side mechanisms, which do not necessarily lead to cell death are shown. On the right the possible abortive infection mechanism of daunorubicin is depicted. On the left it is portrayed how intercalated daunorubicin leads to dsDNA breaks due to steric hindrance. Furthermore, it is illustrated how daunorubicin deters the formation of DNA-protein complexes with e.g. the DNA polymerase, thereby inhibiting DNA replication. And lastly it is depicted how daunorubicin acts in concert with downstream defense systems which leads to the inhibition of phage infection.

A great part of the experiments were planned, performed and discussed with Dr. Larissa Kever in collaboration, therefore her contributions to this work should be recognized in this part especially. The overall, aim of this chapter is to understand the role of daunorubicin mediated chemical defense in the intricate network of phage-host interactions in *E. coli.* Furthermore, we set out to dissect how different characteristics in the phage-host interaction might influence the daunorubicin mediated chemical defense and finally we aimed to integrate the chemical defense into the bigger context of the bacterial immune system.

4.4.1 Daunorubicin alone does not influence the hosts anti-phage defense systems

The first step necessary to understand the chemical defense mediated by daunorubicin was to determine the response of the host organism to the small molecule, especially the change in transcription as response to the small molecule exposure. The goal was to determine whether daunorubicin had a direct effect on the phage infection by interacting with the phage replication

machinery or the phage DNA or whether the effect is indirect by redirecting the host metabolism into a pre-determined stress response which might already fend off phage infection from the beginning. The transcriptomic data of the host strain *E. coli* K12 MG1655 ΔRM however show no general stress response in the way that the bacterial cell would go into a dormant state or downregulate all metabolic pathways (Maslowska, Makiela-Dzbenska, & Fijalkowska, 2019; Žgur Bertok & Podlesek, 2021). In contrast, the transcriptome data in presence of daunorubicin displayed an overall upregulation of genes associated with ribosomal subunits, hinting towards an increase in overall transcription. Furthermore, genes associated with different metabolic pathways are significantly upregulated, which suggests that the cells are in a metabolically active state. Daunorubicin alone does not lead to cell growth arrest or other phenotypes associated with high levels of stress or phage infection (Bhatia, Kirit, Predeus, & Bollback, 2022; Bie et al., 2023). Genes that are significantly upregulated rather hint towards the possibility that *E. coli* metabolizes daunorubicin over time, as several enzymatic pathways and efflux pumps are upregulated (Figure 21, Table S5). Surprisingly, during the analysis of the transcriptomic data only a few DNA regulation associated genes were expressed differently in presence and absence of daunorubicin, even though daunorubicin is expected to intercalate into DNA and thereby lead to steric hindrance of the topoisomerase complex and finally to distortion of the DNA (Alotaibi & Momen, 2020; Bhatia et al., 2022). These seven genes include *nfi* an endonuclease V, *recN* a DNA repair protein, *ruvC* a crossover junction endodeoxyribonuclease, *insC6* an IS2 insertion element repressor, as well as *matA, tdcA,* and *hns,* which are DNA-binding transcriptional regulators (Table S5). Overall the transcriptomic analysis suggests that the host strain is able to cope with daunorubicin at the sub-inhibitory concentrations reasonably well. No drastic stress responses are triggered by the small molecule itself, as significantly less genes are differentially expressed in comparison to stress situations with other antibiotics e.g. kanamycin (Bhatia et al., 2022; Bie et al., 2023). This also fits to the phenotype observed in the growth behaviour of *E. coli*, as it can grow in relatively high concentrations of daunorubicin (up to 80 µM) without any growth defects, even in absence of any antibiotic resistance cassette (Kronheim et al., 2018). The data gained here however only depicted the reaction of the host to the small molecule in absence of any phage infection. It would be crucial to repeat the RNA-seq experiments in presence of phages to assess the cellular response to phage infection in presence and absence of daunorubicin to have more comprehensive insights of the cellular metabolic dynamics in the presence of chemical defense.

4.4.2 Phage genome injection of sensitive phages is not impaired by daunorubicin

The next reasonable step was to determine whether phages, sensitive to daunorubicin mediated chemical defense are actually able to inject their genome into the host cell. Relying here on the method that has been described useful for λ (Boulanger & Letellier, 1988; Kronheim et al., 2018),

potassium efflux assays were performed with different sensitive phages (Figure 20). All tested phages trigger potassium efflux in both conditions, suggesting that daunorubicin has no negative effect on the phage genome injection itself (Figure 22 A-D). An atypical phenotype which was observed for Bas13, Bas20 and λ however is, that the efflux in presence of daunorubicin is faster compared to the efflux in absence of the compound (Figure 22 B, C & D). This could have different reasons, as for example the phage injecting its genome into the host cell might lead to an increase in permeability of the cell wall, thus more daunorubicin can enter the cell and thereby the efflux of potassium ions is enhanced. This is a mere speculation, as only little is known about the injection mechanism, such as the primary and secondary receptor of Bas09, Bas13 and Bas20. However, seeing that those three phages belong to different genera, it might be possible that the injection mechanism of these phages differ greatly (Maffei et al., 2021). Distortion of the cell wall integrity due to phage infection can lead to the efflux of more than just potassium ions, as it was described for phage T4, that different cell envelope components are released into the medium upon phage infection (Loeb, 1974). This extent of which different phages lead to cell-wall distortion might explain the different phenotypes observed in the potassium efflux. Overall, the most important information gained here is that the effect of daunorubicin is most likely intracellular, as all phages are able to infect the cell and inject their genome irrespective of presence or absence of the small molecule (Figure 22 A-D). Therefore, we can reject the hypothesis that daunorubicin acts by blocking the injection of the phage genome, at least for the phages tested here. The growth curves which resemble the conditions used in the potassium efflux assays reveal another interesting phenotype, as Bas09 Bas20 and λ show an abortive infection phenotype in presence of daunorubicin (Lopatina et al., 2020). This means that the infected culture in presence of daunorubicin shows no sign of growth or lysis but seems to be stalled, which is depicted in a flat growth curve (Figure 22). Only for Bas13 a restored growth can be observed in presence of daunorubicin (Figure 22B). The phage titer does not change significantly over the course of the experiment regardless of the small molecule, which was expected due to the short time span of the experiment. Summarising these results two important conclusions can be drawn, i) all phages are able to inject their genome, irrespective of the presence of chemical defense and ii) the mechanism of action of daunorubicin might be different from phage to phage as the growth curves reveal here and abortive infection as a mechanism of action seems highly likely. This underlines once more the hypothesis that chemical defense mediated by daunorubicin is a phage specific trait.

4.4.3 The host genomic background has a bigger impact on chemical defense than the phage genome modification

One outstanding group of phages that was identified to be resistant to daunorubicin mediated chemical defense in the BASEL screening were the *Tevenvirinae,* which include the model phage T4,

and are known for their high degree of DNA modification. T4 for example modifies up to 100 % of its cytosines by adding hydroxymethylglucose groups to the base (Hattman, 2009; Varma et al., 2022). It is already known that these DNA modifications are conferring resistance to nuclease mediated anti-phage defense systems such as CRISPR or RM systems (Bryson et al., 2015; S. Wang et al., 2023). Consequently, the hypothesis arose that hydroxymethyl-glycosylation of the T4 DNA is the cause of resistance towards daunorubicin, as the bulky sugar moiety added to the cytosine's might prevent the intercalation of daunorubicin into the DNA. Due to T4 being a well-studied model phage, different mutants and variants of T4 are available, which was used to investigate the role of DNA modifications in the context of daunorubicin mediated chemical defense. The T4 wild type (~ 100 % glycosylated), the NgTET treated T4 (~ 50 % glycosylated) (Pozhydaieva et al., 2024) and a T4 Δα/β glycosyltransferase mutant were tested in liquid infection experiments. While comparing these T4 variants in liquid infection experiments, it looked like the T4 wild type and the T4 Δα/β glycosyltransferase mutant show resistance to daunorubicin and the NgTET treated T4 was susceptible to the small molecule (Figure 23). However, these results were gained on two different host strains. The T4 wild type and the glycosylation deficient mutant were tested on the *E. coli* MG1655 ΔRM and the NgTET treated T4 was tested on *E. coli* BL21 carrying the plasmid with the active and inactive NgTET enzyme (Table 6). This difference in background strains was probably the reason why a difference in response to the small molecule was observed, since the difference between the T4 wild type and the glycosylation deficient mutant should be the strongest, when the modification alone is reason for the resistance. Investigating this thought further, the T4 wild type and the NgTET treated T4 were compared on different host strains and here it became obvious that the host background is more important for the effect of chemical defense than the genetic modification of the phage tested (Figure 24). The *E. coli* host strains are derivatives of the K12 strain and the B strain which are equipped with different intracellular defense systems and have a different cell envelope (Table S6) (Marisch et al., 2013; Yoon, Jeong, Kwon, & Kim, 2009). It was shown that BL21 has a higher permeability of the membrane compared to K12 derivatives, due to variation in the lipopolysaccharide layer and the reduced expression of efflux pumps (Mee-Jung & Sang Yup, 2012). This difference in the envelope likely enhances the uptake of daunorubicin in the BL21 derivatives, leading to higher intracellular daunorubicin concentrations. When comparing both T4 variants on the different background strains it becomes apparent that there is no difference in infection behaviour between the phages but a clear difference in infectivity between the different *E. coli* strains (Figure 24). The K12 derivatives were infected by either T4 variant in presence and absence of daunorubicin and no difference in the culture collapse was observed. In contrast to this, the B strain derivatives all showed a recovered growth in presence of daunorubicin and neither of the T4 variants could amplify successfully. Phenotypic results

shown in Figure 24 were further supported with intracellular DNA measurements after infection, where again the two tested T4 variants show no significant difference in DNA amplification in presence of daunorubicin (Figure 25). These results contradict the previously stated hypothesis, and suggest that the host genetic background and cell envelope play a crucial role in the effectiveness of chemical anti-phage defense. This statement is further supported by the *in vitro* analysis of interactions between small molecules and DNA from the three T4 variants (Figure S8), where the same interaction pattern of either daunorubicin, apramycin or actinomycin D can be observed for all tested T4 variants. These results showed that chemical defense mediated by daunorubicin is highly complex, as the chemical defense works in concert with the host defense systems (Wu et al., 2024). Both the composition of the hosts' immune system as well as the host cell wall influence the efficiency of chemical defense mediated by daunorubicin. Comparison of T4 infectivity on different *E. coli* strains redirected the focus on this work on the interaction of chemical defense with downstream defense systems and to further identify crucial steps of phage infection that might influence the resistance or sensitivity towards chemical defense systems.

4.4.4 Infection kinetics are crucial for the strength of chemical defense

Phage infection is a precisely coordinated process consisting of multiple stages, each of which may influence the effectiveness of small molecule-mediated anti-phage defense (Wolfram-Schauerte, Pozhydaieva, Viering, Glatter, & Höfer, 2022). In order to decipher the mechanism of action of daunorubicin mediated chemical defense, these stages were investigated in more detail. One main factor that can influence the effectiveness of anti-phage defense systems is the MOI challenging the bacteria. This can already give hints towards the mechanism of action from the resulting growth curves (Aframian & Eldar, 2023; Lopatina et al., 2020; Millman et al., 2022). Here different MOI's of a selection of phages were tested in presence and absence of daunorubicin to assess whether abortive infection phenotypes are present and to elucidate whether the amplification kinetics of the phages play a role in the effectiveness of the chemical defense. In contrast to the results of Figure 24, no abortive infection growth behaviour was observed. However, clear distinctions in the effectiveness of daunorubicin mediated chemical defense can be drawn in respect to the phage amplification speed. In Figure 26 it is shown that slowly replicating phages such as Bas20, Bas30 or λ are completely inhibited by daunorubicin. Fast replicating phages with increased infection kinetics like Bas41, Bas24 or T4 on the other hand show resistance towards the compound (Figure 26). The speed of amplification is for sure not the only reason why some phages are sensitive and others are resistant, however if we place the amplification speed into context of layered anti-phage defense and interaction of different defense systems, this could explain why faster infecting phages are more likely to be resistant to chemical defense. As the bacterial immune system is a highly complex network of

genes, proteins and different triggers, not all phages are fought off with the same system (Hochhauser et al., 2023; Millman et al., 2022). In this case, the host organism used here was devoid of any other intracellular anti-phage defense systems, therefore the daunorubicin was the only instance of defense (Maffei et al., 2021). Here amplification speed might be the turning point, when the small molecule is too slow to associate with the phage DNA, the phage replication cycle is not deterred and the infection can run normally. A phage with a slower replication mechanism, likely dependent on the recruitment of host polymerases, allows more time for the small molecule to associate with phage DNA. This interaction could disrupt the replication complex, ultimately resulting in complete inhibition of phage replication. Considering the two-step intercalation mechanism into the DNA described for doxorubicin, fast replicating phages might disturb the minor-groove binding by starting to replicate and thereby avoiding the anti-phage defense effect of the compound in general (Pérez-Arnaiz et al., 2014). Also abortive infection mechanisms, which are last resort mechanisms of anti-phage defense usually take more time to act, compared to RM systems, which could explain why fast replicating phages show a higher degree of resistance compared to slowly replicating phages (Aframian & Eldar, 2023; Lopatina et al., 2020). An abortive infection mechanism triggered by daunorubicin could also explain the differences observed between different phages, as different phages alter the cell permeability during infection to different degrees (Hu, Margolin, Molineux, & Liu, 2015; Loeb, 1974; Thompson & Wiberg, 1978). This however is very speculative and needs deeper investigation, probably with circular dichroism studies (CD) or nuclear magnetic resonance (NMR) spectroscopy after *in vivo* association of the phage DNA with the small molecule as well as LC-MS measurements of the cytosolic components after infection to gauge if an abortive infection mechanism is taking place. CD or NMR spectroscopy are analytical techniques to measure secondary structures of biomolecules and to provide insights into conformational states, changes, and interactions (Searle, 1993; Subadini, Hota, Behera, & Sahoo, 2022). From these results we can deduce that in an anti-phage defense devoid host cell, fast replicating phages show resistance towards daunorubicin mediated chemical defense, indicating the importance of amplification kinetics as factor in the effectiveness of chemical defense.

4.4.5 *In vitro* synthesis of phage particles reveals different mechanism of action for different phages

A different approach to identify the mechanism of action of daunorubicin mediated chemical defense was the *in vitro* synthesis of phage particles using a TXTL system (Rustad, Eastlund, Jardine, & Noireaux, 2018; Rustad, Eastlund, Marshall, Jardine, & Noireaux, 2017; Shin, Jardine, & Noireaux, 2012). The idea behind this was to identify with certainty where in the cell the daunorubicin is acting and if certain host or phage factors are needed for the anti-phage defense properties of daunorubicin. A TXTL system resembles the cytosolic space, therefore any membrane associated mechanism of the small molecule would fail to function under the given circumstances (Gregorio, Levine, & Oza, 2019;

4. Discussion

Tinafar, Jaenes, & Pardee, 2019). Furthermore, the cell free expression system is not limited by any cell growth limiting factors, as product toxicity can be neglected in the *in vitro* synthesis approach. In this study two phages which showed a different response to daunorubicin were tested, Bas09 of the subfamily of *Tempervirinae* and T7 of the genus *Teseptimavirus*. Bas09 was identified to be sensitive to daunorubicin in the BASEL screening (Figure 20) when tested on the anti-phage defense deficient host strain, whereas T7 was observed to be resistant to lower concentrations of the same host and only elevated concentrations of ~40 µM lead to a decrease in T7 infectivity. T7 was chosen as phage here, since the first bacteriophage particles which were successfully synthetized in TXTL systems were T7 particles (Rustad et al., 2017; Shin et al., 2012). T7 acted as positive control for the synthesis in general and as resistant phage in regard to daunorubicin mediated chemical defense. Surprisingly, the exact opposite of the expected results were observed when manipulating the TXTL reaction with different concentrations of daunorubicin. Here T7 showed sensitivity to daunorubicin, with a stronger decrease in titer at elevated concentrations of daunorubicin (Figure 27) and Bas09 was not impaired in synthesis. It seemed that the synthesis of Bas09 was even stabilized by the small molecule. This can indicate two things for the mechanism of action of daunorubicin; i) daunorubicin mediated inhibition of Bas09 phage infection is associated with the cell wall, which is absent in the TXTL and therefore no inhibition is taking place, or ii) for the inhibition of Bas09 by daunorubicin specific host factor must be present which are lacking in the TXTL master mix. Both of these explanations could hint towards an abortive infection mechanism mediated by daunorubicin. Since T7 encodes its own polymerases, this might explain why T7 is still sensitive to the compound (Adler & Modrich, 1979). Bas09 is devoid of encoded polymerases on its genome and therefore relies on the host polymerases, which are recruited during the process of phage infection (Maffei et al., 2021) or in this case the *in vitro* synthesis. The myTXTL kit used here has the endogenous *E. coli* B strain DNA and RNA polymerase as well as the sigma factor σ_{70} which form the holoenzyme, other polymerases must be added on a plasmid into the mix (Rustad et al., 2017). If daunorubicin is forming a complex with the phage genome and the respective polymerase, it would explain why in this case T7 shows a stronger sensitivity towards the compound compared to Bas09. The association of the T7 RNA polymerase to the T7 DNA is considerably stronger compared to the *E. coli* RNA polymerase to the Bas09 DNA. This hypothesis is however very speculative and needs further investigations, such as EMSA assays comparing the interaction of T7 DNA/T7 RNA polymerase with Bas09 DNA/*E. coli* RNA polymerase and how daunorubicin is acting on these complexes. Even though daunorubicin is primarily described to act on the DNA by intercalating into the bases and leading to steric hindrances, a protein-DNA-daunorubicin complex formation cannot be excluded. Since the SPR biacore measurements with T4 DNA showed that the interaction with DNA and daunorubicin are rather an on/off state than as stable intercalation

(Alotaibi & Momen, 2020; Hajan, Shams, & Parvin, 2009) (Figure S8). Concluding, the cell free synthesis of different phage particles in presence of daunorubicin supports the hypothesis of an abortive infection mechanism triggered by daunorubicin. For phage T7 the sensitivity observed here correlates with the sensitivity observed *in vivo* as well (Kronheim et al., 2018) which is expected considering an abortive infection mechanism, since T7 hijacks the whole host metabolism relatively quickly after injection of the genome and therefore could counteract abortive infection mechanism to a certain degree (Tabib-Salazar et al., 2018). For Bas09 an abortive infection mechanism *in vivo* would explain why the *in vitro* synthesis of Bas09 was not deterred by daunorubicin, as the *in vitro* system lacks the components for an abortive mechanism and is designed to withstand a certain degree of self-toxicity (Rustad et al., 2018; Rustad et al., 2017).

4.5 Synergistic effects between intracellular defense systems and chemical defense lead to efficient inhibition of phage infection

In section 3.4.4 it was shown that rather the host background affected the efficiency than the DNA modification of the phage, therefore it was then hypothesised that there might be an interaction between the daunorubicin mediated chemical defense and the intracellular defense systems. Testing this, different concentrations of daunorubicin were combined with different plasmid based defense systems in the "defense clean" background strain. Six different RM systems, three abortive infection systems with different mechanism of action and two different retron systems were tested in combination with daunorubicin on eleven different phages (Figure 28A). Representatives of the *Drexlerviridae, Siphoviridae* and *Demerecviridae* were tested, as several phages from those groups showed sensitivity to daunorubicin mediated chemical defense in absence of any additional defense system (Figure 20). Synergistic effect for all of the tested intracellular defense systems could be determined (Figure 28A) in a highly phage specific manner. This behaviour was expected regarding the definition of synergism which is that the combined effect of two systems is greater than the addition of the single effects of these systems (Wu et al., 2024). This means that the phages ought to be sensitive to either system, chemical defense or intracellular defense, in order of those two systems to act synergistically. Now the pattern of synergy differs regarding on the concentration of daunorubicin, which is also expected, as each phage has an individual threshold of daunorubicin that it might tolerate as well as a concentration of daunorubicin that alone is sufficient to inhibit the phage, therefore synergistic effects of two defense systems is a "sweet spot" (Figure 28A). These results of synergy between intracellular and chemical anti-phage defense systems support the hypothesis, that daunorubicin is working intracellularly and might interfere with the DNA-protein complex that is formed during either DNA replication (DNA/DNA polymerase) or transcription (DNA/RNA polymerase). This could slow down the phage infection considerably and allow for an abortive

infection mechanism to take over (Lopatina et al., 2020). In liquid infection assays with Bas09 this phenotype of synergism was investigated in detail and strong synergistic effects between daunorubicin and EcoCFT_II and Old could be determined. Those two systems alone were already identified to show anti-phage defense effects on Bas09 (Maffei et al., 2021) as well as sensitivity to daunorubicin was shown in the BASEL screening (Figure 20). In the liquid infection assay it was depicted, that the synergy is not only a factor of concentration of the chemical defense compound but also the concentration of phages that might infect the host strain (Figure 28B). With MOI >1 a growth arrest in presence of daunorubicin was observed, which was considerably faster than the infection induced culture collapse. This supports the hypothesis of an abortive infection mechanism triggered by daunorubicin (Aframian & Eldar, 2023; Lopatina et al., 2020). This phenotype is also resembled in the change in phage titer (Figure 28C), where the titer in the abortive infection phenotype does not change in presence of daunorubicin at the highest MOI. Overall, these results stress out that anti-phage defense mediated by small molecules is a delicate process, influenced by many factors which affect the efficiency of the defense. Furthermore the synergy between intracellular and chemical defense mechanism explain the phenotypes observed on the different host strains in section 3.4.4, as different *E. coli* strains are equipped with different defense systems, which when acting synergistically with daunorubicin, are able to inhibit T4 phage infection (Figure 25). One explanation could be that the retron system of the *E. coli* BL21 strains gets activated in presence of daunorubicin and therefore leads to an inhibition of phage infection. Another explanation would be that the BL21 strains have an increased uptake of daunorubicin compared to the K12 derivatives, which in turn triggers abortive infection mechanism, due to differences in the cell envelope and expression of efflux pumps in those two strains (Mee-Jung & Sang Yup, 2012). With MOI<1 the rescue of growth phenotype, which is shown in Section 3.4.4 could also be explained by abortive infection mechanism. These results also highlight, that chemical defense, as another layer of the bacterial immunity is a highly complex, phage specific and variable kind of defense system, which explains why a direct and distinct mechanism of action was not identified yet (Georjon & Bernheim, 2023; Kever et al., 2022; Kronheim et al., 2018).

4.6 Conclusion and Outlook

Bacteria of the genus *Streptomyces* have proven to be versatile producers of a myriad of specialized metabolites with various different functions, which is known for decades (Bibb, 2013; Gomez-Escribano & Bibb, 2011; Kieser et al., 2000). This work highlights how these specialized metabolites can provide multifunctional protection to *Streptomyces spp.*, conferring protection against both, competing bacteria as well as infectious phage particles (Hardy et al., 2023; Kever et al., 2022; Kronheim et al., 2018). We set out to understand the mechanism of action of small molecule mediated anti-phage defense in both natural producers of anti-phage compounds as well as well-established

model organisms. This work revealed several new insights into the chemical defense of *Streptomyces spp.* such as i) naturally produced aminoglycosides, other than apramycin, are sufficient to inhibit phage infection, even though inhibition differs between different aminoglycosides (Kever et al., 2022); ii) isolation and characterization of novel phages infecting *Streptomyces* species is crucial to broaden our understanding of the interaction between phage and host and how chemical defense interferes with this interaction; iii) chemical defense mediated by small molecules confers protection against a broad range of phages in both closely related species as well as model organism, despite coliphages being mostly resistant to aminoglycosides and lastly iv) daunorubicin mediated chemical defense is specific to the phage and acts synergistically with downstream defense systems. Chemical defense mediated by small molecules which are naturally produced by *Streptomyces spp.* has been proven to be an efficient, yet complex anti-phage defense. It is possible that small molecules interfere with multiple steps of phage amplification and therefore it might be difficult to pin point a singular target or mechanism of action. Especially for daunorubicin mediated chemical defense, it is possible that the compound has more than one way of inhibiting phage infection (see Figure 29). This would explain both the broad range of inhibition as well as the lack of a defined mechanism of action. We could narrow down the mechanism of action for all of the tested susceptible phages to be in the intracellular space, after injection of the phage genome, however between injection of the genome and the onset of genome replication, there are several possibilities where and how daunorubicin could act.

In order to further deepen the understanding of chemical defense and integrate this extracellular anti-phage defense system into the bacterial immune system, several experiments are needed. For further experiments of anti-phage molecule producer strains it would be preferable to have a defense system free *Streptomyces* background host, similar to the *E. coli* K12 MG1655 ΔRM strain in order to disentangle the effect of the chemical defense from the intracellular defense systems. Furthermore, for the mechanism of action of daunorubicin, several measures can be taken to gain more insights. In order to investigate the interaction between daunorubicin and phage DNA-protein complexes for example EMSA assays with purified phage DNA, host polymerases and the compound could be performed. To identify abortive infection mechanisms and the responsible cell suicide factors after infection with high MOI, LC/MS measurements of the cytosolic cell components could be performed. And additionally microscopic imaging on the single cell level would reveal great insight in cells fate after infection when the chemical defense is present.

Overall this work highlights the tremendous potential of *Streptomyces* anti-viral strategies to provide a new, population wide layer of anti-phage defense and stresses out that phage infection as well as the inhibition thereof is a highly orchestrated process. The bacterial immune system, similar to the eukaryotic immune system, consists of different layers of protection that interact with one another in

4. Discussion

order to protect the single cell as well as the population. Broadening our understanding here might help to identify new strategies of protection against eukaryotic viruses as well.

4. Discussion

5. References

Ackermann, H. W. (2006). Classification of bacteriophages. *The bacteriophages, 2*, 8-16.

Ackermann, H. W. (2007). 5500 Phages examined in the electron microscope. *Archives of Virology, 152*(2), 227-243. doi:10.1007/s00705-006-0849-1

Adler, S., & Modrich, P. (1979). T7-induced DNA polymerase. Characterization of associated exonuclease activities and resolution into biologically active subunits. *J Biol Chem, 254*(22), 11605-11614.

Adriaenssens, E., & Brister, J. R. (2017). How to Name and Classify Your Phage: An Informal Guide. *Viruses, 9*(4). doi:10.3390/v9040070

Aframian, N., & Eldar, A. (2023). Abortive infection antiphage defense systems: separating mechanism and phenotype. *Trends in Microbiology, 31*(10), 1003-1012. doi:doi.org/10.1016/j.tim.2023.05.002

Alotaibi, S. H., & Momen, A. A. (2020). Anticancer Drugs' Deoxyribonucleic Acid (DNA) Interactions. *Biophysical Chemistry - Advance Applications*. doi:doi: 10.5772/intechopen.85794

Bair, C. L., & Black, L. W. (2007). A Type IV Modification Dependent Restriction Nuclease that Targets Glucosylated Hydroxymethyl Cytosine Modified DNAs. *J Mol Biol, 366*(3), 768-778. doi:doi.org/10.1016/j.jmb.2006.11.051

Baltz, R. H. (1998). Genetic manipulation of antibiotic producing *Streptomyces*. *Trends in Microbiology, 6*(2), 76-83. doi:doi.org/10.1016/S0966-842X(97)01161-X

Bankevich, A., Nurk, S., Antipov, D., Gurevich, A. A., Dvorkin, M., Kulikov, A. S., . . . Pevzner, P. A. (2012). SPAdes: a new genome assembly algorithm and its applications to single-cell sequencing. *J Comput Biol, 19*(5), 455-477. doi:10.1089/cmb.2012.0021

Barka, E. A., Vatsa, P., Sanchez, L., Gaveau-Vaillant, N., Jacquard, C., Klenk, H.-P., . . . Wezel, G. P. v. (2016). Taxonomy, Physiology, and Natural Products of Actinobacteria. *Microbiology and Molecular Biology Reviews, 80*(1), 1-43. doi:doi:10.1128/MMBR.00019-15

Bentley, S. D., Chater, K. F., Cerdeño-Tárraga, A. M., Challis, G. L., Thomson, N. R., James, K. D., . . . Hopwood, D. A. (2002). Complete genome sequence of the model actinomycete *Streptomyces coelicolor* A3(2). *Nature, 417*(6885), 141-147. doi:10.1038/417141a

Bernheim, A., & Sorek, R. (2020). The pan-immune system of bacteria: antiviral defence as a community resource. *Nat Rev Microbiol, 18*(2), 113-119. doi:10.1038/s41579-019-0278-2

Bhatia, R. P., Kirit, H. A., Predeus, A. V., & Bollback, J. P. (2022). Transcriptomic profiling of *Escherichia coli* K-12 in response to a compendium of stressors. *Scientific Reports, 12*(1), 8788. doi:10.1038/s41598-022-12463-3

Bibb, Mervyn J. (2013). Understanding and manipulating antibiotic production in actinomycetes. *Biochemical Society Transactions, 41*(6), 1355-1364. doi:10.1042/bst20130214

Bie, L., Zhang, M., Wang, J., Fang, M., Li, L., Xu, H., & Wang, M. (2023). Comparative Analysis of Transcriptomic Response of *Escherichia coli* K-12 MG1655 to Nine Representative Classes of Antibiotics. *Microbiology Spectrum, 11*(2), e00317-00323. doi:doi:10.1128/spectrum.00317-23

Bolivar, F., Rodriguez, R. L., Greene, P. J., Betlach, M. C., Heyneker, H. L., Boyer, H. W., . . . Falkow, S. (1977). Construction and characterization of new cloning vehicle. II. A multipurpose cloning system. *Gene, 2*(2), 95-113.

Bondy-Denomy, J., Qian, J., Westra, E. R., Buckling, A., Guttman, D. S., Davidson, A. R., & Maxwell, K. L. (2016). Prophages mediate defense against phage infection through diverse mechanisms. *The ISME Journal, 10*(12), 2854-2866. doi:10.1038/ismej.2016.79

Boulanger, P., & Letellier, L. (1988). Characterization of ion channels involved in the penetration of phage T4 DNA into *Escherichia coli* cells. *Journal of Biological Chemistry, 263*(20), 9767-9775. doi:10.1016/S0021-9258(19)81584-3

5. References

Boulanger, P., & Letellier, L. (1992). Ion channels are likely to be involved in the two steps of phage T5 DNA penetration into *Escherichia coli* cells. *Journal of Biological Chemistry, 267*(5), 3168-3172. doi:doi.org/10.1016/S0021-9258(19)50710-4

Bruni, G. N., & Kralj, J. M. (2020). Membrane voltage dysregulation driven by metabolic dysfunction underlies bactericidal activity of aminoglycosides. *eLife, 9*, e58706. doi:10.7554/eLife.58706

Bryson, A. L., Hwang, Y., Sherrill-Mix, S., Wu, G. D., Lewis, J. D., Black, L., . . . Bushman, F. D. (2015). Covalent Modification of Bacteriophage T4 DNA Inhibits CRISPR-Cas9. *mBio, 6*(3), e00648. doi:10.1128/mBio.00648-15

Burman, N., Belukhina, S., Depardieu, F., Wilkinson, R. A., Skutel, M., Santiago-Frangos, A., . . . Isaev, A. (2024). Viral proteins activate PARIS-mediated tRNA degradation and viral tRNAs rescue infection. *bioRxiv*. doi:10.1101/2024.01.02.573894

Chen, S., Zhou, Y., Chen, Y., & Gu, J. (2018). fastp: an ultra-fast all-in-one FASTQ preprocessor. *Bioinformatics, 34*(17), i884-i890. doi:10.1093/bioinformatics/bty560

Chung, C. T., Niemela, S. L., & Miller, R. H. (1989). One-step preparation of competent *Escherichia coli*: transformation and storage of bacterial cells in the same solution. *Proc Natl Acad Sci U S A, 86*(7), 2172-2175. doi:10.1073/pnas.86.7.2172

Clokie, M. R. J. M., Andrew D.; Letarov, Andrey V.; Heaphy, Shaun. (2011). Phages in nature. *Bacteriophage, 1*(1), 31-45.

Creasy, A., Rosario, K., Leigh, B. A., Dishaw, L. J., & Breitbart, M. (2018). Unprecedented Diversity of ssDNA Phages from the Family *Microviridae* Detected within the Gut of a Protochordate Model Organism (*Ciona robusta*). *Viruses, 10*(8), 404.

d'Herelle, F. H. (1917). Sur un microbe invisible antagoniste des bacilles dysenteriques. . *C. R. Acad. Sci.165:373-375*.

Dion, M. B., Oechslin, F., & Moineau, S. (2020). Phage diversity, genomics and phylogeny. *Nat Rev Microbiol, 18*(3), 125-138. doi:10.1038/s41579-019-0311-5

Donegan-Quick, R., Gibbs, Z. A., Amaku, P. O., Bernal, J. T., Boyd, D. A. M., Burr, A. R., . . . Hughes, L. E. (2017). Genome Sequences of Five Streptomyces Bacteriophages Forming Cluster BG. *Genome Announc, 5*(28). doi:10.1128/genomeA.00502-17

Doron, S., Melamed, S., Ofir, G., Leavitt, A., Lopatina, A., Keren, M., . . . Sorek, R. (2018). Systematic discovery of antiphage defense systems in the microbial pangenome. *Science (New York, N.Y.), 359*(6379), eaar4120. doi:10.1126/science.aar4120

Erdrich, S. H., Luthe, T., Kever, L., Roigé, B. B., Arsova, B., Davoudi, E., & Frunzke, J. (2024). Expanding the phage galaxy: Isolation and characterization of five novel *Streptomyces* siphoviruses Ankus, Byblos, DekoNeimoidia, Mandalore, and Naboo. *bioRxiv*, 2024.2002.2016.580700. doi:10.1101/2024.02.16.580700

Fierer, N. (2017). Embracing the unknown: disentangling the complexities of the soil microbiome. *Nature Reviews Microbiology, 15*(10), 579-590. doi:10.1038/nrmicro.2017.87

Forge, A., & Schacht, J. (2000). Aminoglycoside Antibiotics. *Audiology and Neuro-Otology, 5*, 3-22. doi:10.1159/000013861

Gao, L., Altae-Tran, H., Böhning, F., Makarova, K. S., Segel, M., Schmid-Burgk, J. L., . . . Zhang, F. (2020). Diverse enzymatic activities mediate antiviral immunity in prokaryotes. *Science (New York, N.Y.), 369*(6507), 1077-1084. doi:doi:10.1126/science.aba0372

Garneau-Tsodikova, S., & Labby, K. J. (2016). Mechanisms of Resistance to Aminoglycoside Antibiotics: Overview and Perspectives. *Medchemcomm, 7*(1), 11-27. doi:10.1039/c5md00344j

Garneau, J. R., Depardieu, F., Fortier, L. C., Bikard, D., & Monot, M. (2017). PhageTerm: a tool for fast and accurate determination of phage termini and packaging mechanism using next-generation sequencing data. *Sci Rep, 7*(1), 8292. doi:10.1038/s41598-017-07910-5

Georjon, H., & Bernheim, A. (2023). The highly diverse antiphage defence systems of bacteria. *Nature Reviews Microbiology*. doi:10.1038/s41579-023-00934-x

Georjon, H., Tesson, F., Shomar, H., & Bernheim, A. (2023). Genomic characterization of the antiviral arsenal of Actinobacteria. *Microbiology, 169*(8). doi:doi.org/10.1099/mic.0.001374

5. References

Gomez-Escribano, J. P., & Bibb, M. J. (2011). Engineering *Streptomyces coelicolor* for heterologous expression of secondary metabolite gene clusters. *Microbial Biotechnology, 4*(2), 207-215. doi:doi.org/10.1111/j.1751-7915.2010.00219.x

Gomez-Escribano, J. P., Holmes, N. A., Schlimpert, S., Bibb, M. J., Chandra, G., Wilkinson, B., . . . Bibb, M. J. (2021). *Streptomyces venezuelae* NRRL B-65442: genome sequence of a model strain used to study morphological differentiation in filamentous actinobacteria. *Journal of Industrial Microbiology and Biotechnology, 48*(9-10). doi:10.1093/jimb/kuab035

Gregorio, N. E., Levine, M. Z., & Oza, J. P. (2019). A User's Guide to Cell-Free Protein Synthesis. *Methods and Protocols, 2*(1), 24.

Gurevich, A. I., Kolosov, M. N., Korobko, V. G., & Onoprienko, V. V. (1968). The structure of abikoviromycin. *Tetrahedron Letters, 9*(18), 2209-2212. doi:doi.org/10.1016/S0040-4039(00)89721-X

Hajan, R., Shams, N., & Parvin, A. (2009). DNA-binding Studies of Daunorubicin in the Presence of Methylene Blue by Spectroscopy and Voltammetry Techniques. *Chinese Journal of Chemistry, 27*(6), 1055-1060. doi:doi.org/10.1002/cjoc.200990176

Hanahan, D. (1983). Studies on transformation of *Escherichia coli* with plasmids. *J Mol Biol, 166*(4), 557-580. doi:doi.org/10.1016/S0022-2836(83)80284-8

Hardy, A., Kever, L., & Frunzke, J. (2023). Antiphage small molecules produced by bacteria – beyond protein-mediated defenses. *Trends in Microbiology, 31*(1), 92-106. doi:doi.org/10.1016/j.tim.2022.08.001

Hardy, A., Sharma, V., Kever, L., & Frunzke, J. (2020). Genome Sequence and Characterization of Five Bacteriophages Infecting *Streptomyces coelicolor* and *Streptomyces venezuelae*: Alderaan, Coruscant, Dagobah, Endor1 and Endor2. *Viruses, 12*(10), 1065.

Hatfull, G. F. (2015). Innovations in Undergraduate Science Education: Going Viral. *J Virol, 89*(16), 8111-8113. doi:doi:10.1128/jvi.03003-14

Hatfull, G. F. (2020). Actinobacteriophages: Genomics, Dynamics, and Applications. *Annu Rev Virol, 7*(1), 37-61. doi:10.1146/annurev-virology-122019-070009

Hattman, S. (2009). The first recognized epigenetic signal: DNA glucosylation of T-even bacteriophages. *Epigenetics, 4*(3), 150-151. doi:10.4161/epi.4.3.8444

Hendrix, R. W. (2002). Bacteriophages: Evolution of the Majority. *Theoretical Population Biology, 61*(4), 471-480. doi:doi.org/10.1006/tpbi.2002.1590

Hendrix, R. W., Smith, M. C., Burns, R. N., Ford, M. E., & Hatfull, G. F. (1999). Evolutionary relationships among diverse bacteriophages and prophages: all the world's a phage. *Proc Natl Acad Sci U S A, 96*(5), 2192-2197. doi:10.1073/pnas.96.5.2192

Hochhauser, D., Millman, A., & Sorek, R. (2023). The defense island repertoire of the *Escherichia coli* pan-genome. *PLOS Genetics, 19*(4), e1010694. doi:10.1371/journal.pgen.1010694

Hong, H.-J., Hutchings, M. I., Hill, L. M., & Buttner, M. J. (2005). The Role of the Novel Fem Protein VanK in Vancomycin Resistance in *Streptomyces coelicolor*. *Journal of Biological Chemistry, 280*(13), 13055-13061. doi:10.1074/jbc.M413801200

Hopwood, D. A. (2007). *Streptomyces in Nature and Medicine: The Antibiotic Makers* (1 ed.). OvidSP: Oxford University Press.

Hu, B., Margolin, W., Molineux, I. J., & Liu, J. (2015). Structural remodeling of bacteriophage T4 and host membranes during infection initiation. *Proceedings of the National Academy of Sciences, 112*(35), E4919-E4928. doi:doi:10.1073/pnas.1501064112

Hünnefeld, M., Viets, U., Sharma, V., Wirtz, A., Hardy, A., & Frunzke, J. (2021). Genome Sequence of the Bacteriophage CL31 and Interaction with the Host Strain *Corynebacterium glutamicum* ATCC 13032. *Viruses, 13*(3). doi:10.3390/v13030495

Jensen, E. C., Schrader, H. S., Rieland, B., Thompson, T. L., Lee, K. W., Nickerson, K. W., & Kokjohn, T. A. (1998). Prevalence of Broad-Host-Range Lytic Bacteriophages of *Sphaerotilus natans, Escherichia coli,* and *Pseudomonas aeruginosa*. *Applied and Environmental Microbiology, 64*(2), 575-580. doi:doi:10.1128/AEM.64.2.575-580.1998

5. References

Jiang, Z., Wei, J., Liang, Y., Peng, N., & Li, Y. (2020). Aminoglycoside Antibiotics Inhibit Mycobacteriophage Infection. *Antibiotics, 9*(10), 714.

Katsura, I., & Hendrix, R. W. (1984). Length determination in bacteriophage lambda tails. *Cell, 39*(3 Pt 2), 691-698. doi:10.1016/0092-8674(84)90476-8

Kaur, P., & Russell, J. (1998). Biochemical Coupling between the DrrA and DrrB Proteins of the Doxorubicin Efflux Pump of *Streptomyces peucetius Journal of Biological Chemistry, 273*(28), 17933-17939. doi:doi.org/10.1074/jbc.273.28.17933

Kever, L., Hardy, A., Luthe, T., Hünnefeld, M., Gätgens, C., Milke, L., . . . Storz, G. (2022). Aminoglycoside Antibiotics Inhibit Phage Infection by Blocking an Early Step of the Infection Cycle. *mBio, 0*(0), e00783-00722. doi:doi:10.1128/mbio.00783-22

Kever, L., Zhang, Q., Hardy, A., Westhoff, P., Yu, Y., & Frunzke, J. (2024). Resistance against aminoglycoside antibiotics via drug or target modification enables community-wide antiphage defense. *microLife, 5*. doi:10.1093/femsml/uqae015

Keweloh, H. W., & Bakker, E. P. (1984). Increased permeability and subsequent resealing of the host cell membrane early after infection of *Escherichia coli* with bacteriophage T1. *Journal of bacteriology, 160*(1), 354-359. doi:10.1128/jb.160.1.354-359.1984

Kieser, T., Bibb, M. J., Buttner, M. J., Charter, K. F., & Hopwood, D. A. (2000). *Practical Streptomyces Genetics*: The John Innes Foundation, Norwich, UK

Korn, F., Weingärtner, B., & Kutzner, H. (1978). A study of twenty actinophages: morphology, serological relationship and host range. *Genetics of the Actinomycetales*, 251-270.

Krause, K. M., Serio, A. W., Kane, T. R., & Connolly, L. E. (2016). Aminoglycosides: An Overview. *Cold Spring Harb Perspect Med, 6*(6). doi:10.1101/cshperspect.a027029

Kronheim, S., Daniel-Ivad, M., Duan, Z., Hwang, S., Wong, A., Mantel, I., . . . Maxwell, K. L. (2018). A chemical defence against phage infection. *Nature, 564*(7735), 283-286. doi:10.1038/s41586-018-0767-x

Kronheim, S., Solomon, E., Ho, L., Glossop, M., Davidson, A. R., & Maxwell, K. L. (2023). Complete genomes and comparative analyses of *Streptomyces* phages that influence secondary metabolism and sporulation. *Sci Rep, 13*(1), 9820. doi:10.1038/s41598-023-36938-z

Krupovic, M., Prangishvili, D., Hendrix, R. W., & Bamford, D. H. (2011). Genomics of Bacterial and Archaeal Viruses: Dynamics within the Prokaryotic Virosphere. *Microbiology and Molecular Biology Reviews, 75*(4), 610-635. doi:10.1128/mmbr.00011-11

Krupovic, M., Turner, D., Morozova, V., Dyall-Smith, M., Oksanen, H. M., Edwards, R., . . . Adriaenssens, E. M. (2021). Bacterial Viruses Subcommittee and Archaeal Viruses Subcommittee of the ICTV: update of taxonomy changes in 2021. *Archives of Virology, 166*(11), 3239-3244. doi:10.1007/s00705-021-05205-9

Loeb, M. R. (1974). Bacteriophage T4-mediated release of envelope components from *Escherichia coli*. *J Virol, 13*(3), 631-641. doi:10.1128/jvi.13.3.631-641.1974

Loenen, W. A. M., Dryden, D. T. F., Raleigh, E. A., & Wilson, G. G. (2013). Type I restriction enzymes and their relatives. *Nucleic acids research, 42*(1), 20-44. doi:10.1093/nar/gkt847

Lopatina, A., Tal, N., & Sorek, R. (2020). Abortive Infection: Bacterial Suicide as an Antiviral Immune Strategy. *Annu Rev Virol, 7*(Volume 7, 2020), 371-384. doi:doi.org/10.1146/annurev-virology-011620-040628

Luria, S. E., Delbrück, M., & Anderson, T. F. (1943). Electron microscope studies of bacterial viruses. *Journal of bacteriology, 46*(1), 57-77.

Luria, S. E., & Human, M. L. (1952). A nonhereditary, host-induced variation of bacterial viruses. *Journal of bacteriology, 64*(4), 557-569. doi:doi:10.1128/jb.64.4.557-569.1952

Luthe, T., Kever, L., Hänsch, S., Hardy, A., Tschowri, N., Weidtkamp-Peters, S., & Frunzke, J. (2023a). *Streptomyces* development is involved in the efficient containment of viral infections. *microLife*. doi:10.1093/femsml/uqad002

5. References

Luthe, T., Kever, L., Thormann, K., & Frunzke, J. (2023b). Bacterial multicellular behavior in antiviral defense. *Current Opinion in Microbiology, 74*, 102314. doi:doi.org/10.1016/j.mib.2023.102314

Ly-Chatain , M. H. (2014). The factors affecting effectiveness of treatment in phages therapy. *Frontiers in Microbiology, 5*(51). doi:10.3389/fmicb.2014.00051

MacNeil, D. J., Gewain, K. M., Ruby, C. L., Dezeny, G., Gibbons, P. H., & MacNeil, T. (1992). Analysis of *Streptomyces avermitilis* genes required for avermectin biosynthesis utilizing a novel integration vector. *Gene, 111*(1), 61-68. doi:doi.org/10.1016/0378-1119(92)90603-M

Maffei, E., Shaidullina, A., Burkolter, M., Heyer, Y., Estermann, F., Druelle, V., . . . Harms, A. (2021). Systematic exploration of *Escherichia coli* phage–host interactions with the BASEL phage collection. *PLOS Biology, 19*(11), e3001424. doi:10.1371/journal.pbio.3001424

Makarova, K. S., Wolf, Y. I., Iranzo, J., Shmakov, S. A., Alkhnbashi, O. S., Brouns, S. J. J., . . . Koonin, E. V. (2020). Evolutionary classification of CRISPR–Cas systems: a burst of class 2 and derived variants. *Nature Reviews Microbiology, 18*(2), 67-83. doi:10.1038/s41579-019-0299-x

Makarova, K. S., Wolf, Y. I., Snir, S., & Koonin, E. V. (2011). Defense Islands in Bacterial and Archaeal Genomes and Prediction of Novel Defense Systems. *Journal of bacteriology, 193*(21), 6039-6056. doi:doi:10.1128/JB.05535-11

Marisch, K., Bayer, K., Scharl, T., Mairhofer, J., Krempl, P. M., Hummel, K., . . . Striedner, G. (2013). A comparative analysis of industrial *Escherichia coli* K-12 and B strains in high-glucose batch cultivations on process-, transcriptome- and proteome level. *PLoS One, 8*(8), e70516. doi:10.1371/journal.pone.0070516

Maslowska, K. H., Makiela-Dzbenska, K., & Fijalkowska, I. J. (2019). The SOS system: A complex and tightly regulated response to DNA damage. *Environ Mol Mutagen, 60*(4), 368-384. doi:10.1002/em.22267

McKitterick, A. C., & Bernhardt, T. G. (2022). Phage resistance profiling identifies new genes required for biogenesis and modification of the corynebacterial cell envelope. *eLife, 11*. doi:10.7554/eLife.79981

Mee-Jung, H., & Sang Yup, L. (2012). Comparative Analysis of Envelope Proteomes in *Escherichia coli* B and K-12 Strains. *Journal of Microbiology and Biotechnology, 22*(4), 470-478. doi:10.4014/jmb.1110.10080

Millman, A., Bernheim, A., Stokar-Avihail, A., Fedorenko, T., Voichek, M., Leavitt, A., . . . Sorek, R. (2020). Bacterial Retrons Function In Anti-Phage Defense. *Cell, 183*(6), 1551-1561.e1512. doi:doi.org/10.1016/j.cell.2020.09.065

Millman, A., Melamed, S., Leavitt, A., Doron, S., Bernheim, A., Hör, J., . . . Sorek, R. (2022). An expanded arsenal of immune systems that protect bacteria from phages. *Cell Host & Microbe, 30*(11), 1556-1569.e1555. doi:doi.org/10.1016/j.chom.2022.09.017

Monson, R., & Salmond, G. P. (2012). Genome sequence of a new *Streptomyces coelicolor* generalized transducing bacteriophage, ΦCAM. *J Virol, 86*(24), 13860. doi:10.1128/jvi.02681-12

Montaño, E. T., Nideffer, J. F., Brumage, L., Erb, M., Busch, J., Fernandez, L., . . . Pogliano, J. (2022). Isolation and characterization of *Streptomyces* bacteriophages and *Streptomyces* strains encoding biosynthetic arsenals. *PLoS One, 17*(1), e0262354. doi:10.1371/journal.pone.0262354

Moraru, C., Varsani, A., & Kropinski, A. M. (2020). VIRIDIC-A Novel Tool to Calculate the Intergenomic Similarities of Prokaryote-Infecting Viruses. *Viruses, 12*(11). doi:10.3390/v12111268

Naureen, Z., Dautaj, A., Anpilogov, K., Camilleri, G., Dhuli, K., Tanzi, B., . . . Bertelli, M. (2020). Bacteriophages presence in nature and their role in the natural selection of bacterial populations. *Acta Biomed, 91*(13-s), e2020024. doi:10.23750/abm.v91i13-S.10819

Neri, U., Wolf, Y. I., Roux, S., Camargo, A. P., Lee, B., Kazlauskas, D., . . . Gophna, U. (2022). Expansion of the global RNA virome reveals diverse clades of bacteriophages. *Cell, 185*(21), 4023-4037.e4018. doi:10.1016/j.cell.2022.08.023

5. References

North, S. H., Kirtland, S. E., & Nakai, H. (2007). Translation factor IF2 at the interface of transposition and replication by the PriA-PriC pathway. *Mol Microbiol, 66*(6), 1566-1578. doi:10.1111/j.1365-2958.2007.06022.x

Nouioui, I., Carro, L., García-López, M., Meier-Kolthoff, J. P., Woyke, T., Kyrpides, N. C., . . . Göker, M. (2018). Genome-Based Taxonomic Classification of the Phylum Actinobacteria. *Front Microbiol, 9*, 2007. doi:10.3389/fmicb.2018.02007

Ofir, G., & Sorek, R. (2018). Contemporary Phage Biology: From Classic Models to New Insights. *Cell, 172*(6), 1260-1270. doi:10.1016/j.cell.2017.10.045

Ongenae, V., Azeredo, J., Kropinski, A. M., Rozen, D., Briegel, A., & Claessen, D. (2022a). Genome sequence and characterization of *Streptomyces* phage Pablito, representing a new species within the genus Janusvirus. doi:doi.org/10.21203/rs.3.rs-1784137/v1

Ongenae, V., Kempff, A., van Neer, V., Shomar, H., Tesson, F., Rozen, D., . . . Claessen, D. (2023). Genome sequence and characterization of *Streptomyces* phages Vanseggelen and Verabelle, representing two new species within the genus Camvirus. *Scientific Reports, 13*(1), 20153. doi:10.1038/s41598-023-47634-3

Ongenae, V., Mabrouk, A. S., Crooijmans, M., Rozen, D., Briegel, A., & Claessen, D. (2022b). Reversible bacteriophage resistance by shedding the bacterial cell wall. *Open Biology, 12*(6), 210379. doi:doi:10.1098/rsob.210379

Oppenheim, A. B., Kobiler, O., Stavans, J., Court, D. L., & Adhya, S. (2005). Switches in bacteriophage lambda development. *Annu Rev Genet, 39*, 409-429. doi:10.1146/annurev.genet.39.073003.113656

Paget, M. S. B., Chamberlin, L., Atrih, A., Foster, S. J., & Buttner, M. J. (1999). Evidence that the Extracytoplasmic Function Sigma Factor sigE Is Required for Normal Cell Wall Structure in *Streptomyces coelicolor* A3(2). *Journal of bacteriology, 181*(1), 204-211. doi:doi:10.1128/jb.181.1.204-211.1999

Payne, L. J., Meaden, S., Mestre, M. R., Palmer, C., Toro, N., Fineran, Peter C., & Jackson, Simon A. (2022). PADLOC: a web server for the identification of antiviral defence systems in microbial genomes. *Nucleic acids research, 50*(W1), W541-W550. doi:10.1093/nar/gkac400

Pérez-Arnaiz, C., Busto, N., Leal, J. M., & García, B. (2014). New Insights into the Mechanism of the DNA/Doxorubicin Interaction. *The Journal of Physical Chemistry B, 118*(5), 1288-1295. doi:10.1021/jp411429g

Pingoud, A., Wilson, G. G., & Wende, W. (2014). Type II restriction endonucleases—a historical perspective and more. *Nucleic acids research, 42*(12), 7489-7527. doi:10.1093/nar/gku447

Pleška, M., Qian, L., Okura, R., Bergmiller, T., Wakamoto, Y., Kussell, E., & Guet, Călin C. (2016). Bacterial Autoimmunity Due to a Restriction-Modification System. *Current Biology, 26*(3), 404-409. doi:doi.org/10.1016/j.cub.2015.12.041

Podgorski, J., Calabrese, J., Alexandrescu, L., Jacobs-Sera, D., Pope, W., Hatfull, G., & White, S. (2020). Structures of Three Actinobacteriophage Capsids: Roles of Symmetry and Accessory Proteins. *Viruses, 12*(3), 294.

Pozhydaieva, N., Billau, F. A., Wolfram-Schauerte, M., Ramírez Rojas, A. A., Paczia, N., Schindler, D., & Höfer, K. (2024). Temporal epigenome modulation enables efficient bacteriophage engineering and functional analysis of phage DNA modifications. *PLOS Genetics, 20*(9), e1011384. doi:10.1371/journal.pgen.1011384

Prauser, H. (1976). *Nocardioides*, a New Genus of the Order Actinomycetales. *International Journal of Systematic and Evolutionary Microbiology, 26*(1), 58-65. doi:doi.org/10.1099/00207713-26-1-58

Prauser, H., & Köhler, W. (1965). Untersuchungen zur Lyse von *Streptococcus pyogenes* durch *Streptomyceten*-Enzyme. *Zeitschrift für allgemeine Mikrobiologie, 5*(4), 308-314. doi:doi.org/10.1002/jobm.19650050406

5. References

Prija, F., & Prasad, R. (2017). DrrC protein of *Streptomyces peucetius* removes daunorubicin from intercalated dnrI promoter. *Microbiological Research, 202*, 30-35. doi:doi.org/10.1016/j.micres.2017.05.002

Rackow, B., Rolland, C., Mohnen, I., Wittmann, J., Müsken, M., Overmann, J., & Frunzke, J. (2024). Isolation and characterization of the new *Streptomyces* phages Kamino, Geonosis, Abafar, and Scarif infecting a broad range of host species. *Microbiology Spectrum, 0*(0), e00663-00624. doi:doi:10.1128/spectrum.00663-24

Rao, D. N., Dryden, D. T. F., & Bheemanaik, S. (2013). Type III restriction-modification enzymes: a historical perspective. *Nucleic acids research, 42*(1), 45-55. doi:10.1093/nar/gkt616

Rehman, S., Ali, Z., Khan, M., Bostan, N., & Naseem, S. (2019). The dawn of phage therapy. *Reviews in Medical Virology, 29*(4), e2041. doi:doi.org/10.1002/rmv.2041

Rose, T., Verbeken, G., Vos, D. D., Merabishvili, M., Vaneechoutte, M., Lavigne, R., . . . Pirnay, J. P. (2014). Experimental phage therapy of burn wound infection: difficult first steps. *Int J Burns Trauma, 4*(2), 66-73.

Rostøl, J. T., & Marraffini, L. (2019). (Ph)ighting Phages: How Bacteria Resist Their Parasites. *Cell Host Microbe, 25*(2), 184-194. doi:10.1016/j.chom.2019.01.009

Ruska, H. (1940). Die Sichtbarmachung der bakteriophagen Lyse im Übermikroskop. *Naturwissenschaften, 28*(3), 45-46. doi:10.1007/BF01486931

Rustad, M., Eastlund, A., Jardine, P., & Noireaux, V. (2018). Cell-free TXTL synthesis of infectious bacteriophage T4 in a single test tube reaction. *Synthetic Biology, 3*(1). doi:10.1093/synbio/ysy002

Rustad, M., Eastlund, A., Marshall, R., Jardine, P., & Noireaux, V. (2017). Synthesis of Infectious Bacteriophages in an *E. coli*-based Cell-free Expression System. *JoVE*(126), e56144. doi:doi:10.3791/56144

Salmond, G. P., & Fineran, P. C. (2015). A century of the phage: past, present and future. *Nat Rev Microbiol, 13*(12), 777-786. doi:10.1038/nrmicro3564

Samain, D., Dupin, P., Delrieu, P., & Inchauspe, G. (1987). Multidimensional ion-pair HPLC for the purification of aminoglycoside antibiotics with refractive index detection. *Chromatographia, 24*(1), 748-752. doi:10.1007/BF02688579

Savalia, D., Robins, W., Nechaev, S., Molineux, I., & Severinov, K. (2010). The role of the T7 Gp2 inhibitor of host RNA polymerase in phage development. *J Mol Biol, 402*(1), 118-126. doi:10.1016/j.jmb.2010.07.012

Schindelin, J., Arganda-Carreras, I., Frise, E., Kaynig, V., Longair, M., Pietzsch, T., . . . Schmid, B. (2012). Fiji: an open-source platform for biological-image analysis. *Nature methods, 9*(7), 676-682.

Schindelin, J., Rueden, C. T., Hiner, M. C., & Eliceiri, K. W. (2015). The ImageJ ecosystem: An open platform for biomedical image analysis. *Molecular reproduction and development, 82*(7-8), 518-529.

Scholz, D., Meissner, C., & Rosenthal, H. A. (1979). Differences in sensitivity of T3, T7, T4 and lambda phages to bleomycin and phleomycin. *Z Allg Mikrobiol, 19*(10), 745-752. doi:10.1002/jobm.3630191010

Searle, M. S. (1993). NMR Studies of Drug—DNA interactions. *Progress in Nuclear Magnetic Resonance Spectroscopy, 25*(5), 403-480. doi:doi.org/10.1016/0079-6565(93)80005-E

Seemann, T. (2014). Prokka: rapid prokaryotic genome annotation. *Bioinformatics, 30*(14), 2068-2069. doi:10.1093/bioinformatics/btu153

Sharma, V., Hardy, A., Luthe, T., & Frunzke, J. (2021). Phylogenetic Distribution of WhiB- and Lsr2-Type Regulators in Actinobacteriophage Genomes. *Microbiology Spectrum, 9*(3), e00727-00721. doi:10.1128/Spectrum.00727-21

Shin, J., Jardine, P., & Noireaux, V. (2012). Genome Replication, Synthesis, and Assembly of the Bacteriophage T7 in a Single Cell-Free Reaction. *ACS Synthetic Biology, 1*(9), 408-413. doi:10.1021/sb300049p

5. References

Slomińska, M., Neubauer, P., & Wegrzyn, G. (1999). Regulation of bacteriophage lambda development by guanosine 5'-diphosphate-3'-diphosphate. *Virology, 262*(2), 431-441. doi:10.1006/viro.1999.9907

Smith, M. C. M., Burns, R. N., Wilson, S. E., & Gregory, M. A. (1999). The complete genome sequence of the *Streptomyces* temperate phage φC31: evolutionary relationships to other viruses. *Nucleic acids research, 27*(10), 2145-2155. doi:10.1093/nar/27.10.2145

Smith, M. C. M., Hendrix, R. W., Dedrick, R., Mitchell, K., Ko, C.-C., Russell, D., . . . Hatfull, G. F. (2013). Evolutionary Relationships among Actinophages and a Putative Adaptation for Growth in *Streptomyces spp. Journal of bacteriology, 195*(21), 4924-4935. doi:doi:10.1128/jb.00618-13

Stern, A., & Sorek, R. (2011). The phage-host arms race: Shaping the evolution of microbes. *BioEssays, 33*(1), 43-51. doi:doi.org/10.1002/bies.201000071

Strauch, E., Takano, E., Baylts, H. A., & Bibb, M. J. (1991). The stringent response in *Streptomyces coelicolor* A3(2). *Mol Microbiol, 5*(2), 289-298. doi:doi.org/10.1111/j.1365-2958.1991.tb02109.x

Stutzman-Engwall, K. J., & Hutchinson, C. R. (1989). Multigene families for anthracycline antibiotic production in *Streptomyces peucetius*. *Proceedings of the National Academy of Sciences, 86*(9), 3135-3139. doi:10.1073/pnas.86.9.3135

Subadini, S., Hota, P. R., Behera, D. P., & Sahoo, H. (2022). Circular Dichroism Spectroscopy: Principle and Application. In H. Sahoo (Ed.), *Optical Spectroscopic and Microscopic Techniques: Analysis of Biological Molecules* (pp. 19-33). Singapore: Springer Nature Singapore.

Tabib-Salazar, A., Liu, B., Barker, D., Burchell, L., Qimron, U., Matthews, S. J., & Wigneshweraraj, S. (2018). T7 phage factor required for managing RpoS in *Escherichia coli*. *Proc Natl Acad Sci U S A, 115*(23), E5353-e5362. doi:10.1073/pnas.1800429115

Tal, N., Millman, A., Stokar-Avihail, A., Fedorenko, T., Leavitt, A., Melamed, S., . . . Sorek, R. (2022). Bacteria deplete deoxynucleotides to defend against bacteriophage infection. *Nat Microbiol*. doi:10.1038/s41564-022-01158-0

Tal, N., & Sorek, R. (2022). SnapShot: Bacterial immunity. *Cell, 185*(3), 578-578.e571. doi:doi.org/10.1016/j.cell.2021.12.029

Terzian, P., Olo Ndela, E., Galiez, C., Lossouarn, J., Pérez Bucio, R. E., Mom, R., . . . Enault, F. (2021). PHROG: families of prokaryotic virus proteins clustered using remote homology. *NAR Genom Bioinform, 3*(3), lqab067. doi:10.1093/nargab/lqab067

Tesson, F., & Bernheim, A. (2023). Synergy and regulation of antiphage systems: toward the existence of a bacterial immune system? *Current Opinion in Microbiology, 71*, 102238. doi:doi.org/10.1016/j.mib.2022.102238

Thompson, S., & Wiberg, J. S. (1978). Late effect of bacteriophage T4D on the permeability barrier of *Escherichia coli*. *J. Virol.; (United States), 25:2*, Medium: X; Size: Pages: 491-499 2009-2012-2017.

Tinafar, A., Jaenes, K., & Pardee, K. (2019). Synthetic Biology Goes Cell-Free. *BMC Biology, 17*(1), 64. doi:10.1186/s12915-019-0685-x

Tong, T., Chen, S., Wang, L., Tang, Y., Ryu, J. Y., Jiang, S., . . . Chen, S. (2018). Occurrence, evolution, and functions of DNA phosphorothioate epigenetics in bacteria. *Proceedings of the National Academy of Sciences, 115*(13), E2988-E2996. doi:doi:10.1073/pnas.1721916115

Tse, W. C., & Boger, D. L. (2004). Sequence-Selective DNA Recognition: Natural Products and Nature's Lessons. *Chemistry & Biology, 11*(12), 1607-1617. doi:doi.org/10.1016/j.chembiol.2003.08.012

Turner, D., Kropinski, A. M., & Adriaenssens, E. M. (2021). A Roadmap for Genome-Based Phage Taxonomy. *Viruses, 13*(3). doi:10.3390/v13030506

Twort, F. W. (1915). An investigation on the nature of ulta-microscopic viruses. *The Lancet, 186*(4814), 1241-1243. doi:doi.org/10.1016/S0140-6736(01)20383-3

5. References

Tynecki, P., Guziński, A., Kazimierczak, J., Jadczuk, M., Dastych, J., & Onisko, A. (2020). PhageAI - Bacteriophage Life Cycle Recognition with Machine Learning and Natural Language Processing. *bioRxiv*, 2020.2007.2011.198606. doi:10.1101/2020.07.11.198606

Uyttebroek, S., Chen, B., Onsea, J., Ruythooren, F., Debaveye, Y., Devolder, D., . . . Metsemakers, W.-J. (2022). Safety and efficacy of phage therapy in difficult-to-treat infections: a systematic review. *The Lancet Infectious Diseases, 22*(8), e208-e220. doi:10.1016/S1473-3099(21)00612-5

van den Berg, D. F., van der Steen, B. A., Costa, A. R., & Brouns, S. J. J. (2023). Phage tRNAs evade tRNA-targeting host defenses through anticodon loop mutations. *Elife, 12*. doi:10.7554/eLife.85183

Van Valen, L. (1973). A New Evolutionary Law (1973). *Evol. Theory, 1*.

Varma, S. J., Calvani, E., Grüning, N.-M., Messner, C. B., Grayson, N., Capuano, F., . . . Ralser, M. (2022). Global analysis of cytosine and adenine DNA modifications across the tree of life. *eLife, 11*, e81002. doi:10.7554/eLife.81002

Vassallo, C. N., Doering, C. R., Littlehale, M. L., Teodoro, G. I. C., & Laub, M. T. (2022). A functional selection reveals previously undetected anti-phage defence systems in the *E. coli* pangenome. *Nat Microbiol, 7*(10), 1568-1579. doi:10.1038/s41564-022-01219-4

Vlot, M., Houkes, J., Lochs, S. J A., Swarts, D. C., Zheng, P., Kunne, T., . . . Brouns, S. J J. (2017). Bacteriophage DNA glucosylation impairs target DNA binding by type I and II but not by type V CRISPR–Cas effector complexes. *Nucleic acids research, 46*(2), 873-885. doi:10.1093/nar/gkx1264

Walker, B. J., Abeel, T., Shea, T., Priest, M., Abouelliel, A., Sakthikumar, S., . . . Earl, A. M. (2014). Pilon: An Integrated Tool for Comprehensive Microbial Variant Detection and Genome Assembly Improvement. *PLoS One, 9*(11), e112963. doi:10.1371/journal.pone.0112963

Wang, S., Sun, E., Liu, Y., Yin, B., Zhang, X., Li, M., . . . Tao, P. (2022). The complex roles of genomic DNA modifications of bacteriophage T4 in resistance to nuclease-based defense systems of *E. coli*. *bioRxiv*, 2022.2006.2016.496414. doi:10.1101/2022.06.16.496414

Wang, S., Sun, E., Liu, Y., Yin, B., Zhang, X., Li, M., . . . Tao, P. (2023). Landscape of New Nuclease-Containing Antiphage Systems in *Escherichia coli* and the Counterdefense Roles of Bacteriophage T4 Genome Modifications. *J Virol, 97*(6), e0059923. doi:10.1128/jvi.00599-23

Wang, S., Wan, M., Huang, R., Zhang, Y., Xie, Y., Wei, Y., . . . Wang, L. (2021). SspABCD-SspFGH Constitutes a New Type of DNA Phosphorothioate-Based Bacterial Defense System. *mBio, 12*(2), 10.1128/mbio.00613-00621. doi:doi:10.1128/mbio.00613-21

Wang, X., Kim, Y., Ma, Q., Hong, S. H., Pokusaeva, K., Sturino, J. M., & Wood, T. K. (2010). Cryptic prophages help bacteria cope with adverse environments. *Nat Commun, 1*, 147. doi:10.1038/ncomms1146

Wein, T., & Sorek, R. (2022). Bacterial origins of human cell-autonomous innate immune mechanisms. *Nat Rev Immunol, 22*(10), 629-638. doi:10.1038/s41577-022-00705-4

Wolfram-Schauerte, M., Pozhydaieva, N., Viering, M., Glatter, T., & Höfer, K. (2022). Integrated Omics Reveal Time-Resolved Insights into T4 Phage Infection of *E. coli* on Proteome and Transcriptome Levels. *Viruses, 14*(11), 2502.

Wu, Y., Garushyants, S. K., van den Hurk, A., Aparicio-Maldonado, C., Kushwaha, S. K., King, C. M., . . . Nobrega, F. L. (2024). Bacterial defense systems exhibit synergistic anti-phage activity. *Cell Host & Microbe*. doi:doi.org/10.1016/j.chom.2024.01.015

Xiong, X., Wu, G., Wei, Y., Liu, L., Zhang, Y., Su, R., . . . Wang, L. (2020). SspABCD–SspE is a phosphorothioation-sensing bacterial defence system with broad anti-phage activities. *Nat Microbiol, 5*(7), 917-928. doi:10.1038/s41564-020-0700-6

Yeh, P., Oreglia, J., & Sicard, A. M. (1985). Transfection of *Corynebacterium lilium* Protoplasts. *Microbiology, 131*(12), 3179-3183. doi:doi.org/10.1099/00221287-131-12-3179

Yoon, S. H., Jeong, H., Kwon, S.-K., & Kim, J. F. (2009). Genomics, Biological Features, and Biotechnological Applications of *Escherichia coli* B: "Is B for better?!". In S. Y. Lee (Ed.), *Systems Biology and Biotechnology of Escherichia coli* (pp. 1-17). Dordrecht: Springer Netherlands.

Zambri, M. P., Williams, M. A., & Elliot, M. A. (2022). How *Streptomyces* thrive: Advancing our understanding of classical development and uncovering new behaviors. *Adv Microb Physiol, 80*, 203-236. doi:10.1016/bs.ampbs.2022.01.004

Žgur Bertok, D., & Podlesek, Z. (2021). The *Escherichia coli* SOS Response: Much More than DNA Damage Repair. In M. Starčič Erjavec (Ed.), *Escherichia coli - Old and New Insights*. Rijeka: IntechOpen.

Zhang, Q., Chi, H.-T., Wu, L., Deng, Z., & Yu, Y. (2021). Two Cryptic Self-Resistance Mechanisms in *Streptomyces tenebrarius* Reveal Insights into the Biosynthesis of Apramycin. *Angewandte Chemie International Edition, 60*(16), 8990-8996. doi:doi.org/10.1002/anie.202100687

Zuo, P., Yu, P., Alvarez, P. J. J., & Dozois, C. M. (2021). Aminoglycosides Antagonize Bacteriophage Proliferation, Attenuating Phage Suppression of Bacterial Growth, Biofilm Formation, and Antibiotic Resistance. *Applied and Environmental Microbiology, 87*(15), e00468-00421. doi:doi:10.1128/AEM.00468-21

6. Appendix

6.1 Supplementary material – microscopy images of aminoglycoside producer strains

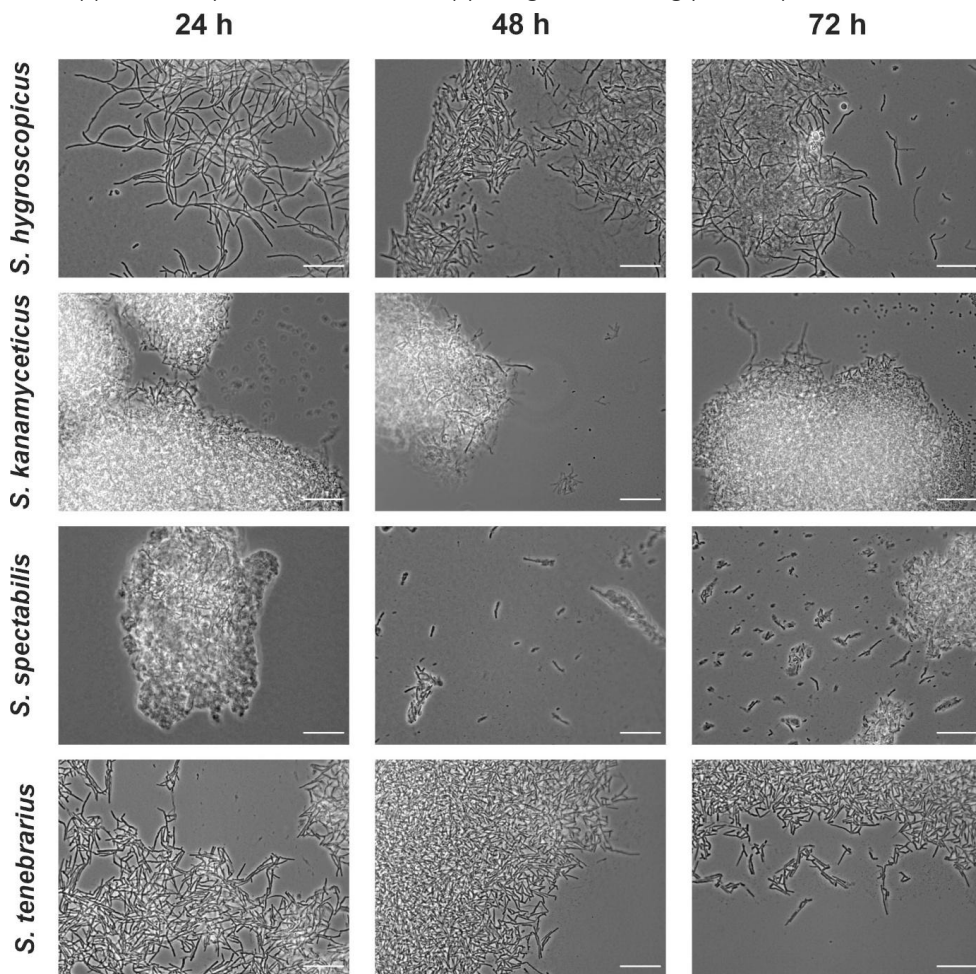**Figure S1: Microscopy images of aminoglycoside producing strains.** Bright field microscopy images of *S. hygroscopicus, S. kanamyceticus, S. spectabilis* and *S. tenebrarius* (top to bottom) at 24 h, 48 h and 72 h of cultivation (left to right) shot the development of the culture over time. The images were taken with a 100 x magnification using a Plan-APOCHROMAT oil immersion objective, scale bar: 20 µm

6.2 Supplementary material – Spent medium assays with remaining producer strains
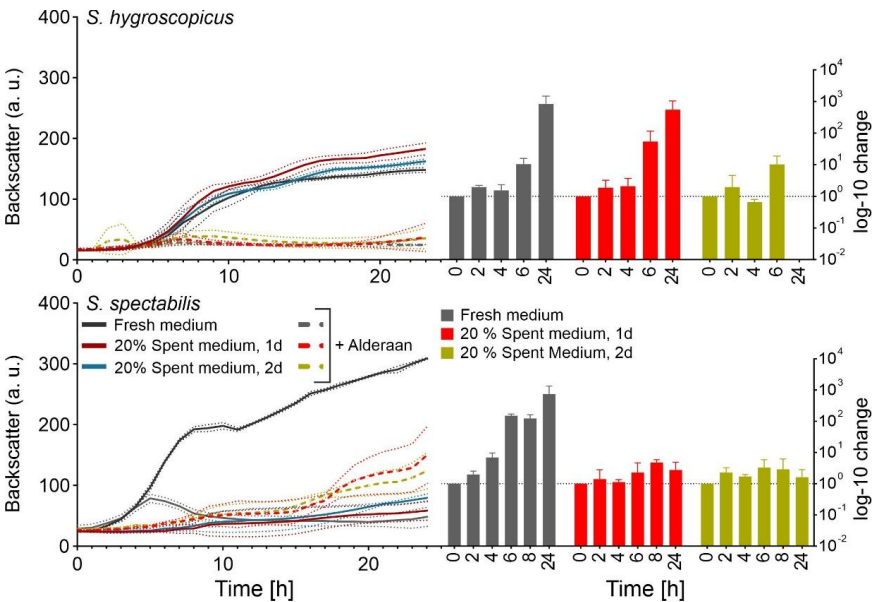

Figure S2: Spent medium assays with the remaining producer strains. . Liquid phage infection assays of phage Alderaan infecting *S. venezuelae* supplemented with 20 % spent medium harvested after 1 or two days of cultivation. On the left growth curves are shown and on the right the corresponding plaque forming units normalized to the T_0. In black is the uninfected culture in fresh GYM medium and in grey dashed lines the infected culture in fresh gym medium, in dark red is the uninfected culture supplemented with 20 % 1-day-old SM and in the bright red dashed line the corresponding infected culture. The turquoise solid line represents the uninfected culture supplemented with 20 % 2-day-old SM and in yellow dashed, the corresponding infected culture. The bar plot colours correspond to the infected cultures with the respective supplement in the medium (grey = GYM, red = 1 d SM, yellow = 2 d SM). The culture was inoculated at an OD_{450}= 0.15 and infected with Alderaan at 10^7 PFU/mL. The left y-axis shows Backscatter in arbitrary units, the right y-axis the $\log_{10}$-fold change normalized to t_0 and the x-axis displays the time in hours. n=3 independent biological replicates, dotted lines in the growth curves and error bars in the bar plot show the standard deviation.

6.3 Supplementary material of Isolation and characterization of new *Streptomyces* phages

Supplementary material of this section was already published in B. Rackow et al. 2024.

Table S1: Bacterial strains used for host range analysis and efficiency of plating. Bacterial strains in this Table were used to perform detailed experiments in the sections describing phage isolation and propagation, infection dynamics, plaque development and phage host range assay with EOP.

Strains	Genotype	Reference
Streptomyces afghaniensis	WT	DSM 40228
Streptomyces albaduncus	WT	DSM 40478
Streptomyces coelicolor A3(2)	WT	DSM 112524
Streptomyces coelicolor A3(2) M145 (host Abafar & Scarif)	*S. coelicolor* A3(2) lacking plasmids SCP1 and SCP2	(Bentley *et al.*, 2002)
Streptomyces albulus	WT	DSM 40492
Streptomyces antibioticus	WT	DSM 40234
Streptomyces avermitilis	WT	DSM 46492
Streptomyces azureus	WT	DSM 40106

Streptomyces celluloflavus	WT	DSM 40839
Streptomyces chartreusis	WT	DSM 40085
Streptomyces clavuligerus	WT	DSM 738
Streptomyces fimbriatus	WT	DSM 40942
Streptomyces fradiae	WT	DSM 40063
Streptomyces galbus	WT	DSM 40089
Streptomyces griseofuscus	WT	DSM 40191
Streptomyces griseorubens	WT	DSM 40160
Streptomyces griseus (host Geonosis)	WT	DSM 40236
Streptomyces humidus	WT	DSM 40263
Streptomyces hygroscopicus	WT	DSM 40578
Streptomyces inusitatus	WT	DSM 41441
Streptomyces kanamyceticus	WT	DSM 40500
Streptomyces kasugaensis (host Kamino)	WT	DSM 40819
Streptomyces lavendulae	WT	DSM 40069
Streptomyces longispororuber	WT	DSM 40599
Streptomyces luridus	WT	DSM 40081
Streptomyces niveus	WT	DSM 40088
Streptomyces nodosus	WT	DSM 40109
Streptomyces olivaceus	WT	DSM 41536
Streptomyces purpurascens	WT	DSM 40310
Streptomyces rimosus	WT	DSM 40260
Streptomyces sulfonofaciens	WT	DSM 41679
Streptomyces thioluteus	WT	DSM 40027
Streptomyces venezuelae NRRL B-65442	WT	DSM 112328
Streptomyces violaceus	WT	DSM 40082
Streptomyces *viridosporus*	WT	DSM 40243

Table S2: Bacterial strains used for host range analysis.

Table S2 includes all *Streptomyces* strains which were used for the host range assay. Strains which showed productive infection were further tested and are mentioned in Table S1 in detail

Streptomyces strains used for the host range	DSM Number
Streptomyces afghaniensis	DSM 40228
Streptomyces albaduncus	DSM 40478
Streptomyces alboniger	DSM 40043
Streptomyces albulus	DSM 40492
Streptomyces anandii	DSM 40535
Streptomyces antibioticus	DSM 40234
Streptomyces avermitilis	DSM 46492
Streptomyces avidinii	DSM 40526
Streptomyces azureus	DSM 40106
Streptomyces bluensis	DSM 40564
Streptomyces celluloflavus	DSM 40839
Streptomyces chartreusis	DSM 40085
Streptomyces chrestomyceticus	DSM 40545
Streptomyces clavuligerus	DSM 738
Streptomyces coelicolor A3(2)	DSM 112524

Streptomyces echinatus	DSM 40013
Streptomyces eurocidicus	DSM 40604
Streptomyces fradiae	DSM 40063
Streptomyces fimbriatus	DSM 40942
Streptomyces galbus	DSM 40089
Streptomyces griseus	DSM 40236
Streptomyces griseofuscus	DSM 40191
Streptomyces griseorubens	DSM 40160
Streptomyces humidus	DSM 40263
Streptomyces inusitatus	DSM 41441
Streptomyces kanamyceticus	DSM 40500
Streptomyces kasugaensis	DSM 40819
Streptomyces lavendulae	DSM 40069
Streptomyces litmocidini	DSM 40164
Streptomyces longispororuber	DSM 40599
Streptomyces luridus	DSM 40081
Streptomyces mutomycini	DSM 41691
Streptomyces niveus	DSM 40088
Streptomyces nodosus	DSM 40109
Streptomyces olivaceus	DSM 41536
Streptomyces purpurascens	DSM 40310
Streptomyces rapamycinicus	DSM 41530
Streptomyces rimosus	DSM 40260
Streptomyces scabiei	DSM 41658
Streptomyces sulfonofaciens	DSM 41679
Streptomyces thioluteus	DSM 40027
Streptomyces venezuelae	DSM 112328
Streptomyces violaceus	DSM 40082
Streptomyces viridosporus	DSM 40243
Streptomyces wellingtoniae	DSM 40632

Table S3: VIRDIC analysis of phages (extra)

VIRDIC analysis of phage genera with comparison of nucleotide sequence identity to other known *Streptomyces* phages. Colouration indicates sequence identity of phages, with red showing no identity, orange and yellow indicating low percentage identity and green indicating high percentage of identity. The newly isolated and characterized phages were clustered into species and genera according to ICTV rules with 95 % and 70 % nucleotide sequence identity over the length of the genome respectively. The numbers in the Table show the percentage of nucleotide sequence identity. spectrum.00663-24-s0002.xlsx

6. Appendix

Table S4: PADLOC analysis of host defense systems (extra)

PADLOC analysis of 34 of the 45 tested *Streptomyces* species for their composition of defense systems. 0 indicates that the respective defense system is absent in the species and 1 indicates that the defense system was found encoded in the genome of the respective species. Abbreviations of defense systems are according to the PADLOC tool. spectrum.00663-24-s0003.xlsx

Supplementary Figure 3

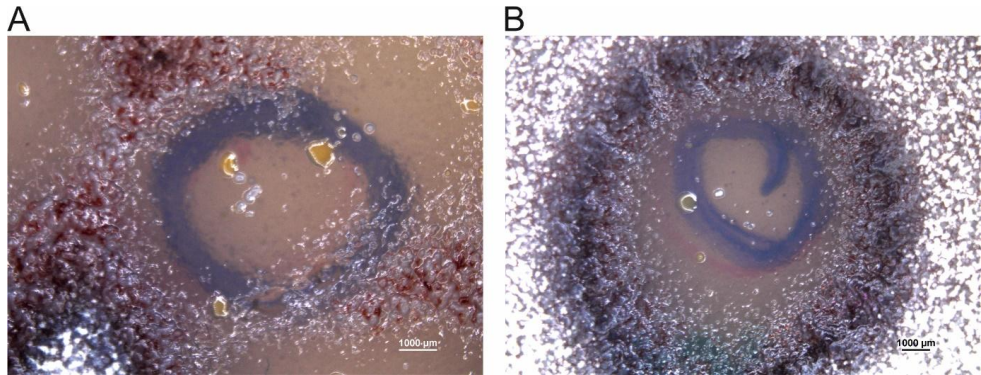**Figure S3:** Plate images of phage Abafar (A) and phage Scarif (B) 72 hours post infection, where the production of actinorhodin as blue pigmentation and undecylprodigiosin as red pigmentation at the edges of the plaques are visible. The blue drawing from underneath the plate marks the initial plaque location. White coloration of the surrounding bacterial lawn indicates sporulation. The scale bar is for both plates 1000 μm.

Supplementary Figure 4

Figure S4: Synteny plot of phage Abafar compared to other manuelviruses at the nucleotide level. The Figure was generated with EasyFig (Sullivan et al., 2011). Colouring is based on the PHROG colour code for functional clusters (Terzian et al., 2021) (orange: integration and excision; blue: head and packaging; purple: transcription; light blue: connector; green: tail; red: lysis; yellow: DNA, RNA and nucleotide metabolism; pink: moron, auxiliary metabolic gene and host takeover; dark grey: other).

Supplementary Figure 5
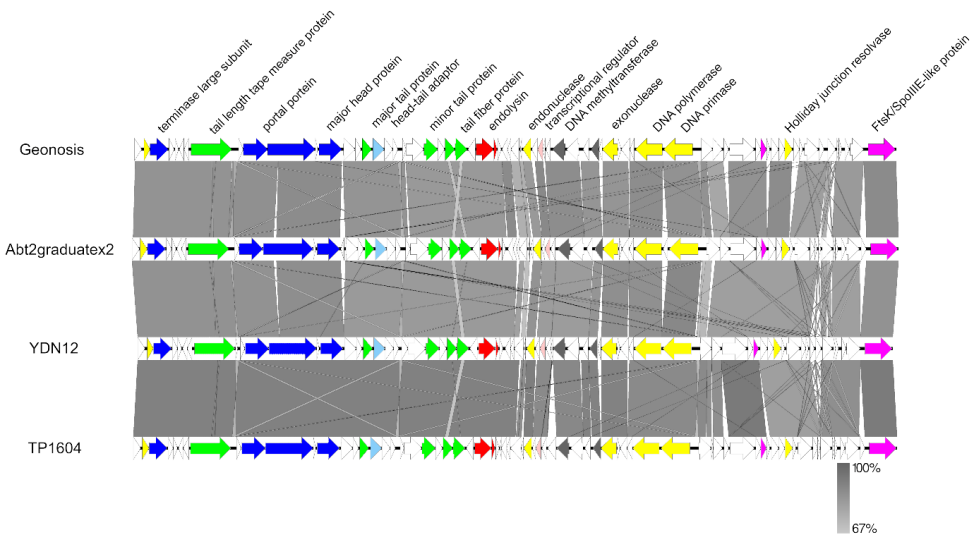
Figure S5: Synteny plot of phage Geonosis compared to other woodruffviruses at the nucleotide level. The Figure was generated with EasyFig (Sullivan et al., 2011). Colouring is based on the PHROG colour code for functional clusters (Terzian et al., 2021) (orange: integration and excision; blue: head and packaging; purple: transcription; light blue: connector; green: tail; red: lysis; yellow: DNA, RNA and nucleotide metabolism; pink: moron, auxiliary metabolic gene and host takeover; dark grey: other).
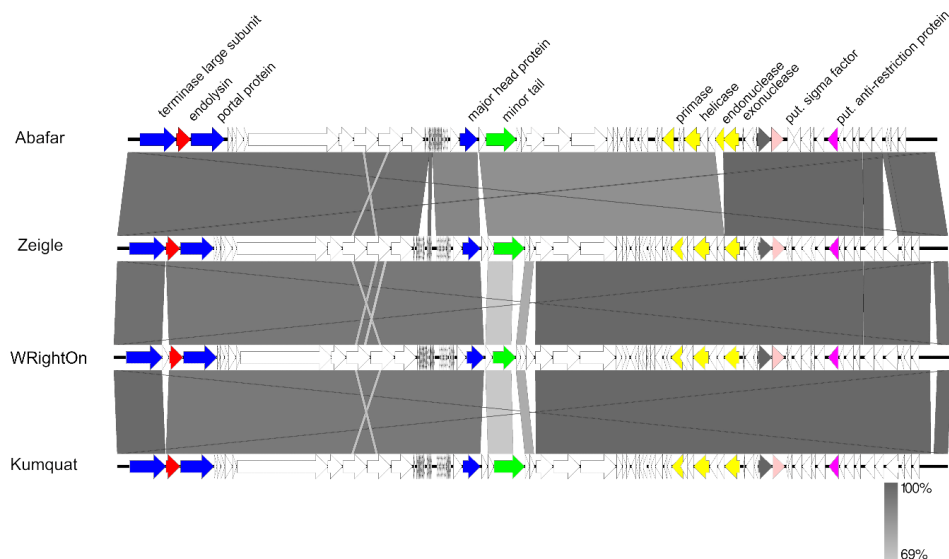
Supplementary Figure 6
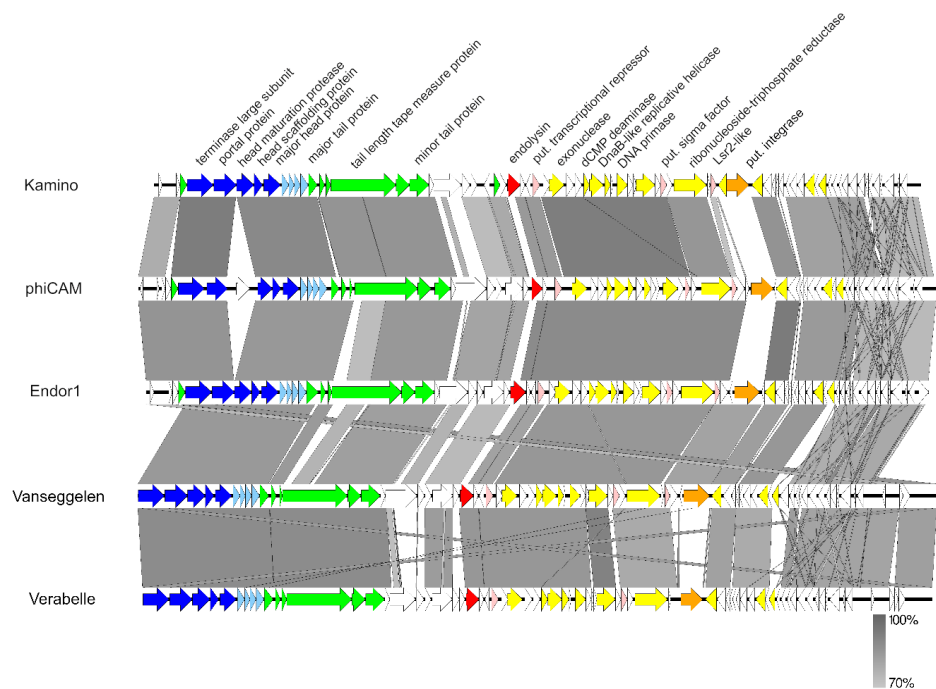
Figure S6: Synteny plot of phage Kamino compared to other camviruses at the nucleotide level. The Figure was generated with EasyFig (Sullivan et al., 2011). Colouring is based on the PHROG colour code for functional clusters (Terzian et al., 2021) (orange: integration and excision; blue: head and packaging; purple: transcription; light blue: connector; green: tail; red: lysis; yellow: DNA, RNA and nucleotide metabolism; pink: moron, auxiliary metabolic gene and host takeover; dark grey: other).

6. Appendix

Supplementary Figure 7

Figure S7: Synteny plot of phage Scarif compared to closely related members of Rimavirus at the nucleotide level. The Figure was generated with EasyFig (Sullivan et al., 2011). Colouring is based on the PHROG colour code for functional clusters (Terzian et al., 2021) (orange: integration and excision; blue: head and packaging; purple: transcription; light blue: connector; green: tail; red: lysis; yellow: DNA, RNA and nucleotide metabolism; pink: moron, auxiliary metabolic gene and host takeover; dark grey: other).
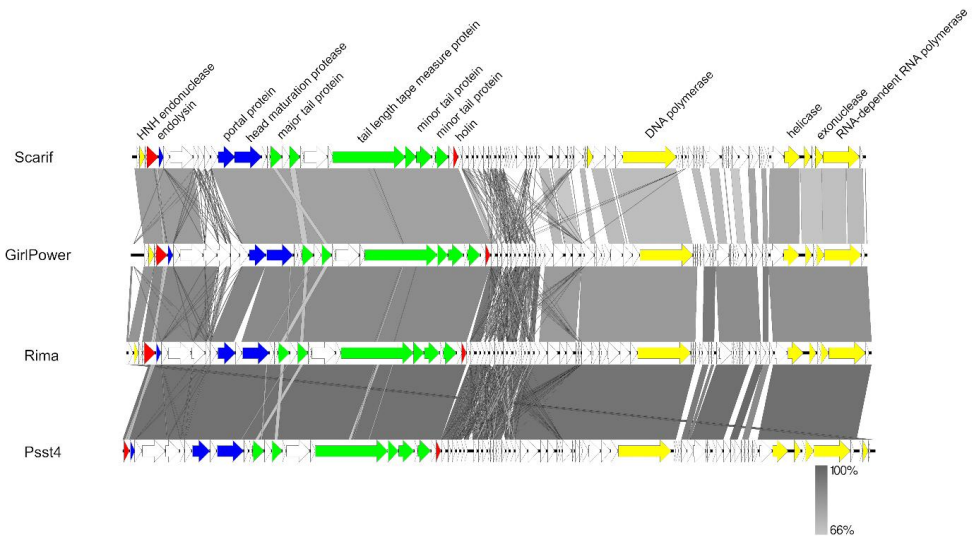
6.4 Supplementary material – representative spot assays of Screening of *Streptomyces* phages
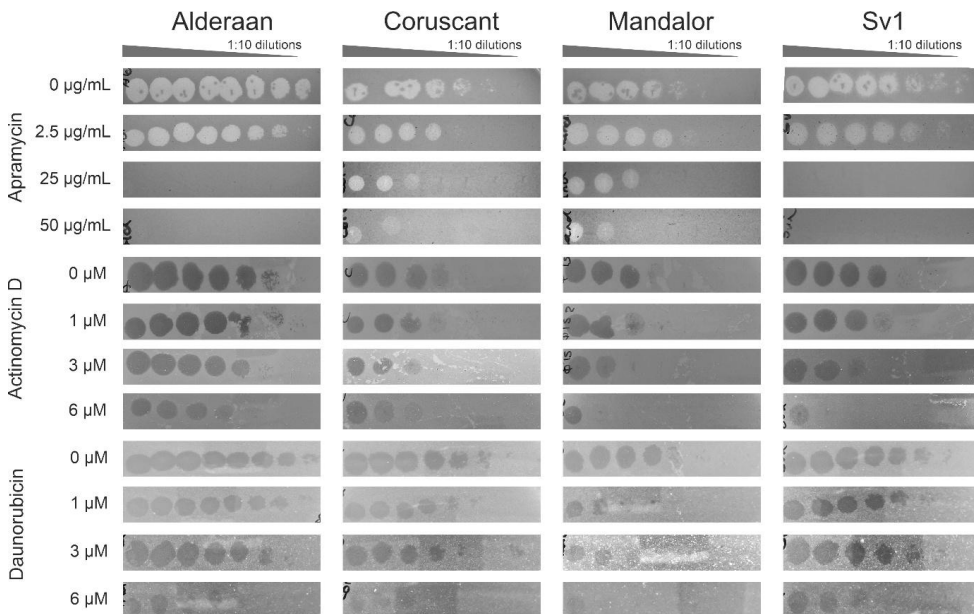
Figure S8: Selection of spot assay images of *S. venezuelae* phages screened on anti-phage molecules. Phage Alderaan, Coruscant, Mandalor and Sv1 (left to right) screened on different concentrations of apramycin (top), actinomycin D (middle) and daunorubicin (bottom). Spotted were serial dilutions of phages on GYM double-agar overlays with the same concentrations of small molecules in both layers of the agar. Reduction in titer corresponds to the heat map in Figure 19.

6.5 Supplementary material – BASEL collection genetic information

The genetic information of all BASEL phages can be found in the publication: Maffei, Enea; Shaidullina, Aisylu; Burkolter, Marco; Heyer, Yannik; Estermann, Fabienne; Druelle, Valentin; et al. (2021). List of all phages used in this study... PLOS Biology. Dataset. https://doi.org/10.1371/journal.pbio.3001424.s005

6.6 Supplementary material – Transcriptome analysis of *E. coli* MG1655 ΔRM +/- dau

Table S5: Transcriptome analysis of *E. coli* MG1655 ΔRM +/- dau, Name, chromosome region, Log$_2$-old change and FDR p-value of significantly differentially expressed genes when comparing +dau vs. -dau.

Name	Chromosome	Region	Log$_2$ fold change	FDR p-value
insD7	U00096	1650881..1651537	11.43665	0.000796
rrfB	U00096	4171637..4171756	9.520385	0.028487
rrfE	U00096	4213040..4213159	9.501239	0.030322
rrlB	U00096	4168641..4171544	7.510629	5.7E-10
rrlE	U00096	4210043..4212946	6.620756	3.65E-06
rrlD	U00096	complement(3423880..3426783)	5.927866	8.43E-09
rrsA	U00096	4035531..4037072	5.639213	1.68E-08

cspG	U00096	1051461..1051673	5.56722	0.046486
rrsC	U00096	3941808..3943349	5.413725	1.69E-07
rbsZ	U00096	3937045..3937278	5.100452	0.000148
rrsG	U00096	complement(2729616..2731157)	5.0089	8.61E-06
rrsD	U00096	complement(3427221..3428762)	4.995932	2.66E-05
rrlC	U00096	3943704..3946607	4.752717	2.15E-05
rrlH	U00096	225759..228662	4.699151	2.66E-05
rrsH	U00096	223771..225312	4.577169	6.63E-07
rrlG	U00096	complement(2726281..2729184)	4.486693	0.000118
torC	U00096	1058084..1059256	4.46099	4.33E-08
rrlA	U00096	4037519..4040423	4.409026	0.000154
yecH	U00096	complement(1989251..1989490)	4.383064	0.005563
yciA	U00096	complement(1311848..1312246)	4.173233	0.039111
glpA	U00096	2352647..2354275	4.149875	5.7E-10
rrsB	U00096	4166659..4168200	4.050839	0.008017
ycaP	U00096	956762..957454	4.015258	0.046486
torA	U00096	1059256..1061802	3.889078	1.00E-16
rrsE	U00096	4208147..4209688	3.778568	0.00031
sgrS	U00096	77367..77593	3.388232	0.033787
fumE	U00096	complement(3074686..3075195)	3.260473	4.01E-05
dcuC	U00096	complement(654583..655968)	3.07942	0.000167
ybcJ	U00096	complement(556661..556873)	3.033215	0.028487
ysaA	U00096	complement(3741109..3741582)	2.98713	0.003165
fdnI	U00096	1551338..1551991	2.979641	0.003276
ubiV	U00096	3302489..3303367	2.932369	9.84E-05
rplE	U00096	complement(3446899..3447438)	2.624878	0.039111
rplJ	U00096	4179996..4180493	2.562689	0.046486
yohK	U00096	2231019..2231714	2.53261	0.000282
hns	U00096	complement(1292509..1292922)	2.510766	0.045893
glpT	U00096	complement(2351016..2352374)	2.401394	1.24E-05
tdcA	U00096	complement(3266127..3267065)	2.285554	0.048736
ybbJ	U00096	complement(514401..514859)	2.284877	0.005563
yohJ	U00096	2230624..2231022	2.282774	0.02807
lomR	U00096	1427389..1428984	2.265642	0.021386
torD	U00096	1061799..1062398	2.243016	0.021591
nirB	U00096	3494011..3496554	2.220536	0.000555
narG	U00096	1279864..1283607	2.18045	0.001084
insC6	U00096	4498272..4498637	2.15617	0.033787
trmJ	U00096	complement(2662583..2663323)	2.129604	0.011406
ubiT	U00096	complement(3300752..3301276)	2.123264	0.001842
nikC	U00096	3616182..3617015	2.10361	0.046486
nuoF	U00096	complement(2400218..2401555)	2.09402	0.023123
nrfA	U00096	4287764..4289200	2.080856	0.048923
ansB	U00096	complement(3099682..3100728)	2.042542	0.023123
yfcC	U00096	2417081..2418601	2.015699	0.046486
cyuA	U00096	complement(3255341..3256651)	1.996429	0.021386

tcyP	U00096	1810934..1812325	1.990345	0.008017
cysW	U00096	complement(2540804..2541679)	1.960467	0.039111
deoC	U00096	4617323..4618102	1.954144	0.001084
dsbA	U00096	4043418..4044044	1.915959	0.014274
rpiA	U00096	complement(3058666..3059325)	1.891343	0.021386
fabZ	U00096	202101..202556	1.857513	0.025475
yohD	U00096	2225801..2226379	1.846557	0.033377
yfeX	U00096	complement(2549646..2550545)	1.775763	0.017786
yeeZ	U00096	complement(2088304..2089128)	1.740664	0.00571
ruvC	U00096	complement(1946855..1947376)	1.719692	0.012922
fkpA	U00096	complement(3476607..3477419)	1.711916	0.014274
yjjI	U00096	complement(4615515..4617065)	1.699732	0.021386
glpD	U00096	3562013..3563518	1.684692	0.000676
pykA	U00096	1937649..1939091	1.676241	0.021386
ybeZ	U00096	complement(692338..693378)	1.675817	0.023551
ravA	U00096	complement(3929597..3931093)	1.641368	0.007388
yhhN	U00096	3605751..3606377	1.588729	0.025709
nfi	U00096	4198790..4199461	1.487012	0.045899
recN	U00096	2751795..2753456	1.4388	0.014455
gatY	U00096	complement(2176350..2177204)	1.356125	0.023551
ucpA	U00096	complement(2543832..2544623)	1.311893	0.021386
queA	U00096	425011..426081	-1.36306	0.046804
livJ	U00096	complement(3598555..3599658)	-1.90637	0.048923
leuB	U00096	complement(80867..81958)	-2.1882	0.00571
sgcC	U00096	complement(4528930..4530243)	-2.26879	0.005304
acs	U00096	complement(4285413..4287371)	-2.38585	8.6E-05
gltI	U00096	complement(686839..687747)	-2.74243	0.000535
lacZ	U00096	complement(363231..366305)	-2.99953	1.5E-07
mglB	U00096	complement(2239350..2240348)	-3.01364	0.014455
ecpA	U00096	complement(310084..310671)	-3.01584	1.26E-06
ecpB	U00096	complement(309358..310026)	-3.49985	0.000676
sgcB	U00096	complement(4530255..4530533)	-3.81478	0.041679
rrfD	U00096	complement(3423668..3423787)	-4.87596	0.046486
matA	U00096	complement(310746..311336)	-5.18809	0.002646
rrfG	U00096	complement(2726069..2726188)	-5.38422	0.021386

6.7 Supplementary material – PADLOC analysis of *E. coli* host strains

Table S6: PADLOC analysis of *E. coli* K12 MG1655

system.number	seqid	system	target.name	hmm.accession	hmm.name	protein.name
5	U00096.2	PDC-S07	b0099	PDLC04899	PDC-S07_WP_110056698.1	PDC-S07
2	U00096.2	Lit	b1139	PDLC02355	Lit	Lit

10	U0009 6.2	RM_type_IV	b1159	PDLC03656	mREase_IV_00002	mREase_IV
6	U0009 6.2	PDC-S07	b1759	PDLC04899	PDC-S07_WP_110056698.1	PDC-S07
7	U0009 6.2	PDC-S12	b1908	PDLC04917	PDC-S12_WP_034891581.1	PDC-S12
12	U0009 6.2	VSPR	b1960	PDLC03397	NEase_II_00006	Vsr
12	U0009 6.2	VSPR	b1961	PDLC03361	MTase_II_00147	MTase_II
14	U0009 6.2	hachiman_type_I	b2627	PDLC00180	HamB1_00007	HamB1
14	U0009 6.2	hachiman_type_I	b2628	PDLC00153	HamA1_00004	HamA1
1	U0009 6.2	CRISPR_array	CRISPR001	NA	NA	CRISPR_array
13	U0009 6.2	cas_type_I-E	b2754	PDLC00934	cas_CT1978	Cas2e
13	U0009 6.2	cas_type_I-E	b2755	PDLC01744	Cas1e_WP_035839043.1	Cas1e
13	U0009 6.2	cas_type_I-E	b2756	PDLC00954	casE_Cse3	Cas6e
13	U0009 6.2	cas_type_I-E	b2757	PDLC00949	casD_Cas5e	Cas5e
13	U0009 6.2	cas_type_I-E	b2758	PDLC00959	casC_Cse4	Cas7e
13	U0009 6.2	cas_type_I-E	b2759	PDLC01283	cd09670	Cas11e
13	U0009 6.2	cas_type_I-E	b2760	PDLC00999	casA_cse1	Cas8e
13	U0009 6.2	cas_type_I-E	b2761	PDLC01767	Cas3e_WP_189128522.1	Cas3e
1	U0009 6.2	CRISPR_array	CRISPR002	NA	NA	CRISPR_array
3	U0009 6.2	PDC-S02	b3220	PDLC04807	PDC-S02_WP_151674975.1	PDC-S02
4	U0009 6.2	PDC-S04	b3361	PDLC04838	PDC-S04_WP_169250289.1	PDC-S04
8	U0009 6.2	PDC-S13	b3645	PDLC04919	PDC-S13_WP_186842295.1	PDC-S13
9	U0009 6.2	RM_type_I	b4348	PDLC03169	Specificity_I_00118	Specificity_I
9	U0009 6.2	RM_type_I	b4349	PDLC03026	MTase_I_00009	MTase_I
9	U0009 6.2	RM_type_I	b4350	PDLC03042	REase_I_00003	REase_I

| 11 | U0009 6.2 | RM_type_IV | b4351 | PDLC03657 | mREase_IV_00003 | mREase_I V |

Table S7: PADLOC analysis of *E. coli* B strain

system.nu mber	seqid	system	target.na me	hmm.acc ession	hmm.name	protein. name
3	NZ_CP014 268.2	PDC-S07	C2566_RS 04235	PDLC0489 9	PDC-S07_WP_110056698.1	PDC-S07
7	NZ_CP014 268.2	retron_II -A	C2566_RS 07945	PDLC0293 0	retron_type_II_A3_ndt _cluster42_1	NDT_II-A
7	NZ_CP014 268.2	retron_II -A	NA	-	TypeIIA3_proteo	msr-msd
7	NZ_CP014 268.2	retron_II -A	C2566_RS 07950	PDLC0294 1	retron_II-A3	RT_II-A
4	NZ_CP014 268.2	PDC-S07	C2566_RS 12580	PDLC0489 9	PDC-S07_WP_110056698.1	PDC-S07
5	NZ_CP014 268.2	PDC-S12	C2566_RS 13380	PDLC0491 7	PDC-S12_WP_034891581.1	PDC-S12
1	NZ_CP014 268.2	CRISPR_ array	CRISPR00 1	NA	NA	CRISPR_ array
1	NZ_CP014 268.2	CRISPR_ array	CRISPR00 2	NA	NA	CRISPR_ array
2	NZ_CP014 268.2	PDC-S04	C2566_RS 20185	PDLC0483 8	PDC-S04_WP_169250289.1	PDC-S04
6	NZ_CP014 268.2	PDC-S13	C2566_RS 21720	PDLC0491 9	PDC-S13_WP_186842295.1	PDC-S13

Table S8: PADLOC analysis of *E. coli* BL21 (DE3)

system.nu mber	seqid	system	target.n ame	hmm.acce ssion	hmm.name	protein.n ame
3	CP0015 09.3	PDC-S07	ECD_00 100	PDLC0489 9	PDC-S07_WP_110056698.1	PDC-S07
9	CP0015 09.3	retron_II -A	ECD_00 830	PDLC0293 0	retron_type_II_A3_ndt_ cluster42_1	NDT_II-A
9	CP0015 09.3	retron_II -A	NA	-	TypeIIA3_proteo	msr-msd
9	CP0015 09.3	retron_II -A	ECD_00 831	PDLC0294 1	retron_II-A3	RT_II-A
4	CP0015 09.3	PDC-S07	ECD_01 728	PDLC0489 9	PDC-S07_WP_110056698.1	PDC-S07
5	CP0015 09.3	PDC-S12	ECD_01 876	PDLC0491 7	PDC-S12_WP_034891581.1	PDC-S12
1	CP0015 09.3	CRISPR_a rray	CRISPR0 01	NA	NA	CRISPR_a rray
1	CP0015 09.3	CRISPR_a rray	CRISPR0 02	NA	NA	CRISPR_a rray
2	CP0015 09.3	PDC-S04	ECD_03 212	PDLC0483 8	PDC-S04_WP_169250289.1	PDC-S04
6	CP0015 09.3	PDC-S13	ECD_03 502	PDLC0491 9	PDC-S13_WP_186842295.1	PDC-S13

7	CP0015 09.3	RM_type _I	ECD_04 215	PDLC0302 6	MTase_I_00009	MTase_I
7	CP0015 09.3	RM_type _I	ECD_04 216	PDLC0304 2	REase_I_00003	REase_I
8	CP0015 09.3	RM_type _IV	ECD_04 217	PDLC0365 7	mREase_IV_00003	mREase_I V

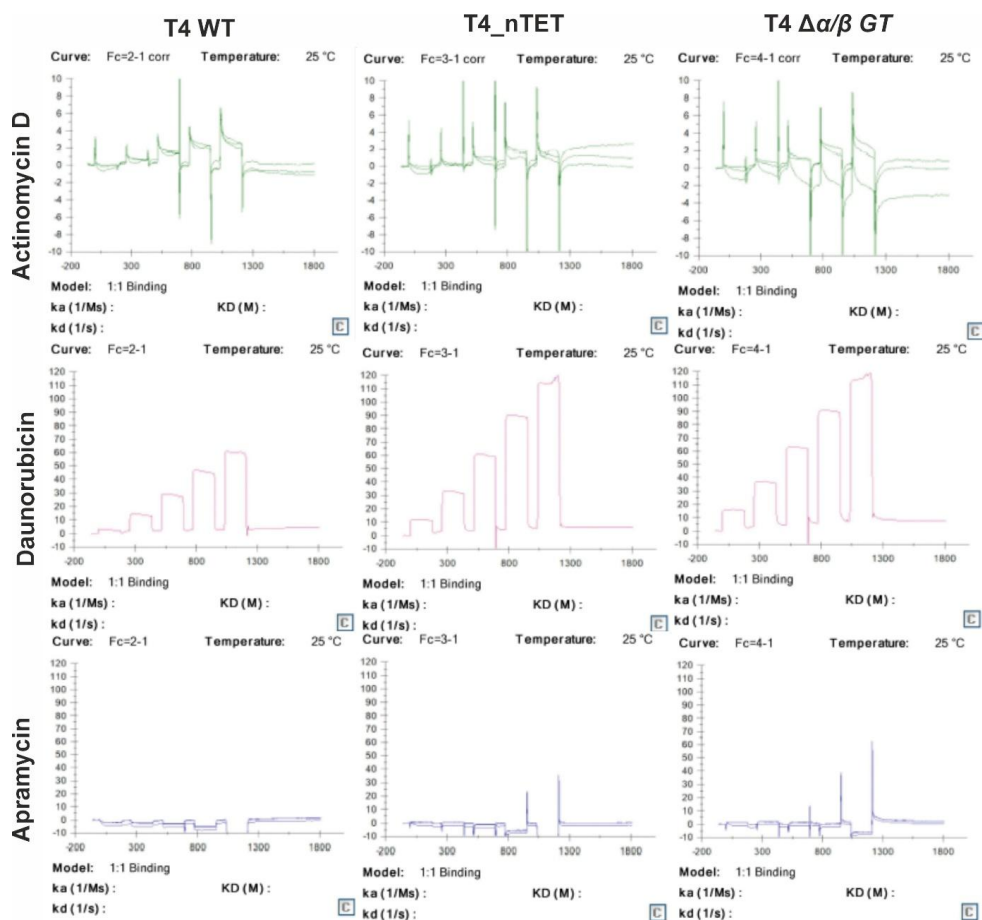## 6.8 Supplementary material – Biacore SPR measurements of T4 DNA

Figure S9: SPR biacore measurements of T4 DNA with varying degrees of glycosylation with Actinomycin D, Daunorubicin and Apramycin as ligand. T4 wild type, T4_nTET and T4 Δα/βGT DNA (left to right) binding kinetics with Actinomycin D (green), Daunorubicin (red) and Apramycin (blue) (top to bottom) are shown. On the y-axis is the Response in response units (RU), on the x-axis the time in minutes. Measurements were performed at 25 °C.

6.9 Supplementary material – Phage titer corresponding to infection kinetics at different MOI
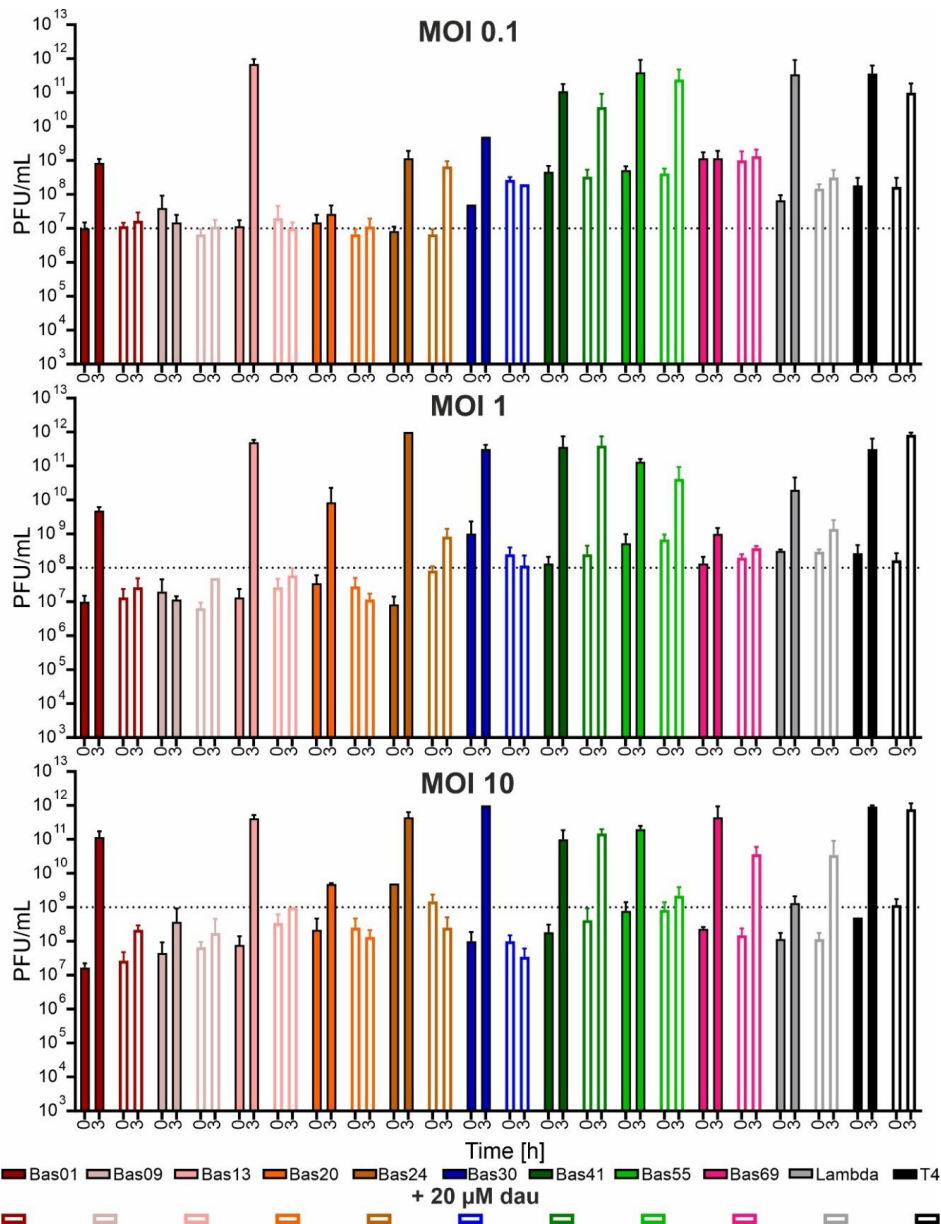

Figure S10: Phage Titer corresponding to infection kinetics at different MOI. Presented here is the monitored phage titer in PFU/mL for liquid infection assays at MOI 0.1, 1 and 10 (top to bottom). In absence of daunorubicin the bar is colour filled with a black outline and in presence of daunorubicin the outline is coloured and the filling is white. Shown are the phages Bas01 (dark red), Bas09 (light red), Bas13 (rosé), Bas 20 (orange), Bas24 (brown), Bas30 (blue), Bas41 (dark green), Bas55 (bright green), Bas69 (pink), λ (grey) and T4 (black) from left to right. The y-axis shows PFU/mL and the x-axis time in hours.

6. Appendix

Acknowledgements

Zuerst einmal möchte ich Prof. Dr. Julia Frunzke dafür danken, dass sie mir ermöglicht hat meine Promotion in Ihrer Arbeitsgruppe zu durchführen zu können. Während dieser Zeit habe ich unfassbar viel gelernt und die Möglichkeit erhalten mich weiterzuentwickeln. Für Julias offene und ehrliche Art bin ich ihr sehr dankbar und weiß die Unterstützung, die konstruktive Kritik und auch die lustigen Group-Evening sehr zu schätzen.

Auch Prof. Dr. Nick Wierckx möchte ich danken, dass er als mein Mentor und Zweitgutachter ist und mir die Möglichkeit gegeben hat seine Geräte zu kapern und nur ein bisschen Kuchen als Gegenleistung erwartet hat.

Ein großer Dank geht auch an alle Kollege und Kolleginnen im ganzen IBG-1, insbesondere der Arbeitsgruppe Frunzke. Ohne euch wäre jede Mittagspause, jeder Group evening, Jeder Retreat und jede Konferenz nur halb so schön gewesen. Ich danke Aileen, Biel, Connie, Doris, Eva, Isabelle, Larissa, Mirco, Moses, Patricia, Philipp, Samy, Sebastian, Sümeyye, Tom und Uli sowie allen ehemaligen Mitgliedern der AG Frunzke dafür, dass wir diese Reise gemeinsam gemacht haben. Mit euch allen wurde es unvergesslich. Ihr wart mir eine große Unterstützung, insbesondere Larissa, und auch Quelle der Inspiration und spaßiger Erlebnisse. Danke!

Auch meinen Freunden und meiner Familie möchte ich danken. Für eure Geduld mit mir, euer Vertrauen in mich und eure bedingungslose Unterstützung. Ohne euch wäre es nicht gegangen. Zu wissen, dass ich bei euch immer Rückendeckung erhalte und ihr mich auffangt hat mich stark gemacht! Dafür danke ich euch von ganzem Herzen, allen voran der besten großen (kleinen) Schwester, Helke, die ich einfach allein gelassen hab mit den Ponys. Aber auch Mama, Papa und Oma, dass ihr stolz auf mich seid hat mich immer wieder angetrieben. Dafür, dass ich auch in 600 km Entfernung immer auf euch zählen konnte bedeutet mir alles! Annika, Nadja & Louisa, auf euch kann ich mich verlassen!

Zu guter Letzt danke ich Christian, meinem Felsen in der Brandung, mein Ruhepol und die kleine Stimme der Vernunft! Ich weiß, gemeinsam mit dir kann ich alles schaffen! Danke!

Erklärung

Hiermit versichere ich an Eides Statt, dass die Dissertation von mir selbstständig und ohne unzulässige fremde Hilfe unter der Beachtung der „Grundsätze zur Sicherung guter wissenschaftlicher Praxis an der Heinrich-Heine-Universität Düsseldorf" erstellt worden ist. Die Dissertation wurde in der vorgelegten oder in ähnlicher Form noch bei keiner anderen Institution eingereicht. Ich habe bisher keine erfolglosen Promotionsversuche unternommen.

Bente Rackow

Band / Volume 286
Ab initio investigation of intrinsic antiferromagnetic solitons
Amal Jawdat Nayef Aldarawsheh (2024), xv, 164 pp
ISBN: 978-3-95806-785-1

Band / Volume 287
Understanding the dynamics of Plant-Bacteria-Bacteriophage interactions as a means to improve plant performance
S. H. Erdrich (2024), ix, 176 pp
ISBN: 978-3-95806-791-2

Band / Volume 288
Prediction of Magnetic Materials for Energy and Information Combining Data-Analytics and First-Principles Theory
R. Hilgers (2024), xv, 215 pp
ISBN: 978-3-95806-795-0

Band / Volume 289
Biodegradation and microbial upcycling of plastics
J. de Witt (2025), XVI, 259 pp
ISBN: 978-3-95806-804-9

Band / Volume 290
Practical Methods for Efficient Analytical Control in Superconducting Qubits
B. Li (2025), 202 pp
ISBN: 978-3-95806-807-0

Band / Volume 291
Ab initio investigation of topological magnetism in two-dimensional van der Waals heterostructures
N. Abuawwad (2025), xviii, 135 pp
ISBN: 978-3-95806-808-7

Band / Volume 292
Tolerance engineering of Pseudomonas for the efficient conversion and production of aldehydes
T. Lechtenberg (2025), XVI, 185 pp
ISBN: 978-3-95806-817-9

Band / Volume 293
Exploring the process window for production of itaconic, 2-hydroxyparaconic, and itatartaric acid with engineered *Ustilago* strains
P. Ernst (2025), x, 145 pp
ISBN: 978-3-95806-825-4

Schriften des Forschungszentrums Jülich
Reihe Schlüsseltechnologien / Key Technologies

Band / Volume 294
**Surface Plasmon Resonance Microscopy for the Characterization of
Cell-Substrate Distances**
J. Bednar (2025), xxiii, 187 pp
ISBN: 978-3-95806-830-8

Band / Volume 295
**Microfluidic-MEA hybrid systems for
electrophysiological recordings of neuronal co-cultures**
J. Stevanović (2025), ix, 186 pp
ISBN: 978-3-95806-831-5

Band / Volume 296
**Structural and Magnetic Properties of Biocompatible Iron Oxide
Nanoparticles for Medical Applications**
A. Nasser (2025), xii, 140 pp
ISBN: 978-3-95806-837-7

Band / Volume 297
**Metabolic engineering of *Pseudomonas taiwanensis* for the
improved production of styrene**
J. Rönitz (2025), XII, 147 pp
ISBN: 978-3-95806-841-4

Band / Volume 298
Elucidation of anti-viral strategies in *Streptomyces*
B. U. Rackow (2025), xii, 148 pp
ISBN: 978-3-95806-842-1

Weitere *Schriften des Verlags im Forschungszentrum Jülich* unter
http://wwwzb1.fz-juelich.de/verlagextern1/index.asp

JÜLICH
Forschungszentrum